
VNIVERSITAT DE VALÈNCIA

# Proof of Concept of Therapeutic Gene Modulation of MBNL1/2 in Myotonic Dystrophy

Doctoral Thesis

**Sarah Overby**

January 2022

Faculty of Biology, Department of Genetics
PhD in Biotechnology and Biomedicine

Director:
Dr. Rubén Artero

Tutor:
Dr. Lola Peñarrubia

Dr. RUBÉN D. ARTERO ALLEPUZ, Catedrático del Departamento de Genética de la Facultad de Ciencias Biológicas de la Universitat de València

**INFORMA**

Que Doña Sarah Joann Overby, con una licenciatura de la escuela de artes y ciencias de Samford University, Birmingham, AL, EE. UU., y una maestría de la escuela de ciencias biológicas y biomoleculares de University College Dublin, Dublín, Irlanda, ha realizado bajo mi supervisión el trabajo de investigación original recogido en la presente memoria titulada "Proof of Concept of Therapeutic Gene Modulation of MBNL1/2 in Myotonic Dystrophy."

Revisado el presente trabajo, expresa su conformidad para la presentación del mismo en el Departamento de Genética de la Universitat de València, por considerar que reúne los requisitos necesarios para ser sometido a discusión ante el Tribunal correspondiente, para optar al grado de Doctora por la Universitat de València dentro del Programa Oficial de Doctorado en Biomedicina y Biotecnología.

En Valencia, a 21 de enero de 2022

Dr. Rubén D. Artero Allepuz

## Acknowledgments

I would like to heartily thank Dr. Ruben Artero for his continued mentorship and wisdom throughout these past 4 years. His passion, creativity, and curiosity are what motivated me to continue through each chapter of investigation. He regularly taught me through his ambitious attitude to think bigger and to use failure as a way to embolden the path ahead. Thank you for believing in me.

This project would not have been possible without the support, expertise, and knowledge exchange from Dr. Estefanía Cerro-Herreros. The strategies discussed in this work are based on groundbreaking research performed in her doctoral thesis. She kindly provided excellent data from previous antagomiR experiments to give context to the new results seen here. I count myself fortunate to have been guided by her consistent leadership, work-ethic, and skill.

I would like to acknowledge Jorge Espinosa-Espinosa for his contribution to the RNA-Seq data seen here. A specialist in bioinformatics, Jorge generously dedicated his time to organizing and analyzing large amounts of data to fit my needs in order to give light to transcriptomic information after therapeutic treatments in DM1 cells.

Finally, Juan Antonio Carbonell-Asíns was a tremendous resource for biostatistical analysis. He instructed me on the correct statistical strategy for data from a biochemical serum and blood assay in mice. I was able to apply this guidance to many other analyses in my work.

## Acknowledgments

For all the mice who were sacrificed with the goal of helping others – may it not be in vain.

1941-1
1941-2
1941-3
1942-1
1942-2
1942-3
1982-1
1982-2
1831-1
1831-3
1833-1
1833-2
1830-1
1982-3
1982-4
1831-2
1831-4
1833-3
1830-2
2445-1
2446-1
2441-1
2444-1
2444-2
2444-3
4993-1
4993-2
4993-3
4992-1
4992-2
4992-3
4357-1
4357-2
4357-3
4357-4
4449-1
4449-2
4449-3
4740-1
4740-2
4740-3
4741-1
4741-2
4741-3
4450-1
4450-2
4450-3
4450-4
4358-2

## Dedication

Dedicated to Jo and Pappy—

who I lost along the way, but never left my side.

The clan: Mom, Dad, Rachel.

Nox, co-author

Pa, Grammy, Elvira, Brittany, and family.

Piotr. Love you. Feed the cat.

Estefanía, mi reina y mamá.

Nerea, Irene, María, Águeda, y lab family ♡

Ari, Miguel, Bea, Juanma, mentores y inspiradores.

Mis gordis: Helena, Agne, Desi, Taylor.

Menú del día C.F. and fans.

Mi querida Valencia.

*Thank you all. Gracias a todos.*

+

1S7:12

## Table of Contents


**Resumen en castellano** ..... **1**

**Introduction** ..... **31**

**I. Myotonic Dystrophy Type 1** ..... **33**

I.I. Clinical overview ..... 33
I.II. Molecular basis of the disease ..... 34
I.III. Role of MBNL proteins and downstream effects ..... 35
I.IV. Other pathways contributing to DM1 pathogenesis ..... 39

**II. Models of DM1** ..... **39**

II.I. Patient-derived cells ..... 39
II.II. *Drosophila melanogaster* ..... 40
II.III. *Mus musculus* ..... 41

**III. RNA therapeutics** ..... **43**

III.I. First generation AONs ..... 44
III.II. Second generation AONs ..... 45
III.III. Third generation AONs ..... 45

**IV. Antisense therapy in DM1** ..... **46**

IV.I. RNAi ..... 47
IV.II. Targeting CUG expansions by antisense blockers ..... 48
IV.III. Targeting CUG expansions by antisense cutters ..... 51
IV.IV. RNA-targeting Cas9 ..... 52
IV.V. Targeting downstream effects ..... 53
IV.VI. Upregulation of MBNLs by miRNA blockers ..... 53

**Objectives** ..... **61**

**Results** ..... **67**

**I. Objective 1: FANA antimiR strategy** ..... **69**

I.I. FANA antimiRs show effective miRNA knockdown by gymnotic delivery ..... 70
I.II. MBNL protein and splicing rescue after treatment with FANA antimiRs ..... 72

**II. Objective 2: LNA blockmiR strategy** ..... **73**

II.I. Pilot screen for blockmiRs in DM1 cells ..... 74
II.II. miRNA binding-site blocking shows rescue at the transcript level ..... 76

II.III. Blocking miR-23b from binding to *MBNL* sites show dose-response MBNL1 protein rescue ..... 78
II.IV. M1-Block-23b-1 shows recovery at the transcriptome level ..... 82
II.V. BlockmiR strategy is highly specific ..... 85
II.VI. miR-23b binding site is conserved in mice ..... 87
II.VII. Testing blockmiRs in an *in vivo* DM1 model ..... 90
II.VIII. Mouse specific blockmiR shows toxicological changes in blood ..... 91
II.IX. BlockmiR treatment increases MBNL1 and rescues DM1 phenotypes in mice muscle ..... 95

**III. Objective 3: P-PMO blockmiR strategy ..... 97**

III.I. Pip9b2-linked PMO blockmiR increases MBNL1 in cells ..... 98
III.II. P-PMO is non-toxic to mice and increases grip strength ..... 100
III.III. BlockmiR induces rescue in $HSA^{LR}$ mice phenotypes ..... 102

**Discussion ..... 107**

**I. FANA antimiRs ..... 109**

I.I. AONs targeting miRNAs can be delivered gymnotically ..... 109
I.II. FANA antimiRs show functional rescue of DM1 phenotypes ..... 111
I.III. FANA antimiR modifications could be a safety improvement to antagomiRs .. 114

**II. LNA blockmiRs ..... 115**

II.I. Targeting miRNA binding sites is effective in cells ..... 115
II.II. BlockmiR strategy is highly specific at transcriptome level ..... 117
II.III. miRNA binding sites are conserved in mice ..... 118
II.IV. BlockmiRs induce toxicological changes ..... 119
II.V. BlockmiRs are also viable *in vivo* ..... 121

**III. P-PMO blockmiRs ..... 123**

III.I. Pip9b2 modified blockmiRs reproduce similar recovery to LNA blockmiRs .... 123
III.II. Cell-penetrating peptide morpholinos are less toxic than LNA-based AONs .. 125

**IV. Preclinical conclusions ..... 127**

IV.I. P-PMO blockmiRs are the safer option ..... 127
IV.II. MiRNA overexpression is part of the DM1 phenotype ..... 128

**Conclusions ..... 131**

**Materials and Methods ..... 137**

## Table of Contents


**I. Materials ..... 139**

I.I. Vectors and constructs ..... 139
I.II. Polymerase Chain Reaction ..... 142
I.III. Antisense oligonucleotides ..... 144
I.IV. Cell culture ..... 145
I.V. Kits ..... 145
I.VI. Antibodies ..... 146
I.VII. Equipment ..... 147
I.VIII. Cell lines ..... 148
I.IX. Mice ..... 149

**II. Methods ..... 149**

II.I. Cell culture ..... 149
II.II. RNA extraction and analysis ..... 153
II.III. Protein extraction and analysis ..... 156
II.IV. Mice handling ..... 160
II.V. Statistics ..... 161

**References ..... 165**

**Annex ..... 183**

# Resumen en castellano

## Introducción

La distrofia miotónica es un trastorno neuromuscular multisistémico de aparición congénita, juvenil, adulta o tardía. Originalmente se pensaba que afectaba a entre 1 y 8000 personas en todo el mundo (Harper, 2009; Suominen et al., 2011), pero se ha demostrado, mediante el cribado genético, que la prevalencia es mayor, acercándose a 5-20 personas por cada 100.000 (Johnson et al., 2021). La forma más grave de esta enfermedad, el tipo 1 (DM1), incluye síntomas como miotonía, debilidad muscular, arritmias cardíacas, disfunción cognitiva y cataratas (OMIM #160900). Los síntomas más graves incluyen la insuficiencia respiratoria y cardíaca, que son las principales causas de muerte en los pacientes con DM1 y contribuyen a acortar la esperanza de vida (de Die-Smulders et al., 1998; Wahbi y Furling, 2020). Otros síntomas de la DM1 son la resistencia a la insulina, la obesidad y la disfunción cardíaca (Mankodi y Thornton, 2002).

La base genética de la DM1 se origina en una expansión repetida de un motivo "CTG" en el gen de la proteína quinasa DM1 (*DMPK*) (Brook et al., 1992). Los individuos sanos presentan entre 5 y 37 repeticiones CTG en la *DMPK*. Los pacientes con DM1 pueden exhibir miles de repeticiones con la cantidad de repeticiones aproximadamente correlacionadas con la gravedad de la enfermedad (Tsilfidis et al., 1992). *DMPK* se transcribe en un transcrito de mRNA mutante que lleva las repeticiones "CUG" que forman estructuras de horquilla. Estos complejos se acumulan como focos en el núcleo y se unen con alta afinidad a proteínas de la familia Muscleblind-like (MBNL) (Miller et al., 2000).

Las proteínas MBNL llevan a cabo la regulación del splicing postranscripcional del desarrollo (Kanadia et al., 2003b; Konieczny et al., 2014) y la regulación del sitio de poliadenilación (Batra et al., 2015). Además, la familia de la proteína de unión al RNA CUG (CELF), que también juega un papel en el splicing alternativo, se activa en los pacientes con DM1 (Philips et al., 1998). Las proteínas CELF y MBNL son funcionalmente antagónicas entre

sí en relación con la regulación de sus mRNA (Wang et al., 2015). La combinación del secuestro de la proteína MBNL y la inducción de la proteína CELF da lugar a numerosos eventos de mis-splicing que comúnmente presentan un patrón de splicing de tipo fetal en las células DM1 adultas (Fernández-Costa et al., 2011; Ladd et al., 2001). La familia Muscleblind consta de tres proteínas: MBNL1, MBNL2 y MBNL3, todas ellas secuestradas por el mRNA de *DMPK* (Jiang et al., 2004; Miller et al., 2000). Las proteínas Muscleblind tienen dos dominios de unión a dedos de zinc en tándem que, en presencia de repeticiones tóxicas, tienen una mayor afinidad de unión a los microsatélites CUG que a sus propias dianas de pre-mRNA (Pascual et al., 2006; Yuan et al., 2007). Cuando funcionan correctamente, MBNL1 y 2 provocan específicamente un cambio del patrón de splicing fetal al adulto durante el desarrollo (Lin et al., 2006).

Las alteraciones en la actividad de MBNL y CELF causan un patrón de splicing fetal anormal de varios transcritos, como el canal de cloruro muscular (*CLCN1*), el receptor de insulina (*INSR*), la troponina T cardíaca (*cTNT*), el canal de sodio cardíaco (*SCN5A*), entre otros, y a su vez dan lugar a síntomas clínicos. Por ejemplo, la miotonía y la resistencia a la insulina están directamente relacionadas con el mis-splicing de *CLCN1* (Wheeler et al., 2007) e *INSR* (Savkur et al., 2001), respectivamente, mientras que *SCN5A* está relacionado con fenotipos cardíacos como defectos de conducción y arritmias (Pang et al., 2018). Otros tejidos afectados son el cerebro, que se ve específicamente afectado por el mis-splicing de la proteína tau asociada a los microtúbulos (*MAPT*) y está implicado en fenotipos neurodegenerativos (Goodwin et al., 2015). La espliceopatía también tiene un efecto sobre la localización de las proteínas MBNL en la célula. Concretamente, la inclusión aberrante del exón 5 en los transcritos de *MBNL1* promueve la localización de MBNL1 en el núcleo (Terenzi y Ladd, 2010). Del mismo modo, la inclusión del exón 7 de *MBNL1* promueve la dimerización de MBNL y la posterior unión de alta afinidad a las repeticiones CUG (Konieczny et al., 2014).

Las innovaciones técnicas han permitido la posibilidad de modular el código genético específico a través de técnicas como los oligonucleótidos antisentido (AON). Los AONs bloquean la expresión génica a través de la unión complementaria a través del impedimento estérico, el bloqueo del splicing, el bloqueo de la tapa 5' y la activación de la RNasa-H (ver revisiones (Chan et al., 2006; Chery, 2016)). Actualmente no hay ningún tratamiento antisentido aprobado por la FDA para la DM1. El éxito de la FDA de los AONs en varias enfermedades neuromusculares y de expansión de microsatélites, como se mencionó anteriormente, ha llevado a los investigadores a explorar las posibilidades de tratamiento antisentido en la DM1 (ver revisión (Overby et al., 2018)).

Recientemente, se han identificado miR-23b y miR-218 como inhibidores de la traducción de MBNL1 y 2 (Cerro-Herreros et al., 2018). El experimento mostró cómo los antagomiRs, que son AONs dirigidos a miRNAs que contienen una fracción de colesterol, eran capaces de silenciar significativamente sus miRNAs diana en mioblastos de pacientes con DM1, así como en ratones $HSA^{LR}$. Sin colesterol, se denominan simplemente antimiRs. La administración de estos antagomiRs llegó al tejido muscular de los ratones y posteriormente aumentó las proteínas Mbnl (Mbnl1 y 2 específicamente) al tiempo que mejoraba los fenotipos distintivos de la enfermedad, incluyendo las alteraciones de splicing, la histopatología y la miotonía. Los antagomiRs han seguido mostrando promesa terapéutica en ratones con DM1 después de que tanto el antagomiR-23b como el antagomiR-218 fueron capaces de provocar una respuesta a la dosis con efectos duraderos (Cerro-Herreros et al., 2020; Cerro-Herreros, 2021).

## Objetivos

Nuestro laboratorio ha demostrado recientemente que dirigirse a los miRNAs que regulan la traducción de los transcritos de MBNL en proteínas también puede rescatar la función de MBNL así como los efectos posteriores.

Específicamente, la focalización de miRNA-23b y miRNA-218 por antagomiRs fue capaz de aumentar la expresión de proteínas MBNL en mioblastos DM1 y aliviar la miotonía, la histopatología y la espliceopatía en modelos de ratón $HSA^{LR}$ DM1 (Cerro-Herreros et al., 2020; Cerro-Herreros, 2021; Cerro-Herreros et al., 2018). El uso de AONs ha crecido exponencialmente en los últimos años para el tratamiento de diversas enfermedades raras, incluyendo algunas con aprobación de la FDA (Rinaldi y Wood, 2018; Roberts et al., 2020). El desarrollo de las modificaciones de tercera generación ha aumentado enormemente la eficacia y la capacidad de entrega de estos oligos. El ya exitoso enfoque antagomiR podría perfeccionarse mediante la mejora selectiva de la química de los oligos para aumentar la especificidad y la potencia. Además, el papel recién descubierto de miR-23b y miR-218 abre la puerta a la exploración de diferentes tácticas para modular su regulación. Aquí se propone el uso de AONs de nuevo diseño dirigidos a la actividad de miR-23b y miR-218 para regular MBNL1 y MBNL2 a través de los siguientes objetivos:

1. Explorar el bloqueo de miRNAs mediante AONs FANA-antimiR *in vitro*.
2. Exploración del bloqueo del sitio de unión del miRNA a través de la estrategia blockmiR *in vitro* e *in vivo* con el uso de modificaciones químicas del LNA.
3. Mejorar la química de la estrategia blockmiR mediante el uso de la tecnología de péptidos de penetración celular *in vitro* e *in vivo*.

## Resultados

### I. Objetivo 1: Estrategia antimiR de FANA

Los antagomiRs dirigidos a miR-23b y miR-218 ya han sido introducidos con éxito en células de DM1 y en ratones provocando un aumento terapéutico de la proteína MBNL1 (Cerro-Herreros et al., 2020; Cerro-Herreros, 2021; Cerro-Herreros et al., 2018). Recientemente, los AONs 2'-Deoxy-

fluoroarabinonucleótidos (FANA) se han convertido en una atractiva mejora de tercera generación de las modificaciones 2'-fluoro de segunda generación porque pueden ser entregados gimnóticamente, es decir, sin el uso de reactivos de transfección. Para probar la eficacia de la entrega gimnótica, se diseñaron antimiRs con las mismas secuencias que los antagomiRs previamente probados y se administraron a cinco concentraciones diferentes según las instrucciones del fabricante para encontrar la concentración óptima de trabajo.

## I.I. Los antimiRs de FANA muestran un derribo efectivo de miRNAs por administración gimnótica

Se diseñó un antimiR de FANA para la unión complementaria a miR-23b y miR-218. También se generó un tercer antimiR con una secuencia codificada (Scramble) como control de la química de FANA. En primer lugar, se evaluó la inhibición del crecimiento celular tras el tratamiento con cada AON en fibroblastos DM1 inmortalizados derivados de pacientes y transdiferenciados en miotubos (células DM1) (Arandel et al., 2017) administrados gimnóticamente.

Los antimiRs de FANA se compararon con los previamente estudiados AntagomiR-23b y -218 con y sin el reactivo de transfección genética X-treme. La viabilidad celular se analizó a 250 nM y 1 $\mu$M para el FANA mientras que los antagomiRs se administraron a sus concentraciones de trabajo anteriores según Cerro-Herreros et al. 2018. Este experimento se realizó dos veces: una con el uso del reactivo de transfección y otra administrando los oligos gimnóticamente. La viabilidad celular fue mucho mayor en los oligos FANA administrados sin reactivo de transfección. También fueron mucho más viables que las células administradas con antagomiR, que se mantuvieron igual que cuando se administraron con el reactivo de transfección.

### I.II. Rescate de la proteína MBNL y del splicing tras el tratamiento con antimiRs de FANA

Dado que se observó el derribo de miRNA y el aumento de *MBNL* incluso en la administración más baja de antimiRs, los experimentos avanzaron a 1 μM. El tratamiento con miR-23b-1 y miR-218-1 también fue capaz de aumentar los niveles de la proteína MBNL1 a esta concentración. Sin embargo, sólo miR-218-1 fue capaz de aumentar MBNL2. Varios eventos de splicing alternativo están presentes en las células afectadas por la DM1, incluyendo los transcritos *BIN1*, *cTNT*, *MBNL1* y *SPTAN*. El tratamiento con miR-23b-1 mostró el rescate de las alteraciones de splicing de *BIN1*, *cTNT* y *MBNL1* en las células de DM1. Curiosamente, *BIN1* también fue rescatado previamente por miR-23b, pero *cTNT* no. Mediante el análisis *in vitro*, los antimiRs de FANA mostraron un rescate comparable al de sus homólogos antagomiR previamente probados, pero con entrega gimnótica. Las modificaciones FANA demostraron ser menos tóxicas que otras modificaciones AON sin perder potencia.

## II. Objetivo 2: estrategia de LNA blockmiR

Para sortear el inconveniente de los efectos inespecíficos, aquí describimos una alternativa a la tecnología antimiR llamada "blockmiRs". En este caso, los blockmiRs se diseñaron con un núcleo de 2'-OMe de 8 polímeros con extremos de LNA asimétricos. De este modo, los oligos tenían la afinidad de unión mejorada de los LNA de tercera generación combinada con la flexibilidad estérica y la tolerabilidad de los 2'-O-metilos naturales.

### II.I. Screen piloto para bloquear miRNAs en células DM1

Los sitios de unión de miR-23b y miR-218 en las 3'UTRs de *MBNL1* y *MBNL2* se predijeron con TargetScan y miRanda y se confirmaron mediante un ensayo de luciferasa dual en el estudio previo de antagomiR en células HeLa (Cerro-Herreros et al., 2018). Se diseñaron BlockmiRs para todos los sitios predichos y confirmados. Se analizaron las células para conocer los niveles

de los transcritos de *MBNL1* y *2* y el nivel de knockdown de miRNAs tras el tratamiento a 1, 2,5 y 5 $\mu$M. El oligo Scramble no tuvo ningún efecto sobre los niveles de transcripción. El tratamiento con miR-23b-1 aumentó tanto *MBNL1* como *2* a 1 $\mu$M en comparación con los niveles de DM1 sin tratar. MiR-218-1 también aumentó ambos transcritos pero a la concentración más alta de 2,5 $\mu$M. Se observó un derribo significativo de miR-23b y miR-218 por sus respectivos AON en todas las concentraciones.

En primer lugar, se comprobó la toxicidad de los blockmiR tras la transfección en células DM1 después de cuatro días diferenciadas a concentraciones crecientes para determinar el TC50 de cada tratamiento. El Scramble mostró la menor toxicidad en comparación con todos los demás blockmiRs, excepto el M2-Block-218-1, lo que puede sugerir que hay otros factores que contribuyen a la toxicidad y no simplemente la estructura química. Todos los blockmiRs estaban por debajo del TC50 a 200 nM, que se determinó como la mayor concentración funcional. Sin embargo, en el estudio anterior (Cerro-Herreros et al., 2018), los antagomiRs para miR-23b mostraron resultados terapéuticos a una concentración de 50 nM y 200 nM para los antagomiRs dirigidos a miR-218. Por lo tanto, se eligió 50 nM para los antagomiRs dirigidos a los sitios de unión de miR-23b y 200 nM para los dirigidos a miR-218 para poder comparar ambos tratamientos.

### II.II. El bloqueo del sitio de unión del miRNA muestra un rescate a nivel de transcripción

Los efectos moleculares del tratamiento con miRNAs bloqueados se analizaron en células DM1 cuatro días después de la transfección y diferenciación. Se administró un control codificado, uno a 50 nM (Scramble 50) y otro a 200 nM (Scramble 200), que no se prevé que tenga ninguna diana específica. Los BlockmiRs M1-Block-23b-1 y M2-Block-23b-1 fueron capaces de aumentar significativamente la expresión relativa de los transcritos *MBNL1* y *MBNL2* en comparación con el tratamiento Scramble. M2-Block-

23b-1 tuvo un mayor efecto sobre los transcritos de *MBNL2*, lo que era de esperar ya que este blockmiR actúa sobre el sitio de unión de la 3'UTR de *MBNL2*. Los blockmiRs dirigidos a los sitios de unión de miR-218 no mostraron ningún aumento en la expresión de *MBNL1* o *2*. De hecho, M2-Block-218-2 y -3 disminuyeron la expresión de *MBNL1* en comparación con Scramble 218 mientras que no ejercieron ningún efecto sobre los transcritos de *MBNL2*.

En las células DM1, se observan patrones de splicing anormales en los transcritos *MBNL1*, *NFIX* y *SPTAN1* (Andre et al., 2019; Charizanis et al., 2012; Konieczny et al., 2014; Nakamori et al., 2013; Wagner et al., 2016) y se pueden observar en comparación con las células control (CNT). De nuevo, M1-Block-23b-1 y M2-Block-23b-1 mostraron una inversión completa de la inclusión del exón 5 en los transcritos de *MBNL1*, mientras que los blockmiRs dirigidos a los sitios de unión de miR-218 no tuvieron ningún efecto. No hubo efecto por parte de ninguno de los blockmiRs en el caso del exón 7 de *NFIX*. Finalmente, todos los blockmiRs dirigidos a miR-218 mostraron un notable rescate con la inclusión del exón 23 en *SPTAN1*. Los blockmiRs dirigidos a miR-23b también mostraron un ligero rescate en la expresión de este exón. *MBNL1* y *NFIX* están regulados por proteínas MBNL1 (Wagner et al., 2016) mientras que *SPTAN1* está regulado por proteínas MBNL2 (Charizanis et al., 2012). Esto podría explicar por qué se observó un mayor rescate con los blockmiRs dirigidos a sitios en MBNL2. Sin embargo, no se puede descartar que esto también podría estar relacionado con el objetivo del miRNA.

### II.III. El bloqueo de miR-23b de la unión a los sitios de MBNL muestra una respuesta a la dosis de rescate de la proteína MBNL1

La función crítica del tratamiento con blockmiR es aumentar la producción de proteínas MBNL mediante el bloqueo de la regulación de miR-23b o miR-218. Por lo tanto, se analizaron y cuantificaron los niveles de la proteína MBNL1 mediante tinción de inmunofluorescencia tras el tratamiento con los

blockmiRs. Las células de control muestran una intensa señal de MBNL1 en todo el núcleo y el citoplasma, lo que indica que la proteína MBNL1 está sana y es funcional. Por el contrario, las células DM1 muestran muy poca señal de MBNL1 en el citoplasma y sólo focos puntuales en el núcleo. La intensidad media de píxeles de la fluorescencia de MBNL1 se calculó para cada célula y se normalizó con respecto al área de la misma. De forma similar al aumento observado en los transcritos de MBNL1, M1-Block-23b-1 y M2-Block-23b-2 presentaron aumentos significativos de la fluorescencia de la proteína MBNL1. También mostraron una localización subcelular citoplásmica difusa que indicaba que el MBNL1 adicional no estaba siendo atrapado en los focos nucleares. Las células tratadas con Scramble 50 y 200 no mostraron ningún aumento de la fluorescencia de MBNL1. Curiosamente, M2-Block-218-2 también mostró un aumento en la intensidad de los píxeles de MBNL1.

### II.IV. M1-Block-23b-1 muestra recuperación a nivel del transcriptoma

Se realizó RNASeq para M1-Block-23b-1 con el fin de investigar la recuperación de la expresión génica tras el tratamiento y compararla con su homólogo antagomiR de estudios anteriores para visualizar el efecto global que tienen los oligos en las células DM1. En este experimento, se dejó que los fibroblastos inmortalizados se diferenciaran cuatro días más antes de la transfección con los AONs y luego se dejaron otros cuatro para su crecimiento con el fin de observar diferencias de expresión más pronunciadas entre las células DM1 y CNT y ver un patrón de expresión más comparable al de los músculos diferenciados *in vivo*.

En primer lugar, se cuantificaron las uniones de splicing utilizando una fórmula de porcentaje de splicing delta (dPSI). Se identificaron 478 alteraciones de eventos de splicing relacionados con la enfermedad entre las células sanas y las de DM1. Estos eventos se filtraron para los datos que tienen un dPSI superior al 25% y que tienen un efecto significativo cuando se

comparan con las células sanas y con las de DM1. Este filtro identificó 20 eventos de splicing en 19 genes.

Se generó otro gráfico de puntos geométricos para visualizar los 25 genes principales que mostraron una recuperación total de la expresión tras el tratamiento con M1-Block-23b-1. El blockmiR y el antagomiR mostraron un patrón de expresión similar en muchos genes, siendo el blockmiR menos intenso. De hecho, el antagomiR tendió a mostrar una recuperación excesiva en comparación con las células de control. El tratamiento con blockmiR todavía mostró cambios en la dirección de rescate de las biopsias para *PODN*, *CLSTN2*, *RAI2* y *MYH6*.

Es importante destacar que, de los genes totalmente recuperados por M1-Block-23b-1, 14 estaban conectados por GOterms sobrerrepresentados, todos los cuales tienen relación con la función muscular y esquelética. Estos genes fueron analizados por STRING y se encontró que tenían vínculos significativos de interacción proteína-proteína. Esto implica al M1-Block-23b-1 en la recuperación de la expresión génica de la infraestructura y los mecanismos neuromusculares vitales en el sistema muscular.

### II.V. La estrategia BlockmiR es altamente específica

Una de las ventajas previstas del enfoque blockmiR es un efecto altamente específico sobre los transcritos MBNL. Se calculó un porcentaje de recuperación para todos los genes relacionados con la enfermedad y se comparó de forma cruzada con cada tratamiento. En comparación con las células sanas, el blockmiR y el antagomiR fueron capaces de un rescate parcial y total. El blockmiR mostró una mayor recuperación parcial mientras que el antagomiR mostró una mayor recuperación total e incluso 108 casos de sobre recuperación. El blockmiR también fue capaz de recuperar algunos genes que el antagomiR no pudo y viceversa. El antagomiR tiene un mayor efecto sobre el transcriptoma total.

Por último, para investigar la especificidad de los tratamientos con respecto a miR-23b, se analizaron los datos de RNASeq específicamente para los transcritos dirigidos por miR-23b. De las 57 dianas confirmadas identificadas mediante miRTarBase, sólo 1 de ellas mostró una alteración en la expresión tras el tratamiento con M1-Block-23b-1 en comparación con las células DM1 no tratadas. Por el contrario, las células tratadas con antagomiR mostraron alteraciones en 28 de las dianas. Cuando se comparan con los controles sanos, las células tratadas con blockmiR mostraron más similitud con las células de control que las antagomiR. Esto indica que la estrategia blockmiR de dirigirse a los sitios de unión del miRNA es un método mucho más específico que dirigirse al propio miRNA.

### II.VI. El sitio de unión de miR-23b está conservado en los ratones

El éxito de los bloqueadores del blockmiR *in vitro* llevó a realizar pruebas *in vivo* en ratones. Pero antes de que este experimento pudiera llevarse a cabo, era necesario confirmar el sitio de unión de miR-23b en el ratón. Para confirmar los sitios predichos, se realizó otro ensayo de luciferasa en células C2C12 de ratón utilizando construcciones *Mbnl1* 3'-UTR. La expresión endógena de la unión de miR-23b en las células C2C12 se hizo evidente a través del aumento de la luminiscencia en los plásmidos de deleción del sitio de unión de miR-23b en comparación con el tipo salvaje. Por el contrario, la señal GLuc disminuyó tras la transfección con los plásmidos de unión perfecta. Esto confirma que miR-23b se une directamente a estos sitios.

### II.VII. Pruebas de blockmiRs en un modelo *in vivo* de DM1

El sitio de unión conservado 1 para miR-23b en ratones tiene un nucleótido de diferencia en comparación con el sitio humano. Por lo tanto, se generó un nuevo compuesto, M1-Block23b-M, teniendo en cuenta esta diferencia y se administró a 12,5 mg/kg mediante inyección subcutánea en ratones del modelo $HSA^{LR}$ DM1 (n = 5). La versión humana del blockmiR, M1-Block23b-H, también se inyectó a la misma concentración (n = 5). A un grupo de ratones

sanos FVB (n = 5) y a un grupo de ratones $HSA^{LR}$ (n = 5) se les administró PBS como dos controles separados. Después de cuatro días, se sacrificaron los ratones y se extrajeron sus músculos gastrocnemios y cuádriceps para el análisis molecular.

## II.VIII. El blockmiR específico de ratón muestra cambios toxicológicos en la sangre

Tras el tratamiento con las versiones humana y de ratón de M1-Block23b, se extrajo y analizó la sangre y el suero. Se realizó un recuento diferencial de glóbulos blancos (WBC) después de cada tratamiento y se comparó con los niveles empíricos de FVB. También se añadieron mediciones externas de FVB como referencia, pero variaron mucho entre los estudios (Bogue et al., 2020; Schneck et al., 2000). Los niveles de FVB más similares a los medidos empíricamente en nuestro laboratorio fueron los de los machos de 8 semanas (§) (Bogue et al., 2020). Estos FVB también coincidían con las proporciones típicas normales de los ratones sanos en general: neutrófilos 20-30%, eosinófilos 0-7%, linfocitos: 70-80%, monocitos <2%, basófilos: 0-1% (O'Connell et al., 2015). Los tratamientos con PBS y M1-Block23b-H se mantuvieron dentro de estos rangos. Sin embargo, se observó un aumento de monocitos y linfocitos tras el tratamiento con M1-Block23b-M.

Se realizó un recuento sanguíneo completo (CBC) y un análisis bioquímico para cada muestra y se comparó con los niveles de FVB. Con esta comparación, M1-Block23b-M mostró varios cambios, entre ellos un aumento significativo de la hemoglobina corpuscular media (HCM), de la concentración de hemoglobina corpuscular media (HCM), de las plaquetas y de la fosfatasa alcalina, así como una disminución significativa del volumen corpuscular medio (VCM), de la anchura de distribución de los glóbulos rojos (ADE), de la amilasa, del aspartato transaminasa (AST), de la creatina quinasa (CPK) y del lactato deshidrogenasa (LDH). En la mayoría de los casos, el M1-Block23b-H se mantuvo cerca del mismo nivel que el PBS.

Cuando se comparó el M1-Block23b-H con los niveles de FVB, sólo hubo un aumento significativo de la glucosa y el colesterol, que es un fenotipo de la enfermedad de los ratones $HSA^{LR}$, así como una ligera disminución de la AST.

## II.IX. El tratamiento con BlockmiR aumenta el MBNL1 y rescata los fenotipos de DM1 en el músculo de los ratones

Cuatro días después de la inyección, se sacrificaron los ratones y se extrajeron los músculos de las patas traseras, gastrocnemio y cuádriceps, para su examen molecular. Se observó un aumento significativo de la expresión del transcrito *Mbnl1* en ambos músculos tras el tratamiento con M1-Block23b-M. Asimismo, se produjo un aumento similar que alcanzó los niveles normales de la proteína Mbnl1 del FVB tras el tratamiento con M1-Block23b-M.

M1-Block23-M también indujo un aumento fisiológico de la fuerza de agarre. El porcentaje de fuerza normal se calculó normalizando la fuerza de los ratones en un medidor de fuerza de agarre a su peso antes y después del tratamiento y luego comparándolo con los niveles de PBS. Se analizó el splicing de tres transcritos después del tratamiento, incluyendo *Atp2a1*, *Clcn1* y *Mbnl1*. Se observaron ligeros aumentos del porcentaje de recuperación del splicing (PSR) en *Atp2a1* y *Clcn1*. Sin embargo, al observar los ratones tratados individualmente, dos ratones en particular mostraron una gran cantidad de rescate.

La migración de los núcleos de las fibras musculares hacia el centro de las mismas es un fenotipo bien conocido del músculo de los ratones $HSA^{LR}$ (Mankodi et al., 2000). Por lo tanto, se realizó una tinción de hematoxilina y eosina (H&E) en el músculo gastrocnemio y en el cuádriceps para visualizar el porcentaje de fibras musculares que contienen núcleos centrales. En ambos tejidos, M1-Block23b-M mostró una reducción significativa del

porcentaje de núcleos centrales en comparación con los controles de PBS. De hecho, las fibras tratadas con M1-Block23b-M son más similares morfológicamente a las de los ratones FVB.

## III. Objetivo 3: Estrategia de P-PMO blockmiR

Los morfolinos de carga neutra (PMO) y los morfolinos ligados a péptidos que penetran en la célula (P-PMO) basados en AONs dirigidos a las repeticiones tóxicas *DMPK* fueron capaces de bloquear la unión de las proteínas MBNL (Leger et al., 2013; Wheeler et al., 2009). Los PMOs tienen una carga neutra que crea un compuesto altamente estable y facilita la entrega eficiente a la célula. Los antimiRs y antagomiRs han sido bien caracterizados por su viabilidad para bloquear la actividad de los miRNAs (Lopez Castel et al., 2019; Rupaimoole and Slack, 2017). En este caso, se diseñaron blockmiRs de PMO químicamente mejorados con el péptido Pip9b2 contra un sitio de unión de miR-23b en *MBNL1* y se probaron en fibroblastos DM1 inmortalizados derivados de pacientes y transdiferenciados en miotubos (células DM1) (Arandel et al., 2017). El péptido está diseñado para facilitar la entrada eficiente en la célula sin el uso de reactivos de transfección y, por lo tanto, disminuir los efectos secundarios tóxicos. La carga neutra también mejorará la estabilidad del compuesto *in vivo*.

### III.I. El PMO blockmiR ligado a Pip9b2 aumenta la MBNL1 en las células

Pip9b2 es un péptido que penetra en las células sin necesidad de un reactivo de transfección. Para comprobar la toxicidad celular, el P-PMO blockmiR y un péptido enlazado con un PMO Scramble (P-SC), un control químico, se administraron en células DM1 a concentraciones crecientes. Los oligos ligados a péptidos mostraron poca o ninguna inhibición del crecimiento celular en todas las concentraciones, en contraste con los tratados con el reactivo de transfección, que empezaron a mostrar una inhibición del

crecimiento celular del 50% después de 50 nM. Por lo tanto, para el resto de los experimentos, P-PMO y P-SC se administraron a 1 $\mu$M según la recomendación del fabricante.

Las células DM1 mostraron un aumento de los niveles de expresión de los transcritos *MBNL1* y *2* tras el tratamiento con P-PMO blockmiR. Los patrones de splicing fetal aberrante en los transcritos *MBNL1* y *NFIX* muestran un fuerte fenotipo en las células DM1. Tras el tratamiento con el blockmiR, se observó un ligero pero significativo retorno al patrón de splicing adulto. Las células también mostraron un llamativo aumento de la inmunofluorescencia de la proteína MBNL1 mediante el análisis de imágenes de microscopía confocal. Desde un punto de vista cualitativo, las células tratadas con el péptido penetrante blockmiRs eran visiblemente más prolíficas y mostraban un gran aumento de la fluorescencia de MBNL1 en el citoplasma. La cuantificación de la intensidad media de los píxeles de cada célula confirmó este aumento.

### III.II. P-PMO no es tóxico para los ratones y aumenta la fuerza de agarre

El éxito del P-PMO blockmiR *in vitro* llevó a su administración en ratones $HSA^{LR}$. Se generó un nuevo P-PMO que tenía en cuenta la diferencia de un nucleótido entre los ratones y los humanos y se administró por vía intravenosa a 10 mg/kg. Se midió la fuerza de agarre de los ratones antes y después del tratamiento y se calculó el porcentaje de fuerza normal para cada grupo. Los ratones tratados con P-PMO mostraron un gran aumento del porcentaje de fuerza normal. Tras el tratamiento, se extrajo el suero sanguíneo de los ratones para su análisis bioquímico. Los niveles de FVB se establecieron como el nivel de control sano con el que se compararon todos los demás tratamientos. Uno de los pocos cambios significativos fue la disminución de los niveles de creatina fosfocinasa (CPK). Las cantidades más bajas observadas aquí indican la ausencia de daño tisular y están dentro

del rango de niveles normales en ratones sanos. También son significativamente diferentes a los de FVB los niveles de amilasa tras el tratamiento con el P-PMO y, curiosamente, el control PBS. Sin embargo, tras un examen más detallado, estos niveles también estaban dentro del rango normal para ratones sanos. Es importante destacar que el resto de los parámetros que indican hepatotoxicidad o daño tisular, incluyendo ALT, AST, bilirrubina, ácidos biliares y LDH, permanecieron sin cambios tras el tratamiento con blockmiR. Otros indicadores de salud, como la creatinina, el colesterol, la glucosa y los triglicéridos, así como el peso del ratón, también se mantuvieron estables. No se observaron cambios en los niveles de expresión relativa de *Mbnl1* o *2*.

### III.III. BlockmiR induce el rescate de los fenotipos de los ratones $HSA^{LR}$

Después de ver resultados prometedores a nivel fisiológico, se analizaron los ratones a nivel molecular para ver si había cambios en el fenotipo DM1 específicamente en el músculo cuádriceps de la pierna. No se observaron cambios en ningún parámetro en el músculo gastrocnemio, por lo que los resultados se excluyeron del análisis. Los transcritos *Atp2a1*, *Clcn1*, *Mbnl1* y *Nfix* muestran patrones anormales de splicing fetal en el modelo de ratones DM1 (Dixon et al., 2015; Du et al., 2010; Lin et al., 2006; Tanner et al., 2021). Tras la administración de blockmiR, se observó una corrección en los cuatro transcritos. El porcentaje de recuperación del splicing comparado con el control P-SC mostró un rescate significativo.

Como se observó en la microscopía de células DM1, el P-PMO también aumentó la cantidad de proteína Mbnl1. El P-PMO mostró un aumento significativo en comparación con el P-SC y el control $HSA^{LR}$ PBS. Por último, se realizó un análisis histológico de secciones de 10 $\mu$m del músculo del cuádriceps. Tras la tinción con H&E, se cuantificó el porcentaje de fibras musculares con núcleos centrales. Aunque no fue estadísticamente

significativo al promediar los seis ratones, se observó una disminución del porcentaje de fibras con núcleos centrales en comparación con las muestras de P-SC. Hubo dos ratones específicos que mostraron un rescate particularmente fuerte. La imagen muestra un sorprendente parecido con los cortes FVB.

## Conclusiones

En resumen, se pueden extraer las siguientes conclusiones:

1. Los antimiRs con modificaciones FANA dirigidos a miR-23b y miR-218 administrados sin el uso de un reactivo de transfección son una alternativa adecuada a los antagomiRs con modificaciones 2'-O-metilo y una fracción de colesterol debido a su mayor viabilidad celular en las células DM1 incluso a concentraciones más altas.
2. La administración gimnótica de los antimiRs de FANA muestra una recuperación terapéutica comparable a la de los antagomiRs en las células DM1 al aumentar los transcritos de *MBNL1* y *MBNL2*, reducir miR-23b y miR-218, y aumentar la proteína MBNL1 en las células DM1. MiR-218-1 fue capaz de aumentar la proteína MBNL2 y MiR-23b-1 fue capaz de rescatar el splicing en el exón 11 de *BIN1*, el exón 5 de *cTNT* y el exón 5 de *MBNL1*.
3. Se demostró que los blockmiRs dirigidos a los sitios de unión de miR-23b o miR-218 también eran capaces de tener efectos terapéuticos en las células DM1. Específicamente, M1-Block-23b-1 y M2-Block-23b-1 aumentaron los transcritos de *MBNL1* y *MBNL2*, rescataron los patrones de splicing del exón 5 de *MBNL1* y del exón 23 de *SPTAN*, y aumentaron la inmunofluorescencia y corrigieron la localización subcelular de la proteína MBNL1.
4. El bloqueo del sitio de unión de miR-23b por los blockmiRs causó aproximadamente un 40% menos de cambios en el transcriptoma relacionado con la enfermedad que la unión directa de miR-23b por los antagomiRs.

5. Los dos sitios de unión de miR-23b predichos en la 3'UTR de *Mbnl1* de ratón fueron confirmados tras un ensayo de luciferasa dual. El sitio 3 para la unión de miR-218 en *Mbnl1* 3'UTR fue confirmado, así como el sitio 1 y posiblemente el sitio 2 en *Mbnl2* 3'UTR.
6. M1-Block-23b-1, denominado LNA blockmiR, es viable *in vivo* y muestra un aumento de la fuerza de agarre y del transcrito y la proteína Mbnl1 en los músculos cuádriceps y gastrocnemio de ratones $HSA^{LR}$. También mostró una disminución significativa en los núcleos centrales.
7. El P-PMO blockmiR muestra un efecto terapéutico similar al LNA blockmiR sin toxicidad en células DM1.
8. P-PMO blockmiR también es viable *in vivo* mostrando un aumento de la fuerza de agarre y sin cambios tóxicos. En el músculo del cuádriceps de los ratones $HSA^{LR}$, P-PMO también mostró un aumento de la proteína Mbnl1, y rescató eventos de splicing en el exón 22 de *Atp2a1*, el exón 7a de *Clcn1*, el exón 5 de *Mbnl1* y el exón 7 de *Nfix*.
9. El papel de los miRNAs en la DM1 posiciona las estrategias antimiR y blockmiR en la vanguardia de la terapia potencial de la DM1.

## Metodología

### I. Condiciones de cultivo celular

Todas las células utilizadas en este trabajo se cultivaron a 37°C en una atmósfera humidificada al 5% de $CO_2$. Las células DM1, los fibroblastos CNT y las células C2C12 se cultivaron en medio de crecimiento DMEM + 4,5 g/L de glucosa suplementado con 10% de FBS y antibióticos. Para iniciar el programa miogénico, las células DM1 y CNT se cultivaron entonces en medio de diferenciación según Arandel et al., 2017 que las transdiferencia a miotubos mediante la activación con doxiciclina.

#### I.I. Transfección

24 h antes de la transfección, las células se sembraron a 100.000 células por mL en una placa de 24 pocillos (inmunofluorescencia), una placa de 96 pocillos (ensayo de toxicidad), una placa de Petri de 3 mL (extracción de ARN) o una placa de Petri de 10 mL (extracción de proteínas). Para la administración gimnótica, los oligos se sonicaron y se agitaron vigorosamente en vórtex antes de administrarlos en el medio de diferenciación y dejarlos incubar. La mezcla de transfección se hizo mezclando X-treme Gene y el respectivo blockmiR en medio Optimem.

## I.II. Ensayo de toxicidad

Para los ensayos de proliferación celular de los antimiRs de FANA y los blockmiRs de LNA y P-PMO, se sembraron células en placas de 96 pocillos y se transfectaron a concentraciones crecientes por cuadruplicado. Para medir la viabilidad de las células, se añadieron 20 µl de sal de tetrazolio MTS/PMS del ensayo de proliferación celular no radiactivo CellTiter 96 a cada pocillo y se incubaron las células durante cuatro horas a 37°C en una cámara humidificada con un 5% de $CO_2$. La conversión de MTS en formazán soluble se midió por absorbancia a 490 nm utilizando un lector de placas Infinite 200 PRO.

## I.III. Transformación de células competentes

Las células competentes se transformaron con plásmidos. En primer lugar, se añadió el DNA del plásmido a las células competentes descongeladas y se sometió a un choque térmico durante 2 minutos a 37°C y luego 1,5 minutos a 42°C (Froger y Hall, 2007). Las células se incubaron en hielo durante 1-2 minutos y luego se añadieron a LB líquido y se incubaron durante 1 hora a 37°C. A continuación, las células se centrifugaron, se resuspendieron y se extendieron en placas de agar LB recubiertas de ampicilina. Después de la incubación a 37°C durante la noche, se seleccionaron las colonias y se añadieron a LB líquido con ampicilina para incubar una vez más durante la noche a 37°C (Maniatis et al., 1982).

### I.IV. Ensayo de luciferasa dual

La luminiscencia de la luciferasa gaussiana (GLuc) y de la fosfatasa alcalina (SEAP) se midió utilizando el kit de luminiscencia dual de pares secretados, de acuerdo con los protocolos del fabricante. La actividad de la luciferasa gaussiana se normalizó con la actividad de la fosfatasa alcalina (GLuc/SEAP). La luminiscencia se midió utilizando un lector de placas Infinite M200 PRO. Se diseñaron plásmidos reporteros de *Mbnl1* y *Mbnl2* 3'UTR pEZX-MT05 que contenían *Mbnl1* y *Mbnl2* de tipo salvaje (WT), deleción de la región semilla de miR-23b o miR-218 (Del), o coincidencia perfecta de la secuencia completa de miR-23b o miR-218 (PM). Se repitió el mismo ensayo con células C2C12 co-transfectadas con el mímico miR-23b o miR-218, el mímico codificado (pVmiR) y los controles sin mímico.

## II. Extracción y análisis de RNA

### II.I. Extracción de células y tejidos de ratón

El RNA total se aisló de miotubos transdiferenciados o de músculo gastrocnemio o cuádriceps de ratón utilizando el reactivo de lisis QIAzol y el RNeasy Mini Kit siguiendo las recomendaciones del fabricante. Se analizó la calidad y la concentración total de los productos mediante Nanodrop. Para las células, se lisaron con QIAzol y se rasparon las placas. En el caso de los ratones, los tejidos se añadieron a un tubo Eppendorf de 2 mL junto con una bola metálica de lisado y el reactivo QIAzol. Los tubos se agitaron enérgicamente con la máquina TissueLyser durante 5 minutos.

### II.II. DNA plasmídico de células competentes

Tras la selección de colonias y la incubación, se aisló el DNA plasmídico utilizando el kit de aislamiento de plásmidos de alta pureza. Tras la extracción, se analizó la calidad de las muestras mediante Nanodrop y se sometió a la digestión de las enzimas de restricción AsiSI y SpeI. El producto se pasó por electroforesis en gel para confirmar que los plásmidos habían aceptado las construcciones y tenían el tamaño correcto (Maniatis et al., 1982).

## II.III. RT-PCR

Se llevó a cabo la transcripción inversa de la PCR para todos los aislados utilizando 1 μg de RNA total para obtener el cDNA. En primer lugar, las muestras se trataron con DNasa con un control sin transcriptasa inversa (NRT) para confirmarlo. La transcripción inversa fue seguida de una RT-PCR semicuantitativa sobre el cDNA. El producto de la PCR se corrió en un gel de electroforesis de agarosa al 2% con una escalera biomolecular para determinar el tamaño de los amplicones (Friedmann y Rossi, 2007). En el caso del análisis de miRNA, se añadió un paso adicional al principio de este protocolo utilizando la polimerasa A y el ATP para añadir una cola 3' poli-A a los miRNA.

El índice de recuperación de splicing (PSR) se definió como el valor %SI menos $\bar{\mathbf{X}}\%_{DSI}$, dividido por $\bar{\mathbf{X}}\%_{DSI}$ menos $\bar{\mathbf{X}}\%_{HSI}$ (donde SI es la inclusión de splicing de cada muestra, DSI es la inclusión de splicing de la enfermedad, y HSI es la inclusión de splicing saludable).

## II.IV. RT-qPCR

Para la PCR cuantitativa basada en Taqman, se añadieron sondas marcadas con FAM o MAX junto con cebadores específicos para que todas las muestras pudieran ser normalizadas por controles endógenos en el mismo pozo. Todas las muestras se ejecutaron por triplicado en un sistema de PCR en tiempo real QuantStudio 5. Para la PCR cuantitativa de miRCURY basada en Sybr, cada miRNA se cuantificó en un pozo separado y se normalizó con respecto a los snRNA U6 y U1. Los niveles de expresión se normalizaron con respecto al gen de referencia utilizando el método $2^{-\Delta\Delta Ct}$ (Livak y Schmittgen, 2001).

## II.V. RNASeq

Los fibroblastos DM1 inmortalizados se sembraron a 100.000 células por mL en placas de Petri de 3 mL. Las células se trataron con medio de diferenciación y se dejaron transdiferenciar durante cuatro días. A

continuación, se transfectaron M1-Block-23b-1 y AntagomiR-23b a 50 nM y se dejaron durante cuatro días más. Al octavo día, se extrajo el RNA total siguiendo el protocolo de extracción de RNA. El siguiente análisis bioinformático se realizó amablemente en colaboración con Jorge Espinosa-Espinosa (Universitat de Valencia). Las bibliotecas se prepararon utilizando el kit de preparación de bibliotecas de ARNm TruSeq Stranded siguiendo los protocolos de Illumina y se secuenciaron utilizando NextSeq 550 de extremo pareado en el centro de genómica de la Universitat de Valencia. Se obtuvieron unos 20 millones de lecturas de cada muestra. Un control de calidad eliminó cualquier lectura con un valor q inferior a 30 utilizando el programa Trim Galore! (RRID:SCR_011847, versión 0.6.4_dev). Todas las lecturas aceptadas se alinearon con la versión del genoma GRCh38.p12 utilizando el software STAR (versión 2.7.3a). A continuación, los resultados bam se analizaron con el software RSEM (versión v1.3.2) para obtener recuentos de genes. Se utilizó el paquete R edgeR (versión 3.28.1) para realizar una prueba de expresión génica diferencial (DGE). El umbral para una llamada DGE fue un valor p ajustado < 0,05 y un log2FoldChange de 1. La recuperación de la expresión génica, es decir, los genes que se acercaban a un patrón de expresión normal, se realizó para todos los genes relacionados con la enfermedad utilizando esta fórmula: $\%\ Recovery = \frac{mean\ treated\ gene\ counts - mean\ disease\ gene\ counts}{mean\ control\ gene\ counts - mean\ disease\ gene\ counts}$.

Para el análisis STRING, la puntuación de interacción mínima requerida se fijó en una confianza media (0,400). Las fuentes de interacción activas incluyeron textmining, experimentos, bases de datos, coexpresión, vecindad, fusión de genes y coocurrencia. Los nodos desconectados se ocultaron de la red.

## III. Extracción y análisis de proteínas

### III.I. Extracción de células y ratones

Para la extracción de proteínas totales, las células se sonicaron y homogeneizaron en el tampón RIPA de Pierce (Thermo Fisher Scientific) complementado con cócteles de inhibidores de proteasas y fosfatasas (Roche). La cuantificación de la proteína total se realizó con un kit de ensayo de proteínas BCA (Pierce) utilizando albúmina de suero bovino como estándar. Para el tejido de ratón, se utilizó el mismo tampón, pero en lugar de sonicarse, los tubos se agitaron enérgicamente con la máquina TissueLyser durante 5 minutos.

### III.II. Jess Simple Western

Para el ensayo de inmunodetección en las células DM1 se utilizó el sistema Jess Simple Western para cuantificar MBNL1 por quimioluminiscencia utilizando anti-MBNL1 (1:50, 4A8, anti-ratón). A continuación, los capilares se sometieron a un paso Replex y se evaluó de nuevo la proteína total mediante quimioluminiscencia. Para los tejidos de ratón, se utilizó Jess para cuantificar la quimioluminiscencia de la proteína Mbnl1 utilizando anti-MBNL1 (1:10, ab45899, anti-conejo) y se normalizó a la fluorescencia de la proteína total sin el paso Replex.

### III.III. Western Blot

Se mezclaron 20 μg de proteína total con tampón de carga 6x y H2O y se hirvieron durante 5 min y se transfirieron a hielo. Las proteínas se separaron por electroforesis en geles de acrilamida/bisacrilamida SDS-PAGE con el sistema de electroforesis Mini-protean en tampón de electroforesis a 12 mA según el protocolo de electroforesis de poliacrilamida de BioRad. Como marcador molecular se utilizó el Precision Plus Protein Dual Color Standard (Bio-Rad).

Tras la electroforesis, las membranas y el papel de filtro se empaparon en tampón de transferencia y se transfirieron a una membrana de nitrocelulosa (GE Healthcare) utilizando la célula de transferencia semiseca Trans-Blot SD

según el protocolo de protein blotting de BioRad. Después, las membranas se tiñeron con Ponceau para confirmar la transferencia de proteínas y, a continuación, se lavaron con agua del grifo hasta eliminar la tinción. A continuación, las membranas se bloquearon con una solución de bloqueo durante al menos 1 h. Las membranas se incubaron con los anticuerpos primarios disueltos en la solución de bloqueo durante la noche a 4°C. Tras la incubación, las membranas se lavaron con 1x PBST, tres veces durante 5 minutos agitando, y se incubaron con anticuerpos secundarios conjugados con peroxidasa de rábano picante durante 1 h a temperatura ambiente agitando. Tras la incubación, las membranas se lavaron con 1x PBST y se detectó la quimioluminiscencia con el sustrato de máxima sensibilidad SuperSignal West Femto. Posteriormente, las membranas fueron despojadas de los anticuerpos adheridos para ser reutilizadas para la detección de la proteína de control endógena. Una vez eliminados los anticuerpos, se bloquearon las membranas y se volvió a realizar la inmunodetección como se ha descrito anteriormente La quimioluminiscencia se visualizó con ImageQuant LAS 4000 (GE Healthcare).

### III.IV. Inmunofluorescencia

Tras la transfección y cuatro días de diferenciación, las células DM1 se fijaron con PFA al 4%. Los miotubos se permeabilizaron con PBS-T y se bloquearon. A continuación, se incubaron con el anticuerpo primario MBNL1 (1:200, 4A8) a 4°C durante toda la noche. Después de tres lavados con PBS-T, las células se incubaron con un anti-IgG de ratón biotinilado (1:200) y posterior amplificación de Avidina-Biotina (kit Elite ABC). A continuación, se realizaron tres lavados con PBS-T y la incubación con fluoróforo estreptavidina-FITC (1:200). Después de tres lavados con PBS, las células se montaron con medio de montaje Vectashield que contenía 2 μg/mL de DAPI para detectar los núcleos. Se tomaron imágenes de las células DM1 en un microscopio confocal Olympus FluoView FV100 (Beesley, 1993). Las imágenes se tomaron con un aumento de 40x y se cuantificaron utilizando Image J con la siguiente fórmula con un umbral de 10: Intensidad media de

píxeles=valor de gris/área según la guía de ImageJ de la Dra. Christine Labno (Universidad de Chicago) (Schneider et al., 2012).

## IV. Manejo de ratones

La manipulación de los ratones y los procedimientos experimentales se ajustaron a la legislación europea relativa al cuidado y la experimentación con animales de laboratorio (2003/65/CE) y fueron aprobados por la Conselleria de Agricultura de la Generalitat Valenciana ("Respuesta terapéutica a blockmiRs modificados en un modelo de ratón de DM1", número de referencia 2020/VSC/PEA/0203).

### IV.I. Fuerza de agarre

La fuerza de agarre de la extremidad anterior se midió con un medidor de fuerza de agarre según el protocolo de BioSeb. La medición se realizó tres veces consecutivas a intervalos de 30 s. La medición del peso corporal se realizó en paralelo. El porcentaje de fuerza normal se calculó normalizando la fuerza media después del tratamiento a la fuerza antes del tratamiento y dividiendo este valor por el peso corporal de cada ratón.

### IV.II. Bioquímica sanguínea

Se recogió el suero sanguíneo de cada ratón y se analizaron los parámetros bioquímicos en los Laboratorios Montoro Botella (Valencia, España).

### IV.III. Inmunohistoquímica

Se cortaron secciones congeladas de 10 μm de los músculos gastrocnemio y cuádriceps de los ratones con un criostato. A continuación, las secciones se tiñeron con hematoxilina y eosina y se montaron con el medio de montaje Vectashield (Feldman y Wolfe, 2014). Las imágenes se tomaron con un aumento de 100x con un microscopio Leica DM2500. Se cuantificó el porcentaje de fibras que contenían núcleos centrales en una media de 500

fibras en cada ratón. Todas las imágenes fueron etiquetadas al azar durante la cuantificación para facilitar un análisis ciego.

## V. Estadísticas

Todos los análisis estadísticos se realizaron utilizando Prism 8.2.1 (GraphPad) con la asistencia especial del Dr. Juan Carbonell (Bioestadístico, INCLIVA, Valencia, España). Se asumió una distribución normal para comparar las muestras utilizando la prueba t de Student. Se utilizó la corrección de Welch en caso de varianza desigual. Cuando no se pudo asumir una distribución normal, específicamente en el análisis bioquímico de la sangre, se utilizó la prueba no paramétrica de Kruskal Wallis con la corrección de Wilcoxon cuando fue necesario.

# Introduction

# I. Myotonic Dystrophy Type 1

## I.I. Clinical overview

Myotonic Dystrophy is a multi-systemic neuromuscular disorder with congenital, juvenile, adult, or late onset. Originally thought to affect 1 and 8000 people worldwide (Harper, 2009; Suominen *et al.*, 2011), it has been shown through genetic screening that the prevalence is higher at closer to 5-20 people per 100,000 (Johnson *et al.*, 2021). The most severe form of this disease, type 1 (DM1), includes symptoms such as myotonia, muscle weakness, cardiac arrhythmias, cognitive dysfunction, and cataracts (OMIM #160900). DM1 carries a high disease burden. Patients report that muscle weakness, fatigue, and pain regularly cause difficulties in daily life and impact their interpersonal relationships (Landfeldt *et al.*, 2019). Up to 84% of patients have difficulty walking and 3% of patients must use a wheelchair (Bouchard *et al.*, 2015).

The most severe symptoms include respiratory and heart failure, which are the primary causes of death in DM1 patients and contribute to shortened life expectancy (de Die-Smulders *et al.*, 1998; Wahbi and Furling, 2020). Indeed, the probability of survival in a 15 year period was 49±5% for DM1 patients in Belgrade (Mladenovic *et al.*, 2006). More recently, it was shown that DM1 patients are at an increased risk to contracting a severe case of COVID-19 due to impaired respiratory muscle function (Dhont *et al.*, 2020). Other symptoms of DM1 include insulin resistance, obesity, and cardiac dysfunction (Mankodi and Thornton, 2002), which also increase the risk of severe COVID-19 symptoms.

Myotonic Dystrophy Type 2 (DM2) has similar symptoms to DM1 such as myotonia and cataracts but other symptoms are generally less severe (Machuca-Tzili *et al.*, 2005). Indeed, the pattern of muscle weakness is much more variable and there are little reported cardiac and respiratory symptoms.

Disease onset is consistently later into adulthood in DM2 with no known congenital cases.

## I.II. Molecular basis of the disease

The genetic basis of DM1 originates in a repeat expansion of a "CTG" motif in the DM1 Protein Kinase (*DMPK*) gene (Brook *et al.*, 1992). Healthy individuals exhibit between 5-37 CTG repeats in *DMPK*. Patients with DM1 can exhibit thousands of repeats with the amount of repetitions approximately correlating to the severity of the disease (Tsilfidis *et al.*, 1992). Indeed, a significant correlation was found between patients reporting muscle weakness and the number of CTG repeats found on the *DMPK* allele (Bouchard *et al.*, 2015; Landfeldt *et al.*, 2019). A higher number of repeats is also related with the time of disease onset and death (de Die-Smulders *et al.*, 1998; Mladenovic *et al.*, 2006). *DMPK* is transcribed into a mutant mRNA transcript carrying the "CUG" repeats that form hairpin structures. These complexes accumulate as foci in the nucleus and bind with high affinity to proteins from the Muscleblind-like (MBNL) family (Miller *et al.*, 2000) (Figure I1).

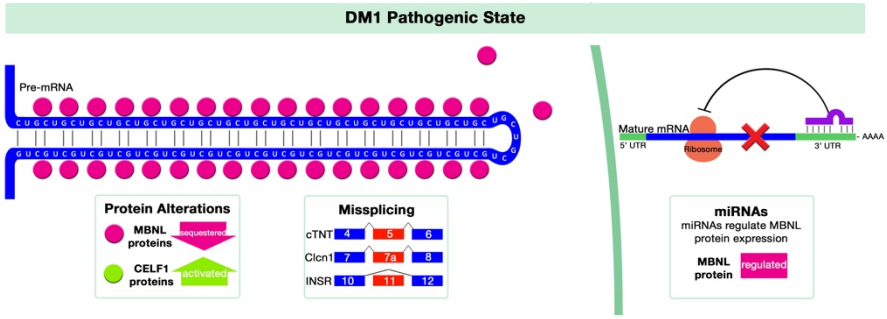


**Figure I1. DM1 pathogenic state.** The DM1 pathogenic state includes the sequestration of MBNL proteins by toxic DMPK transcripts, CELF1 protein activation, and fetal-like splicing patterns. Concurrently, the transcription of *MBNL* into protein is regulated by miRNAS on the 3'UTR. Figure from (Overby *et al.*, 2018).

## I.III. Role of MBNL proteins and downstream effects

MBNL proteins perform developmental post-transcriptional splicing regulation (Kanadia *et al.*, 2003b; Konieczny *et al.*, 2014) and polyadenylation site regulation (Batra *et al.*, 2015). Additionally, the CUG RNA-Binding Protein (CELF) family, which also plays a role in alternative splicing, is activated in DM1 patients (Philips *et al.*, 1998). CELF and MBNL proteins are functionally antagonistic to one another in relation to the regulation of their mRNAs (Wang *et al.*, 2015). The combination of MBNL protein sequestration and CELF protein induction results in numerous mis-splicing events most commonly exhibited by a fetal-like splicing pattern in adult DM1 cells (Fernandez-Costa *et al.*, 2011; Ladd *et al.*, 2001). The Muscleblind family consists of three proteins: MBNL1, MBNL2, and MBNL3, all of which are sequestered by *DMPK* mRNA (Jiang *et al.*, 2004; Miller *et al.*, 2000). The Muscleblind proteins have two zinc finger binding domains in tandem which, in the presence of toxic repeats, have a higher binding affinity to CUG microsatellites than their own pre-mRNA targets (Pascual *et al.*, 2006; Yuan *et al.*, 2007). When functioning properly, MBNL1 and 2 specifically cause a shift from fetal to adult splicing pattern during development (Lin *et al.*, 2006). The activation and repression of mRNAs takes place in the nucleus and the cytoplasm depending on the localization of the target transcript (Wang *et al.*, 2012). MBNL1 is believed to play a larger role in cardiac and skeletal muscle while MBNL2 likely plays a larger role in the brain contributing to DM1 central nervous system (CNS) phenotypes (Charizanis *et al.*, 2012; Kanadia *et al.*, 2003a). MBNL3 plays a role in a developmental capacity contributing to progressive muscle degeneration and age associated pathologies in DM1. It is also related to the impairment of muscle regeneration and repression of myogenesis (Choi *et al.*, 2016; Lee *et al.*, 2010; Lee *et al.*, 2008; Pascual *et al.*, 2006; Poulos *et al.*, 2013).

Critically low levels of MBNL protein function in DM1 is considered the primary contribution to the DM1 phenotype. This is evidenced by a mouse model knockout (KO) for *Mbnl1*, *Mbnl1*$^{\Delta E3/\Delta E3}$, which reproduces myotonia,

alterations in alternative splicing, and cataracts (Kanadia *et al.*, 2003a). Conversely, *Mbnl1* overexpression in DM1 skeletal cells and DM1 model mice increased proliferation and rescued muscle myopathy, respectively (Chamberlain and Ranum, 2012; Song *et al.*, 2020). It has also been described that *Mbnl1*$^{\Delta E2/\Delta E2}$ mutants develop prominent cardiac problems (cardiac hypertrophy, interstitial fibrosis, alterations in transcript splicing), which suggests a key role of Mbnl1 in the initiation of heart problems in DM1 (Dixon *et al.*, 2015). However, KO *Mbnl1* does not recapitulate the full range of DM1 symptoms so it has been hypothesized that Mbnl2 could be compensating for the lack of Mbnl1 function in these mice. *Mbnl2*$^{\Delta E2/\Delta E2}$ KO mice show typical neurological phenotypes of DM1 such as mis-splicing in brain tissues and impaired memory and learning (Charizanis *et al.*, 2012). When making a compound loss of *Mbnl1* and *Mbnl2*, the mice do not survive (Lee *et al.*, 2013). Instead, *Mbnl1*$^{-/-}$; *Mbnl2*$^{+/-}$ mice were generated and developed cardinal aspects of the disease, including reduced half-life, cardiac conduction blockage, severe myotonia, atrophic fibers, and progressive skeletal muscle weakness. According to the compensation hypothesis, the levels of Mbnl2 are high in KO *Mbnl1*$^{-/-}$ and Mbnl2 can regulate exons normally regulated by Mbnl1. Finally, *Mbnl3*$^{\Delta E2}$ KO mice show delays in muscle regeneration and muscle function impairment (Poulos *et al.*, 2013).

In corresponding gain-of-function experiments, overexpression of a Muscleblind isoform in a *Drosophila* DM1 model partially manages to rescue muscle atrophy (Bargiela *et al.*, 2015). Overexpression of CUGBP1, a CELF family protein, also exacerbated muscle degeneration in flies (de Haro *et al.*, 2006). Mbnl1 administration to DM1 model mice by adeno-associates rescues myotonia and alterations in alternative splicing typical of DM1, which supports that Mbnl1 lack of function can be supplemented with more protein (Kanadia *et al.*, 2006).

The alterations in MBNL and CELF activity cause an abnormal fetal splicing pattern of several transcripts, such as muscle chloride channel (*CLCN1*), insulin receptor (*INSR*), cardiac troponin T (*cTNT*), cardiac sodium channel (*SCN5A*), among others (see Table I1) and in turn lead to clinical symptoms. For example, myotonia and insulin resistance are directly related to *CLCN1* (Wheeler *et al.*, 2007) and *INSR* (Savkur *et al.*, 2001) mis-splicing, respectively, while *SCN5A* is related to cardiac phenotypes like conduction defects and arrhythmias (Pang *et al.*, 2018). Other affected tissues include the brain which is specifically affected by the mis-splicing of microtubule associated protein tau (*MAPT*) and is implicated in neurodegenerative phenotypes (Goodwin *et al.*, 2015). Spliceopathy also has an effect on the localization of MBNL proteins in the cell. Concretely, the aberrant inclusion of exon 5 in *MBNL1* transcripts promotes MBNL1 localization in the nucleus (Terenzi and Ladd, 2010). Likewise, the inclusion of *MBNL1* exon 7 promotes MBNL dimerization and subsequent high affinity binding to CUG repeats (Konieczny *et al.*, 2014).

**Table I1. Examples of splicing alterations in DM1 adults.** Adapted from (Lopez-Martinez *et al.*, 2020).

| Gene | Exon exclusion /inclusion | Functional implications | Tissue Expression | | | References |
|---|---|---|---|---|---|---|
| | | | Skeletal Muscle | Brain | Heart | |
| *ATP2A1 (SERCA1)* | 22 exc. | $Ca^{2+}$ reuptake for muscle contraction; muscle dysfunction | ✓ | | | (Kimura *et al.*, 2005; Tang *et al.*, 2012; Vihola *et al.*, 2013) |
| *BIN1* | 11 exc. | T-tubule formation; muscle weakness | ✓ | | | (Fugier *et al.*, 2011) |
| *CLCN1* | 7a inc. | Chloride channel ion conduction; myotonia | ✓ | ✓ | | (Charlet *et al.*, 2002; Lueck *et al.*, 2007; Mankodi *et al.*, 2002; Nakamori *et al.*, 2013; Wheeler *et al.*, 2007) |

| | | | | | | |
|---|---|---|---|---|---|---|
| *CACNA1S* | 29 exc. | Excitation-contraction coupling; muscle weakness | ✓ | | | (Tang *et al.*, 2012) |
| *cTNT (TNNT2)* | 5 inc. | Calcium sensitivity for muscle contraction | | | ✓ | (Dixon *et al.*, 2015; Ho *et al.*, 2004; Philips *et al.*, 1998) |
| *DMD* | 78 exc. | Membrane integrity; muscle fiber maintenance | ✓ | | | (Rau *et al.*, 2015) |
| *INSR* | 11 exc. | Insulin signaling; insulin resistance | ✓ | | | (Savkur *et al.*, 2001) |
| *LDB3 (ZASP)* | 11 inc. | Z disc muscle contraction; abnormal cardiac fibers | | ✓ | ✓ | (Lin *et al.*, 2006; Nakamori *et al.*, 2013) |
| *MAPT (TAU)* | 2 exc. | Microtubule stabilization; neurodegeneration | | ✓ | | (Carpentier *et al.*, 2014; Goodwin *et al.*, 2015) |
| *MBNL1* | 5 inc. | MBNL1 subcellular localization; alternative splicing | ✓ | | | (Konieczny *et al.*, 2014; Lin *et al.*, 2006; Terenzi and Ladd, 2010) |
| | 7 inc. | MBNL1 dimerization, alternative splicing | ✓ | | | (Konieczny *et al.*, 2014; Nakamori *et al.*, 2013) |
| *MBNL2* | 7 inc. | Alternative splicing | | ✓ | | (Konieczny *et al.*, 2014; Lin *et al.*, 2006; Nakamori *et al.*, 2013) |
| *NFIX* | 7 inc. | Transcription factor; myogenesis | ✓ | | | (Konieczny *et al.*, 2014; Yamashita *et al.*, 2012) |
| *SCN5A* | 6a inc. | Cardiac arrhythmia | | | ✓ | (Freyermuth *et al.*, 2016; Pang *et al.*, 2018) |
| *TTN (Titin)* | Mex5 inc. | Cytoskeletal assembly | | | ✓ | (Lin *et al.*, 2006; Yamashita *et al.*, 2012) |

### I.IV. Other pathways contributing to DM1 pathogenesis

As mentioned above, the traditional focus of the DM1 pathogenic phenotype has been rooted in the loss-of-function of the MBNL protein family through toxic repetition sequestration. Also of mention are the many signaling cascades that are implicated in contributing to this phenotype. For example, diminished signaling of protein kinase B (AKT), which regulates CELF1, is correlated to an increase in autophagy and apoptosis in this disease. Mis-regulation of CELF1 by AKT and protein kinase C (PKC) both contribute to the pathogenic pathway in DM1 (see review ((Ozimski *et al.*, 2021)). Similarly, less studied translational regulators such as miRNAs are known to play a role in DM1 pathology, (see review (Lopez Castel *et al.*, 2019)) but will be discussed in more detail later.

## II. Models of DM1

Myotonic Dystrophy can be studied through the use of model organisms. Live models of the disease can produce similar phenotypes to those seen in humans which can be studied for better understanding of disease mechanisms. Also, experimental study of potential therapies through mice, flies, and patient cells has the advantage of producing results contextually similar to human patients and are important for pre-clinical milestones.

### II.I. Patient-derived cells

DM1 is studied *in vitro* through the use of DM1 cell cultures using muscle cells, cardiac cells, and neurons (see review (Matloka *et al.*, 2018)). The most commonly used patient-derived cells are fibroblasts and myoblasts taken from patient biopsies. Primary fibroblasts are derived from the skin and therefore easier to procure but do not differentiate into myotubes. However primary myoblasts from skeletal muscle can activate the myogenic program. To circumvent this, fibroblasts can be virally transduced to express myogenic differentiation protein 1 (*MYOD1*) in order to force their differentiation into

myoblasts. Furthermore, these myoblasts and fibroblasts can avoid cell senescence by immortalization through the expression of human telomerase reverse transcriptase (*hTERT*) and over-expression of cyclin-dependent kinase 4 (*CDK4*) (Arandel *et al.*, 2017). These cells reproduce DM1 phenotypes such as fetal splicing patterns, nuclear foci, and activation of pathogenic pathways like autophagy (Table I2).

Human pluripotent stem cells are also used to develop tissues that are more difficult to harvest such as cardiac and neuronal cells (see review (Kalra *et al.*, 2016)). Models have been developed using human embryonic stem cells (hESCs) as well as human induced pluripotent stem cells (hiPSCs). These cells can be reprogrammed into different cell types in order to model typical tissue-specific characteristics of DM1 such as heart defects and CNS phenotypes (Denis *et al.*, 2013; Gao *et al.*, 2016; Marteyn *et al.*, 2011; Martineau *et al.*, 2018; Ueki *et al.*, 2017; Xia *et al.*, 2013; Yanovsky-Dagan *et al.*, 2015).

### II.II. *Drosophila melanogaster*

*In vitro* studies are limited to a single tissue, whereas *in vivo* models allow for testing in a multi-systemic organism. Therefore, a DM1 model was generated in *Drosophila melanogaster* by introducing 480 CTG repeats in the context of a non-coding RNA (de Haro *et al.*, 2006; Garcia-Lopez *et al.*, 2008). This model reproduces molecular, genetic, and histological aspects of the disease such as nuclear foci, morphological eye phenotype, and muscle degeneration through the *Myosin heavy chain* (*Mhc*)-Gal4 driver. This causes the expansions to express specifically in muscles causing muscle atrophy and therefore a flightless phenotype. This same model was introduced with a heat-shock driver so that the toxic repetitions could be studied in adult form with no developmental contribution (Bargiela *et al.*, 2015).

Another *Drosophila* model was developed by driving 250 CTG repeats in a cardiomyocyte-specific driver *GMH5*-Gal4 in order to model heart-specific

phenotypes including arrhythmias and contractility defects (Chakraborty *et al.*, 2015). Both *Drosophila* models have been important tools for discovering new components in the pathogenesis pathway and potential drugs for DM1 treatment (Chakraborty *et al.*, 2018; Chakraborty *et al.*, 2015; Garcia-Lopez *et al.*, 2011; Llamusi *et al.*, 2014).

### II.III. *Mus musculus*

*Mus musculus* as an animal model has the advantage of being a mammalian species which can more accurately mimic the human system and has also been used for the study of DM1 (see review (Gomes-Pereira *et al.*, 2011)). The first model developed for this disease was the Mbnl KO *Mbnl1*$^{\Delta E3/\Delta E3}$ (Kanadia *et al.*, 2003a; Matynia *et al.*, 2010). This model was able to replicate aberrant splicing patterns, myotonia, and some cardiac and CNS events.

**Table I2. Examples of DM1 models.**

| | Model | Mechanism | Phenotypes: Nuclear foci | Spliceopathy | Cardiac | CNS defects | Muscle | Myotonia | References |
|---|---|---|---|---|---|---|---|---|---|
| Cells | Primary myoblasts | DM1 patient biopsies | ✓ | ✓ | | | | | (Furling *et al.*, 2001) |
| | Immortalized myoblasts | hTERT, CDK4 immortalization | ✓ | ✓ | | | | | (Arandel *et al.*, 2017; Bigot *et al.*, 2009) |
| | Immortalized transdifferentiated fibroblasts | hTERT immortalization; MyoD transdifferentiation | ✓ | ✓ | | | | | (Arandel *et al.*, 2017) |
| | hESCs | Differential reprogramming | ✓ | ✓ | ✓ | ✓ | | | (Denis *et al.*, 2013; Marteyn *et al.*, 2011; Yanovsky-Dagan *et al.*, 2015) |

| | | | | | | | | | |
|---|---|---|---|---|---|---|---|---|---|
| | hiPSCs | Differential reprogramming | ✓ | ✓ | ✓ | ✓ | | | (Gao *et al.*, 2016; Martineau *et al.*, 2018; Ueki *et al.*, 2017; Xia *et al.*, 2013) |
| **Flies** | i(CTG)480 | *Mhc*-Gal4 driver | ✓ | ✓ | | | ✓ | | (Garcia-Lopez *et al.*, 2008) |
| | CUG(250x) | *GMH5*-Gal4 driver | ✓ | | ✓ | | | | (Chakraborty *et al.*, 2015) |
| | i(CTG)480 | *Hs*-Gal4 driver | ✓ | | | | ✓ | | (Bargiela *et al.*, 2015) |
| **Mice** | *Mbnl1*$^{\Delta E3/\Delta E3}$ | Mbnl1 knockout | ✓ | ✓ | ✓ | ✓ | | ✓ | (Kanadia *et al.*, 2003a; Matynia *et al.*, 2010) |
| | HSA$^{LR}$ | Long repeats in *HSA* | ✓ | ✓ | | | ✓ | ✓ | (Mankodi *et al.*, 2000) |
| | DM500/ DMSXL | Long repeats in *DMPK* | ✓ | ✓ | ✓ | ✓ | ✓ | ✓ | (Gomes-Pereira *et al.*, 2007; Seznec *et al.*, 2001) |

But without the presence of repetitions, the model was limited. HSA$^{LR}$ transgenic mice have been engineered to express CUG long repeats (LR) in the human skeletal actin (*HSA*) gene. Expression of this toxic CUG expansion causes mice to exhibit molecular abnormalities similar to those of patients with DM1, such as spliceopathy and accumulation of RNA foci, as well as clinical manifestations like myotonia (Mankodi *et al.*, 2000). However, HSA$^{LR}$ mice are restricted by exclusive expression of repeats in skeletal musculature and their inability to reproduce the typical muscle degeneration of the pathology.

The DM500 mouse model systemically expresses a 45 kb fragment of DM1 patient DNA that includes 500 CTG repeats and the entire *DMPK* gene (Seznec *et al.*, 2001). They exhibit phenotypic characteristics such as histological muscle abnormalities, myotonia, and the presence of nuclear foci. Also of mention are DMSXL mice, which are derived from DM500 mice differing only in having over a 1000 repeats instead of 500 (Gomes-Pereira *et al.*, 2007). DM500 and DMSXL mice have the advantage of being able to

reproduce cardiac and CNS phenotypes that are not seen in $HSA^{LR}$ mice. However, they are limited by difficult breeding and repeat instability.

## III. RNA therapeutics

Correcting mutations at the DNA or RNA level can have a potentially higher therapeutic impact than targeting downstream effects at the splicing or protein level. Technical innovations have allowed the possibility of modulating specific genetic code through techniques like RNA interference (RNAi), antisense oligonucleotides (AONs), clustered regularly interspaced short palindromic repeats (CRISPR), and catalytic RNAs (Burnett and Rossi, 2012; Chery, 2016; Roberts *et al.*, 2020; Zhou and Rossi, 2017).

RNAi uses the endogenous chemistries of short interfering RNAs (siRNAs) and micro RNAs (miRNAs) to regulate gene expression (see review (Kubowicz *et al.*, 2013)). Protein levels are regulated by siRNAs and miRNAs *in vivo* through specific base-pair binding to target RNAs. The RNase III enzyme Dicer cuts double stranded RNA (dsRNA) or short hairpin RNA (shRNA) into short interfering RNAs with an average length of 21 bp. Complexes of Argonaute-type endoribonuclease (Ago) and RISC proteins bind and unwind the double stranded siRNA so that a single strand can be used to guide the protein complex. Once the siRNA guide strand recognizes and specifically binds to RNA of the complementary sequence, the transcript can be signaled for repression or degradation. A similar process is done with miRNAs, which are converted to mature miRNAs by Dicer and subsequently linked to an Argonaute complex to target complementary RNA and regulate expression. From a therapeutic perspective, these RNAs can be chemically synthesized to base-pair complement disease-causing genes in order to repress expression and potentially alleviate symptoms.

RNAi has been applied to a wide range of medicine with some molecules currently undergoing clinical trials and on the market (see reviews (Chery,

2016; Hu *et al.*, 2020; Kubowicz *et al.*, 2013; Roberts *et al.*, 2020)). However, RNAi as gene therapy must overcome the challenges of effective delivery to the cell as siRNAs are typically degraded by RNases before ever reaching the target transcripts (see review (Garber, 2017)). Vector delivery has improved sustainability of the drug. For example, RNAi-mediated knockdown of the *FRG1* gene improved myopathy in transgenic mice modeling muscular defects related to facioscapulohumeral muscular dystrophy (FSHD). *FRG1* knockdown was achieved through the use of miRNAs delivered using the adeno-associated viral (AAV) vector system (Wallace *et al.*, 2011).

Antisense oligonucleotides enter the cell through endocytosis and bind to mRNA in the cytoplasm (see review (Geary *et al.*, 2015)). They are single-stranded made up of typically 15 – 25 DNA or RNA nucleotides. Like RNAi, AONs block gene expression through complementary binding, but through different mechanisms such as steric hindrance, splicing blocking, 5′ cap blocking, and activation of RNase-H (see reviews (Chan *et al.*, 2006; Chery, 2016)). Specifically, steric hindrance blocks the binding of ribosomal subunits to mRNA by binding the AON to the start codons of the transcript. The mechanism by which AONs can direct degradation is recruitment of RNase-H endonucleases to bind and degrade the target RNA determined by the plethora of chemical modifications and structure of the antisense compounds (see review ((Roberts *et al.*, 2020)).

### III.I. First generation AONs

Like siRNAs, AONs have challenges with delivery and off-target effects (see reviews (Dowdy, 2017; Geary *et al.*, 2015)), however improvements have been made for cellular uptake by modifying their chemical structure (see review (Khvorova and Watts, 2017)). The first generation of modifications to combat degradation by nucleases is a phosphorothioate (PS) backbone which substitutes one non-bound phosphoryl oxygen for a sulfur (Figure I2). PS modifications on oligonucleotides increase stability and cellular uptake while

also being compatible with the RNase-H pathway to degradation. Methylphosphonate (MP) backbones are highly similar but have a methyl group instead of a sulfur attached to the phosphate group (Reynolds *et al.*, 1996).

### III.II. Second generation AONs

The PS and MP backbones alone are not enough to combat nuclease degradation therefore a second generation of sugar modifications was generated including 2′-*O*-methyl (2′-OMe), 2′-*O*-methoxyethyl (2′-MOE), and 2′-fluoro (2′-F). These have been used to improve binding affinity and stability and elicits less of an immune response. 2′-OMe modifications have even shown gymnotic cell uptake in DM1 myoblasts (Gonzalez-Barriga *et al.*, 2017). However, these sugar modifications do not support the recruitment of RNase-H pathway. To circumvent this, a gap can be added between the modified nucleotides with natural nucleotides to allow room for the RNase-H protein to bind. AONs of this nature are termed "gapmers".

### III.III. Third generation AONs

The third generation of AONs are characterized by even more stable chemical conformations that allow for even greater cell acceptance. For example, 2′-Deoxy-fluoroarabinonucleotides (FANA) also support RNase-H activation through gapmer design. They can also be interspaced with RNA/DNA nucleotides to improve affinity and stability and still be recognized by RNase-H (Souleimanian *et al.*, 2012). They also have the attractive feature of being able to be delivered to cells gymnotically, that is, without the use of transfection or delivery agents. Locked 2′- Nucleic Acids (LNAs), 2′, 4′-$BNA^{NC}$[NMe] ($BNA^{NC}$), and constrained ethyl (cEt) are other forms of 3rd generations AONs but without RNase-H compatibility. However, the 2′-oxygen 4′-carbon link in the ribose substantially increases affinity and decreases nuclease degradation in delivery by making the oligo less flexible.

Finally, there are AONs carrying chemical changes that exhibit an overall neutral charge in order to increase stability. For example, phosphoroamidate morpholino oligomers (PMO) are made up of morpholino rings and phosphoroamidate linkages and Peptide Nucleic Acids (PNAs) have a polyamide backbone. By substituting these for phosphodiester backbones, these AONs are highly stable with high binding affinity and are hardly recognized by nucleases due to their conformational differences from natural nucleic acids. This has significantly increased their delivery efficiency. Indeed, some of these AONs have already been approved for clinical use by the FDA (Roberts *et al.*, 2020), for instance, the PMO Eteplirsen, marketed as Exondys 51, treats Duchenne Muscular Dystrophy (McDonald *et al.*, 2021), and Nusinersen, marketed as Spinraza, for the treatment of Spinal Muscular Atrophy (Neil and Bisaccia, 2019).

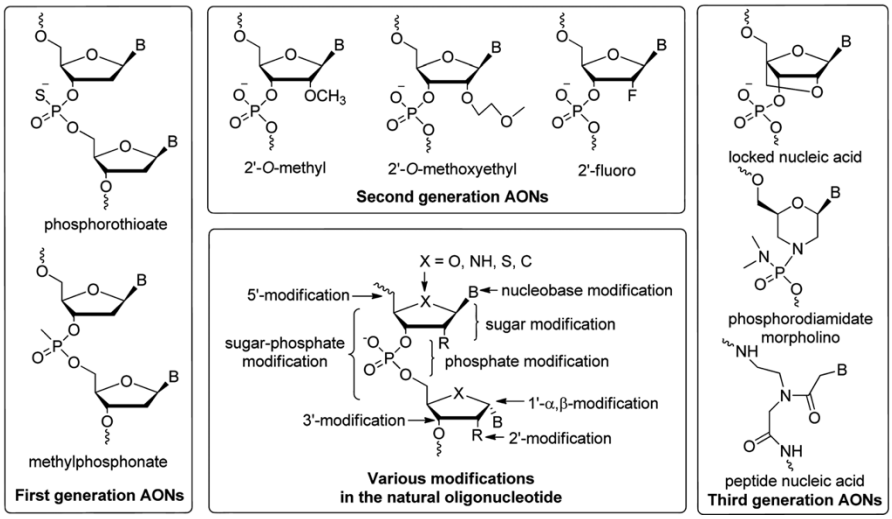


**Figure I2. Antisense oligonucleotide modifications.** AONs have been progressively improved over time starting from first generation to third generation modifications. All modifications aim to stabilize oligos and increase their uptake and affinity for targets. Figure from (Sharma *et al.*, 2014).

## IV. Antisense therapy in DM1

Currently there is no FDA approved antisense treatment for DM1. The FDA success of AONs in various neuromuscular and microsatellite expansion

diseases, as mentioned above, has led researchers to explore the possibilities of antisense treatment in DM1 (see review (Overby *et al.*, 2018)). RNA medicine shows particular promise in DM1 therapeutics through the targeting of toxic CUG expansions (Figure I3). However, one of the major difficulties in antisense technology and RNAi is effective delivery. In fact, a study investigating the membrane integrity of DM1 patient muscle found that the membrane is no more permeable than healthy patients (Gonzalez-Barriga *et al.*, 2015). Therefore, DM1 therapies must overcome the barrier of a fully functional membrane in regard to drug delivery. Consequently, a diverse array of potential therapeutic molecules has been developed in response to the mutation found in this disease.

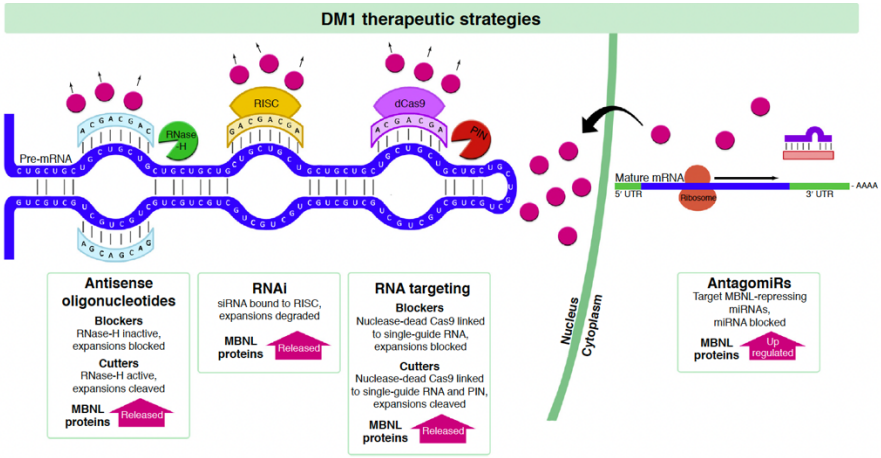


**Figure I3. DM1 therapeutic mechanisms.** Therapeutic strategies for DM1 targeting CUG-expanded transcripts include antisense oligonucleotides, RNAi, and RNA-targeting nuclease dead Cas9. The goal of these methods is to restore MBNL protein function. ASOs either work through the RNase-H pathway or by other routes such as steric hindrance to release MBNL from sequestration. Likewise, dCas9 can function by PIN-activated cleavage of mRNA or by steric blocking to release MBNL. Furthermore, recent studies have shown that blocking miRNAs that regulate MBNL transcripts can increase MBNL protein expression. Figure from (Overby *et al.*, 2018).

## IV.I. RNAi

Small RNAs have been engineered to target the CUG expanded RNA transcripts in DM1 cells for therapeutic benefit. Using the lentiviral vector

pHIV7, shRNAs complementary to *DMPK* mRNA were cloned and transduced into human DM1 myoblasts. The shRNAs, labeled DM10 and DM130, down-regulated wild-type *DMPK* mRNA as well as mutant *DMPK* mRNA, even though the mutant RNA does not localize outside the nucleus. Additionally, a synthetic siRNA, termed ssiDM10, also effectively reduced levels of *DMPK* RNA transcripts in both wild-type and DM1 mutants. The siRNA was delivered through N-methylpurine DNA glycosylase enzyme (MPG) peptide transfection, which assists in nuclear transport of the siRNA. These results suggest that RNAi machinery may not exist exclusively in the cytoplasm but may as well appear in the nuclear region (Langlois *et al.*, 2005).

A subsequent group aimed to knockdown CUG-expanded RNA by siRNAs in $HSA^{LR}$ mice. To accomplish this, they designed their siRNAs to target the CUG repeats directly and delivered them through transfection by electroporation. These siRNAs specific to the repeats were successful in reducing CUG repeat RNA as well as nuclear foci. Several splicing alterations were improved as well, such as *Atp2a1* and *Clcn1* (Sobczak *et al.*, 2013). Systemic delivery of RNAi machinery has also had a therapeutic effect in $HSA^{LR}$ mice. Recombinant AAV vector RNAi expression cassettes were delivered to mice through intravenous tail vein injection to express shRNAs targeting the 3′ untranslated region (UTR) of the *HSA* mRNA. The molecule rAAV6-HSA10 was particularly successful in reducing the level of *HSA* mRNA, myotonia, known up-regulated pathogenic genes *Atp1 β 4* and *Mustn1,* and nuclear foci. It also corrected splicing for *Atp2a1*, *Clcn1*, *m-Ttn* transcripts (Bisset *et al.*, 2015).

### IV.II. Targeting CUG expansions by antisense blockers

Antisense therapy through the use of RNase inactive oligo designs have also shown success in DM1 treatment. MBNL1 loss-of-function was restored in DM1 mice models using a 25 base-pair PMO. This morpholino, termed CAG25, functions by RNA blocking and is incompatible with RNase-H

degradation. In this way, non-toxic endogenous repeat transcripts are protected from being destroyed. CAG25 treatment in $HSA^{LR}$ mice by intramuscular injection released Mbnl1 from sequestration, which in turn restored splicing abnormalities for at least 14 weeks after injection as well as reduced myotonia. Curiously, delivery of this oligonucleotide caused around a 50% reduction in toxic mRNA. However, the PMO did not reduce any endogenous "CUG" repeats (Wheeler *et al.*, 2009).

In an experiment from the same year, $HSA^{LR}$ mice and DM500 mice cells were used to test the effect of a 2-*O*-methyl-phosphorothioate oligonucleotide. AONs with 2'-OMe modifications are predicted to be incompatible with nuclease degradation. This oligonucleotide also caused a reduction in toxic mRNA in DM500 mouse model myotubes and myoblasts. This effect was observed for as long as 10 days after transfection and was preferential only to the toxic repeat RNAs. The AON also reduced the appearance of nuclear foci in DM500 muscle cells as well as rescued the abnormal fetal splicing pattern in $HSA^{LR}$ mice (Mulders *et al.*, 2009). However, myotonia was not rescued as it was in the Wheeler *et al.*, 2009 study.

An experiment by the same group investigated the efficacy of a variety of AONs with regards to CUG repeat transcript knockdown in DM1 cell models. It was found that AONs with 2'-OMe modifications can more efficiently knockdown CUG repeat transcripts in DM500 myotubes if they contain more than four CAG triplets. Similar to their previous results, 2'-OMe and morpholino AONs caused a reduction in CUG repeat transcripts when they should only block, not degrade the transcript (Gonzalez-Barriga *et al.*, 2013). Taken together, this points to the possibility that the transcripts undergo degradation by another pathway once released from binding with MBNL proteins after AON treatment. In fact, a study using RNase active and inactive AONs showed that both were equally capable of reducing CUG-expanded RNA. These AONs were LNA modified with one group being

gapmers (RNase active) and one group termed "mixmers" (RNase inactive) (Nakamori *et al.*, 2011).

Another RNA-mediated blocker engineered by Francois *et al.*, is the U7-small nuclear RNA transcript containing an antisense sequence complementary to expanded-CUG mRNA. After transduction into DM1 human myoblasts, the toxic *DMPK* transcripts were selectively decreased by 71-82%. Nuclear foci were significantly reduced, and adult splicing patterns were restored. The mechanism for this molecule is not completely understood as it is not designed to activate RNase-H nor did it show evidence of following the RNAi pathway (Francois *et al.*, 2011).

A study using LNA oligomers showed that alternative splicing in DM1 patient myoblasts and $HSA^{LR}$ mice models can be corrected without activating RNase-H, keeping CUG transcripts intact. The oligomers contained *all*-LNA units instead of spaced out LNA units like mixmers or gapmers. The AONs effectively and stably bound to CUG repeat transcripts preventing the sequestration of MBNL proteins and the appearance of nuclear foci and mis-splicing without a strong reduction in expanded CUG transcripts (Wojtkowiak-Szlachcic *et al.*, 2015).

In order to study the effects of systemic delivery, a peptide-linked morpholino (P-PMO) was administered to $HSA^{LR}$ mice targeting expanded CUG transcripts. The cationic peptide links were utilized to facilitate delivery to all tissues, not just muscle. The treatment was well tolerated by the mice and was also able to rescue abnormal splicing patterns, normalize Mbnl1 distribution, and reduce myotonia (Leger *et al.*, 2013). Likewise, an arginine-rich peptide called Pip6a was conjugated to a PMO against the toxic repeats (Klein *et al.*, 2019). Pip6a-PMO was able to rescue *Clcn1*, *Mbnl1*, and *Atp2a1* mis-splicing in both gastrocnemius and quadriceps muscles of $HSA^{LR}$ mice.

## IV.III. Targeting CUG expansions by antisense cutters

Other therapeutic strategies include the direct employment of the RNase-H degradation pathway. Considering that RNase-H degradation is predominantly carried out in the nucleus, Wheeler *et al.*, 2012 used the nuclear retention of expanded CUG transcripts to their advantage. They used oligonucleotides stabilized by MOE modifications and a 10-nucleotide gap for RNase activation. Interestingly, the gapmers were designed to target the 3'UTR region or the coding region of the human *HSA* gene in the $HSA^{LR}$ mice instead of the repeats directly. After injection of the MOE gapmers, alternative splicing and Mbnl sequestration were rescued and myotonia was reduced. Indeed, the use of RNase-H activated antisense technology may provide a "therapeutic advantage" in releasing nuclear sequestered MBNL proteins (Wheeler *et al.*, 2012).

After the promising results shown by Wheeler *et al.*, 2012, the same group designed additional gapmers targeting the 3'UTR region of the mutant *DMPK* mRNA instead of the CUG repeats (Pandey *et al.*, 2015). In this study, the gapmer, termed ISIS 486178, contained cEt oligonucleotides. The cEt successfully reduced toxic repeat RNA and nuclear foci in human patient DM1 myoblasts. ISIS 486178 was also tested *in vivo* in DMSXL mice. The cEt reduced expanded CUG RNA in heart and skeletal tissues and were well tolerated by the mice. The safety of this AON was also tested in Cynomolgus monkeys and wild-type mice for 13 weeks and 6 weeks respectively. Interestingly, both species tolerated the drug well despite the knockdown of endogenous *DMPK* mRNA. More recently, the same gapmer was shown to also improve body weight and muscle strength in DMSXL mice after 9 weeks of treatment (Jauvin *et al.*, 2017). Jauvin *et al.*, 2017 also tested a previously identified MOE gapmer, termed ISIS 445569, targeting the 3'UTR of the *DMPK* gene (Wheeler *et al.*, 2012). As in the earlier study, ISIS 445569 was effectively able to reduce (CUG)exp mRNA as well as nuclear foci (Jauvin *et al.*, 2017).

To test the efficacy of CUG-repeat knock-down between LNA and $BNA^{NC}$ gapmers, which are structurally similar in their ribose bridge modifications, a study was performed using CUG-repeat transfected COSM6 cells. The $BNA^{NC}$ gapmers were divided between those that target the CUG repeats directly ($BNA^{NC}$-CAG), or those that target the *DMPK* transcript upstream of the repetitions ($BNA^{NC}$-DMPK). Likewise, there was an LNA-CAG gapmer and an LNA-DMPK gapmer. Both LNA and $BNA^{NC}$ gapmers successfully reduced toxic *DMPK* transcripts, however the $BNA^{NC}$-DMPK gapmer was noticeably more effective and more selective than $BNA^{NC}$-CAG in knocking down expanded CUG-repeats. $BNA^{NC}$ gapmers also reduced nuclear foci and rescued several mis-splicing events. All the gapmers except LNA-CAG showed no induction of caspase activity (Manning *et al.*, 2017).

## IV.IV. RNA-targeting Cas9

CRISPR technology has also been used to target toxic *DMPK* mRNA in DM1 cells. CRISPR Cas9 was used to permanently cut CUG repeats in DM500 mice myoblasts, DM1 patient myoblasts, and control patient myoblasts (van Agtmaal *et al.*, 2017). This treatment was able to improve cytoplasmic localization of *DMPK* transcripts and reduction of ribonuclear MBNL1 foci in both human and mouse DM1 myoblasts without disturbing the expression of neighboring gene *SIX5* or impairing their ability to differentiate into myotubes.

Through the use of a modified CRISPR nuclease-dead Cas9 (dCas9) protein, mutant CUG-repeat RNA was targeted and degraded in COSM6 cells expressing 105 CTG repeats (Batra *et al.*, 2017) as well as $HSA^{LR}$ mice (Batra *et al.*, 2021). In both models, RNA-targeting CRISPR-Cas9 (rCas9) was capable of knocking down toxic repeat RNA and rescue of abnormal splicing patterns as well as reduction of ribonuclear foci and myotonia in mice. CRISPR-Cas9 was also capable of foci elimination and transcriptome-wide

splicing correction in DM1 iPSC-derived cardiomyocytes (Dastidar *et al.*, 2021).

### IV.V.Targeting downstream effects

The loss-of-function of MBNL proteins and activation of CELF1 has been associated with an array of splicing errors evident in DM1 affected patients in pre-mRNAs including *CLCN1*, *INSR*, *cTNT*, *BIN1*, *SCN5A* (Freyermuth *et al.*, 2016; Fugier *et al.*, 2011; Ho *et al.*, 2004; Ladd *et al.*, 2001; Mankodi *et al.*, 2002). In particular, MBNL and CELF1 have been observed to act antagonistically to one another. CELF1 proteins induce skipping of exon 11 in *INSR* (Savkur *et al.*, 2001) but MBNL proteins promote its inclusion (Ho *et al.*, 2004). Variations in expression of CELF1 and MBNL proteins cause an imbalance of splicing regulation leading to aberrant isoforms of several mRNAs and, consequently, clinical symptoms.

Antisense technology in DM1 cells has also been able to correct downstream effects such as mis-splicing. For example, a morpholino AON was used to target exon 7a in *Clcn1* pre-mRNA in $HSA^{LR}$ mice which is normally excluded in healthy cells (Wheeler *et al.*, 2007). By using the morpholino to restore the reading frame, *Clcn1* transcripts were corrected and myotonia reduced in $HSA^{LR}$ mice tibialis anterior muscle. A subsequent study used a similar morpholino to target exon 7a in *Clcn1* RNA however using a different delivery technique (Koebis *et al.*, 2013). The bubble liposome-ultrasound delivery method was used to administer the PMO more efficiently and less invasively. Consequently, exon 7a was correctly excluded and myotonia was alleviated in $HSA^{LR}$ mice.

### IV.VI. Upregulation of MBNLs by miRNA blockers

Therapeutic Gene Modulation (TGM) aims to up or down-regulate endogenous gene expression in order to alleviate a determined pathological state. Altering the expression of the Muscleblind-family of genes is especially

important in this disease, given that their loss-of-function is the principal cause of alterations seen in DM1 (Kanadia *et al.*, 2006; Lee *et al.*, 2013). TGM has already been applied through up-regulation of MBNL proteins and has

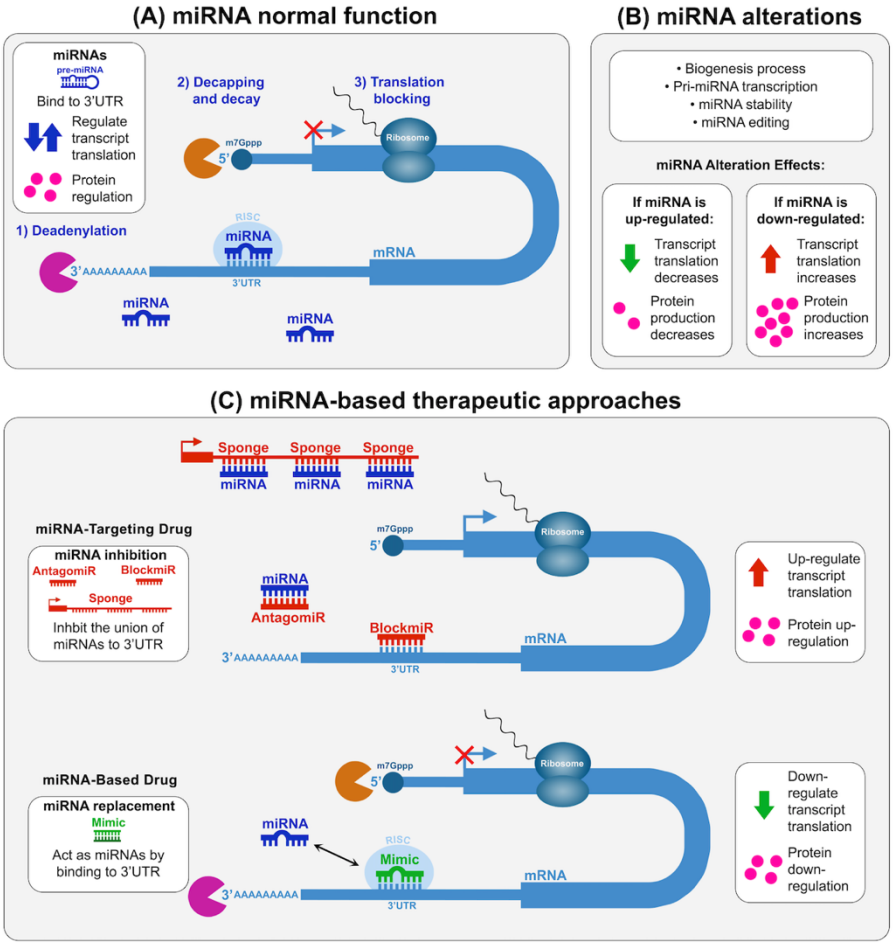


**Figure I4. Micro RNA (miRNA) mechanisms for mRNA translation, regulation, and therapeutic intervention. (A)** The interaction between miRNA and mRNA targets trigger different mechanisms for transcript regulation through the RISC complex in order to achieve normal cellular protein levels (pink circles) **(B)** Alterations in miRNA biogenesis, editing, or in its biological stability, among others, may cause pathological upregulation or downregulation leading to decreased or increased target transcript translation regulation and final protein levels, respectively. **(C)** When a miRNA is upregulated, inhibition can be conducted by using antimiRs, blockmiRs, or sponges. When a miRNA is downregulated, mimics can be used to restore its function. Figure from (Lopez Castel *et al.*, 2019).

alleviated certain DM1 symptoms. For example, overexpression of Mbnl1 in $HSA^{LR}$ mice skeletal muscle rescues myotonia and splicing abnormalities (Kanadia *et al.*, 2006) and is well tolerated over long-term administration (Chamberlain and Ranum, 2012). Overexpression of *mblC* in DM1 model flies ameliorates muscle wasting as well as decreased expression of autophagy related genes (Bargiela *et al.*, 2015). Cardiac dysfunctions such as arrhythmia and contractility have been rescued in a DM1 heart model in flies after increasing *mblC* expression (Chakraborty *et al.*, 2018). It is evident through these studies that the restoration of MBNL function is key to alleviating the most common and detrimental pathological characteristics of the disease.

A less explored method of rescuing MBNL function in DM1 is through the targeting of miRNAs that regulate the expression of MBNL1 and 2 (Figure I4). MiRNA roles have been linked to key cellular pathways such as stem-cell self-renewal, cellular development, differentiation, proliferation, and apoptosis, etc. (Wienholds and Plasterk, 2005) with some ubiquitously expressed but others displaying tissue-specific expression. MiRNAs have been found to be mis-regulated in numerous diseases, including muscle and neurodegenerative ones (Li and Kowdley, 2012) as well as in Myotonic Dystrophy (Figure I5) (Lopez Castel *et al.*, 2019).

This approach was first tested in flies (Cerro-Herreros *et al.*, 2016) where endogenous expression of the single fly MBNL homolog, *muscleblind*, was found to be under direct control of the miRNAs miR-277 and miR-304. Sequestration of each miRNA by sponge constructs boosted *muscleblind* protein expression in both wildtype and DM1 model flies expressing CUG trinucleotide repeats throughout the musculature. De-repression of *muscleblind* was sufficient to rescue significant splicing alterations in DM1 fly models as well as improve pathological phenotypes, including muscle function and lifespan. Subsequently, specific miRNAs have been identified as regulators of MBNL proteins, for example, miR-30a-5p and miR-30e-5p (Zhang *et al.*, 2016), and miR-10b (Teplyuk *et al.*, 2016), which could serve as

other future candidates for miRNA modulation in order to increase the expression of endogenous MBNL.

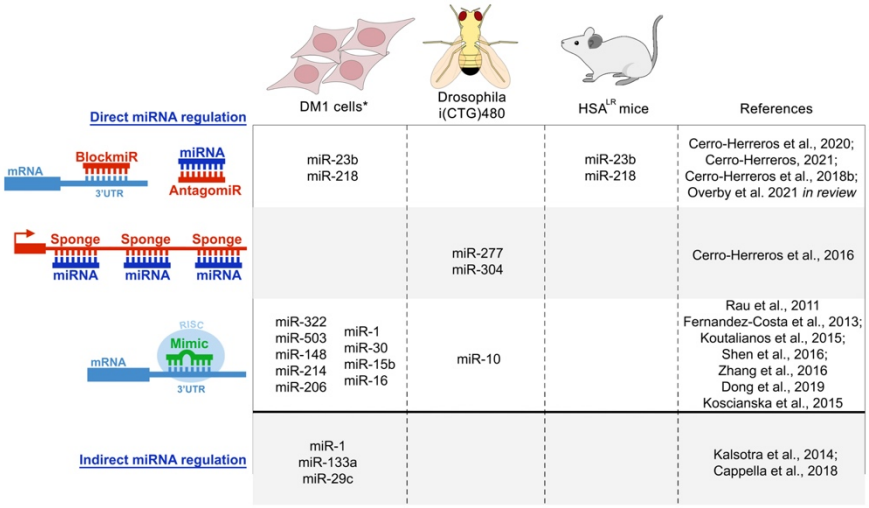


**Figure I5. Therapeutic proof-of-concept approaches for DM based on the modulation of miRNA levels.** Currently three different model systems have been used for evaluation: cells* (human and murine lines), flies, and mice. *In vivo* miRNA interventions were performed in disease backgrounds to directly assess the therapeutic potential in DM. *Cell approaches used DM and non-disease lines indistinctly for therapeutic evaluation and for conceptual modulation of DM-related targets, respectively. Figure adapted from (Lopez Castel *et al.*, 2019).

Recently, miR-23b and miR-218 have been identified as inhibitors of translation of *MBNL1* and 2 (Cerro-Herreros *et al.*, 2018). The experiment showed how antagomiRs, which are miRNA-targeting AONs containing a cholesterol moiety, were capable of significantly silencing their target miRNAs in DM1 patient myoblasts as well as HSA$^{LR}$ mice. Without cholesterol, they are simply termed antimiRs. The administration of these antagomiRs reached the muscle tissue of the mice and subsequently increased Mbnl proteins (Mbnl1 and 2 specifically) while improving hallmark phenotypes of the disease including splicing alterations, histopathology, and myotonia. The antagomiRs have continued to show therapeutic promise in DM1 mice after both antagomiR-23b and antagomiR-

218 were able to provoke a dose response with long-lasting effects (Cerro-Herreros *et al.*, 2020; Cerro-Herreros, 2021).

An attractive alternative to direct miRNA inhibition is the blockmiR strategy. BlockmiRs are similar to antimiRs in that they both use antisense technology to reduce miRNA regulation. However, instead of binding to miRNAs, they bind specifically to the 3'UTR binding site on the target transcript. This blocks interaction with miRNAs thereby allowing translation to occur. In this way, blockmiRs are site-specific and not miRNA-specific. BlockmiRs have already shown success in the study of angiogenesis. Concretely, miR-27a was identified as a regulator of VE-Cadherin. MiR-27a upregulation blocks capillary tube formation and angiogenesis. Therefore, a blockmiR was designed against the binding site of miR-27a on the VE-cadherin 3'UTR (Young *et al.*, 2013). When injected into mice after ischemic injury, the blockmiR blocked the regulation of miR-27a which promoted the formation of new blood vessels and reduced vascular leak. After the proof of concept, the 2'-*O*-methyl based blockmiR termed CD5-2 was tested in the context of diabetes-related retinal dysfunction which breaks down the blood-retinal-barrier and leads to retinal damage and inflammation and, in some in cases, even blindness (Ting *et al.*, 2019). CD5-2 again reduced vascular leakage and inflammation in diabetic mouse models.

Further investigation is needed for the better understanding of miRNA roles in DM1. Additionally, proof-of-concept experiments testing different AON chemistries and strategies will help with this pursuit. New therapeutic strategies are key for revealing the full mechanisms of DM1 and the roles of MBNL proteins and miRNAs thereby bringing patients one step closer to life-changing pharmaceuticals.

# Objectives

## Objectives

The primary focus of current therapeutic methods in DM1 is to restore the function of Muscleblind-like proteins, be that through repeat-expansion targeting or MBNL protein up-regulation, as discussed in detail in the introduction. Moreover, our lab has recently shown that targeting miRNAs regulating the translation of *MBNL* transcripts into proteins can also rescue MBNL function as well as the downstream effects. Specifically, the targeting of miRNA-23b and miRNA-218 by antagomiRs was capable of increasing MBNL protein expression in DM1 myoblasts and alleviating myotonia, histopathology, and spliceopathy in DM1 $HSA^{LR}$ mouse models (Cerro-Herreros *et al.*, 2020; Cerro-Herreros, 2021; Cerro-Herreros *et al.*, 2018). The miRNAs were targeted by antagonistic antisense oligonucleotides termed "antagomiRs" containing a cholesterol moiety to facilitate cell entry.

The use of AONs has grown exponentially in recent years for the treatment of various rare diseases including some with FDA approval (Rinaldi and Wood, 2018; Roberts *et al.*, 2020). The development of 3rd generation modifications has greatly increased the efficacy and deliverability of these oligos. The already successful antagomiR approach could be refined by targeted improvement of the oligo chemistry to increase specificity and potency. Additionally, the newly discovered role of miR-23b and miR-218 opens the door to exploring different tactics in modulating their regulation. Proposed here is the use of newly designed AONs targeting miR-23b and miR-218 activity in order to regulate MBNL1 and MBNL2 through the following objectives:

1. Exploration of miRNA blocking through FANA-antimiR AONs *in vitro*.

2. Exploration of miRNA binding site blocking through blockmiR strategy *in vitro* and *in vivo* with the use of LNA chemical modifications.

3. Improve the chemistry of the blockmiR strategy through the use of cell penetrating peptide technology *in vitro* and *in vivo*.

# Results

## I. Objective 1: FANA antimiR strategy

AntagomiRs targeting miR-23b and miR-218 have already been successfully introduced into DM1 cells and mice causing a therapeutic increase of MBNL1 protein (Cerro-Herreros *et al.*, 2020; Cerro-Herreros, 2021; Cerro-Herreros *et al.*, 2018). The AONs used in these experiments are composed of 2'-*O*-methyl modified nucleic acids with a cholesterol moiety to enhance cell uptake. The 2'-*O*-methyl, 2'-*O*-methoxyethyl, and 2'-fluoro modifications are part of the second generation of 2'-carbon (C-2) modified AONs (Sharma *et al.*, 2014). Recently, 2'-Deoxy-fluoroarabinonucleotides (FANA) AONs have become an attractive third generation improvement of the second generation 2'-fluoro modifications. In these oligos, the fluorine is added to the C-2 on the sugar in the arabino conformation instead of in the C-2 ribo conformation. This modification allows increased stability and "gymnotic" delivery to cells without the use of transfection reagents (Souleimanian *et al.*, 2012). The FANA technology also exhibits enhanced resistance to nucleases and much lower cell toxicity (Ferrari *et al.*, 2006).

The use of FANA modified oligos have shown successful silencing in various disease contexts. For example, the CD39 enzyme is downregulated in Crohn's disease and is implicated in immunosuppression. Blocking of endogenous CD39 regulators using FANA based antisense oligonucleotides allows this enzyme to return to healthy levels in cells and in mice and ameliorates some disease symptoms (Harshe *et al.*, 2020). FANA AONs have also already been successfully delivered gymnotically in mouse fibroblasts (Della Valle *et al.*, 2020).

To test the efficacy of gymnotic delivery, antimiRs were designed with the same sequences as the previously tested antagomiRs, but with FANA modifications and no cholesterol moiety. The FANA modifications were isolated to the extremities of the oligos to leave room for RNase-H binding thereby allowing target degradation. Just like antagomiRs, antimiRs

complementary bind to miR-23b and miR-218 so that MBNL can be up-regulated through protein synthesis activation. MiR-218 has three confirmed binding sites on *MBNL2* 3'UTR while miR-23b has one binding site on both *MBNL1* and *MBNL2* 3'UTRs (Cerro-Herreros *et al.*, 2018). Recently, another site on the on the *MBNL1* 3'UTR was also confirmed for miR-218 (Cerro-Herreros *et al.*, 2021). The FANA antimiRs were administered at five different concentrations per manufacturer's instructions in order to find the optimal working concentration.

## I.I. FANA antimiRs show effective miRNA knockdown by gymnotic delivery

A FANA antimiR was designed for complementary binding to miR-23b or miR-218 (Figure R1A). A third antimiR was also generated with a scrambled sequence (Scramble) as a control for the FANA chemistry. First, cell growth inhibition was assessed after treatment with each AON in immortalized patient-derived DM1 fibroblasts transdifferentiated into myotubes (DM1 cells) (Arandel *et al.*, 2017) gymnotically delivered (Figure R1B). Cells were treated at five different concentrations: 0.5 $\mu$M, 1 $\mu$M, 2.5 $\mu$M, 5 $\mu$M, and 10 $\mu$M, and a toxic concentration level at 50% (TC50) was calculated for each treatment. Compound miR-218-1 showed the lowest toxicity while the Scramble and miR-23b-1 showed a TC50 near 8 $\mu$M, which was nearly the highest dose.

The FANA antimiRs were also compared against the previously studied AntagomiR-23b and -218 with and without X-treme gene transfection reagent (Figure R1C-D). Cell viability was analyzed at 250 nM and 1 $\mu$M for the FANA while the antagomiRs were administered at their previous working concentrations according to Cerro-Herreros *et al*. 2018. This experiment was performed twice: once with the use of transfection reagent and once delivering the oligos gymnotically. Cell viability was much higher in FANA oligos administered without transfection reagent. They were also much more

viable than the antagomiR administered cells which stayed the same as when delivered with transfection reagent.

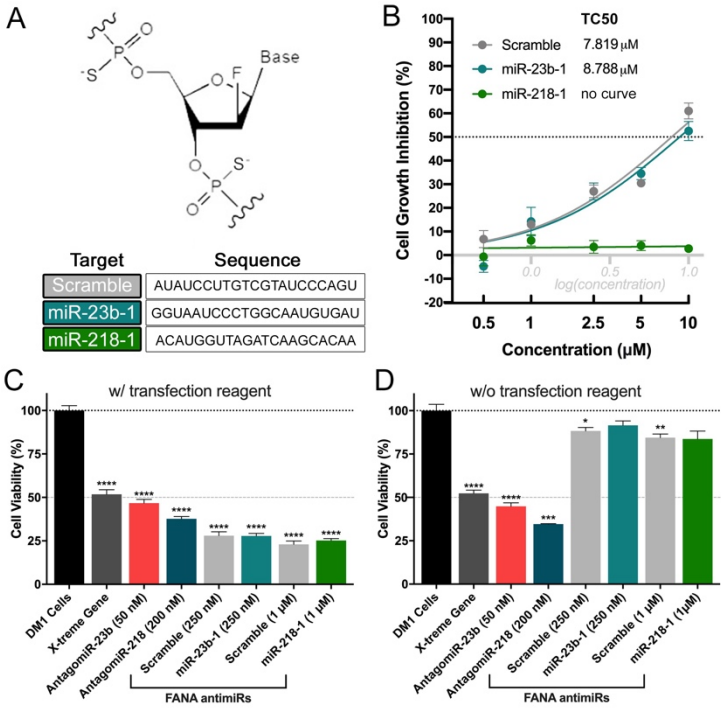


**Figure R1. FANA chemistry shows low toxicity in cells. (A)** The oligos seen here have phosphorothioate linkages combined with a C-2 fluorine substitution. **(B)** DM1 cells were treated with miR-23b or miR-218 FANA antimiRs at five increasing concentrations (x-axis in black) along with a scrambled control. The percent of cell growth inhibition is shown in comparison with the log transformation of each concentration (x-axis in grey). The toxic concentration level at 50% (TC50) for each compound is shown untransformed in μM in the legend above. Cell viability percent was assessed in comparison to AntagomiR-23b and -218 treatment **(C)** with transfection reagent and **(D)** without transfection reagent. X-treme gene is a transfection reagent only control. All samples were compared to DM1 cells control and statistically analyzed with Student's t-Test. P-value GP style: 0.1234 (ns), 0.0332 (*), 0.0021 (**), 0.0002 (***), <0.0001 (****). Error bars = SEM.

Cells were analyzed for levels of *MBNL1* and *2* transcripts and level of miRNA knockdown after treatment at 1, 2.5, and 5 μM (Figure R2). The Scramble oligo had no effect on transcript levels. Treatment with miR-23b-1 increased both *MBNL1* and *2* at 1 μM in comparison to untreated DM1 levels. MiR-218-1 also increased both transcripts but at the higher concentration of

2.5 μM. Significant knockdown of miR-23b and miR-218 was observed by their respective AON at all concentrations. This is to be expected since the FANA oligos were designed as gapmers capable of RNase-H degradation. Curiously, knockdown was also observed after treatment with the Scramble. But in all concentrations, the targeted treatment had a lower knockdown than the Scramble and was statistically significant in most cases.

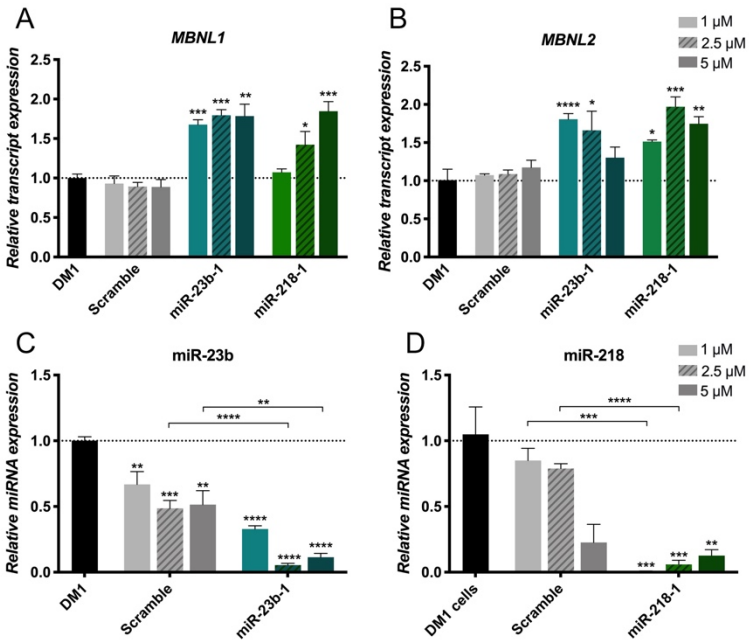


**Figure R2. FANA oligos increase *MBNL1* and *2* transcripts through miRNA functional knockdown.** DM1 cells were measured for **(A)** *MBNL1* and **(B)** *MBNL2* transcripts after treatment at 3 different concentrations (see legend). Samples were normalized to *GAPDH* endogenous control. The same samples were also quantified for **(C)** miR-23b or **(D)** miR-218 knockdown. Samples were normalized to *U1* and *U6* endogenous controls. All samples were compared to DM1 cells control and statistically analyzed with Student's t-Test. P-value GP style: 0.1234 (ns), 0.0332 (*), 0.0021 (**), 0.0002 (***), <0.0001 (****). Error bars = SEM.

## I.II. MBNL protein and splicing rescue after treatment with FANA antimiRs

Since miRNA knockdown and *MBNL* up-regulation was seen even at the lowest antimiR administration, experiments moved forward at 1 μM. Treatment with miR-23b-1 and miR-218-1 were also able to increase levels of

MBNL1 protein at this concentration (Figure R3A-B). However, only miR-218-1 was able to increase MBNL2. Several alternative splicing events are present in DM1 affected cells including *BIN1*, *cTNT*, *MBNL1*, and *SPTAN* transcripts. Treatment with miR-23b-1 showed rescue of *BIN1*, *cTNT*, and *MBNL1* splicing alterations in DM1 cells (Figure R3C). Interestingly, *BIN1* was also rescued previously by antagomiR-23b but *cTNT* was not.

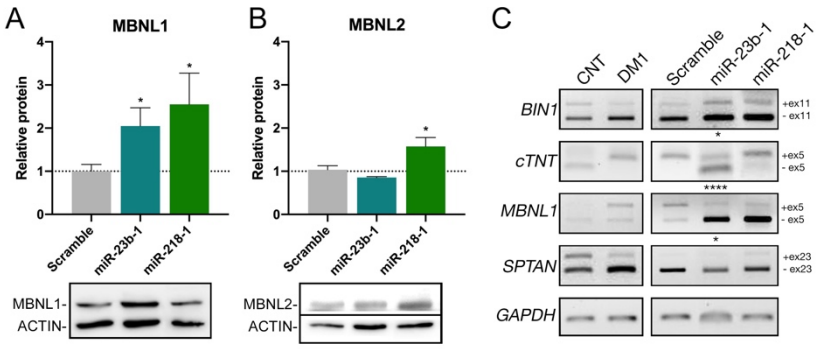


**Figure R3. MBNL protein and splicing rescue after treatment with FANA antimiRs.** Western blot was used to quantify the relative **(A)** MBNL1 and **(B)** MBNL2 protein after FANA treatment at 1 μM. Representative membranes can be seen below the graphs. Band intensity was quantified using Image J. Samples were normalized to β-Actin endogenous control. **(C)** The same samples were analyzed for alternative splicing through semiquantitative RT-PCR. Representative gels can be seen below for each sample which were quantitated with Image J. Samples were tested for *GAPDH* as an endogenous control and were statistically analyzed by Student's t-Test. P-value GP style: 0.1234 (ns), 0.0332 (*), 0.0021 (**), 0.0002 (***), <0.0001 (****). Error bars = SEM.

Through the analysis *in vitro*, FANA antimiRs showed comparable rescue to their previously tested antagomiR counterparts but with gymnotic delivery. The FANA modifications proved to be less toxic than other AON modifications without losing potency.

## II. Objective 2: LNA blockmiR strategy

AntagomiRs and antimiRs have been well characterized for their viability in blocking miRNA activity (Lopez Castel *et al.*, 2019; Rupaimoole and Slack, 2017). However, because miRNAs can have hundreds of target transcripts

(Bartel, 2009), it is difficult to set apart the specific effects on MBNLs versus the additional effects on their other mRNA targets. To circumvent this drawback, here we describe an alternative to antimiR technology called "blockmiRs".

LNA and 2'-*O*-methyl based blockmiRs with phophorothioate linkages were designed against the binding sites of miR-23b and miR-218 on *MBNL1* and *MBNL2* 3'UTR and tested in immortalized patient-derived DM1 fibroblasts transdifferentiated into myotubes (DM1 cells) (Arandel et al., 2017). Third generation LNA modifications are stabilized by a carbon bridge between the sugar C2 and C4 (Figure R4B). The combination of LNA and 2'-*O*-methyl modifications as CUG-repetition blockers has been tested before but without success in DM1 mouse myoblasts (Christou *et al.*, 2020). There, LNA and 2'-OMe nucleotides were interspaced which may have decreased their binding affinity. All-LNA based AONs have been tested in DM1 mice through intramuscular injection with success (Wojtkowiak-Szlachcic *et al.*, 2015). However, these AONs were only 8 to 10-mer, much shorter than the typical 15 to 25-mer AON. Here, the blockmiRs were designed with an 8-mer 2'-OMe core with asymmetrical LNA ends. In this way, the oligos had the enhanced binding affinity of third generation LNAs combined with the steric flexibility and tolerability of naturally occurring 2'-*O*-methyls.

### II.I. Pilot screen for blockmiRs in DM1 cells

The binding sites of miR-23b and miR-218 on the 3'UTRs of *MBNL1* and *MBNL2* were predicted with TargetScan and miRanda and confirmed by dual luciferase assay in the previous antagomiR study in HeLa cells (Cerro-Herreros *et al.*, 2018). BlockmiRs were designed for all predicted and confirmed sites (Figure R4A; Table MM8). BlockmiRs for the confirmed binding sites are separated and highlighted in the following results. Analysis of blockmiRs for the unconfirmed binding sites can be found in additional figures (Figures R6 & R8G-I). Three blockmiRs were designed for the *MBNL2*

3'UTR for miR-218. One blockmiR was designed for the *MBNL1* 3'UTR and one for the *MBNL2* 3'UTR for miR-23b. Finally, a scrambled control (Scramble) was designed as a non-binding control in order to observe any effects related to the LNA chemistry.

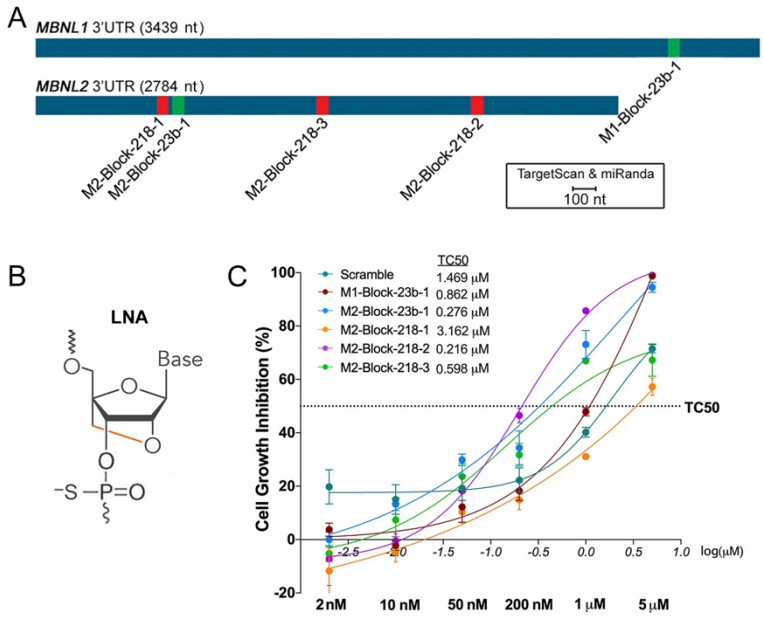


**Figure R4. BlockmiRs designed according to confirmed binding sites. (A)** Predicted miRNA binding sites on *MBNL1* and *MBNL2* 3'UTRs were found using TargetScan and miRanda and confirmed with dual luciferase assay. **(B)** The blockmiRs were designed with LNA modifications and phosphorothioate linkages. **(C)** BlockmiRs were designed for each of the confirmed binding sites and screened for cell viability at increasing concentrations in DM1 cells. Samples were run in quadruplicate. Data are shown log(x) transformed and the toxic concentration values at 50% (TC50) for each compound can be seen on the table next to the legend. Error bars = SEM.

The blockmiRs were first tested for toxicity after transfection into DM1 cells after four days differentiated at increasing concentrations to determine the TC50 of each treatment (Figure R4C). The Scramble showed the lowest toxicity in comparison to all the other blockmiRs, except M2-Block-218-1, which may suggest that other factors are contributing to toxicity rather than simply chemical structure. All the blockmiRs were below the TC50 at 200 nM which was determined to be the highest working concentration. However, in

the previous study (Cerro-Herreros *et al.*, 2018), antagomiRs for miR-23b showed therapeutic results at a concentration of 50 nM and 200 nM for the antagomiRs targeting miR-218. Therefore, 50 nM was chosen for the blockmiRs targeting miR-23b binding sites and 200 nM was chosen for those targeting miR-218 so that the two treatments could be compared.

### II.II. miRNA binding-site blocking shows rescue at the transcript level

The molecular effects of blockmiR treatment were analyzed in DM1 cells four days after transfection and differentiation. A scrambled control was administered, one at 50 nM (Scramble 50) and another at 200 nM (Scramble 200), which is not predicted to have any specific targets. BlockmiRs M1-Block-23b-1 and M2-Block-23b-1 were both able to significantly increase the relative expression of *MBNL1* and *MBNL2* transcripts in comparison with Scramble treatment (Figure R5A-B). M2-Block-23b-1 had a greater effect on *MBNL2* transcripts which is to be expected since this blockmiR acts upon the *MBNL2* 3'UTR binding site. The blockmiRs targeting miR-218 binding sites showed no increase in *MBNL1* or *2* expression. Indeed, M2-Block-218-2 and -3 both decreased the expression of *MBNL1* compared to Scramble 218 while exerting no effect on *MBNL2* transcripts.

In DM1 cells, abnormal splicing patterns are seen in *MBNL1*, *NFIX*, and *SPTAN1* transcripts (Andre *et al.*, 2019; Charizanis *et al.*, 2012; Konieczny *et al.*, 2014; Nakamori *et al.*, 2013; Wagner *et al.*, 2016) and can be observed in comparison to control cells (CNT) (Figure R5C). Again M1-Block-23b-1 and M2-Block-23b-1 showed complete reversal of exon 5 inclusion in *MBNL1* transcripts while blockmiRs targeting miR-218 binding sites had no effect. There was no effect by any of the blockmiRs in the case of *NFIX* exon 7. Finally, all the miR-218 blockmiRs showed remarkable rescue with the inclusion of exon 23 in *SPTAN1*. BlockmiRs targeting miR-23b also showed slight rescue in this exon's expression. *MBNL1* and *NFIX* are regulated by MBNL1 proteins (Wagner et al., 2016) while *SPTAN1* is regulated by MBNL2

proteins (Charizanis et al., 2012). This could explain why greater rescue was seen by blockmiRs targeting sites on *MBNL2*. However, it cannot be dismissed that this could also be related to the miRNA target.

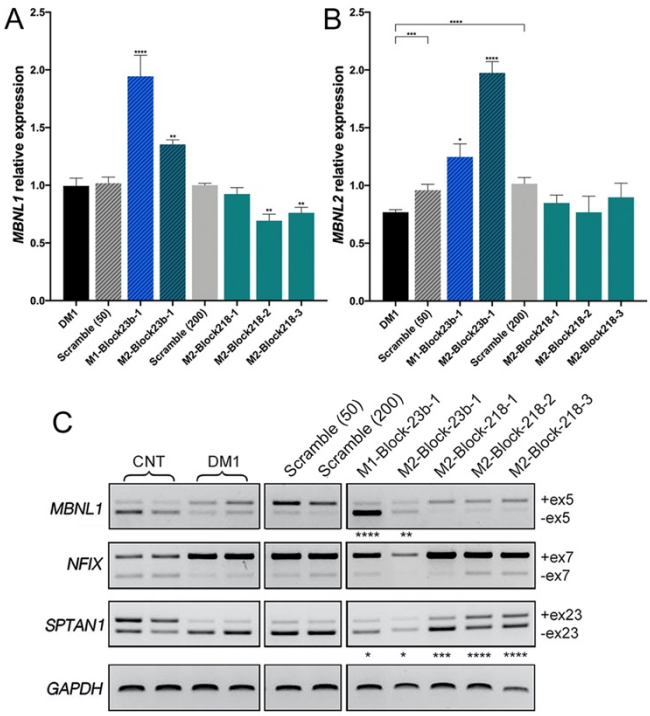


**Figure R5. BlockmiR effects on transcript expression and splicing.** Expression of **(A)** *MBNL1* and **(B)** *MBNL2* transcripts was relatively quantified in quadruplicate after treatment with blockmiRs through semiquantitative RT-qPCR. Scramble 50 serves as a control for samples transfected at 50 nM while Scramble 218 serves for samples transfected at 200 nM. *GAPDH* was used as an endogenous control and MBNL levels were calibrated with the levels in the respective Scrambles. **(C)** Alternative splicing was analyzed for transcripts *MBNL1*, *NFIX*, and *SPTAN1* with *GAPDH* used as an endogenous control through semi-quantitative RT-PCR. Healthy cells (CNT) and DM1 cells are shown in duplicate as splicing controls. A representative gel is seen above. In total, three different gels were run for statistical analysis using Image J. All statistical comparisons were performed against the respective Scrambles (50 or 200) via Student's t-test. P-value GP style: 0.1234 (ns), 0.0332 (*), 0.0021 (**), 0.0002 (***), <0.0001 (****). Error bars = SEM.

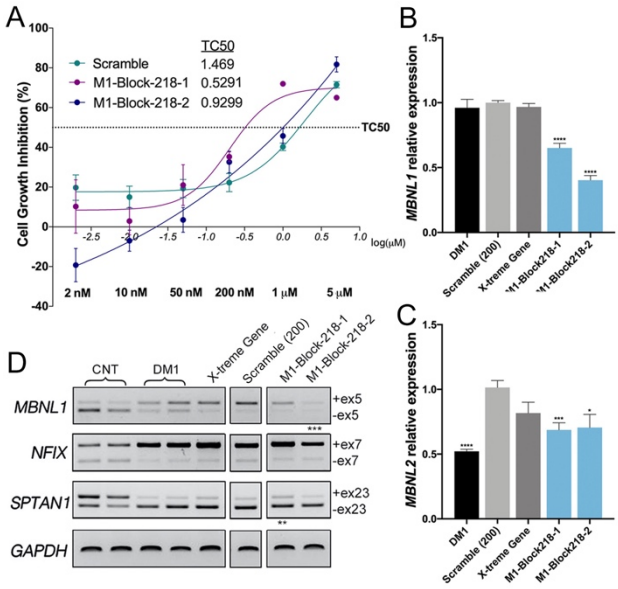


**Figure R6. Treatment with blockmiRs for unconfirmed binding sites. (A)** BlockmiRs with miRNA binding sites not confirmed with dual luciferase assay were screened for cell viability at increasing concentrations in DM1 cells. The toxic concentration values at 50% (TC50) for each compound can be seen on the table. Samples were run in quadruplicate. Expression of **(B)** *MBNL1* and **(C)** *MBNL2* transcripts was relatively quantified in quadruplicate after treatment with blockmiRs. MiR-23b targets were transfected at 50 nM while miR-218 targets were transfected at 200 nM. *GAPDH* was used as an endogenous normalization control and MBNL levels were calibrated with the levels in the respective Scrambles. The DM1 control was calibrated to both Scrambles. All statistical comparisons were performed against the respective Scrambles via Student's t-test. **(D)** Alternative splicing was analyzed for transcripts *MBNL1*, *NFIX*, and *SPTAN1* with *GAPDH* used as an endogenous control after semiquantitative RT-PCR. Healthy cells, CNT, and DM1 cells are shown in duplicate as splicing controls. A representative gel is seen above. In total, three different gels were run for statistical analysis using Image J. All statistical comparisons were performed against the respective Scrambles (50 or 200) via Student's t-test. P-value GP style: 0.1234 (ns), 0.0332 (*), 0.0021 (**), 0.0002 (***), <0.0001 (****). Error bars = SEM.

## II.III. Blocking miR-23b from binding to *MBNL* sites show dose-response MBNL1 protein rescue

The critical role of blockmiR treatment is to increase the production of MBNL proteins by blocking the regulation of miR-23b or miR-218. Therefore, the levels of MBNL1 protein were analyzed and quantified through immunofluorescence staining after treatment with the blockmiRs. Representative images can be seen showing MBNL1 in green and nuclear

DAPI in blue (Figure R7A-F). Control cells show intense MBNL1 signal

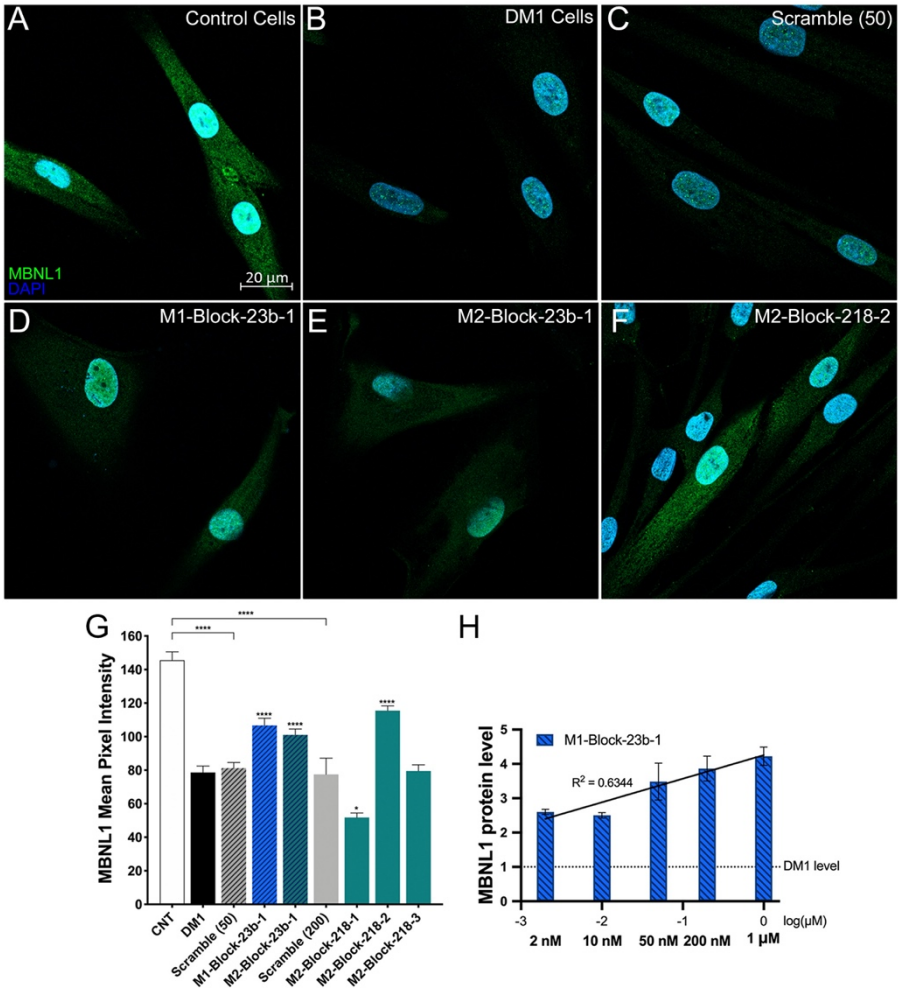


**Figure R7. Immunofluorescence and quantification of MBNL1 protein. (A-F)** CNT and DM1 cells were stained in parallel for MBNL1 protein (green) and nuclei (DAPI blue). **(A)** Healthy control cells show intense signal and disperse localization of MBNL1 fluorescence throughout the entire cell. **(B)** DM1 cells show only punctate fluorescence of MBNL1 in nuclear foci. (Cell count: CNT n=63; DM1 n=106; Scramble 50 n=105; M1-Block-23b-1 n=86; M2-Block-23b-1 n=145; M2-Block-218-2 n=155) **(G)** MBNL1 protein fluorescence was quantified by measuring pixel intensity using Image J with a threshold of 10 and normalized by cell area. All samples were compared to their respective Scrambles (50 or 200) via Student's t-test. **(H)** Quantitative dot blot (QDB) analysis of MBNL1 levels calibrated to GAPDH levels in DM1 cells after treatment with M1-Block-23b-1 at increasing concentrations. Data are shown log(x) transformed and normalized relative to untreated DM1 cell MBNL1 levels. Samples were run in quadruplicate. Black line represents linear regression with $R^2$ value seen above. P-value GP style: 0.1234 (ns), 0.0332 (*), 0.0021 (**), 0.0002 (***), <0.0001 (****). Error bars = SEM.

throughout the nucleus and the cytoplasm, indicative of healthy and functional MBNL1 protein. Conversely, DM1 cells show very little MBNL1 signal in the cytoplasm and only punctate foci in the nucleus. The mean pixel intensity of MBNL1 fluorescence was calculated for each cell and normalized to cell area (Figure R7G). Similar to the increase seen in *MBNL1* transcripts, M1-Block-23b-1 and M2-Block-23b-2 had significant increases of MBNL1 protein fluorescence. They also showed a diffuse cytoplasmic subcellular localization indicating that additional MBNL1 was not being trapped in nuclear foci. Cells treated with Scramble 50 and 200 showed no increase in MBNL1 fluorescence. Curiously, M2-Block-218-2 also showed an increase in MBNL1 pixel intensity. Only the cell images treated with blockmiRs showing rescue are shown in Figure R7. The remaining treatment photos can be found in Figure R8A-F.

With all the results taken together, the most promising and consistent rescue observed in DM1 cells was seen after treatment with M1-Block-23b-1 and M2-Block-23b-1. Both compounds increased MBNL1 transcripts and protein levels a significant amount as well as showed splicing rescue in *MBNL1* and *SPTAN1*. They also showed toxicity levels below the TC50 at the lower concentration of 50 nM while still inducing phenotypic improvements in the DM1 cells. M2-Block-218-2 also showed an increase in MBNL1 fluorescence and *SPTAN1* exon 23 inclusion but failed to increase MBNL1 and 2 transcripts or rescue other splicing events.

With future *in vivo* experiments in mind, human *MBNL1* transcripts show more homology to mice than *MBNL2*. Indeed, there are no predicted binding sites for miR-23b on the mouse *Mbnl2* 3'UTR. Therefore, M1-Block-23b-1 was chosen as the candidate compound and promoted for further analysis and optimization. Five different concentrations of the blockmiR were administered to DM1 cells and were measured for MBNL1 protein level through quantitative dot blot (QDB) (Figure R7H). With exception of the 10 nM treatment, the treatment shows a dose response increase of MBNL1. The

50 nM treatment was also consistent with the results seen in immunofluorescence image quantification.

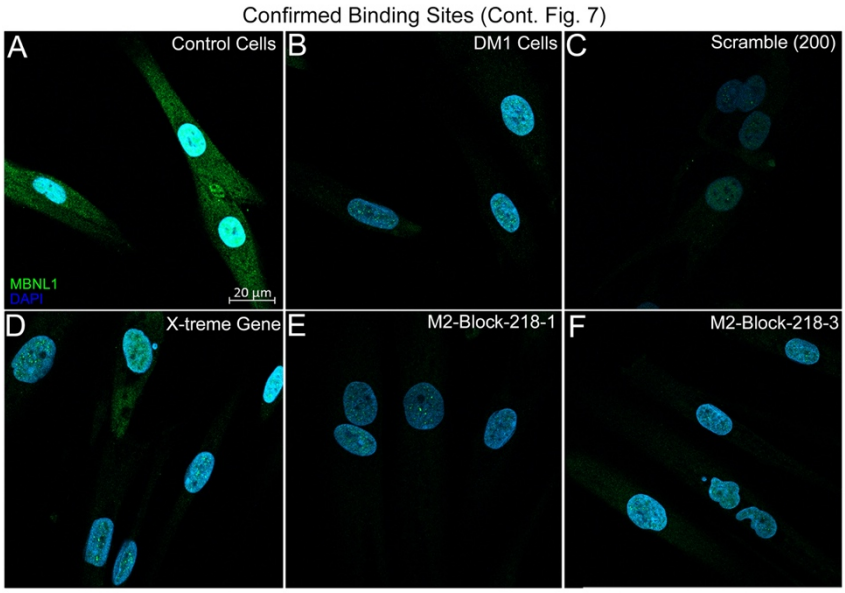


Figure 8. Unconfirmed Binding Sites

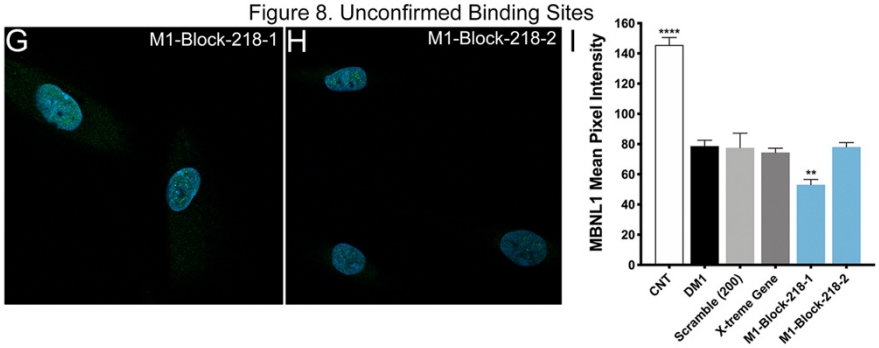


**Figure R8. Immunofluorescence of MBNL1 protein for additional blockmiRs. (A-F)** Continuation of Figure 7 depicting the immunofluorescence of MBNL1 after treatment with the remaining site-confirmed blockmiRs. DM1 cells were stained for MBNL1 protein (green) and nuclei (DAPI) blue (Cell count: CNT n=63; DM1 n=106; Scramble 200 n=17; X-treme Gene n=119; M2-Block-218-1 n=108; M2-Block-218-3 n=109) **(G-H)** Immunofluorescence detection of DM1 cells transfected with blockmiRs targeting unconfirmed binding sites. (Cell count: M1-Block-218-1 n=79; M1-Block-218-2 n=91) **(I)** MBNL1 protein fluorescence was quantified by measuring pixel intensity using Image J with a threshold of 10 and normalized by cell area. All samples compared to Scrambles as a reference via Student's t-test. P-value GP style: 0.1234 (ns), 0.0332 (*), 0.0021 (**), 0.0002 (***), <0.0001 (****). Error bars = SEM.

## II.IV. M1-Block-23b-1 shows recovery at the transcriptome level

RNASeq was performed for M1-Block-23b-1 to investigate gene expression recovery after treatment and compare it to its antagomiR counterpart from previous studies to visualize the global effect the oligos have in DM1 cells. In this experiment, the immortalized fibroblasts were allowed to differentiate four extra days before transfection with the AONs and then left another four for growth in order to observe more pronounced expression differences between the DM1 and CNT cells and to see a more comparable pattern of expression to differentiated muscles *in vivo*.

First, splicing junctions were quantified using a delta percent spliced-in (dPSI) formula. 478 disease related splicing event alterations were identified between healthy and DM1 cells. These events were filtered for data that has a dPSI over 25% and have a significant effect when compared to both healthy and DM1 cells. This filter identified 20 splicing events in 19 genes (Figure R9A). Geometric points are shown only for events with 10 reads or more. 17 out of the 20 events showed a reversal of the splicing event frequency after treatment with M1-Block-23b-1. The splicing recovery events included *SORBS1*, which plays a role in insulin signaling and which is regulated by MBNL1 and CELF1 proteins (Suenaga et al., 2012; Wang et al., 2009). Also recovered was *MLH3*, which is part of the DNA mismatch repair pathway (MMR) and is implicated in somatic expansion of CAG repeats in DM1 and Huntington's disease (Flower *et al.*, 2019; Pinto *et al.*, 2013). Also of mention is the recovery of *BAG4*, which is a known target of miR-1 regulation (Fleming et al., 2013). This miRNA has a varied expression pattern in DM1 tissues and is a likely regulator of *DMPK* expression (Koscianska *et al.*, 2015; Lopez Castel *et al.*, 2019).

Another geometric point graph was generated to visualize the top 25 genes that showed total expression recovery after treatment with M1-Block-23b-1 (Figure R9B). For this reason, the far-right column shows no geometric points due to the fact that there is no difference in expression levels between control

cells and DM1 cells treated with M1-Block-23b-1. The blockmiR and antagomiR showed a similar pattern of expression in many genes with the blockmiR being less intense (see Figure R9B gold box). Indeed, the antagomiR

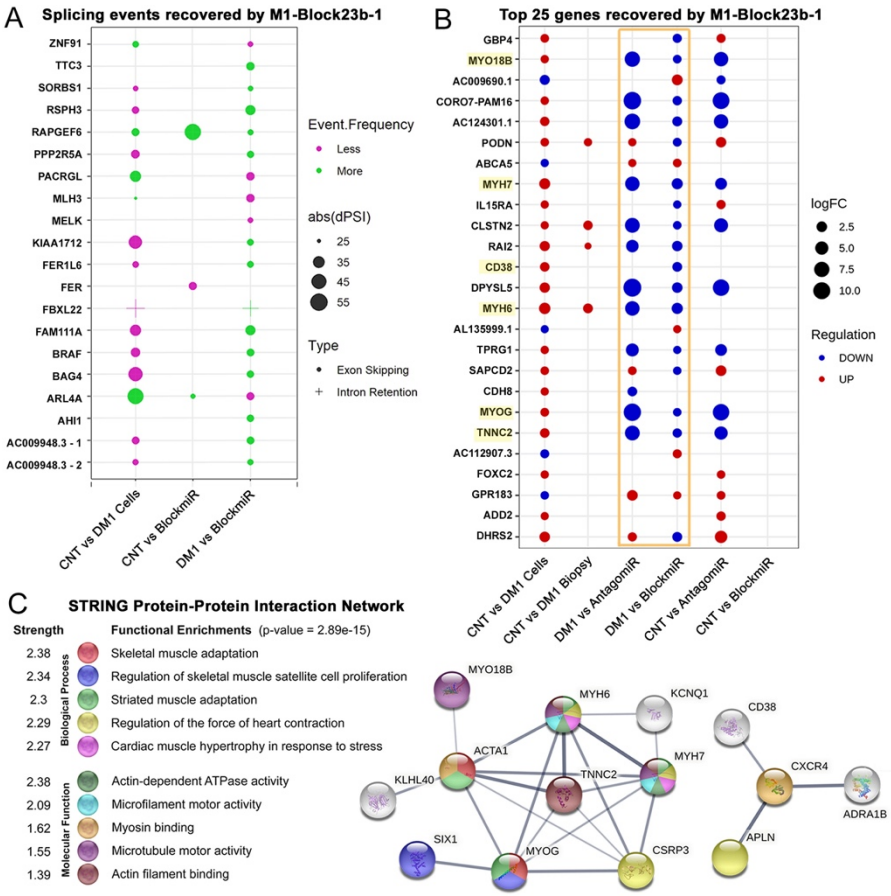


**Figure R9. BlockmiR recovery through RNASeq transcriptome analysis. (A)** Splicing events were analyzed through exon/intron junctions and quantified using delta percent spliced-in (dPSI). Only events with greater than 25% dPSI, adjusted p-value <0.05, and with >10 reads are shown. Geometric points are shown for each event in green for more frequency and pink for less frequency for each comparison. **(B)** Geometric points are shown for the top 25 genes that are totally recovered after treatment with the blockmiR. The size of each point represents the intensity of the change in log2 fold change, while the color represents the over or under expression of each comparison. **(C)** GOterm analysis was performed for the 135 genes with total recovery by the blockmiR. 14 edges were found with overrepresented GOterms. The edges were analyzed by STRING protein indicating both functional and physical protein associations. Line thickness indicates the strength of data support.

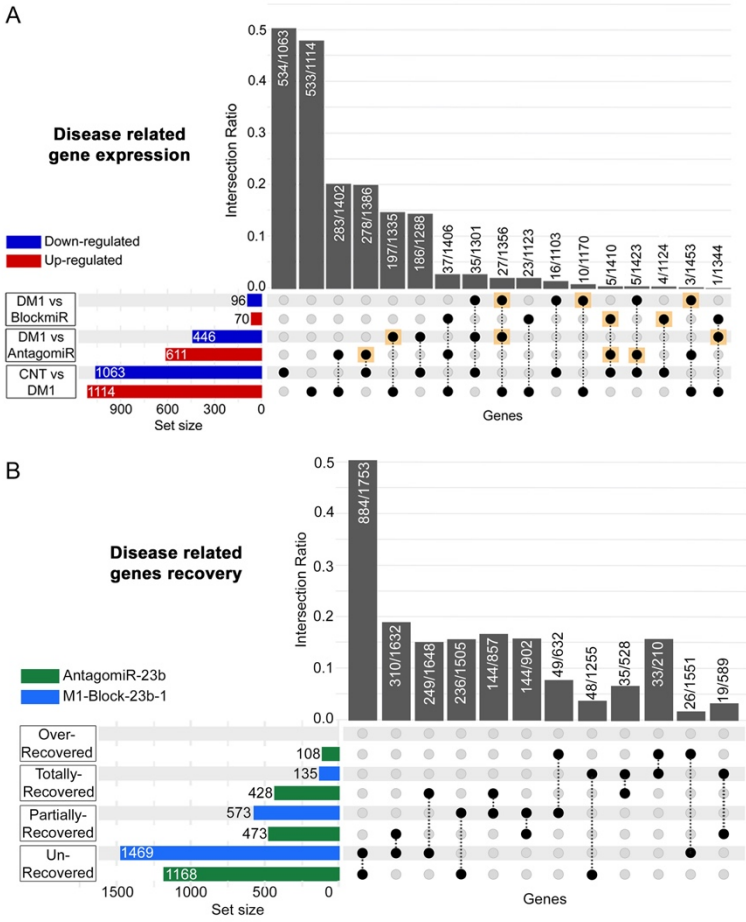


**Figure R10. Comparison of blockmiR- and antagomiR-treated DM1 transcriptomes. (A)** After comparing healthy control cells and DM1 cells, 2177 genes were altered and identified as disease related genes. antagomiR-23b (antagomiR) and M1-Block-23b-1 (blockmiR) treated cells were compared to untreated DM1 cells and a total of 1057 genes and 166 genes respectively had altered expression. The number of genes up- or down-regulated for each comparison can be seen in the respective red and blue horizontal bars to the left. The black circles and dotted lines show which groups share the same altered genes. The intersection ratio is the number of altered genes found in common between groups divided by the total number of unaffected genes from the groups. Gold squares represent genes whose expression was reversed after treatment. **(B)** The percent recovery of disease related genes in comparison to normal expression was calculated for both antagomiR and blockmiR. Unrecovered <10%; partially recovered between 10% and 50%; total recovery between 50% and 150%; over recovered > 150%. The number of genes for AntagomiR or BlockmiR treated cells in each recovery group can be seen in the horizontal bars to the left. The black circles and dotted lines show which groups share genes in the same percent recovery range. The intersection ratio is the number of genes found in common between percent recovery groups divided by the total number of genes not found in common.

tended to show over recovery when compared to the control cells. RNASeq data was also retrieved from http://DMSeq.org for DM1 muscle biopsies to compare the cellular models (Wang et al., 2019). DMSeq.org is deep sequencing data repository for transcriptome data from DM biopsies, autopsies, and animal models. There is a marked difference between the biopsies and the DM1 cell model with many genes showing expression alterations in the DM1 transdifferentiated myotubes while the biopsies showed no difference. However, blockmiR treatment still showed changes in the direction of rescue of biopsies for *PODN*, *CLSTN2*, *RAI2*, and *MYH6*.

Importantly, of the genes totally recovered by M1-Block-23b-1, 14 were connected by overrepresented GOterms all of which have relation to muscular and skeletal function (Figure R9C). These genes were analyzed by STRING and were found to have significant protein-protein interaction linkages. This implicates M1-Block-23b-1 to the gene expression recovery of vital neuromuscular infrastructure and mechanisms in the muscle system.

### II.V. BlockmiR strategy is highly specific

BlockmiR technology builds off of the already effective antagomiR strategy outlined in our previous study (Cerro-Herreros *et al.*, 2018). BlockmiRs have a similar goal in recovering MBNL protein functionality through the blocking of miR-23b and -218 binding sites but without affecting the total levels of these miRNAs. One anticipated advantage of the blockmiR approach is a highly specific effect on *MBNL* transcripts. When comparing DM1 cells and healthy control cells, 2177 genes were found to be altered (Figure R10A). These genes were termed "disease related genes". Of these genes, antagomiR-23b had 1057 altered genes while M1-Block-23b-1 had 166 when compared to untreated DM1 controls. Of the 1057 genes altered by antagomiR treatment, 48.53% were reversed in their disease related expression (see Figure R10A gold squares). As for the blockmiR treated cells, 29.52% were reverted. These reversals suggest an approach to a normal

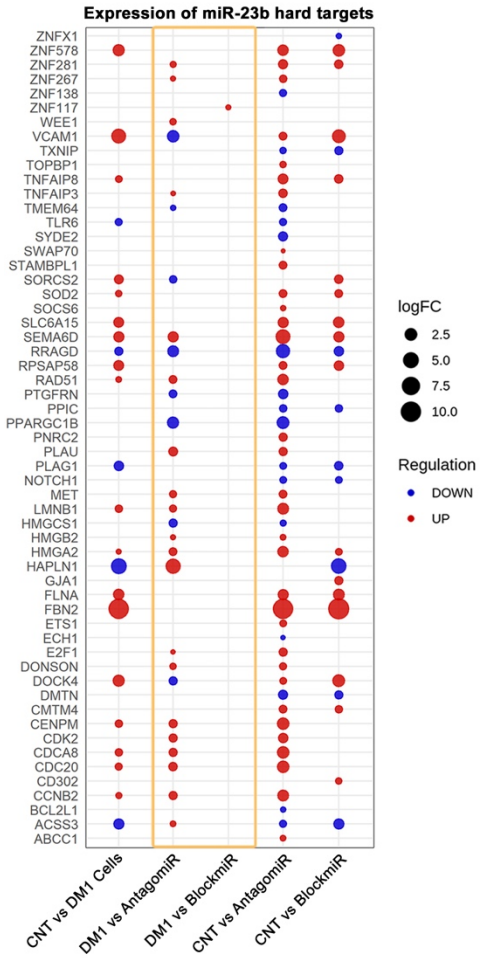


**Figure R11. Geometric point graph of blockmiR- and antagomiR-treated DM1 transcriptomes.** Geometric points are shown for the targets of miR-23b after treatment with the blockmiR or antagomiR. The size of each point represents the intensity of the change in log2 fold change, while the color represents the over or under expression of each comparison.

expression pattern but cannot assume so. Therefore, in order to further quantify the exact recovery patterns, a recovery percentage was calculated for all the disease related genes and cross compared to each treatment (Figure 10B). In comparison to healthy cells, the blockmiR and antagomiR were capable of partial and total rescue. The blockmiR showed greater partial recovery while the antagomiR showed greater total recovery and even 108 cases of over recovery. The blockmiR was also able to recover some genes that the antagomiR could not and vice versa. Combined with the data seen in Figure 9B, the antagomiR has a stronger effect on the total transcriptome.

Finally, to investigate the specificity of the treatments in regard to miR-23b, RNASeq data was analyzed specifically for the transcripts targeted by miR-23b. Of the 57 confirmed targets identified using miRTarBase, only 1 of these showed an alteration in expression after treatment with M1-Block-23b-1 in comparison to untreated DM1 cells (see Figure R11 gold box). On the contrary, the antagomiR treated cells showed

alterations in 28 of the targets. When compared to the healthy controls, the blockmiR treated cells showed more similarity to the control cells than the antagomiR. This indicates that the blockmiR strategy of targeting the miRNA binding sites is a much more specific method than targeting the miRNA itself.

## II.VI. miR-23b binding site is conserved in mice

The success of the blockmiRs *in vitro* led to *in vivo* testing in mice. But before this experiment could take place, the binding site of miR-23b needed to be confirmed in mouse. Site 1 on the *MBNL1* 3'UTR has previously been confirmed in HeLa cells through dual luciferase assay (Cerro-Herreros *et al.*, 2018). This site shares sequence homology with Site 2 of the two predicted miR-23b binding sites in mice save for one nucleotide. To confirm these predicted sites, another luciferase assay was performed in mouse C2C12 cells using *Mbnl1* 3'UTR constructs. Three reporter plasmids were generated, one containing the wildtype *Mbnl1* (WT), one with deletion of the respective miR-23b seed region in the binding site (Del), and one with a complementary

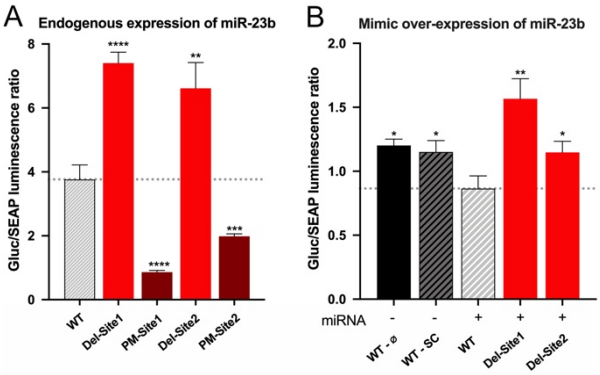


**Figure R12. Dual luciferase assay confirms conservation of miR-23b binding site. (A)** Gluc and SEAP luminescence was quantified in C2C12 mouse cells after transfection with reporter plasmids containing the 3'UTR of Mbnl1 either wildtype (WT), the miR-23b seed region deleted (Del) or perfect match to miR-23b (PM). **(B)** To further confirm the luminescence observed was due to miR-23b, the experiment was repeated with co-transfection of a miRNA mimic of miR-23b. Two mimic controls were used, one with no mimic (WT-∅) and one with a scrambled mimic (WT-SC). All dual luciferase assays were normalized to SEAP and compared to WT for statistical comparison using Student's t-Test. P-value GP style: 0.1234 (ns), 0.0332 (*), 0.0021 (**), 0.0002 (***), <0.0001 (****). Error bars = SEM.

perfect match to the full miR-23b sequence (PM). The plasmids were transfected in C2C12 cells and the GLuc and SEAP luminescence was read after 48 h. If miRNA binding occurs, GLuc translation is inhibited and therefore luminescence decreases. SEAP is constitutively translated as a normalization control. Endogenous expression of miR-23b binding in the C2C12 cells was apparent through the increase of luminescence in the miR-23b binding site deletion plasmids in comparison to the wildtype (Figure 12A). In contrast, GLuc signal was decreased upon transfection with perfect match plasmids. This confirms that miR-23b is directly binding to these sites.

In order to further validate these binding sites, the experiment was repeated using a miR-23b mimic (Figure 12B). Upon seed region deletion, GLuc luminescence increased once again. Also supporting this information was the wildtype no-mimic control and the wildtype scrambled-mimic control which both showed less miRNA repression compared to wildtype and mimic co-transfection.

In scanning for potential binding sites to the 3'UTR in mouse *Mbnl1* and *Mbnl2*, potential sites were also recognized for miR-218 (Figure R13A). M2-Block-218-2 showed a strong increase in MBNL1 protein fluorescence in DM1 cells (Figure R7F). All miR-218 blockmiRs also showed significant *SPTAN* rescue (Figure 5C). The potential for blockmiRs targeting miR-218 binding sites could not be dismissed. Therefore, for the sake of future study, the binding sites of miR-218 were also assessed by dual luciferase assay in C2C12 cells (Figure R13B). The procedure was conducted in the same manner as Figure 12B but using a miR-218 mimic and also including the perfect match plasmids. Of the four potential sites on *Mbnl1*, only Site 3 showed increased luminescence after deletion. All perfect match samples showed a significant decrease in luminescence while the wildtype scrambled miR-218 mimic showed an increase. This indicates that the co-transfection was successful. On the other hand, the PM-Site 2 on *Mbnl2* did not show a decrease in luminescence suggesting that the mimic may not have been accepted by the

cells or was inadvertently skipped during transfection. Indeed, the sample was significantly increased in comparison to the WT showing the lack of mimic but is still slightly less than the WT-SC suggesting that endogenous miR-218 is still binding to the perfect match. However, upon deletion of site 2, luminescence increased meaning that the binding site is most likely viable. Del-Site1 and PM-Site1 on *Mbnl2* also confirmed existence of a binding site.

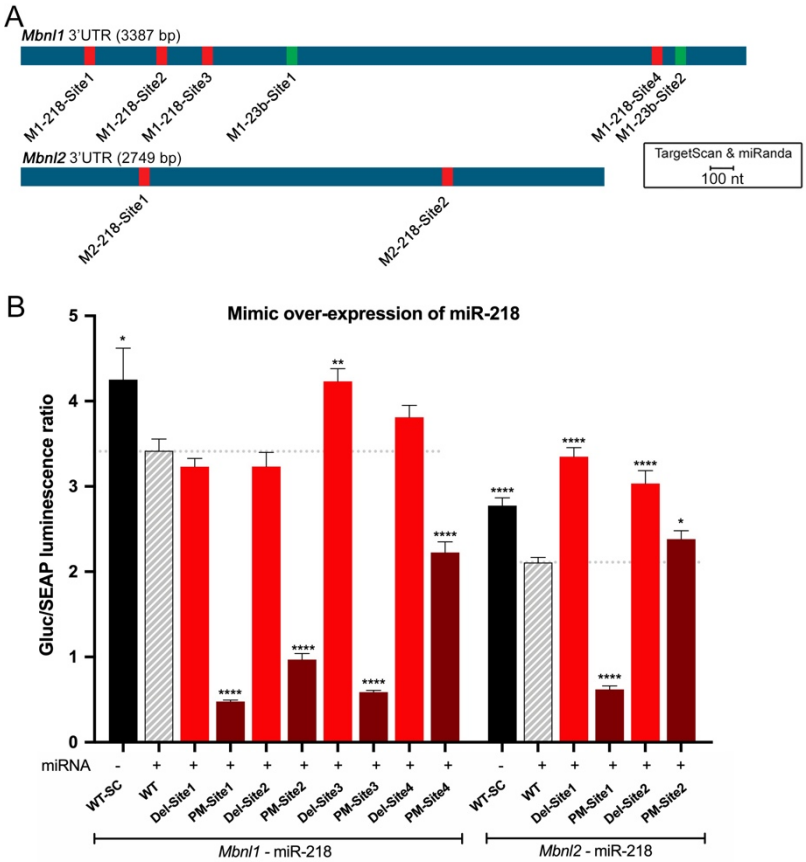


**Figure R13. miR-218 also binds to *Mbnl1* and *Mbnl2* 3'UTR. (A)** Predicted binding sites for miR-23b and miR-218 on *Mbnl1* and *Mbnl2* were scanned using bioinformatic tools TargetScan and miRanda. **(B)** Gluc and SEAP luminescence was quantified in C2C12 mouse cells after transfection with reporter plasmids containing the 3'UTR of *Mbnl1* either wildtype (WT), the miR-23b seed region deleted (Del) or perfect match to miR-23b (PM). They were co-transfected with a miR-218 mimic as well as a scrambled mimic control (WT-SC). The dual luciferase assays were normalized to SEAP and compared to WT for statistical comparison using Student's t-Test. P-value GP style: 0.1234 (ns), 0.0332 (*), 0.0021 (**), 0.0002 (***), <0.0001 (****). Error bars = SEM.

M2-Block-218-2 shares strongest homology with M2-218-Site2 with only two nucleotide differences. The co-transfection for PM-Site2 could be repeated to further confirm the existence of M2-218-Site2 before moving forward with this blockmiR *in vivo*.

## II.VII. Testing blockmiRs in an *in vivo* DM1 model

Through these luciferase assays, Sites 1 and 2 were both confirmed as miR-23b binding sites in the mouse *Mbnl1* 3'UTR. Therefore, the blockmiR was approved for testing *in vivo*. The conserved binding Site 1 for miR-23b in mice has one nucleotide difference in comparison to the human site (Figure R14). Therefore, a new compound, M1-Block23b-M, was generated accounting for this difference and was administered at 12.5 mg/kg through subcutaneous injection in $HSA^{LR}$ DM1 model mice (n = 5). The human version of the blockmiR, M1-Block23b-H, was also injected at the same concentration (n = 5). A group of FVB healthy mice (n = 5) and a group of $HSA^{LR}$ mice (n = 5) were administered PBS as two separate controls. After four days, mice were sacrificed and their gastrocnemius and quadriceps muscles were extracted for molecular analysis.

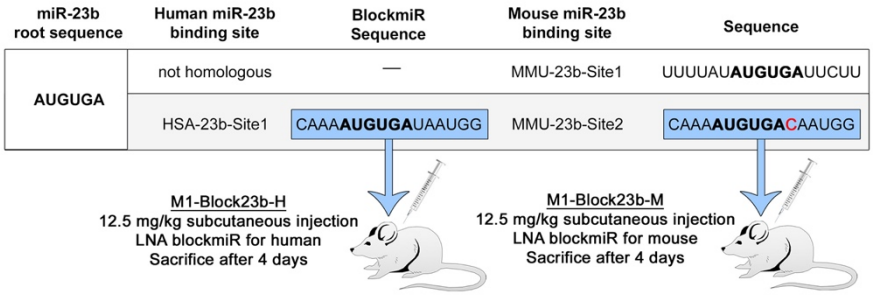


**Figure R14. In vivo blockmiR administration.** The blockmiR sequence used in DM1 cells has one nucleotide difference (red) for the same site in mice. A new blockmiR adjusting for this small difference was synthesized for more precise binding in $HSA^{LR}$ mice. Both the human and mouse version of blockmiRs were administered at a single dose of 12.5. mg/kg to $HSA^{LR}$ mice. After four days, the mice were sacrificed and the gastrocnemius and quadriceps muscle were extracted for analysis.

## II.VIII. Mouse specific blockmiR shows toxicological changes in blood

After treatment with both human and mouse versions of M1-Block23b, blood and serum were extracted and analyzed. A differential white blood cell (WBC) count was performed after each treatment and compared to empirical FVB levels (Figure R15). Outside FVB measurements were also added as reference but varied greatly between study (Bogue *et al.*, 2020; Schneck *et al.*, 2000). The most similar FVB levels to those empirically measured in our lab were those of 8 week males (§) (Bogue *et al.*, 2020). These FVB also coincided with typical normal ratios of healthy mice in general: neutrophils: 20-30%, eosinophils: 0-7%, lymphocytes: 70-80%, monocytes: <2%, basophils: 0-1% (O'Connell *et al.*, 2015). PBS and M1-Block23b-H treatments both stayed within these ranges. However, an increase in monocytes and lymphocytes was observed after treatment with M1-Block23b-M.

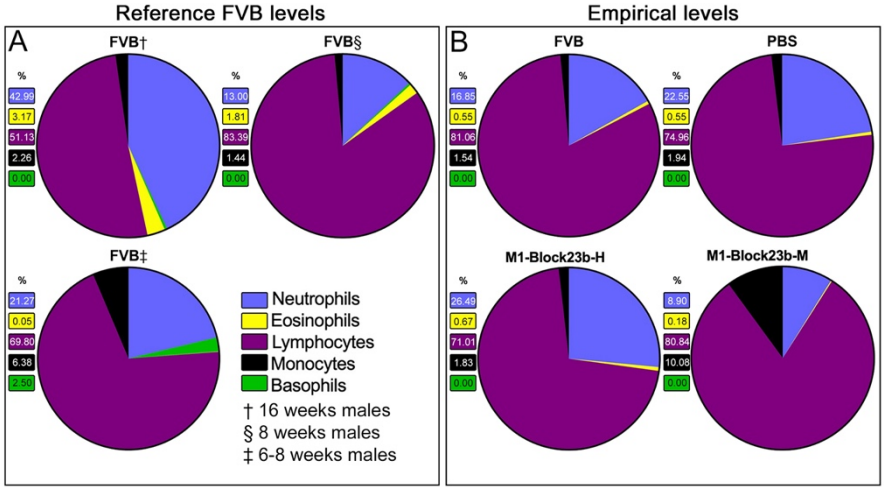


**Figure R15. Differential WBC count. (A)** Reference FVB levels from outside sources. **(B)** Empirical FVB levels measured in this study. All ratios sum to a total of 100%.

A complete blood count (CBC) and biochemical analysis were performed for each sample and compared to the FVB levels (Figure R16). With this

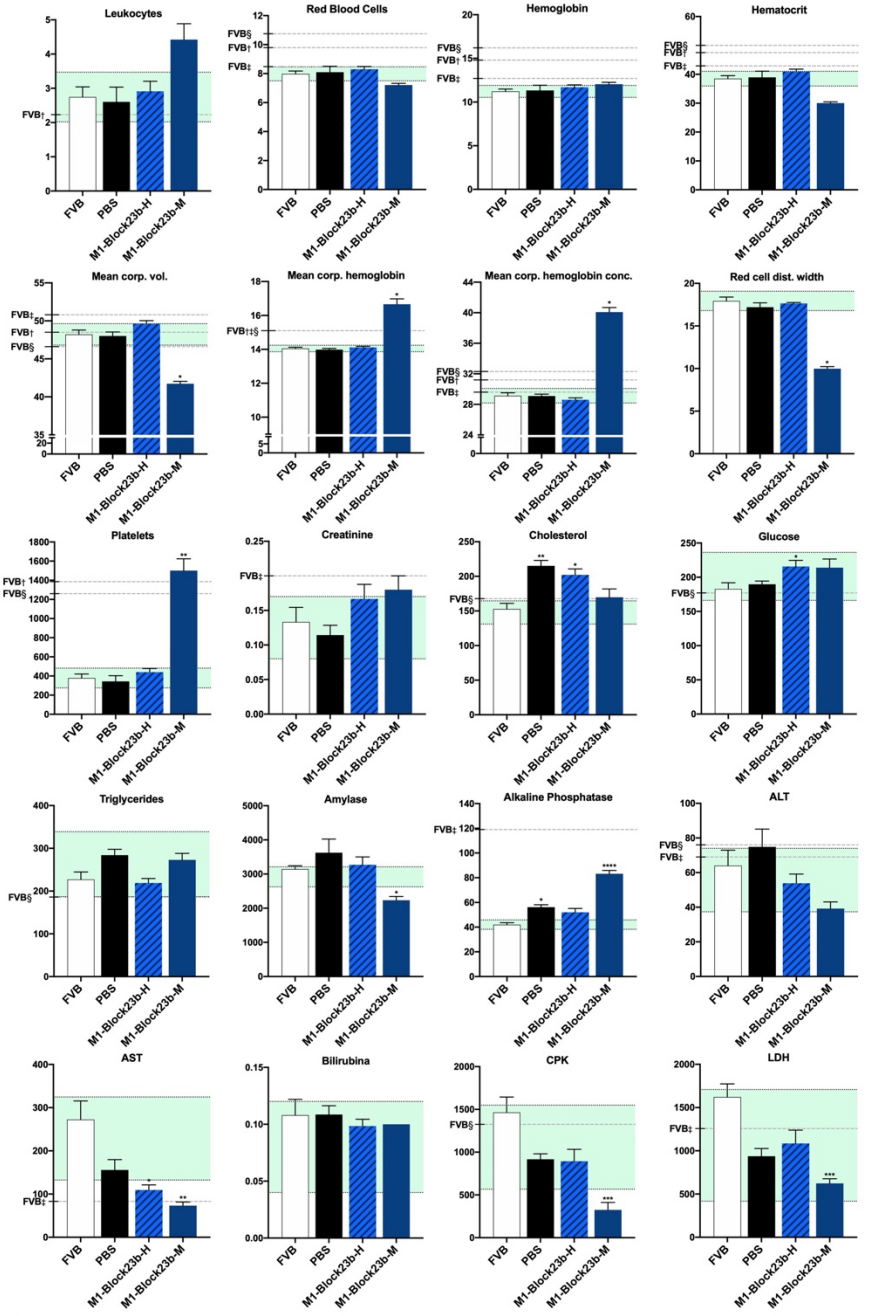


**Figure R16. Serum and blood biochemical analysis.** Blood and serum parameters were analyzed for all treatment groups and compared to empirical FVB controls through one-way ANOVA. The range of empirical FVB levels are shown in green. Reference FVB levels are shown by dashed grey lines (see legend). P-value GP style: 0.1234 (ns), 0.0332 (*), 0.0021 (**), 0.0002 (***), <0.0001 (****). Error bars = SEM.

comparison, M1-Block23b-M showed various changes including a significant increase in mean corpuscular hemoglobin (MCH), mean corpuscular hemoglobin concentration (MCHC), platelets, and alkaline phosphatase as well as a significant decrease in mean corpuscular volume (MCV), red cell distribution width (RDW), amylase, aspartate transaminase (AST), creatine kinase (CPK), and lactate dehydrogenase (LDH). In most cases, M1-Block23b-H remained near the same level as PBS. When M1-Block23b-H was compared to the FVB levels, there was only a significant increase in glucose and cholesterol, which is an $HSA^{LR}$ mice disease phenotype, as well as slight decrease in AST.

The acceptable ranges of biochemical parameters in blood differ between mouse strains (Champy *et al.*, 2008). To better understand the acceptable ranges of each measurement, empirical data from 12 male FVB mice between 12-18 weeks old from our lab were averaged and their upper and lower standard deviation was added to each graph in green. Averages of male FVB mice ‡6-8 weeks old

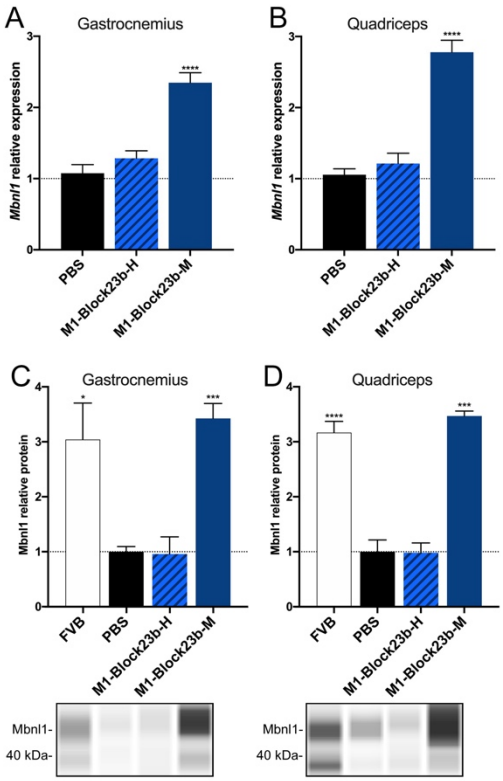


**Figure R17. Molecular outcomes of blockmiR treatment.** Relative expression of *Mbnl1* transcripts was relatively quantified in triplicate from muscles after treatment with the blockmiRs in mice **(A)** gastrocnemius and **(B)** quadriceps muscles. Values were normalized to *Gapdh* endogenous control. **(C-D)** Relative Mbnl1 protein was also quantified in each muscle using Jess Simple Western technology and normalized to total protein. A representative lane view shows the bands observed below each graph. All statistical comparisons were performed against PBS via Student's t-test. P-value GP style: 0.1234 (ns), 0.0332 (*), 0.0021 (**), 0.0002 (***), <0.0001 (****). Error bars = SEM.

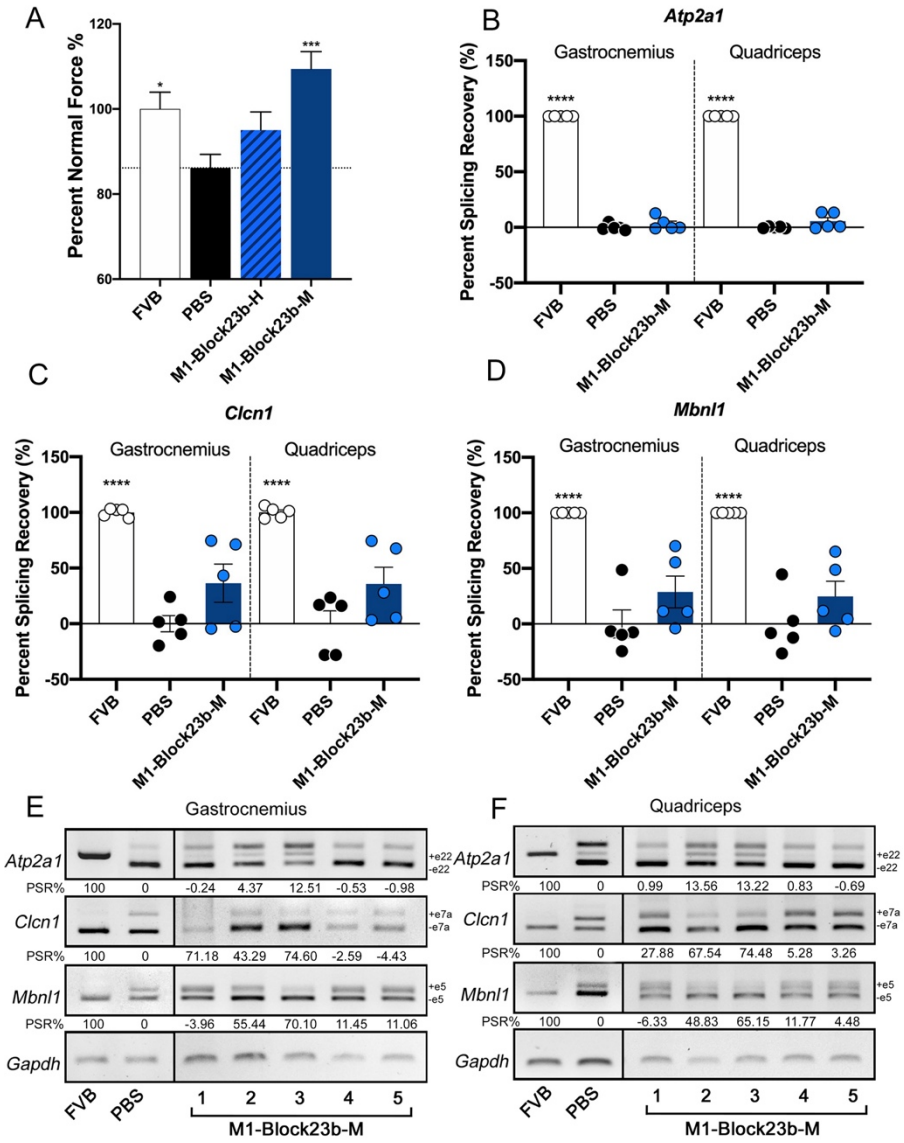


**Figure R18. Physiological and splicing outcomes of blockmiR treatment. (A)** Mouse grip strength was measured before and after treatment with M1-Block23b-M by grip meter to calculate the percent of normal force normalized to mouse weight. Semiquantitative RT-PCR was performed to analyze alternative splicing patterns in exons of interest for **(B)** *Atp2a1* **(C)** *Clcn1* and **(D)** *Mbnl1* transcripts. *Gapdh* was run as an endogenous control. PSR was calculated normalized to FVB samples. Representative gels can be seen below for **(E)** gastrocnemius and **(F)** quadriceps. The PSR for each sample can be found below each gel. Individual mice are labeled below *Gapdh* by numbers after treatment with M1-Block23b-M. Statistical comparison was performed against PBS via Student's t-test. P-value GP style: 0.1234 (ns), 0.0332 (*), 0.0021 (**), 0.0002 (***), <0.0001 (****). Error bars = SEM.

(Schneck *et al.*, 2000), †16-week and §8-week males (Bogue *et al.*, 2020) were added with a dashed grey line when data was available. With these results in context, some of the values that were significantly changed after M1-Block23b-M treatment were still within the known values of healthy FVB ranges.

### II.IX. BlockmiR treatment increases Mbnl1 and rescues DM1 phenotypes in mice muscle

Four days after injection, mice were sacrificed and their hind leg muscles, gastrocnemius and quadriceps, were extracted for molecular examination. A significant increase was observed in *Mbnl1* transcript expression in both muscles after treatment with M1-Block23b-M (Figure R17). Likewise, a similar increase reaching normal levels of FVB Mbnl1 protein was achieved after M1-Block23b-M treatment.

M1-Block23-M also induced physiological increase of grip strength (Figure R18A). The percent normal force was calculated by normalizing the strength of mice on a grip strength meter to their weight before and after treatment and then comparing to the PBS levels. Splicing for three transcripts was analyzed after treatment including *Atp2a1*, *Clcn1*, and *Mbnl1* (Figure R18B-F). Slight increases of percent splicing recovery (PSR) were observed in *Mbnl1* and *Clcn1*. However, when looking at the treated mice individually, two mice in particular showed a large amount of rescue in all transcripts (see mice 2 and 3 in Figure R18E-F).

The migration of muscle fiber nuclei towards the center of the muscle fibers is a well-known phenotype of $HSA^{LR}$ mice muscle (Mankodi *et al.*, 2000). Therefore, hematoxylin and eosin (H&E) staining was performed on both gastrocnemius and quadriceps muscle to visualize the percent of muscle fibers containing central nuclei (Figure R19). In both tissues, M1-Block23b-M showed significant reduction in the percentage of central nuclei in

comparison to PBS controls. Indeed, the fibers treated with M1-Block23b-M are more morphologically similar to the FVB mice. Nuclei quantification was done blindly after randomizing images to avoid bias. Detailed statistical information can be found in Table R1 including SEM and number of fibers counted for each individual mouse.

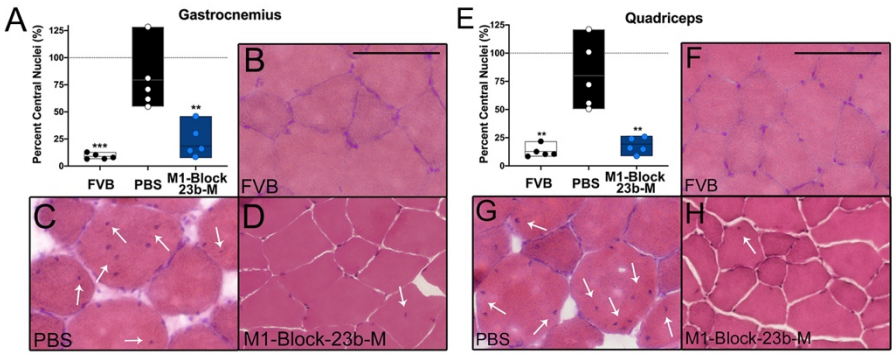


**Figure R19. Histological improvements from blockmiR therapy.** First, 10 µm sections of quadriceps and gastrocnemius muscle were cut and stained with hematoxylin and eosin in order to visualize the localization of central nuclei within the muscle fibers. **(A & E)** An average of 600 fibers were analyzed and quantified per mouse. Representative images of each treatment can be seen for **(B-D)** gastrocnemius and **(F-H)** quadriceps. Black scale bar = 100 µm. The white arrows signal nuclei that have central localization. All samples were statistically compared to PBS through Student's t-Test. P-value GP style: 0.1234 (ns), 0.0332 (*), 0.0021 (**), 0.0002 (***), <0.0001 (****). Error bars = SEM. SEM and number of fibers for panels A and E can be found in Table R1.

**Table R1. Statistical data for histological image quantification in Figure R19.**

| Mouse | Gastrocnemius | | | Quadriceps | | |
|---|---|---|---|---|---|---|
| | Mean | SEM | # of fibers | Mean | SEM | # of fibers |
| FVB1 | 6.61 | ±1.67 | 514 | 10.51 | ±1.32 | 465 |
| FVB2 | 6.83 | ±1.46 | 595 | 8.43 | ±1.39 | 473 |
| FVB3 | 7.92 | ±1.11 | 538 | 21.74 | ±8.65 | 483 |
| FVB4 | 10.38 | ±2.51 | 446 | 10.40 | ±3.85 | 480 |
| FVB5 | 12.86 | ±2.30 | 434 | 12.63 | ±1.56 | 416 |
| PBS1 | 54.82 | ±6.90 | 428 | 50.45 | ±11.11 | 269 |
| PBS2 | 128.33 | ±17.77 | 327 | 121.04 | ±14.77 | 273 |
| PBS3 | 70.73 | ±5.18 | 363 | 72.08 | ±7.20 | 433 |
| PBS4 | 61.73 | ±4.95 | 726 | 55.60 | ±10.54 | 352 |

| | | | | | | |
|---|---|---|---|---|---|---|
| PBS5 | 80.96 | ±13.25 | 348 | 100.96 | ±11.66 | 297 |
| M1-Block23b-1-M1 | 15.94 | ±1.97 | 1157 | 23.97 | ±1.93 | 932 |
| M1-Block23b-1-M2 | 14.29 | ±1.56 | 962 | 8.64 | ±0.96 | 1249 |
| M1-Block23b-1-M3 | 7.50 | ±1.07 | 1461 | 15.77 | ±1.27 | 867 |
| M1-Block23b-1-M4 | 8.41 | ±0.92 | 1416 | 26.62 | ±2.48 | 692 |
| M1-Block23b-1-M5 | 45.96 | ±5.84 | 314 | 14.72 | ±1.13 | 816 |

## III. Objective 3: P-PMO blockmiR strategy

Charge-neutral morpholino (PMO) and cell-penetrating peptide-linked morpholino (P-PMO) based AONs targeting the toxic *DMPK* repetitions were able to block the binding of MBNL proteins (Leger *et al.*, 2013; Wheeler *et al.*, 2009). PMOs have a neutral charge that create a highly stable compound and facilitate efficient delivery to the cell. A PMO called Eteplirsen has already obtained FDA approval for the treatment of Duchenne muscular dystrophy (DMD) (Lim *et al.*, 2017). PMOs can also be covalently linked with cell penetrating peptides to further promote cell uptake. For example, the Pip6a-PMO compound has shown cardiac improvements in DMD mouse models (Blain *et al.*, 2018; Forand *et al.*, 2020). Pip6a-PMO has also been used for the treatment of DM1 by targeting the toxic repeat sequence in DMPK (Klein *et al.*, 2019). A P-PMO has also produced therapeutic results in DM1 $HSA^{LR}$ mice, including splicing rescue, myotonia and reduction of nuclear foci (Leger *et al.*, 2013).

AntimiRs and antagomiRs have been well characterized for their viability in blocking miRNA activity (Lopez Castel *et al.*, 2019; Rupaimoole and Slack, 2017). And as seen in Objective 2, the blockmiR strategy targeting miRNA binding sites showed proof of concept in DM1 cells and mice. Therefore, M1-Block23b-M needed more study and refinement. Here, chemically improved Pip9b2 peptide-linked PMO blockmiRs were designed against a binding site of miR-23b on *MBNL1* and tested in immortalized patient-derived DM1 fibroblasts transdifferentiated into myotubes (DM1 cells) (Arandel *et al.*,

2017). The peptide is designed to facilitate efficient entry into the cell without the use of transfection reagents and therefore decrease toxic side effects. The neutral charge will also improve the stability of the compound *in vivo*.

## III.I. Pip9b2-linked PMO blockmiR increases MBNL1 in cells

Pip9b2 is a cell penetrating peptide that contains two flanking regions enriched with arginines (cationic amino acids) and a central hydrophobic core (Figure R20A). The peptide-linkage to the PMO blockmiR is designed to facilitate cell entry without the need for transfection reagent. To test for cell

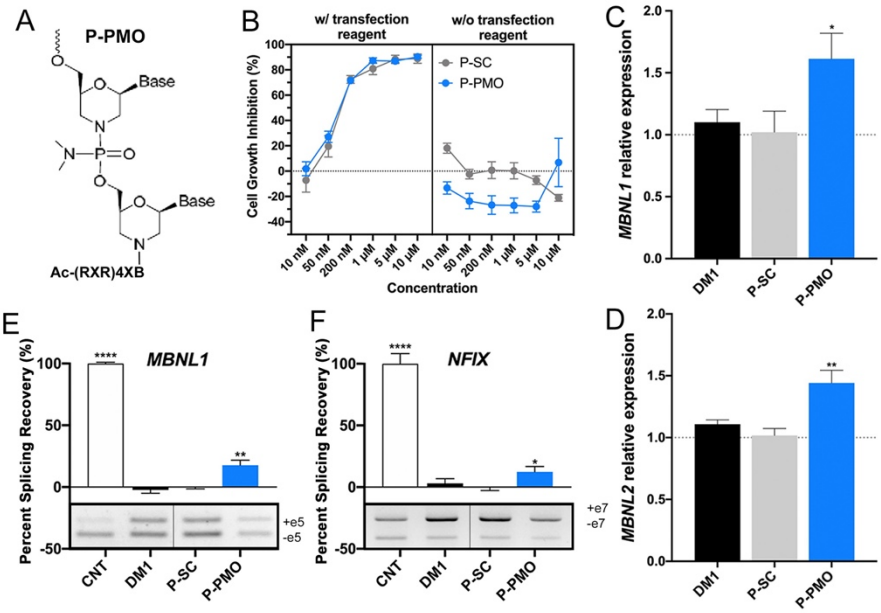


**Figure R20. P-PMO blockmiR effects on DM1 cells. (A)** The P-PMO blockmiR along with the scramble control (P-SC) was tested for cell viability at increasing concentrations with and without the use of transfection reagent. The peptide conjugation is designed to penetrate the cell without the need for transfection reagent. Expression of **(B)** *MBNL1* and **(C)** *MBNL2* transcripts was relatively quantified in triplicate from cells after treatment with the P-PMO blockmiR at 1 µM. Values were normalized to endogenous *Gapdh* and compared to P-SC using Student's t-Test. Percent Splicing Recovery (PSR) was calculated after semiquantitative RT-PCR and exon band quantification for **(D)** *MBNL1* exon 5 and **(E)** *NFIX* exon 7 and normalized to CNT samples. Representative gels can be seen below each graph. *GAPDH* was run as an endogenous control (see Figure R25). Values were compared to P-SC using Student's t-Test. P-value GP style: 0.1234 (ns), 0.0332 (*), 0.0021 (**), 0.0002 (***), <0.0001 (****). Error bars = SEM.

toxicity, the P-PMO blockmiR and a peptide-linked with a scrambled PMO (P-SC), a chemistry control, were administered in DM1 cells at increasing concentrations (Figure R20B). The peptide-linked oligos showed little to no cell growth inhibition across all concentrations in contrast to those treated with transfection reagent which began to show 50% cell growth inhibition after 50 nM. Therefore, for the rest of the experiments, P-PMO and P-SC were administered at 1 $\mu$M per manufacturer's recommendation.

DM1 cells showed an increase in *MBNL1* and 2 transcript expression levels after P-PMO blockmiR treatment (Figures R20C-D). Aberrant fetal splicing patterns in *MBNL1* and *NFIX* transcripts show a strong phenotype in DM1 cells. After treatment with the blockmiR, a slight but significant return to the adult splicing pattern was observed (Figure R20E-F).

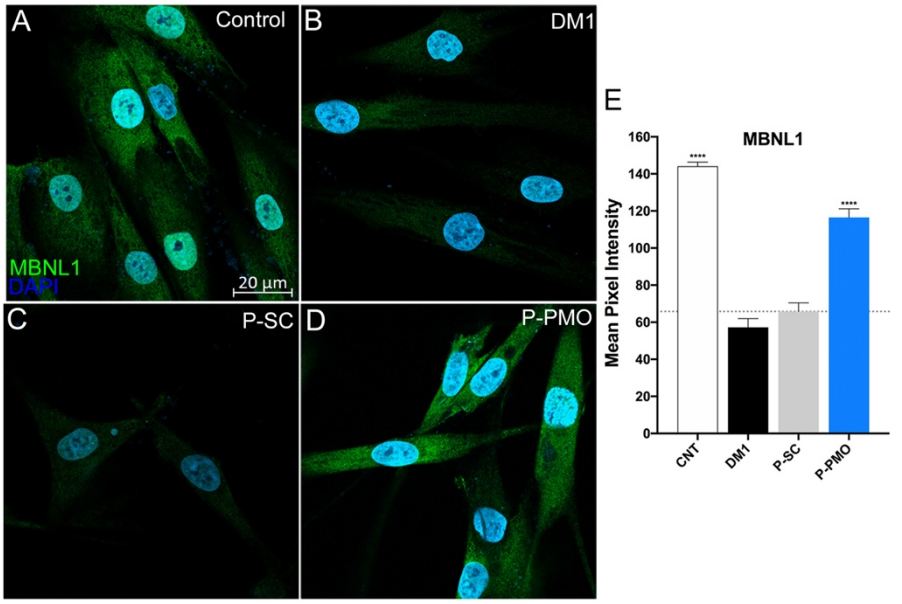


**Figure R21. P-PMO blockmiR effects on DM1 cells.** Immunofluorescence of MBNL1 protein (green) and DAPI (blue) was observed in **(A)** controls cells, **(B)** DM1, **(C)** P-SC treated DM1 cells, and **(D)** P-PMO treated DM1 cells. **(E)** The mean pixel intensity of each was quantified. Cell count: CNT n=118, DM1 n=83, P-SC n=96, P-PMO n=108. All statistical comparisons were performed against P-SC via Student's t-test. P-value GP style: 0.1234 (ns), 0.0332 (*), 0.0021 (**), 0.0002 (***), <0.0001 (****). Error bars = SEM.

The cells also showed a striking increase in MBNL1 protein immunofluorescence through analysis of confocal microscopy images (Figures R21A-D). From a qualitative standpoint, the cells treated with cell-penetrating peptide blockmiRs were visibly more prolific and showed a large increase in MBNL1 fluorescence in the cytoplasm. Quantification of the mean pixel intensity for each cell confirmed this increase (Figure R21E).

## III.II. P-PMO is non-toxic to mice and increases grip strength

The success of P-PMO blockmiR *in vitro* led to its administration in $HSA^{LR}$ mice. A new P-PMO was generated accounting for the one nucleotide difference between mice and humans and was administered intravenously at 10 mg/kg (Figure R22).

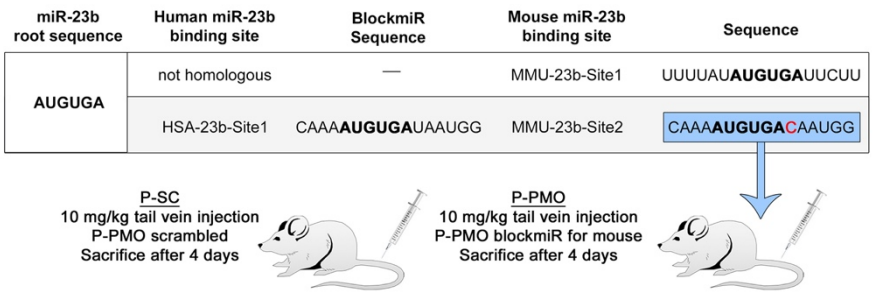


**Figure R22. P-PMO administration *in vivo*.** A new P-PMO was generated for treatment in mice to account for the one nucleotide difference. Then P-SC and P-PMO were administered by tail vein injection at 10 mg/kg. After four days, the mice were sacrificed and their blood and tissues analyzed.

Mice grip strength was measured before and after treatment and the percent normal force was calculated for each group (Figure R23A). The P-PMO treated mice showed a large increase in percentage of normal force. The change was statistically significant compared to the same mice treated with PBS through Student's t-Test. After treatment, blood serum was extracted from the mice for biochemical analysis (Figure R23B). The FVB levels were set as the healthy control level to which all other treatments were compared. One of the few significant changes was a decrease in creatine phosphokinase

(CPK) levels. CPK is released into the blood during muscle tissue damage (Veenstra *et al.*, 1994). The lower amounts seen here indicate a lack of tissue damage and are within the range for normal levels in healthy mice. Also significantly different from FVB are the amylase levels after treatment with the P-PMO and, curiously, the PBS control. However, after closer look, these levels were also within the normal range for healthy mice. Importantly, the

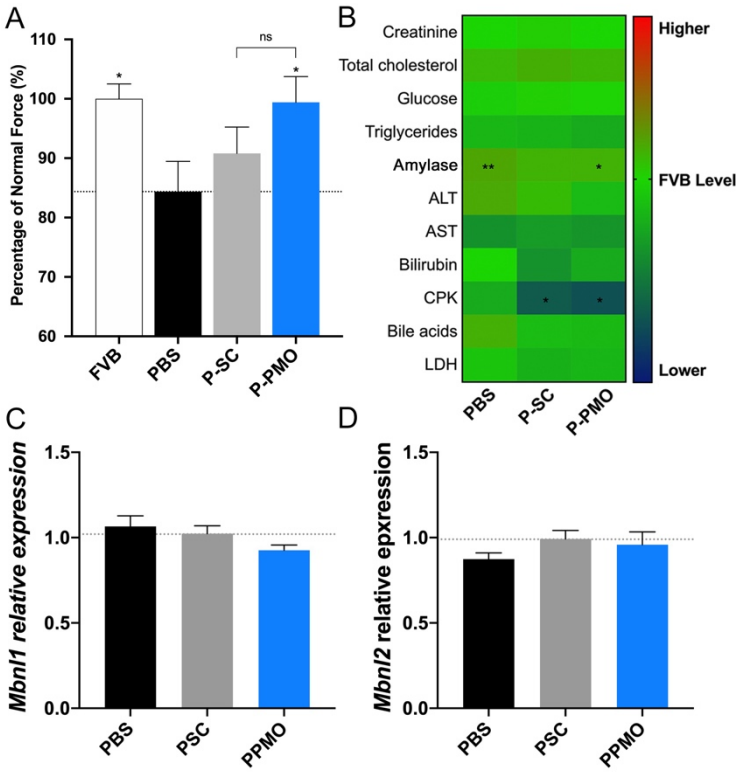


**Figure R23. Pip9b2-linked blockmiR affects grip strength without toxicity. (A)** Mouse grip strength was measured before and after treatment with P-PMO or P-SC by grip meter to calculate the percent of normal force normalized to mouse weight. Student's t-Test was used for statistical comparison. **(B)** Blood serum biochemistry was analyzed after treatments. All samples were statistically compared to FVB mice through Kruskal-Wallis ANOVA and Wilcoxon test if applicable. All parameters were within the normal range for healthy mice. Relative expression of **(C)** *Mbnl1* and **(D)** *Mbnl2* transcripts was relatively quantified in triplicate from muscles after treatment with P-PMO and P-SC in quadriceps muscles. Values were normalized to endogenous *Gapdh* and compared to P-SC using Student's t-Test. P-value GP style: 0.1234 (ns), 0.0332 (*), 0.0021 (**), 0.0002 (***), <0.0001 (****). Error bars = SEM.

rest of the parameters indicating hepatotoxicity or tissue damage, including ALT, AST, bilirubin, bile acids, and LDH, remained unchanged after blockmiR treatment. Other health indicators such as creatinine, cholesterol, glucose, and triglycerides, as well as mouse weight were also stable. No change was observed in the levels of *Mbnl1* or *2* relative expression (Figure 23C-D).

### III.III. BlockmiR induces rescue in HSA$^{LR}$ mice phenotypes

After seeing promising results at the physiological level, the mice were analyzed at the molecular level for changes in the DM1 phenotype specifically in the quadriceps leg muscle. Little change was observed in any parameter in gastrocnemius muscle therefore the results have been excluded from analysis. Transcripts *Atp2a1*, *Clcn1*, *Mbnl1*, and *Nfix* all show abnormal fetal splicing patterns in the DM1 mice model (Dixon *et al.*, 2015; Du *et al.*, 2010; Lin *et al.*, 2006; Tanner *et al.*, 2021). After blockmiR administration, correction was seen in all four transcripts (Figures R24A-D). The percent splicing recovery compared to the P-SC control showed significant rescue.

As seen in DM1 cell microscopy, the P-PMO also increased the amount of Mbnl1 protein (Figure R24E-F). Jess Simple Western technology was used to quantify the level of Mbnl1 normalized to the total protein level. The P-PMO showed significant increase compared to the P-SC and the HSA$^{LR}$ PBS control.

Finally, a histological analysis was made of 10 $\mu$m sections of the quadriceps muscle (Figure R24G-K). After H&E staining, the percent of muscle fibers with central nuclei were quantified. Although not statistically significant when averaging all six mice, a decrease in the percent of fibers with central nuclei was observed in comparison to the P-SC samples. There were two specific mice that showed particularly strong rescue. The image in Figure

R24K is representative of one of these mice and shows a striking resemblance to the FVB cuts.

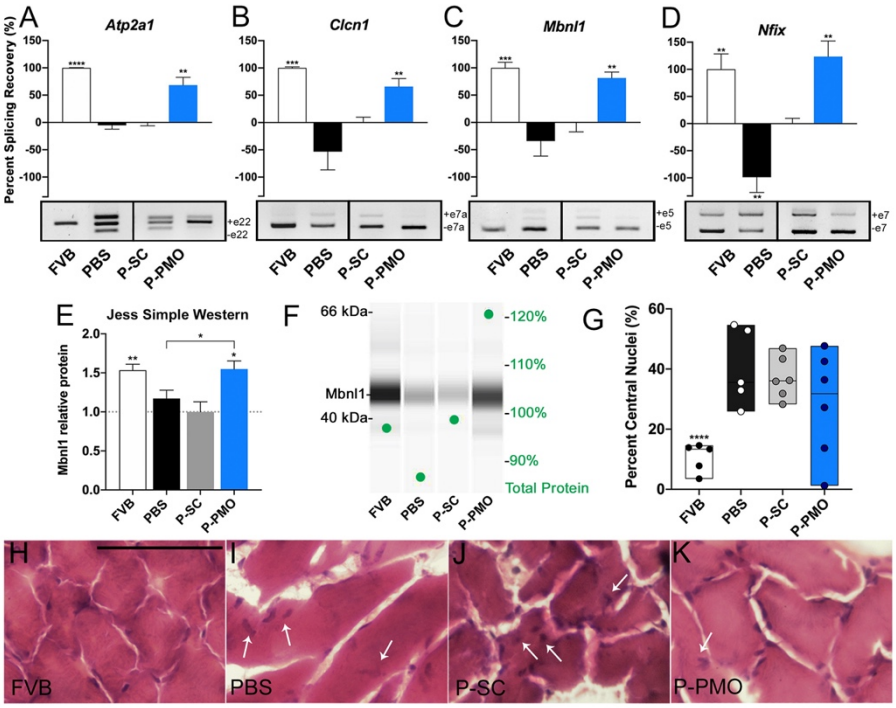


**Figure R24. P-PMO blockmiR rescues molecular and histological phenotypes of HSA$^{LR}$ mice.** Semiquantitative RT-PCR was performed to analyze alternative splicing patterns in exons of interest for **(A)** *Atp2a1* **(B)** *Clcn1* **(C)** *Mbnl1* and **(D)** *Nfix* transcripts. *Gapdh* was run as an endogenous control (see Figure R24). PSR was calculated normalized to FVB samples. Representative gels can be seen below each graph. **(E)** Relative protein was quantified using Jess Simple Western technology. **(F)** A representative lane view shows the bands observed compared to total protein normalization (green dots and scale). Finally, 10 µm sections of quadriceps muscle were cut and stained with hematoxylin and eosin in order to visualize the localization of central nuclei within the muscle fibers. **(G)** An average of 500 fibers were analyzed per mouse. Representative images of each treatment can be seen in **(H-K)**. Black scale bar = 50 µm. The white arrows signal nuclei that have central localization. All samples were statistically compared to P-SC through Student's t-Test. P-value GP style: 0.1234 (ns), 0.0332 (*), 0.0021 (**), 0.0002 (***), <0.0001 (****). Error bars = SEM. SEM and number of fibers for panel G can be found in Table R2.

**Table R2. Statistical data for histological image quantification in Figure R24G.**

| Mouse | Mean | SEM | # of fibers |
|---|---|---|---|
| FVB1 | 38.91 | ±0.32 | 1791 |
| FVB2 | 39.61 | ±0.57 | 455 |
| FVB3 | 32.79 | ±0.38 | 877 |
| FVB4 | 28.50 | ±0.71 | 452 |
| FVB5 | 38.36 | ±0.34 | 816 |
| PBS1 | 77.86 | ±1.38 | 276 |
| PBS2 | 50.92 | ±1.00 | 297 |
| PBS3 | 60.57 | ±1.24 | 424 |
| PBS4 | 79.69 | ±0.98 | 342 |
| PBS5 | 57.89 | ±0.75 | 799 |
| P-SC1 | 68.36 | ±1.42 | 214 |
| P-SC2 | 71.89 | ±0.98 | 575 |
| P-SC3 | 56.83 | ±1.09 | 332 |
| P-SC4 | 60.90 | ±1.21 | 178 |
| P-SC5 | 53.32 | ±0.67 | 738 |
| P-SC6 | 61.24 | ±1.02 | 482 |
| P-PMO1 | 61.41 | ±1.48 | 238 |
| P-PMO2 | 39.29 | ±0.59 | 1325 |
| P-PMO3 | 72.69 | ±1.28 | 180 |
| P-PMO4 | 26.22 | ±0.93 | 325 |
| P-PMO5 | 52.22 | ±0.86 | 953 |
| P-PMO6 | 67.55 | ±2.26 | 88 |

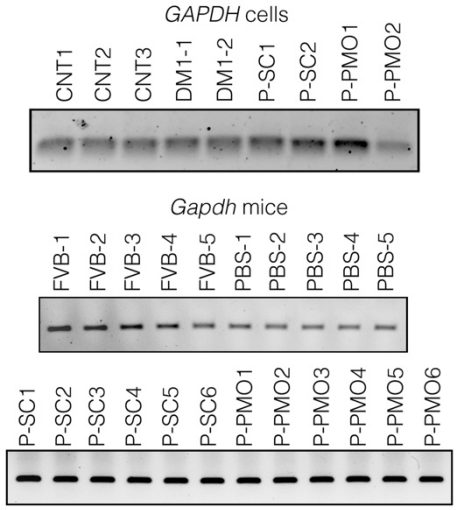


**Figure R25. Endogenous GAPDH controls.** Semiquantitative RT-PCR was performed to analyze alternative splicing patterns in exons of interest for *Atp2a1*, *Clcn1, Mbnl1*, and *Nfix* transcripts in DM1 cells and mice. *GAPDH* and *Gapdh* was run as endogenous controls.

# Discussion

There are currently no disease-modifying therapies that address more than one symptom in DM1. Despite all the encouraging results obtained in animal models using different oligonucleotide-based approaches in DM1 treatment, only one AON-based drug has ever entered past phase 2 clinical trials (ClinicalTrials.gov Identifier: NCT02312011) (Pascual-Gilabert *et al.*, 2021). The primary goals of the clinical trial were to use dose escalation to evaluate safety, tolerability, and muscle tissue effects of the drug as well as search for drug interaction biomarkers.

Despite the relevant results achieved using this AON in murine models, the development of this drug was discontinued because of inadequate therapeutic benefit in short-term trials in DM1 patients (see Ionis Pharmaceutical Report (Mignon, 2017)). However, IONIS pharmaceuticals have reported pertinent conclusions from this study. First, that heterogeneity of the patient population within and across dosing groups complicated the interpretation of results. Second, that the limited effect of the treatment may be because the drug did not reach target concentrations in muscle tissue of trial participants. Therefore, more potent chemistries or improved muscle delivery technologies would circumvent the poor efficacy of this drug in patients. Once the barrier of delivery in human patients is surmounted, the promising therapeutic effects of antisense technology may be realized. At least five AON pharmaceuticals are currently in preclinical phase study (Pascual-Gilabert *et al.*, 2021). To this end, the advancement of efficient drug possibilities was the overarching aim of this thesis divided into three objectives.

## I. FANA antimiRs

### I.I. AONs targeting miRNAs can be delivered gymnotically

Building upon the success of antagomiR-23b and antagomiR-218 in DM1 cells (Cerro-Herreros *et al.*, 2018), new AONs were designed to target miR-23b and miR-218. The antisense technology used to target miRNAs incorporated third

generation 2'-fluoro modifications, also known as FANA antimiRs. The most distinguishing feature of FANA is that they can be delivered gymnotically to cells without the use of transfection reagent. As seen in Figures R1C and R1D, the transfection reagent causes a significant reduction in cell viability. Importantly, the FANA antimiRs are also less toxic to cells than the antagomiRs even when both were delivered gymnotically. Strictly from a chemical perspective, it can be deduced that FANA modifications cause less cell death in DM1 cells 4 days after transfection than those with 2'-*O*-methyl modifications, even at higher concentrations.

Interestingly, second generation 2'-fluoro gapmer AONs have shown toxicity in HeLa cells and hepatotoxicity in mice (Shen *et al.*, 2018). This is interesting because FANA modifications only differ from second generation 2'-fluoro AONs in that the fluorine on C2 is conformationally trans to the phosphate group instead of cis (Figure D1). Similarly, the *O*-methyl group on 2'-OMe oligos is also cis to the phosphate group. Perhaps the trans conformation of modifications on C2 is key to reducing toxic response of second generation AONs. Indeed, in endogenous RNA, C2 only carries a small cis -OH group while DNA has just a hydrogen. It is possible that the size of the *O*-methyl or fluorine groups attached in the cis conformation on C2 is sterically bulkier than in the trans conformation. The trans C2 fluorine could be balancing the sugar molecule making it more stable and tolerable as seen in these results.

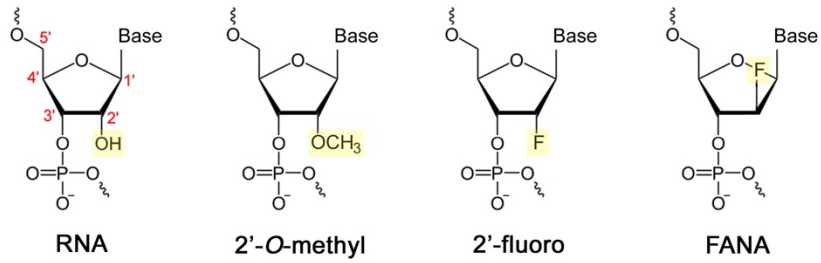


**Figure D1. Chemical modifications on C2 of the nucleotide sugar.** Each carbon is numbered in red and the C2 modifications are highlighted in yellow.

## I.II. FANA antimiRs show functional rescue of DM1 phenotypes

Not only did the antimiRs have low toxicity, but they also were able to improve other DM1 dysfunction in cells. *MBNL1* and *MBNL2* expression were both increased after treatment with miR-23b-1 and miR-218-1. Similar to antagomiR-218 in Cerro-Herreros *et al.*, 2018, even miR-218-1 was able to increase *MBNL1* expression at higher concentrations (Figure R2A) even though it has no binding sites on the *MBNL1* 3'UTR but could have binding sites elsewhere. MiR-218-1 also showed a 2.5-fold increase in MBNL1 protein at 1 μM. This could be due to the partial redundancy of the MBNL1 and 2 proteins and regulatory feedback loops existing between the two (Konieczny *et al.*, 2017). In this way, increase in one protein could be expected in the other.

Indeed, miR-218 has already been shown to be over-expressed in several DM1 models including, $HSA^{LR}$ mice, patient-derived myotubes and biopsies (Cerro-Herreros, 2021). The overexpression of miR-218 was also positively correlated to the number of CTG repeats found in the patient biopsies. Therefore, miR-218 is not only a regulator of MBNL1 translation but its overexpression is a part of the DM1 phenotype. AntagomiR-218 was just as capable of rescuing MBNL1 relative protein expression as AntagomiR-23b (Table D1). This suggests the existence of signaling between miRNA regulation and *MBNL* transcripts in DM1.

AntagomiR-23b had higher rescue of *MBNL1* expression at three times the level of SC treated DM1 controls, whereas FANA miR-23b-1 increased the expression by 1.7 times the controls (Table D1). MiR-218-1 only had rescue of *MBNL1* transcript when administered at higher concentrations. For *MBNL2* transcript expression, both FANA antimiRs showed similar rescue to the antagomiRs by increasing the transcript approximately 1.5-1.7 times.

**Table D1. AntagomiR-23b and -218 and FANA effects in DM1 cells (Cerro-Herreros *et al.*, 2018).** All values listed are approximate fold changes.

| | **AntagomiR-23b** (50 nM) | **AntagomiR-218** (200 nM) | **FANA miR-23b-1** (1 μM) | **FANA miR-218-1** (1 μM) |
|---|---|---|---|---|
| ***MBNL1*** | 3X increase | 1.9X increase | 1.7X increase | No change |
| ***MBNL2*** | 1.5X increase | 1.5X increase | 1.7X increase | 1.5X increase |
| **miR-23b** | 0.1X decrease | -- | 0.3X decrease | -- |
| **miR-218** | -- | 0.3X decrease | -- | Total reduction |
| **MBNL1** | 5X increase | 4X increase | 2X increase | 2.5X increase |
| **MBNL2** | 2.3X increase | 3.5X increase | No change | 1.5X increase |
| ***BIN1 ex11*** | Rescue | Rescue | Rescue | No change |
| ***cTNT ex5*** | No change | No change | Rescue | No change |
| ***MBNL1 ex5*** | -- | -- | Rescue | No change |

Recently, the competing endogenous RNA (ceRNA) hypothesis has given possible explanation to the finely tuned balance of RNA regulation (Ala, 2020). In this hypothesis, it is proposed that RNAs that are targeted by the same miRNAs can indirectly regulate one another due to the competitive binding of these miRNAs from shared miRNA response elements (MREs). For instance, in DM1, miR-23b has binding sites on both *MBNL1* and *MBNL2* 3'UTRs. According to the theory of ceRNAs, competitive binding of miR-23b between *MBNL1* and *2*, could cause decreased miRNA regulation of both transcripts through indirect crosstalk of ceRNAs between the *MBNL1* and *2*. Taking into account this hypothesis, decreasing the amount of miR-23b by antimiRs would have an effect on both transcripts.

This hypothesis also applies to the increase in *MBNL1* at higher concentrations of miR-218-1. When miR-218-1 derepresses the expression of *MBNL2*, higher levels of *MBNL2* transcripts could sponge more miR-23b and in turn also derepress expression of *MBNL1* since miR-23b regulates both transcripts. Thus, the ceRNA hypothesis could help explain why RNA transcripts sharing MREs may have coordinated changes in expression patterns.

Importantly, FANA antimiRs reduced the relative expression of their respective miRNAs by half or more when compared to DM1 controls. (Figure R2C-D). This is the same amount of reduction seen by antagomiRs when compared to their SC controls (Table D1). Curiously, the FANA scrambled controls also showed a decrease in miRNA levels even though they are not predicted to have any specific binding. However, even compared to these scrambles, the FANA antimiRs still provoked a stronger reduction. As previously stated, the levels of miRNA regulation are dependent on a complex system of direct and indirect signaling through miRNA 3'UTR binding as well as ceRNA crosstalk. Although the scrambles are not predicted to bind to miR-23b or miR-218, this does not preclude the existence of shared MREs with other miRNAs which could affect these levels.

Also of note are the technical difficulties of precise miRNA quantification after treatment with AONs. The short length of miRNAs makes RT-qPCR particularly difficult, which is why a precursor Poly-A adaptor step is taken during reverse transcription to increase the length of the sequences and therefore the efficiency of binding of specific miRNA primers. However, this step does not preclude the interaction of the antimiRs themselves. As they are also short sequences, it is possible that RT-qPCR could be quantifying the antimiRs along with the miRNAs of interest. It is also unknown how strongly, or reversible, the binding is between miRNA and its respective antimiR. The RNA extraction and purification process also complicates this factor. Finally, although the FANA antimiRs are predicted to be RNase-H active, destruction is not guaranteed, and RT-qPCR could still be detecting non-functional miRNA. However, as evidenced by the low expression levels of miR-23b and miR-218 after treatment with FANA antimiRs compared to controls, it is most likely that true miRNA destruction is occurring.

Finally, the FANA antimiRs also showed effective MBNL1 and 2 protein increase as well as functional rescue of certain splicing patterns (Figure R3). In comparison, antagomiRs-23b and -218 effectively quadrupled the amount

of MBNL1 while miR-23b-1 and miR-218-1 doubled it (Table D1). The antagomiRs also showed higher rescue of MBNL2 protein. MiR-23b-1 was unable to rescue MBNL2 levels while miR-218-1 did significantly increase them 1.5 times. On the contrary, miR-218-1 failed to rescue splicing patterns, however miR-23b-1 was able to significantly recover *BIN1*, *cTNT* and *MBNL1* exon splicing (Figure R3C). An additional transcript, *SPTAN*, which is known to be regulated by MBNL2 was also analyzed in order to see if miR-218-1 only had effects on *MBNL2* regulated transcripts. A slight increase in the inclusion of exon 23 can be seen but is not statistically significant. AntimiR miR-23b-1 had a qualitatively similar, but slightly weaker, pattern of rescue of *BIN1* as antagomiR-23b (Table D1). Interestingly, miR-23b-1 was able to significantly rescue *cTNT* exclusion when antagomiR-23b could not.

### I.III. FANA antimiR modifications could be a safety improvement to antagomiRs

The results seen in this objective are encouraging advances in the safety of AONs. The use of 2-*O*-methyl antagomiRs with a cholesterol moiety showed stunning improvements in disease related phenotypes in Cerro-Herreros *et al.*, 2018. FANA antimiRs miR-23b-1 and miR-218-1 were designed and administered with the hypothesis of providing similar therapeutic effects of the antagomiRs while causing less cell death. This was achieved with the increase of *MBNL1* and *2* transcripts and the decrease of miR-23b and miR-218 to their respective AON all while having significantly fewer toxic effects in DM1 cells in comparison to the antagomiRs. Additionally, the antimiRs were also capable of improving molecular defects such as increasing MBNL1 and MBNL2 proteins. MiR-23b-1 also showed promising recovery of splicing patterns.

To conclude, FANA modifications could be a potential improvement to the already successful antagomiR strategy in DM1 therapy. Although FANA antimiRs had more subtle disease recovery effects, they were still able to

reproduce the same molecular improvements with higher cell viability. This could be due to the non-toxic fluorine modifications which are less toxic than 2'-OMe modifications. However, the cholesterol moiety of the antagomiRs may have been key to their higher potency *in vivo*. Cholesterol conjugations are popular attachments to other larger drugs such as polymers for its natural permeability to cell membranes (Misiak *et al.*, 2020). Indeed, the cholesterol-conjugation on siRNAs has helped with association to plasma lipoproteins (Seth *et al.*, 2019).

Most informative would be future experiments in mice to test for physiological improvements and blood and serum inflammatory biomarkers. This could also be performed in the form of dose and time response experiments. Also of interest could be to test the delivery of both antimiRs at once targeting miR-23b and miR-218 at the same time.

## II. LNA blockmiRs

### II.I. Targeting miRNA binding sites is effective in cells

After exploring the effects of FANA AONs, a new possibility was explored using an alternative pathway for modulating miRNAs implicated in DM1. The use of blockmiR technology is a highly specific method of blocking miRNA binding sites in order to restore MBNL protein function in DM1 cells without disturbing the regulation of other non disease-related miRNA targets. The goal of the blockmiRs was to cause meaningful improvements in the DM1 phenotype with little toxicity and off-target effects. This strategy is a refinement of the already successful antagomiR study which identified miR-23b and miR-218 as regulators of Muscleblind-like proteins.

For proof-of-concept, a set of five blockmiRs targeting each binding site on *MBNL1* or *MBNL2* were first tested in cells. The third generation LNA-based oligos showed an increase in the expression of *MBNL* transcripts as well as corrected alternative splicing (Figure R5). Specifically, M1-Block-23b-1 and

M2-Block-23b-1 showed particular rescue of *MBNL1* and *2* transcripts as well as *MBNL1* and *SPTAN1* mis-splicing. Importantly, *MBNL1* exon 5 inclusion is associated with the nuclear localization of MBNL1 proteins (Tran *et al.*, 2011; Wang *et al.*, 2018). Indeed, the same blockmiRs with exon 5 rescue made a significant change in the intensity and subcellular localization of MBNL1 proteins in the cell. This is a critical therapeutic effect in DM1 treatment, as MBNL sequestration in the nucleus is the limiting factor in this disease. M1-Block-23b-1 specifically showed a dose response increase of MBNL1 protein when treated at increasing concentrations.

It is curious that M1-Block-23b-1 was able to upregulate the activity of *MBNL2* due to the fact that the blockmiR is specific only to *MBNL1* and vice versa for M2-Block-23b-1. An explanation for the case of M1-Block-23b-1 could be that the increase in *MBNL1* transcripts after blockmiR treatment logically increases available binding sites for miRNAs. In turn, these transcripts act as "sponges" for miRNAs relative to *MBNL2*. This is also related to the previously mentioned theory of ceRNAs in which transcripts with the same MREs can have crosstalk through competitive binding (Kartha and Subramanian, 2014). Concretely, *MBNL1* and *MBNL2* share common MREs. As *MBNL1* expression is increased, so is miRNA binding to *MBNL1*, leading to less miRNAs downregulating *MBNL2* thereby increasing its relative expression as well. This also could explain why slight rescue was seen in *SPTAN1* alternative splicing after treatment with M1-Block-23b-1 even when *SPTAN1* is regulated by MBNL2 proteins. This "decoy" theory has already been described in relation to *PTEN* and its respective miRNAs (Rigoutsos and Furnari, 2010).

Curiously, the M2-Block-218-2 showed a large increase in MBNL1 pixel intensity without any *MBNL1* or *-2* transcript increase or *MBNL1* splicing rescue (Figure R7). This could also be due to MBNL protein functional overlap mentioned previously. Another hypothesis is that perhaps the de-regulation of *MBNL2* transcripts and subsequent increase in MBNL2 protein

could increase competitive binding to the *DMPK* repetitions. In this way it is possible that an increase in MBNL2 could trigger an increase in functional MBNL1 that has been released from *DMPK* repetitions.

It is also curious that though MBNL1 protein was increased after treatment with M2-Block-218-2, there was no discernable splicing rescue in MBNL1 exon 5. Indeed, exon 5 inclusion is associated with the nuclear localization of MBNL1 proteins. However, the exclusive distribution of MBNL1 in the nucleus relies on the concurrent inclusion of exon 5 and exon 6 in *MBNL1* (Tran *et al.*, 2011). Therefore, even though the DM1 cells still showed exon 5 inclusion after treatment with M2-Block-218-2, exon 6 exclusion could be responsible for contributing to the cytoplasmic subcellular distribution. There is also evidence for the role of exon 7 in the effects on MBNL1 localization (Konieczny *et al.*, 2014).

Another explanation for this splicing pattern could be due to the site-specific nature of the blockmiRs. Unlike antagomiR technology, blockmiRs only block binding sites of miRNAs, not the miRNAs themselves. In this way, the miRNA of interest is still free to bind to other target sites. In the context of this experiment, miR-218 could still bind to other binding sites on *MBNL2* while M2-Block-218-2 is bound and cause regulation of the transcript. Repression of miR-218 on *MBNL2* could cause an overcompensation of miR-218 activity on other 3'UTR binding sites. Perhaps blocking all miR-218 sites at one time would increase effectiveness such as the combinatorial usage of M2-Block-218-1 and -2, and -3. Also, DM1 model cells can show repeat instability which could cause potential variability in treatment (Tome and Gourdon, 2020).

### II.II. BlockmiR strategy is highly specific at transcriptome level

M1-Block-23b-1 was chosen as the candidate compound after the preliminary screening due to its performance in cells and due to the fact that this is the

only binding site for miR-23b in human *MBNL1* 3'UTR. Therefore, potential effects could be more easily interpreted. After performing RNA sequencing and looking at the top 25 genes rescued by M1-Block-23b-1 treatment, a network of important proteins involved in muscle function and infrastructure was revealed through STRING analysis (Figure R9C). Most notably the myosin heavy chain (MYH) family of proteins and myogenin protein (MYOG) are critical in cell signaling for myogenic differentiation of myoblasts into mature skeletal muscle (Jang and Baik, 2013). Indeed, upregulation of the MYH family of proteins is strongly associated with DM patient biopsies (Vihola et al., 2010).

When compared to the previously studied antagomiR-23b, M1-Block-23b-1 showed gene expression recovery less dramatically than antagomiR-23b (Figure R10). Indeed, the antagomiR is a miRNA specific technology while the blockmiRs are site-specific. However, there were no cases of blockmiR induced over-recovery unlike antagomiR treated cells where 108 genes were over-recovered. Finally, the blockmiR had no effect on other miR-23b targets whereas antagomiR-23b had many (Figure R11). This confirmed the hypothesis that the blockmiR strategy has highly specific effects on the cell transcriptome and merits further study *in vivo*.

### II.III. miRNA binding sites are conserved in mice

Through dual luciferase assay, the two predicted binding sites of miR-23b were confirmed on the *Mbnl1* 3'UTR (Figure R12). This is of key significance when it comes to the preclinical analysis of blockmiRs and the future of miR-23b investigation in the context of DM1. *Mus musculus* models are critical for preclinical testing any potential human therapy due to its homology with humans. But although they are similar, the human and mouse binding site does contain one nucleotide difference. For this reason, both a human and a mouse version of the blockmiR were generated. This is because, though the human version may not bind with high specificity, it can still give us critical

information about the chemistry's specificity, delivery, tolerability and will be valuable for other future *in vivo* testing. Therefore, if the drug performs well in mice, there is a foundation already established *in vivo* for the human version.

If predicted binding site 2 had not been conserved in mice, M1-Block-23b-1 would have been unable to move forward in this model and a substitute would have been necessary. For instance, M2-Block-218-2 showed considerable therapeutic value in DM1 myoblasts. The binding site for this blockmiR closely matches predicted binding Site 2 in mouse *Mbnl2* 3'UTR. This compound could have certainly been a viable backup for further study if the miR-23b binding site was absent. This also allows for the possibility of future combinatorial experiments such as co-transfecting M1-Block-23b-1 and M2-Block-218-2. In this way, two different implicated miRNAs could be blocked on two different important transcripts: *MBNL1* and *MBNL2*. Perhaps the simultaneous dosage of these two blockmiRs could have a synergistic effect. Clearly, the modulation of even just one miRNA binding site has shown to have effects on both MBNL1 and MBNL2. It is possible that dual administration could have a compounded effect like increasing the expression of *MBNL1* and *2* transcripts caused by M1-Block-23b-1 while also incorporating the strong *SPTAN* splicing rescue and immunofluorescence of M2-Block-218-2.

### II.IV. BlockmiRs induce toxicological changes

After the WBC, CBC, and biochemical blood and serum analysis, M1-Block23b-M showed various changes when compared to FVB while M1-Block23b-H remained near the same level as PBS. First in the WBC count, there was a large variation in the reference FVB levels (Figure R15). This could be due to differences in age, diet, and other living conditions becoming variables in different laboratories. Curiously, our labs 12-18 week-old FVB mice and $HSA^{LR}$ mice (PBS) most closely matched the ratios seen in 8 week

males from Bogue *et al.*, 2020. In comparison to the PBS treated mice in our lab, treatment with M1-Block23b-H increased the number of neutrophils slightly, while decreasing lymphocytes. M1-Block23b-M treatment most notably increased monocytes and lymphocytes, decreasing neutrophils. High monocytes and lymphocytes usually occur after an infection as an immune response. This suggests an inflammatory response to M1-Block23b-M as, according to O'Connell *et al.*, 2015, general mice monocyte levels are typically seen at <2%.

Many significant changes were observed when comparing M1-Block23b-M to FVB levels in the CBC and biochemical analysis. However, when these results are put in context of the added reference FVB levels, some of the values that were significantly changed were still within the known values of healthy FVB ranges such as platelets, alkaline phosphatase, and LDH.

In some cases, M1-Block23-M caused a favorable change such as lowering cholesterol, RDW, AST, ALT, and CPK (Cabaniss, 1990; Evans and Jehle, 1991; Gowda *et al.*, 2009; Senior, 2012; Tabas, 2002). Indeed, in this case, the decreases in ALT and AST also caused the AST:ALT ratio to decrease. An AST:ALT ratio closer to 1 is considered healthy (Botros and Sikaris, 2013). Additionally, CPK, cholesterol, LDH, and ALT have all been found increased in DM2 (Heatwole *et al.*, 2011). Therefore, their decrease after treatment with M1-Block23b-M could be interpreted as favorable. When comparing to all-LNA gapmers that showed high toxicity in hepatic biomarkers in CD-1 mice (Burdick *et al.*, 2014), ALT, AST, and alkaline phosphatase levels of blockmiR treated mice were well within the control values as well.

Some results are less clear, concretely the decreased levels of MCV and increased MCH. Typically, the amount of hemoglobin mirrors the cell volume (Sarma, 1990). While lower levels of MCV are not necessarily cause for alarm, the inverse changes to this level in comparison to the MCH is unusual and could indicate anemia or vitamin deficiency. This is supported

by the increase in MCHC which can have similar causes (Northrop-Clewes and Thurnham, 2013; Sharma *et al.*, 2010). Finally, low amylase is linked to insulin resistance, a common symptom in DM1 patients (Nakajima, 2016). Overall, the drug was tolerated generally well with no significant changes in weight. But there is room for improvement on the acceptance of this particular chemistry. More information on hepatic reporter RNA levels would be helpful to better understand the exact of the effects of this drug.

## II.V. BlockmiRs are also viable *in vivo*

M1-Block23b-M, administered at the same concentration and treatment time as antagomiR-23b (12.5 mg/kg; 4 days), was able to make stunning increases in *Mbnl1* transcript expression and protein. *Mbnl1* expression and Mbnl1 protein were increased 2.8 – 3.2-fold after blockmiR treatment in quadriceps. To compare, antagomiR-23b when treated in mice, increased *Mbnl1* transcript by 1.5 and Mbnl1 protein by 2 (Table D2).

Mice grip strength was also fully restored with the use of M1-Block23b-M (Figure R18) just as antagomiR-23b (Table D2). The percentage of central nuclei was also decreased by M1-Block23b-M similar to antagomiR treatment. FVB quadriceps percentages stayed around 15% while fibers from M1-Block23b-M treated mice had on average 20% central nuclei; a significant decrease compared to PBS (Figure R19).

**Table D2. AntagomiR-23b and -218 effects in HSA$^{LR}$ mice quadriceps (Cerro-Herreros *et al.*, 2018 and 2020).** All values listed are approximate fold changes or percentages.

| | **AntagomiR-23b** (50 nM) | **LNA blockmiR** (50 nM) | **P-PMO blockmiR** (1 μM) |
|---|---|---|---|
| ***MBNL1*** | 1.5X increase | 2.8X increase | No change |
| **MBNL1** | 2X increase | 3.2X increase | 1.5X increase |
| **Grip strength** | 90% | 110% | 100% |
| **% of fibers w/ central nuclei** | 15% | 20% | No change |
| ***Atp2a1 ex22*** | Rescue | No change | Rescue |
| ***Clcn1 ex7a*** | Rescue | No change | Rescue |

| | | | |
|---|---|---|---|
| ***Mbnl1 ex5*** | -- | No change | Rescue |
| ***Nfix ex7*** | Rescue | -- | Rescue |

In splicing, blockmiRs showed less consistent results (Figure R18). However, mice 2 and 3 showed exceptional rescue of fetal splicing patterns in *Atp2a1*, *Clcn1*, and *Mbnl1*. The qualitative splicing patterns of mice 2 and 3 after blockmiR treatment showed similar patterns to antagomiR-23b rescued samples in transcripts *Atp2a1* and *Clcn1*. The rescue of these transcripts is of clinical importance to DM1. *Atp2a1* exon 22 exclusion is associated with muscle dysfunction, *Clcn1* exon 7a inclusion is associated with myotonia, and *Mbnl1* exon 5 inclusion is associated with MBNL1 subcellular localization (Table I1). Indeed, antagomiR-23b which also showed *Clcn1* splicing restoration in mice, showed a tendency towards a reduction in myotonia.

Overall, M1-Block23b-M showed curative effects in DM1 cells and $HSA^{LR}$ mice that were comparable to previously studied antagomiR-23b. The experiments seen here demonstrate a proof of concept that site-specific binding by AONs to miRNA 3'UTR regulation sites can have similar effects to targeting the miRNAs themselves. The important advantage to this method was shown through RNA-Seq in that the blockmiRs had less effects on the wider transcriptome in human cells. High specificity is a key goal for AON design in order to mitigate undesired off-target effects.

However, of singular importance in drug development is safety and tolerability. Third generation LNAs are certainly an improvement of previous AON stability due to the bridged carbons on the sugar molecule. But the chemistry could be lacking in regards to *in vivo* immune response. Indeed, M1-Block23b-M was able to ameliorate certain disease related biochemical parameters such as cholesterol however some of the WBC and CBC parameters showed unexplained changes (Figures R15-16). Reference values from healthy FVB mice were added to the results to help interpret the significance of these changes. These values can vary greatly depending on

mouse age, sex, and general laboratory conditions. Furthermore, there simply is not enough data on the baseline values of $HSA^{LR}$ mice to make meaningful conclusions. Consequently, the development of a similar AON is necessary in order to introduce the lowest amount of toxicological perturbations. To this end, cell-penetrating peptide, Pip9b2, conjugated morpholinos were developed.

## III. P-PMO blockmiRs

### III.I. Pip9b2 modified blockmiRs reproduce similar recovery to LNA blockmiRs

A significant increase in MBNL1 protein was observed after treatment with P-PMO blockmiR in cells through immunofluorescence analysis and in mice through Simple Western. Importantly, the treatment also did not over rescue the abundance of MBNL1 as the levels reached were comparable to the healthy controls. The MBNL1 protein increase was also functional as evidenced by the significant splicing rescue in cells and mice. MBNL proteins play a critical role in the alternative splicing patterns of the transcripts. Specifically, a recent study comparing mis-spliced transcripts in $HSA^{LR}$ mice to Mbnl1−/− and Mbnl2+/− knockout mice showed 81% overlap which included *Atp2a1*, *Clcn1*, *Mbnl1*, and *Nfix* (Tanner *et al.*, 2021). Indeed, *ATP2A1*, *MBNL1*, and *NFIX* splicing correction showed a dose response to *MBNL1* knockout in human cells (Wagner *et al.*, 2016). Likewise, *Clcn1* also shows response to *Mbnl* knockout (Choi *et al.*, 2015). The results of P-PMO blockmiR treatment not only indicates an increase in MBNL1 protein but the rescue of the various transcripts in cells and mice also indicates an upstream rescue of MBNL1 functionality. The functionality of Mbnl1 is also evidenced by the increase in mice grip strength.

Curiously, the splicing improvements in mice by P-PMO blockmiR were much superior to the splicing patterns seen after treatment with LNA-based M1-Block23b-M (henceforth referred to as LNA blockmiR). Both P-PMO and

LNA blockmiR had similar increases of MBNL relative protein expression and grip strength. Conversely, in the case of histochemistry, the LNA blockmiR had a more consistent and stronger effect than P-PMO blockmiR. The abundance of central nuclei decreased greatly for two mice in particular after treatment with P-PMO blockmiR but was not statistically significant.

Interestingly, P-PMO blockmiRs showed no increase in either *Mbnl1* or *Mbnl2* transcripts even when they were both increased after treatment in DM1 cells. *Mbnl* transcript increase is not required for increase in Mbnl protein but is expected and has been seen after antagomiR and LNA blockmiR treatment. As more Mbnl is translated from miRNA de-regulation, it is likely that internal feedback loops can signal for the increase in even more Mbnl translation. In the case of P-PMO blockmiR, a large increase in Mbnl1 protein is observed as well as impressive splicing improvements. Just like 2'-OMe modifications, morpholinos are not predicted to activate the RNase-H degradation pathway. Therefore, it is curious that the *Mbnl* transcripts do not correspond to the increase in protein. A future immunofluorescent microscopy experiment tagging the localization of *Mbnl* transcripts or P-PMO blockmiRs could give valuable information as to the subcellular quantities and locations of *Mbnl* after treatment.

One of the principal delimiting factors in antisense therapy is transporting the AONs across the cell membrane barrier (Crooke *et al.*, 2017). In an experiment testing the cell membrane of $HSA^{LR}$ mice, it was concluded that their cell membranes have a fully functional barrier (Gonzalez-Barriga *et al.*, 2015). Therefore, all ASO treatments in DM1 must consider the integrity of the cell. The therapeutic effects of P-PMO blockmiR seen here in cells and mice suggest that the cell-penetrating peptides are indeed capable of crossing the cell membrane. However, the most troubling observation here is the unsuccessful delivery to gastrocnemius muscle. Indeed, no significant therapeutic change was observed in gastrocnemius muscle after treatment with P-PMO. This weakness suggests inadequate delivery method rather

than ineffective chemistry because P-PMO blockmiR was capable of tremendous recovery in quadriceps. More likely, the dosage was not enough to reach all tissues or tail vein injection is not the most efficient administration method. Perhaps an intramuscular injection would be more effective. The P-PMOs should also be labelled and quantified in each tissue after injection to identify weaknesses.

Other possibilities include the use of tissue-specific AONs (Seth *et al.*, 2019). For example, Transferrin receptor 1 (TfR1; also known as CD71) -mediated delivery has been used for siRNAs in mice (Sugo *et al.*, 2016). TfR1 is an iron-binding glycoprotein found in abundance in cardiac and skeletal cells. By targeting TfR1 antibodies, anti-CD71 conjugated siRNAs were able to knockdown genes specifically in the heart and skeletal muscle and was particularly effective in gastrocnemius. Perhaps a more tissue targeted approach could improve the P-PMO delivery.

### III.II. Cell-penetrating peptide morpholinos are less toxic than LNA-based AONs

While both blockmiR chemistries were similar in the amount of MBNL protein rescue and splicing in cells, a striking difference was noticeable through toxicity assays. First, LNA blockmiR treated cells valued TC50 at 0.862 $\mu$M (Figure R4). P-PMO blockmiRs showed virtually no toxicity after treatment in DM1 cells even at concentrations as high as 10 $\mu$M (Figure R20). This difference was even perceptible through microscopy. Although, the immunofluorescence intensity of MBNL1 was nearly the same for both treatments, the P-PMO treated cells were visually much more proliferative. The P-PMOs are designed for safe cell entry without the use of transfection reagent. Qualitatively and quantitatively, the chemical safety advantages of cell-penetrating peptide technology are extremely apparent in cells.

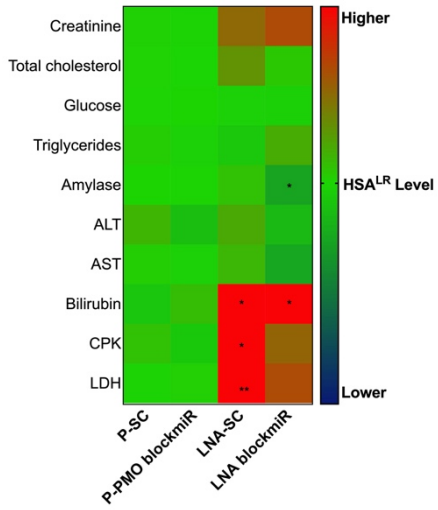


**Figure D2. Comparing P-PMO and LNA toxicity in mice.** Data compiled from Figures R15 and Figures R22. $HSA^{LR}$ mice treated with PBS were used as the normalization standard and all samples were compared to P-PMO blockmiR using Kruskal-Wallis ANOVA and Wilcoxon test if applicable. P-value GP style: 0.1234 (ns), 0.0332 (*), 0.0021 (**), 0.0002 (***), <0.0001 (****).

In agreement with results seen in cells, the P-PMO blockmiR showed significantly less changes in the biochemical parameters measured than LNA blockmiR. When compared to the levels of FVB, P-PMO blockmiR only showed a significant decrease in CPK and a slight increase in amylase. As mentioned before, increase in CPK is an indicator for muscle injury. The decrease seen here is well within the range of healthy levels of CPK. Additionally, amylase levels are significantly increased in PBS as well, indicating that this may be a disease related symptom and that the P-PMO has actually lowered this value.

To compare the toxicological differences, all biochemical parameters were combined from LNA and P-PMO treatments into a comprehensive heatmap compared to the average of PBS treated $HSA^{LR}$ mice from both experiments (Figure D2). This differs from previous figures that compared all treatments to the level of FVB mice. Here in figure D2, no conclusions are being drawn on whether the changes observed are therapeutic. Rather it is simply comparing which AONs induce significant changes in $HSA^{LR}$ mice. Compared to P-PMO blockmiR, the LNA-based scramble and blockmiR both induced significant changes in amylase, bilirubin, CPK, and LDH. Creatinine was also increased but not statistically significant.

Systemic administration of LNA gapmers have been known to show increased hepatotoxicity outside of DM1 (Burdick *et al.*, 2014; Swayze *et al.*, 2007). Burdick *et al.*, 2014 delivered mice a 3-8-3 gapmer design with LNAs on the ends at a concentration of 25 mg/kg. While Swayze *et al.*, 2007 tested various gapmer combinations in mice such as 4-10-4, 3-10-3, 3-12-3, and 2-14-2 at concentrations as high as 4.5 μM/kg. Here, LNA blockmiR has a 6-8-2 configuration in order to avoid such symmetry. It was also tested at 12.5 mg/kg (~2.3 μmol/kg) which is much lower than the toxic concentrations seen in previous studies. However, perhaps the LNA – 2'-OMe gapmer pattern is simply not well tolerated *in vivo*.

## IV. Preclinical conclusions

### IV.I. P-PMO blockmiRs are the safer option

While both LNA and P-PMO blockmiR were able to provoke significant beneficial changes in both DM1 cells and mice, it is clear through toxicological analysis that the P-PMO is better received in both disease models. Through cell-penetrating technology and highly stable morpholino design, the P-PMO was able to enter DM1 cells without the use of transfection reagent. Confocal microscopy showed that cells were intense and diffuse with MBNL1 fluorescence and highly proliferative. Subsequent toxicological analysis *in vivo* showed similar receptibility especially when compared to the LNA blockmiR. The P-PMO blockmiR also induced a stronger mis-splicing pattern reversal which could be interpreted as a stronger functional MBNL increase. The P-PMO chemistry has a critical safety advantage and merits further *in vivo* study that could potentially be applied to other antisense treatment strategies. Its disadvantage in lack of gastrocnemius muscle delivery is a challenge that could be overcome with further refinement. Just as was seen in the only DM1 AON clinical trial, sufficient delivery into the muscle tissue is one of the biggest obstacles in AON development.

## IV.II. MiRNA overexpression is part of the DM1 phenotype

Recently, Cerro-Herreros *et al*., 2018 published another significant contribution showing that miR-218 is over-expressed in several DM1 models including, $HSA^{LR}$ mice and patient-derived myotubes and biopsies. Preliminary data from our lab has shown that miR-23b also shows the same overexpression pattern in these samples. This discovery gives even greater significance to the potential therapeutic benefits of AONs targeting miRNAs in DM1. This finding also supports the incredible results seen from blockmiR treatment.

Since, miR-218 and miR-23b have both been shown to be a part of the DM1 disease phenotype, their modulation therefore merits the same focus that has already been given to AONs targeting CUG repetitions. Perhaps the future of DM1 therapy lies not in invasive repetition cutting and degradation, but in more subtle fine-tuning of the many miRNAs in balance. Indeed, with treatments like FANA antimiRs targeting just one miRNA, non-toxic improvements were seen in DM1 cells that mirror similar effects seen by preclinical phase DM1 drugs. Even more refined and specific blocking of miRNA binding sites with the use of LNA and P-PMO blockmiRs also showed potent therapeutic effects *in vitro* and *in vivo*. Most importantly, these experiments showed proof of concept that miRNA binding-site blocking has less off-target effects in the transcriptome than direct miRNA binding. Finally, the antisense chemistries tested in this study give elucidating information on the tolerability in cells and mice. Some of these drugs have never before been tested in the context of DM1 and the immunological responses documented here will be hugely beneficial for future selection of AON design. To conclude, the *in vivo* and *in vitro* success of miRNA modulation in DM1 is edifying evidence for antimiR and blockmiR marketability as restorative medicine for DM1 patients. Coupling the potency of miRNA knockdown with the safety and deliverability of state-of-the-art AON chemistries, potential is on the rise for an effective treatment for those suffering from DM1.

# Conclusions

## Conclusions

In sum, the following conclusions can be made:

1. AntimiRs with FANA modifications targeting miR-23b and miR-218 administered without the use of transfection reagent are a suitable alternative to antagomiRs with 2'-*O*-methyl modifications and a cholesterol moiety due to their increased cell viability in DM1 cells even at higher concentrations.
2. Gymnotic delivery of FANA antimiRs shows comparable therapeutic recovery to antagomiRs in DM1 cells by increasing *MBNL1* and *MBNL2* transcripts, reducing miR-23b and miR-218, and increasing MBNL1 protein in DM1 cells. MiR-218-1 was capable of increasing MBNL2 protein and MiR-23b-1 was capable of splicing rescue in *BIN1* exon 11, *cTNT* exon 5, and *MBNL1* exon 5.
3. Proof of concept was shown that blockmiRs targeting the binding sites of miR-23b or miR-218 were also capable of therapeutic effects in DM1 cells. Specifically, M1-Block-23b-1 and M2-Block-23b-1 both increased *MBNL1* and *MBNL2* transcripts, rescued *MBNL1* exon 5 and *SPTAN* exon 23 splicing patterns, and increased immunofluorescence and corrected subcellular localization of MBNL1 protein.
4. MiR-23b binding site blocking by blockmiRs caused approximately 40% less changes in the disease related transcriptome than direct miR-23b binding by antagomiRs.
5. The two predicted miR-23b binding sites on mouse *Mbnl1* 3'UTR were confirmed after dual luciferase assay. Site 3 for miR-218 binding on *Mbnl1* 3'UTR was confirmed, as well as Site 1 and possibly Site 2 on *Mbnl2* 3'UTR.
6. M1-Block-23b-1, termed LNA blockmiR, is viable *in vivo* showing an increase in grip strength and Mbnl1 transcript and protein in $HSA^{LR}$ mice quadriceps and gastrocnemius muscle. It also showed a significant decrease in central nuclei.

7. P-PMO blockmiR shows similar therapeutic effect to LNA blockmiR with no toxicity in DM1 cells.
8. P-PMO blockmiR is also viable *in vivo* showing increased grip strength and no toxic changes. In the quadriceps muscle of $HSA^{LR}$ mice, P-PMO also showed increased Mbnl1 protein, and rescued splicing events in *Atp2a1* exon 22, *Clcn1* exon 7a, *Mbnl1* exon 5, *Nfix* exon 7.
9. The role of miRNAs in DM1 positions antimiR and blockmiR strategies at the forefront of potential DM1 therapy.

# Materials and Methods

# I. Materials

## I.I. Vectors and constructs

### *I.I.I. Cloning vectors*

The plasmid vector pEZX-MT05 (Table MM1) was used to subclone *Mbnl1* and *Mbnl2* 3′UTR constructs (Table MM2). The vector is part of the Secrete Pair Dual Luciferase Assay containing a GLuc and SEAP reporter system under the control of a SV40 promoter. It also contains an ampicillin resistance gene. The 5′ restriction site can be cut with *Asi*SI and *Eco*RI while the 3′ restriction site can be cut with *Xho*I and *Spe*I.

**Table MM1. Vectors and enzymes.**

| **Vector** | **Application** | **Provider** |
|---|---|---|
| pEZX-MT05 | Dual Luciferase Assay | Genecopoeia |
| **Restriction Enzyme Used** | **Site** | **Provider** |
| *Spe*I | 5' cutting site | Thermo Fisher Scientific |
| *Asi*SI | 3' cutting site | Thermo Fisher Scientific |

### *I.I.II. Constructs*

Various constructs were developed for the Secrete Pair Dual Luciferase Assay including wildtype 3′UTRs for mouse *Mbnl1* and *Mbnl2*. Other constructs were made with deletions of predicted binding sites of miR-218 and miR-23b as well as perfect matches for these miRNAs.

**Table MM2. Predicted binding sites on wildtype**

miR-218-5p predicted sites Human blockmiRs miR-218

miR-23b-3p predicted sites Human blockmiRs miR-23b

Predicted by: *Target Scan †miRDB ‡microrna.org

***Mbnl1* 3'UTR Wildtype**

(NCBI: NM_020007.4)

```
CCACAAGTATGTTACCCAGATGTAGAGCTGTCGTCACAAAACAATCATACAAAGAGGAAAGGACAGTGTG
CTTGATTAGAGTAAGGACGACGTCATTAGCCATATTGTATATACCGTCAAGCAACACATACAAAAATCCC
TCAGCCACAAGACATCCACATATTGCATGTTAACCAGAAGAAACGACAACATGGGAACCTGCTGCACACT
```

GTTGCCTACACACTTTGTACATTCAGTTGGTATTTGTGCTGAGGTGATATTCCTATCTAAAACAACAACA
TTGTCTTTCTTTTGTAGCACA‡GAGTTATGCATTAAAATATGCATACGTAATTAGTTTCCTATATATTCA
TGCCATCTTGAAAAGACAGACTATGGTGTGACCATGATTCTATTATGTATTGGTACGTCTGTAGACCAAG
ATATAATTTTTTAAAAATAAGTTTATTTCTTTCAAGGTTTACAAGTAACCAAGGTGCACCTTGTATTTAA
AATCGCCGTTAGAGCTGAGAGCGCGCATGCAGAGTCATTTTTGTTTGAGAGTAATATTTTTACTGTAATA
GATTGTACGACATGGTGAGGGAGGGAACTGACAGATGAATGTGCCAAGCAAAACCACAACTGTGTATATT
TTAAAGCACA*††CCATGGCTTTAAGTACCATGTTGTTAAGGATTCTCATGAAGTGCCATAGACTGTACAT
CAAATTAGAGTATTATTTCTTCAGTGTTATTGTTTCTGGAGCCACATTTTGTTGCTTATTTGCTAGTACT
AATCAATCAAAGGGCACCATTCTTTTCTTTTTTGTTTTTGAAACCAAAGCTGTCTCAGAAATGGCCAATT
TAACTTTACAGTAACAATAGACAGCACA*††ACACAAACTCAATACAGATAACCTTTCACATACTGGAGAT
ATATATGATAGATATATAAAATTATTTTAATGCATTGTAGTGTAATATTTATGCATACTCTACTATATAA
CATGTTATTCAAAAGGGATATGCCATTTCTGAGACACAATAACAAAAAATGTTTGAGGAAATTATTTTGC
TTCTATTTATAGCCTCTGTCAAAAGTCAAAAGACTATAAATGCTTTGCAGAAATGGGTTCACGTTTGCTT
AAACGCTTCATCACAGTCACATTCAAAATAGTGACTCTAAACAAAGAGAACAGCACTGTCATCAGATGCA
TGATAAACCAAAATATGAAAATGGGAAATGTTTAATTAACCTAGTAATTGGGTGGGTTAAGTACATGGGT
GAATTTTATATGTGA‡TTCTTTTGTTCAGATTAACTGCTTATAGCCTTAGAAAGCCTTTTAAAAAATTTT
AAAAATAGATGTGCATTCAGTTTTTAAGAATGGATTCATCCAAAGGAATTCCCCTTTTTTGTGGTTTGGA
TGTTGCAGCTAGGAAAGGCTATTTTTGCTCTGTTCAGCAGTTCTAAAATCGCTGAGTAGGGGCCAGGTCA
CTGGCAGTTCTAGTGTGGAATGGGAGAAGTGAGAGTTCTGTTATAGAACTTTCCATACTTCCAAGTTTAC
TGCAAGTTTTTATGCTTGAGAGAGATGCTTTCTAATATAAGACTGATGTGTTGATTTTCCTGATTGTACT
GTACATCTATTAAAGCCTTAGATTATTACATTACGGGTTGGAACCCATACCAATGTAATTTCAATCGTGT
TAAGAGAGTAATGGTGACTTCACATGTTATTGTAGTTAGTTACGTTATAGAATATTACTTATTTTTCTTG
TTAAAATGTAGTTTTTCATTTCCTACATTTATTGGATTTTCATTTTCTATTAACAGTTGAATACCATTTC
AGTTTTTAGACTATTGTTTTATTAGATTTTACCAATGAATTTTTCAAAATACAAAAAAATTAAAGTAGTT
TTTTCTTCATAACATACTCAGTTTTAAATTACATGTAGTGTCATATGAATATCCGTATTATTGTTAACTA
AATGATTTATATTTTACTGATTTAATATTACAGTGTAAGAATGTCAGTCATTGTTCTTGTCTAGTTTTCA
TTAAAAGAACAAAGATCTTTTATATGGATATCTTATAAATATATAATCATTGCTAAGTAAGAAGTTAAGT
TGTTGCTATGGCAACAATCCTGGCAGACAATTGAGTAATATTTTGATGATTTATTTTGTTTGTAATTAGT
TATTATGAGAAGATCTAGATCCTAGATATTAGAATAAAATTTATTTTCTACTGTATCCATTTCAAATGTT
AAAGTATTGTTTAATATTTTTGAAATCCCTGAATATCAGGCCTTGTTATAAATAAGCTGCATAATCAATA
AATAGAACAAGGGACTTTTTGTTGATAATCCAAATACTCAAAGTTTACGTAATGAGAATTTTAGCGTGTG
TGCAAACTCTTGAGGGTTGATGATGCTGCAATTTAGCATGTTGGAAAGTCTAGAGAGAAGGTTGACTTTT
TGCACTTCTGTATATAGTCAAAAGAGAGAAACCTGTATAATAGCAAGATCTTATTTTGAATAAAAACGTC
TATAATTACAAGGAGTTTTGTTAAGGCTAATGAAATGACAGACTGAGCAAAATTGCTTGCAAAAGTGGCA
CAGAGTTAGCACTCCATACCCTTCAAACACGTCGCTTTGCTTTTTGTGGACAGCTTGTAGTTTGCCAGGA
TTTTTCAGCTGGAAAGATTTGCCATCCTTCCAAGATCTCATGACTGACAAAACTCCATTGGGCCAAATCT
GCCTGAAGATCATTACCAAAAAATAGCAGGTACTTCAGCCACTAAGATGAAATCATGGATCAGATATCCC
TTACATTGTTTTCAAAACTACTGCATGTTTAAAACTTCAACAAAAAGAGAGAAAGAACTATGCTAAGGAC
ATATATTATTCAGATCGATATCTACCAATTTCAGTGGTTTAATGTTCACAAAATGAAATCTTGAAAATAA
CTATTGACTTTCACAAAATTTTAACCATAAACAGGCAAACCAAACAGCACA‡CCTGTAGTTGTTCTGTGA
TTGTTTTTTAATTGCTGTAGATCATGTTCTTTCCGCAGGTGGAAAAAAAAAAAAAAAAAAAAAAAGAAGT
TCAAATTTCACAGTTTTAATTTTCAACTCAGAAGCAAAAGAGCAAAATGTGA‡CAATGGCCACTTGTTTA
ATGACTTGGTTGCCCAGCTGTCACTGCAGCTGGCTACTGATGTTGCACTTACCAGCAACCCACCCACCTT
CATCTGCCGAAAGGACAGTGAGCTTGGTTTTACGATTATGTAATCACAACTTACTTTCTGCTTGTAGTGG
CTTAAAATTATGTATTTTGTCTAGGGCTGCAATTTGTTTTTATGCTTACTTTATTATTACTGCAGTAGTTG
ACTTTGCTGTATGGAAAAATAAAGCGAAATTGCCCTAATAAAACTTCTCTTTCTTAAGTATAAAAAAAAA
AAAAAAAAAA

***Mbnl2* 3'UTR Wildtype**

(NCBI: NM_175341.4)

TCAACAGAAATGGAATGGAATGCCAAGAATCTGCATTGAGAATAACTAAACATTGTTACTGTACATATT
ACCCCGTTTCCTCCTCAATAGAATTGCCACAAACTGCATGCTAAATTTAGTTCTTCTGGACAGACCACA
ACCCTAAGGCTAGTTCTGCTATGTCATATATGAGTATTAAATATGGTATGCTTAGTATACTCCAGCCTA
AGATAGTTAACCACCTGAGACCAGCTGTGATGTTCGAAGACATACAGGATGAGGTTTTCTTTCACAGGG
TTCTGAGCATAGTTTCTGTCCCAGGAATATTGTCTTATCTCCATAACTATAGCTGATGCAGAAAGTCCA
GACAATATACTCATTTCGACTCAGAATATTTCAAATTTAGCAATAAACAGTTAGCTTTAGTTTTAAGTA
CCTATTCCAAGGGCAGGTTCGATTGTAACTCCAATCACAACCATTTCATTTCCTGACTGGATCGAAGGG

TATGATTCACTTCTTGAGGAGACGGACAGTCGCAGCAGAGAGAAGTGAAGTAAAACATACGCCTGCCTC
GCAGGTCTAAAGTCTGAGTGGCAGCTCAAGCACA*††ATTGCCAGGGGACACATCAGAGTGTGGGGTTC
GCTTTGCCAGGAGATGCCGCACTGAATCATGGGATTCTAGAATAACATTGCATAGATTGAAAAAAAAAA
AAAAACTTTGCACGGTATGAGCTTCATACCCAACCCAACAAAGTCTTGAAGGTATTATTTTACAAGTAT
ATTTTTAAAGTTGTTTTATAAGAGAGACTTTGTAGAAGTGCCTAGATTTTGCCAGACTTCATCCAGCTT
GACAAGAATGAAAGGCTCATGCCAATAGTCGAATCTAAGGGATTGGTCTTTCAAACTCGCCCTCCGGTT
GCCTGTTACCGAATAACTCTTCTAAACTAAAACCTAGTCAAACAGGGAAGCTGTAGGTGAGGAGGTCTG
TATAATATTCCAGTTTAAGTACGTCTGAGTTTAGTCACTACAGATGCAAACTGTGACTTTAATCTAAAT
TACTATGTAAACGAAAAAAAAAAGTAGATAGTTTCACTTTTTAAAAACTCCATTACTGTTTTTGCATTT
TAAGAGTTGGATTAAAGGGTTGTAAGTAACTGCAGCATGGAAAAATAGTTCTTTTAATTCTTTCACCTT
AAAGCATATTTTATGTCTCAAAAGTATAAAAAACTTTAATACAAGTACACACATATTATATATACACAT
ACATATATATACTATATATGGATGAAACATATTTTAATGTTGTTTACTTTTTTTAAATACTTGGTTGAT
CTTCAAGGTAATAGCGATACAATTAAATTTTGTTCAGAAAGTTTGTTTTAAAGTTTATTTTAAGCACTA
TCGTACCAAATATTTCATATTTCACATTTTATATGTTGCACATAGCCTACACAGTACCTACATAGTTTT
TAAATTATTGTTTAAGAAATGAAACAGCTGTTATAAATGGATATTATGTGTAATTGTTTAAAACATCCA
TTTTCTTTGTGAACATTTTAGTGATTGAAGTATTTTGACTTTTGAGATTGAATGTAAAATATTTTAAAT
TTTGGTATCATCGCCTGTTCTGAAAACTAGAGGCATCCAACCATATCATTTTTTTTGATTGAAAAAAGA
TCTGCATTTAATTCATGTTGGTCAAAGTCTAATTACTATTTATCTTACATCATAGATCTGATAACTGTA
TCGAAAAGAGAAATCACATTCTGAGTGTAATCTTGCATAGTGCTTGTGTCGTGTTTGTTTTTAATTTGT
GGAAAGGTATTGTATCTAACTTGTATCACCTTGATAGTTCTCATCTTTATGTATTATTGATATTTGTAA
TTTCCTCAGCTATAACAATGTAGTTACGCTACAACTTGCCTAAAACACTCATACTTTTTTTTTCTTTA
CTTACTCATTTAAACTCATTGAGAAGATAGTAGACTAAAAAGGTAAATTATGGGAATCACTGAAATATT
TTTGTAGACTAATTGTTGTAACTGTCCTTTCTTCCTTTCATTTCATGATTTTTATTTTAAAAATTATTA
GCACA‡TAGCTATTTTCAGCCCTTTAATAACTGATCATCAAAACATCACCTGTATCCCCCAGCCAATAT
AGATGACTGTATTTTTTACTATGATATCCATTTTCCAGAATTGTGATTATAATATGCAGAGTCAAATAT
GCCATTTACAATAAGGAGGAGGCCAGGCAAATGCATAGATGTACAAATATATGTACAACAGATTTTGCT
TTTTATTTATTTATAATGTAATTTTATAGAATAATTCTGGGATTTGAGAGGATCTAAAACTATTTTTCT
GTATAAATATTATTTGCCAAAAGTTTGTTTATATTCAGAAGTCTGACTATGATGGATAAATCTTAAATG
CTTTGTTTAATTACAAAAACAAAATCACCAATATCCAAGACAGGAAGATCTCAGTTCAACAGCTCCGGT
AGTTAGGGAACTAACTCCACTTGCACAGGACTTCATTTCACTCTTGGTTTTCAGGCTATAACAGCACTT
CACAGAACTATTCTTTCAGCCATACACCACTGGTCACATTTCTACTAAATCTTTCTGTAACACTTCTTA
AAGAATTCCCTCATTCGTTATCTTACAGTGTAAACAGGACTCTAATTTGTATCAATTATATGTTTTGGT
TGTAATATTCAGTTCACTCACCCAATGTACAACCAATGAAATAAAAGAAGCATTTAAAAGGAAAAAAAA
AAAAAAAAAAAAAAAAAAA

**Table MM3. Constructs**

Highlighted in green and blue are the respective miRNA seed regions.

| | Mature miRNA sequence | | |
|---|---|---|---|
| **miR-218-5p** | ACATGGTTAGATCAAGCACAA | **miR-23b-3p** | GGTAATCCCTGGCAATGTGAT |

| Predicted Site | Deletion | Perfect Match |
|---|---|---|
| **M1-218 Site1** | TTCTTTTGTAGCACAGAGTTATGCA | TACATGGTTAGATCAAGCACAAAGTTATGCA |
| **M1-218 Site2** | ATATTTTAAAGCACACCATGGCTTT | CACATGGTTAGATCAAGCACAACATGGCTTT |
| **M1-218 Site3** | ACAATAGACAGCACACACAAACTC | AACATGGTTAGATCAAGCACAACACAAACTC |
| **M1-218 Site4** | AAACCAAACAGCACACCTGTAGTTG | AACATGGTTAGATCAAGCACAACTGTAGTTG |
| **M1-23b Site1** | GAATTTTATATGTGATTCTTTTGTT | AGGTAATCCCTGGCAATGTGATTCTTTTGTT |
| **M1-23b Site2** | AAGAGCAAAATGTGACAATGGCCAC | AGGTAATCCCTGGCAATGTGATAATGGCCAC |
| **M2-218 Site1** | GGCAGCTCAAGCACAATTGCCAGGG | CACATGGTTAGATCAAGCACAATTGCCAGGG |
| **M2-218 Site2** | AAAATTATTAGCACATAGCTATTTT | AACATGGTTAGATCAAGCACAAGCTATTTT |

## I.II. Polymerase Chain Reaction

The following section details the materials used for conducting polymerase chain reaction (PCR) assays. This includes semiquantitative RT-PCR, miRNA-specific RT-PCR, and qRT-PCR.

### *I.II.I. Enzymes*

Enzymes used in PCR experiments can be found in Table MM4.

**Table MM4. Enzymes and enzyme mixes used for PCR.**

| Enzyme and Enzyme Mixes | Application | Provider |
|---|---|---|
| DNase | RT-PCR | Zymo Research |
| Superscript II Reverse Transcriptase | RT-PCR | Invitrogen |
| Poly(A) polymerase | miRNA RT-PCR | New England Biolabs |
| GoTaq G2 DNA Polymerase | RT-PCR | Promega |
| HOT FIREPol Probe Universal qPCR Mix | qRT-PCR | Solis Biodyne |
| miRCURY LNA Sybr Green | miRNA qRT-PCR | Bionova |

### *I.II.II. Primers for semiquantitative RT-PCR*

Primers used in RT-PCR experiments can be found in Table MM5. All RT-PCRs were run with 30 cycles.

**Table MM5. Primer and probe sequences used in RT-PCR.**

| Primers | Sequence (5' – 3') | Tm (°C) |
|---|---|---|
| *GAPDH* F | CAACGGATTTGGTCGTATTGG | 55 |
| *GAPDH* R | TGATGGCAACAATATCCACTTTACC | |
| *MBNL1* exon 5 F | AGGGAGATGCTCTCGGGAAAAGTG | 60 |
| *MBNL1* exon 5 R | GTTGGCTAGAGCCTGTTGGTATTGGAAAATAC | |
| *NFIX* exon 7 F | GAGCCCTGTTGATGACGTGTTCTA | 55 |
| *NFIX* exon 7 R | CTGCACAAACTCCTTCAGTGAGTC | |
| *SPTAN1* exon 23 F | GATTGGTGGAAAGTGGAAGTGAACGAT | 60 |
| *SPTAN1* exon 23 R | TGATCCATTGCTGTAGTTCATTCGCT | |

| | | |
|---|---|---|
| *Atp2a1* exon 22 F | GGGTCAGTGCCTCAGCTTTG | 58 |
| *Atp2a1* exon 22 R | GCTCATGGTCCTCAAGATCTCAC | |
| *Clcn1* exon 7a F | GTCCTCAGCAAGTTTATGTCC | 58 |
| *Clcn1* exon 7a R | GAATCCTCGCCAGTAATTCC | |
| *Gapdh F* | GAACGGATTTGGCCGTATTGG | 58 |
| *Gapdh R* | GATGGCAACAATCTCCACTTTGCC | |
| *Mbnl1* exon 5 F | AGGGGAGATGCTCTCGGGAAAAGTG | 66 |
| *Mbnl1* exon 5 R | GTTGGCTAGAGCCTGTTGGTATTGGAAAATAC | |
| *Nfix* exon 7 F | TCGACGACAGTGAGATGGAG | 58 |
| *Nfix exon 7 R* | CAAACTCCTTCAGCGAGTCC | |

### *I.II.III. Primers for qRT-PCR*

Primers and probes used for quantitative RT-PCR experiments can be found in Table MM6.

**Table MM6. Primer and probe sequences used in RT-qPCR.**

| Primers | Sequence (5' – 3') |
|---|---|
| *MBNL1* F | CTGCATCTGTCTATGCCAAACT |
| *MBNL1* R | GGGAATCTCCTCACAGCTGAAT |
| *MBNL1* FAM-labelled probe | ACCGATTGCACCACCAAACTCCATTGCA |
| *MBNL2* F | CCACCACGCCTGTTATTGTT |
| *MBNL2* R | CAGTCCTGAGAAGTTTCTGAGTTG |
| *MBNL2* FAM-labeled probe | ACCGGTCACTGTCCCGGGCTCAACT |
| *GAPDH* F | CAACGGATTTGGTCGTATTGG |
| *GAPDH* R | TGATGGCAACAATATCCACTTTACC |
| *GAPDH* MAX-labelled probe | CGCCTGGTCACCAGGGCTGCT |
| *Mbnl1* F | TACCGATTGCACCACCAAAC |
| *Mbnl1* R | GCTGCTTTCAGCAAAGTTGTC |
| *Mbnl1* FAM-labeled probe | TCGCAAATCAGCTGTGAGGAGATTCCCT |
| *Mbnl2* F | GAGACAGACTGCCGCTTTG |
| *Mbnl2* R | GGTTACGGTGTTGTCGTTTGT |
| *Mbnl2* FAM-labeled probe | CCCGGCAGACAGCACCATGATCGA |
| *Gapdh* F | GAACGGATTTGGCCGTATTGG |

| | |
|---|---|
| *Gapdh* R | GATGGCAACAATCTCCACTTTGCC |
| *Gapdh* MAX-labeled probe | CGCCTGGTCACCAGGGCTGCT |

## I.III. Antisense oligonucleotides

The sequences of the AONs used in this study can be seen in Table MM7-9. In Table MM7, the FANA modifications are localized to the extremities of the oligo to leave room for RNase-H binding.

**Table MM7. FANA antimiR design.**

| Name | Sequence (5' – 3') | Concentration |
|---|---|---|
| AUM-miR-23b-3p-1 | GGUAAUCCCTGGCAAUGUGAU | 1, 2.5, & 5 µM |
| AUM-miR-218-5p-1 | ACAUGGUTAGATCAAGCACAA | 1, 2.5, & 5 µM |
| AUM-SC-1 | AUAUCCUTGTCGTAUCCCAGU | 1, 2.5, & 5 µM |

AON modifications can be found in Table MM8 legend for the LNA based blockmiRs.

**Table MM8. LNA blockmiR design.**

**Legend:**
2'-O-Methyl-Nucleotides: lower-case a, g, c, u
LNA Nucleotides: Ab Gb Tb Cb
Phosphorothioate linkages: s
* Not confirmed in Cerro-Herreros *et al*., 2018 luciferase assay

| Name | Sequence (5' – 3') | Concentration |
|---|---|---|
| M1-Block-23b-1 | CbsCbsAbsTbsTbsAbsuscsascsasususususTbsGb | 50 nM |
| M2-Block-23b-1 | AbsuscsascsasusgsasTbsTbsCbsAbsAbsCbsGb | 50 nM |
| M1-Block-218-1* | GbsAbsusgsusgscsusususAbsAbsAbsTbsAbsTb | 200 nM |
| M1-Block-218-2* | GbsususgsusgscsusgsTbsCbsTbsAbsTbsTbsGb | 200 nM |
| M2-Block-218-1 | AbsCbsTbsusgsusgscsususGbsAbsAbsusTbsTb | 200 nM |
| M2-Block-218-2 | GbsTbsTbsGbsusgsusgscsusasasTbsAbsAbsTb | 200 nM |
| M2-Block-218-3 | CbsGbsAbsTbsAbsgsusgscsususAbsAbsAbsAb | 200 nM |
| Scramble | TbsGbscsascscsusususgsTbsTbsAbsTbsTbsTb | 50 & 200 nM |

Finally, the sequence for the PMO blockmiRs can be found in Table MM9. Each PMO was conjugated with Pip9b2 described below.

**Table MM9. P-PMO blockmiR design**

X = aminohexanoic acid; B = β-alanine

| Name | Sequence (5' – 3') | Concentration |
|---|---|---|
| PMO | CCATTATCACATTTTGCTCTT | 1 μM |
| SC | TCTTACCTCAGTTACAATTTA | 1 μM |
| | **Peptide Conjugate** | |
| Pip9b2 (P) | Ac-RXRRBRR FQILY RBRXRB-pmo | |

## I.IV. Cell culture

Table MM10 describes all reagents used in cell culture.

**Table MM10. Cell culture reagents**

| Reagents | Provider |
|---|---|
| apo-Transferrin human (10 mg/mL) | Sigma Aldrich |
| Corning PBS (1X) | Thermo Fisher Scientific |
| Doxycycline (10 mg/mL) | Sigma Aldrich |
| Gibco Dulbecco's Modified Eagle Medium (DMEM) with 4.5 g/L glucose | Thermo Fisher Scientific |
| Gibco FBS | Thermo Fisher Scientific |
| Gibco Horse Serum | Thermo Fisher Scientific |
| Gibco Opti-MEM with GlutaMAX | Thermo Fisher Scientific |
| Gibco Penicillin/Streptomycin | Thermo Fisher Scientific |
| Gibco Trypsin-EDTA 0.25% | Thermo Fisher Scientific |
| Insulin (10 mg/mL) | Sigma Aldrich |
| X-tremeGENE HP DNA Transfection Reagent | Roche |

## I.V. Kits

Kits used in this work along with the commercial provider can be found in Table MM11.

**Table MM11. Commercial kits**

| Kit | Provider |
|---|---|
| BCA Protein Assay | Pierce |
| CellTiter 96 AQueous Non-Radioactive Cell Proliferation Assay | Promega |
| ECL Western blotting substrate | Pierce |
| High Pure Plasmid Isolation Kit | Roche |
| RNeasy Mini Kit | Qiagen |
| Protein Normalization Assay Module for Jess | ProteinSimple |
| Quantitative Dot Blot (QDB) plates | Quanticision Diagnostics |
| Secrete-Pair™ Dual Luminescence Assay Kit | GeneCopoeia |
| SuperSignal West Femto Maximum Sensitivity Substrate | Pierce |
| Vectastain elite ABC-peroxidase Staining Kit | Vector |

## I.VI. Antibodies

Antibodies and stains were used in various assays including western blot, quantitative dot blot, Jess Simple Western, and immunofluorescence staining. These antibodies and their concentrations can be found in Table MM12.

**Table MM12. Antibodies**

| Primary | | | | | |
|---|---|---|---|---|---|
| **Antibody** | **Target** | **Host** | **Application** | **Dilution** | **Provider** |
| Anti-MB1a (4A8) | MBNL1 Mbnl1 | Mouse | Western blot | 1:200 | Developmental Studies Hybridoma Bank |
| | | | Immunofluorescence | | |
| | | | Jess Simple Western | 1:50 | |
| Anti-MBNL1 (ab77017) | MBNL1 Mbnl1 | Mouse | Western blot | 1:1000 | Abcam |
| | | | QDB | | |
| Anti-MBNL1 (ab45899) | MBNL1 | Rabbit | Jess Simple Western | 1:10 | Abcam |
| Anti-MB2a (3B4) | MBNL2 Mbnl2 | Mouse | Western blot | 1:100 | Developmental Studies Hybridoma Bank |
| | | | Jess Simple Western | 1:10 | |
| Anti-β-ACTIN (AC-15) | ACTIN | Mouse | Western blot | 1:5000 | Sigma Aldrich |

| | | | | | |
|---|---|---|---|---|---|
| Anti-GAPDH (G-9) | GAPDH Gapdh | Mouse | Western blot | 1:3000 | Santa Cruz Biotechnology |
| | | | QDB | 1:500 | |
| | | | Jess Simple Western | 1:2000 | |

**Secondary**

| Antibody | Host | Application | Dilution | Provider |
|---|---|---|---|---|
| Anti-Mouse IgG | Goat | Western blot | 1:3500 | Sigma Aldrich |
| | | Immunofluorescence | 1:200 | |
| Anti-Rabbit IgG | Goat | Western blot | 1:3500 | Sigma Aldrich |

**Other stains**

| Name | Application | Dilution | Provider |
|---|---|---|---|
| DAPI | Immunofluorescence | 2 $\mu$g/mL | Vectashield |
| Streptavidin-FITC | Immunofluorescence | 1:200 | Vector |

## I.VII.Equipment

Table MM13 includes a list of all the equipment and model used in this work.

**Table MM13. Equipment**

| Equipment | Model |
|---|---|
| Centrifuges | 5430 Eppendorf<br>5810R Eppendorf<br>5417R Eppendorf<br>Legend Micro 21R, Sorvall |
| Cell counter | Countess II FL, Thermo Fisher Scientific |
| Spectrophotometer | Nanodrop 2000, Thermo Fisher Scientific |
| Plate reader | Infinite M2000 Pro, Tecan |
| Microscopes | DM2500, Leica<br>DM4000 B, Leica<br>MZ 6, Leica<br>FluoView FV1000 Olympus |
| Ultrasonic Processor UP100H | Hielscher |
| Imagers | ImageQuant LAS 4000, GE Healthcare<br>Gel Documentation System – BL, Axygen<br>Image Quant 800 Imager, Amersham |
| Water purification system | Milli-Q, Millipore |

| | |
|---|---|
| Protein transfer | Trans-Blot SD semi-dry transfer cell, Bio-Rad |
| Thermocycler | Gene Max Tc-s-B Thermocycler, BIOER<br>QuantStudio 5 Real-Time PCR System<br>Mastercycler Gradient, Eppendorf |
| Simple Western | Jess, Protein Simple |
| Cryostat | Leica CM1950 |
| Tissue homogenizer | TissueLyser II, Qiagen |
| Shakers and incubators | KS 250 basic, IKA<br>Drying Oven, JP Selecta<br>Shaking Incubator SH maxi, Controltecnica<br>GyroMini Nutating Mixer, Labnet<br>Orbital shaker, SBS Tecman |
| Laboratory Hoods | PCR Workstation UVT-S-AR, Grant-bio<br>Laminar flow AH-100, Telstar<br>Fume hood B ST 1200, Burdinola<br>LabGard Class II NV-437-400E, Nuaire |
| Electrophoresis | Wide Mini-Sub Cell GT, Bio-Rad<br>Mini-protean Electrophoresis System, Bio-Rad |
| Grip strength meter | BIO-GS3, Bioseb |

## I.VIII. Cell lines

### *I.VIII.I. Immortalized patient-derived DM1 and CNT fibroblasts*

The cells in this study were developed from DM1 patient fibroblasts taken from skin biopsies that were immortalized using human TERT re-expression (Lee *et al.,* 2004). The immortalized fibroblasts were transduced to express MYOD1 under activation by doxycycline (Arandel *et al.,* 2017). This initiates the myogenic program which trans-differentiates the fibroblasts into myotubes. Control fibroblasts (CNT) were developed in the same way from healthy patients. These cell lines were kindly provided by Dr. Denis Furling (Institute of Myology, Paris).

#### *I.VIII.II. C2C12*

C2C12 cells are immortalized fibroblasts developed from a subclone of *Mus musculus* leg muscle that quickly differentiate into myotubes (Blau *et al.*, 1985). They are commonly used for the study of myogenesis and differentiation.

### I.IX. Mice

#### *I.IX.I. HSA$^{LR}$*

The HSA$^{LR}$ (line 20 b) mouse strain is a transgenic line expressing approximately 250 CUG long repeats (LR) in the human skeletal actin (HSA) gene (Mankodi *et al.*, 2000). Homozygous mice were kindly provided by Prof. Charles Thornton (University of Rochester Medical Center, Rochester, NY, USA).

#### *I.IX.II. FVB*

FVB mice are an inbred strain of mice carrying the same genetic background as HSA$^{LR}$ mice and are therefore used as healthy controls. This strain was outbred from the Swiss mouse NIH general purpose mouse (Taketo *et al.*, 1991).

## II. Methods

### II.I. Cell culture

#### *II.I.I. Culture conditions*

All cells used in this work were cultured in 37°C in a humidified atmosphere at 5% $CO_2$. DM1, CNT fibroblasts, and C2C12 cells were grown in DMEM + 4.5 g/L glucose growth medium supplemented with 10% FBS and antibiotics (Table MM13). All cells are adherent therefore cell passage was performed at confluency by washing with PBS 1X and adding trypsin 0.25% for 3 min to

release from the flask. Then fresh growth medium was added which deactivates the trypsin. To initiate the myogenic program, DM1 and CNT cells were then grown in differentiation medium according to Arandel *et al*., 2017 which trans-differentiates them into myotubes through doxycycline activation.

**Table MM13. Cell culture mediums**

| Reagents | Details |
|---|---|
| Growth medium | DMEM (1x) + 4.5 g/L glucose<br>10% FBS<br>1% Penicillin/Streptomycin |
| Differentiation medium | DMEM (1x)<br>2% Horse Serum<br>1% apo-transferrin<br>1% Penicillin/Streptomycin<br>0.02% Doxycycline<br>0.1% Insulin |

### *II.I.II. FANA antimiR transfection*

24 h before transfection, cells were seeded at 100,000 cells per mL in either 96 well plate (toxicity assay), 3 mL petri dish (RNA extraction), or 10 mL petri dish (protein extraction). For gymnotic delivery, FANA were administered in differentiation medium and left to incubate. See Table MM7 for concentrations used.

### *II.I.III. LNA blockmiR transfection*

24 h before transfection, cells were seeded at 100,000 cells per mL in either 24 well plate (immunofluorescence), 96 well plate (toxicity assay), 3 mL petri dish (RNA extraction), or 10 mL petri dish (protein extraction). Transfection mix was made by mixing X-treme Gene and the respective blockmiR in Optimem medium and was allowed to incubate for 30 min at room temperature to form the transfection complex. The transfection mix was then administered dropwise to the plates. 4 h later, differentiation medium was

added, and the cells were left to incubate. See Table MM7 for concentrations used.

### *II.I.IV. P-PMO blockmiR transfection*

24 h before transfection, cells were seeded at 100,000 cells per mL in either 24 well plate (immunofluorescence), 96 well plate (toxicity assay), 3 mL petri dish (RNA extraction), or 10 mL petri dish (protein extraction). For gymnotic delivery, P-PMOs were sonicated and vortexed vigorously before being administered in differentiation medium and left to incubate. See Table MM8 for concentrations used.

### *II.I.V. Toxicity assay*

For the cell proliferation assays for FANA antimiRs and LNA and P-PMO blockmiRs, cells were seeded in 96 well plates and transfected at increasing concentrations in quadruplicate (see Table MM13). To measure cell viability, 20 µl of MTS/PMS tetrazolium salt from the CellTiter 96 Aqueous Non-Radioactive Cell Proliferation Assay was added to each well and cells were incubated for four hours at 37°C in a humidified chamber with 5% $CO_2$. The conversion of MTS into soluble formazan was measured by absorbance at 490 nm using an Infinite 200 PRO plate reader.

**Table MM13. Toxicity assay concentrations**

| AON | Tested concentrations |
|---|---|
| FANA antimiRs | 0.5, 1, 2.5, 5, 10 µM |
| LNA blockmiRs | 0.002, 0.01, 0.05, 0.2, 1, 5 µM |
| P-PMO blockmiRs | 0.01, 0.05, 0.2, 1, 5, 10 µM |

### *II.I.VI. Transformation of competent cells*

Competent cells were transformed with plasmids from Table MM1 containing constructs from Table MM2. First, plasmid DNA was added to

thawed competent cells and heat shocked for 2 min at 37°C then 1.5 min at 42°C (Froger and Hall, 2007). The cells were incubated on ice for 1-2 min and then added to liquid LB and incubated for 1 h at 37°C. The cells were then centrifuged, resuspended, and spread onto ampicillin coated LB agar plates. After 37°C incubation overnight, colonies were selected and added to liquid LB with ampicillin to incubate once more overnight at 37°C (Maniatis *et al.*, 1982).

### *II.I.VII. Dual Luciferase Assay*

Luminescence of Gaussian luciferase (GLuc) and alkaline phosphatase (SEAP) were measured using the secreted pair dual luminescence kit according to the manufacturer's protocols. Gaussian luciferase activity was normalized to alkaline phosphatase activity (GLuc/SEAP). Luminescence was measured using a Infinite M200 PRO plate reader. *Mbnl1* and *Mbnl2* 3'UTR reporter pEZX-MT05 plasmids were designed containing wildtype *Mbnl1* and *Mbnl2* (WT), deletion of miR-23b or miR-218 seed region (Del), or perfect match of the full miR-23b or miR-218 sequence (PM). C2C12 cells were seeded into 24 well plates and transfected with the respective plasmid in triplicate. Each sample was given 500 ng of the respective construct in 200 µL of Optimem in an X-treme gene transfection complex (Table MM14). The next day, the EGFP control was checked for fluorescence to confirm cell entry. Fresh medium was added to each well and time 0 h was recorded. Medium was collected and luminescence was measured after 24 h. The same assay was repeated with C2C12 cells co-transfected with miR-23b or miR-218 mimic, scrambled mimic (pVmiR), and no mimic controls. Full plasmid sequences can be found in Table MM2.

**Table MM14. Dual luciferase assay transfection guide**

| Mix | Mimic | 500 ng (µL) | 3'UTR Construct | 500 ng (µL) | X-treme Gene (µL) | Optimem (µL) |
|---|---|---|---|---|---|---|
| Mix 1 | miR-23b | 1 | Mbnl1 WT | 1.31 | 3 | 200 |
| Mix 2 | miR-23b | 1 | Mbnl1 Del-Site-1 | 2.75 | 3 | 200 |

| | | | | | | |
|---|---|---|---|---|---|---|
| Mix 3 | miR-23b | 1 | Mbnl1 Del-Site-2 | 3.35 | 3 | 200 |
| Mix 4 | miR-23b | 1 | Mbnl1 PM-Site-1 | 2.22 | 3 | 200 |
| Mix 5 | miR-23b | 1 | Mbnl1 PM-Site-2 | 2.96 | 3 | 200 |
| Mix 6 | miR-218 | 0.5 | Mbnl1 WT | 1.31 | 3 | 200 |
| Mix 7 | miR-218 | 0.5 | Mbnl1 Del-Site-1 | 3.13 | 3 | 200 |
| Mix 8 | miR-218 | 0.5 | Mbnl1 Del-Site-2 | 4.15 | 3 | 200 |
| Mix 9 | miR-218 | 0.5 | Mbnl1 Del-Site-3 | 3.39 | 3 | 200 |
| Mix 10 | miR-218 | 0.5 | Mbnl1 Del-Site-4 | 4.03 | 3 | 200 |
| Mix 11 | miR-218 | 0.5 | Mbnl1 PM-Site-1 | 3.21 | 3 | 200 |
| Mix 12 | miR-218 | 0.5 | Mbnl1 PM-Site-2 | 2.45 | 3 | 200 |
| Mix 13 | miR-218 | 0.5 | Mbnl1 PM-Site-3 | 3.66 | 3 | 200 |
| Mix 14 | miR-218 | 0.5 | Mbnl1 PM-Site-4 | 3.09 | 3 | 200 |
| Mix 15 | pVmiR | 1 | Mbnl1 WT | 1.31 | 3 | 200 |
| Mix 16 | NONE | -- | Mbnl1 WT | 1.31 | 3 | 200 |
| Mix 17 | miR-218 | 0.5 | Mbnl2 WT | 1.38 | 3 | 200 |
| Mix 18 | miR-218 | 0.5 | Mbnl2 Del-Site-1 | 3.63 | 3 | 200 |
| Mix 19 | miR-218 | 0.5 | Mbnl2 Del-Site-1 | 2.93 | 3 | 200 |
| Mix 20 | miR-218 | 0.5 | Mbnl2 PM-Site-1 | 3.58 | 3 | 200 |
| Mix 21 | miR-218 | 0.5 | Mbnl2 PM-Site-2 | 4.64 | 3 | 200 |
| Mix 22 | pVmiR | 1 | Mbnl2 WT | 1.38 | 3 | 200 |
| Mix 23 | NONE | -- | Mbnl2 WT | 1.38 | 3 | 200 |
| | | | EGFP | 1.00 | 1 | 200 |

## II.II. RNA extraction and analysis

### *II.II.I. Cell and mouse tissue extraction*

Total RNA was isolated from transdifferentiated myotubes or mouse gastrocnemius or quadriceps muscle using QIAzol Lysis Reagent and RNeasy Mini Kit following manufacturer's recommendations. The products were analyzed for quality and total concentration by Nanodrop. For cells, the plates were washed with PBS 1X and lysed with QIAzol. The plates were scraped and the lysate was collected and extraction continued following the RNeasy kit. For mice, the tissues were added to a 2 mL Eppendorf tube along with a metal lysing ball and QIAzol reagent. The tubes were then shaken vigorously by the TissueLyser machine for 5 min. Following this step, the extraction continued following the RNeasy kit.

### *II.II.II. Plasmid DNA from competent cells*

After colony selection and incubation (see section *II.I.VI*), plasmid DNA was isolated using the High Pure Plasmid Isolation Kit. After extraction, the samples were analyzed for quality by Nanodrop and subjected to *Asi*SI and *Spe*I restriction enzyme digestion. The product was run on gel electrophoresis to confirm the plasmids had accepted the constructs and were the correct size (Maniatis *et al.*, 1982).

### *II.II.III. RT-PCR*

Reverse transcription PCR was performed for all isolates using 1 μg of total RNA in order to make cDNA. First the samples were treated with DNase at 37°C for 10 min to ensure there was no genomic DNA contamination. A no reverse-transcriptase (NRT) control was always added to confirm this. The DNase treatment was inactivated by EDTA at 65°C for 10 min. Then the samples received a universal hexanucleotide and dNTPs at 65°C for 5 min followed by 5X Buffer, DTT, and RNase Out at 25°C for 2 min. Finally, the samples (except for NRT) received superscript II and began at 25°C for 10 min, 42°C for 50 min, and finally 70°C for 15 min. Reverse transcription was followed by semiquantitative RT-PCR on the cDNA using primers in Table MM4. PCR product was then run on a 2% agarose electrophoresis gel with a biomolecular ladder to determine amplicon sizes (Friedmann and Rossi, 2007)

In the case of miRNA analysis, an extra step was added to the beginning of this protocol using Polymerase A and ATP to add a 3' poly-A tail to the miRNAs. This lengthens the miRNAs and allows them to be recognized by an RT primer followed by conventional reverse transcription (Shi *et al.*, 2012).

Percentage splice recovery (PSR) index was defined as value %SI minus $\overline{X}\%_{DSI}$, divided by $\overline{X}\%_{DSI}$ minus $\overline{X}\%_{HSI}$ (where SI is splicing inclusion of each

sample, DSI is disease splicing inclusion, and HSI is healthy splicing inclusion).

### *II.II.IV. RT-qPCR*

For Taqman based quantitative PCR, cDNA from reverse transcription was diluted 1:50. FAM or MAX-labelled probes were added along with specific primers from Table MM5 so that all samples can be normalized by endogenous controls in the same well. All samples were run in triplicate on a QuantStudio 5 Real-Time PCR System. For Sybr based miRCURY quantitative PCR, cDNA from reverse transcription was diluted 1:60. Each miRNA was quantified in a separate well and normalized to U6 and U1 snRNAs. The expression levels were normalized to the reference gene using the $2^{-\Delta\Delta Ct}$ method (Livak and Schmittgen, 2001).

### *II.II.V. RNASeq*

Immortalized DM1 fibroblasts were plated at 100,000 cells per mL in 3 mL petri dishes. The cells were treated with differentiation medium and allowed to transdifferentiate for four days. Then M1-Block-23b-1 and AntagomiR-23b were both transfected at 50 nM and left for four more days. On the eighth day, total RNA was extracted following the RNA extraction protocol mentioned in section *II.II.I.* The following bioinformatics analysis was kindly conducted in collaboration with Jorge Espinosa-Espinosa (Universitat de Valencia). Libraries were prepared using the TruSeq Stranded mRNA library preparation kit following Illumina protocols and were sequenced using paired-end NextSeq 550 in the Universitat de Valencia genomics core facility. Around 20 million reads were obtained from each sample. A quality check eliminated any read with a q-value under 30 using the Trim Galore! (RRID:SCR_011847, version 0.6.4_dev) software. All accepted reads were aligned to genome version GRCh38.p12 using the software STAR (version 2.7.3a). Next, the bam results were analyzed with RSEM (version v1.3.2)

software to obtain gene counts. R package edgeR (version 3.28.1) was used to perform a differential gene expression (DGE) test. The threshold for a DGE call was an adjusted p-value < 0.05 and log2FoldChange of 1. Gene expression recovery, i.e. genes that approached a normal expression pattern, was performed for all disease-related genes using this formula: $\%\ Recovery = \frac{mean\ treated\ gene\ counts - mean\ disease\ gene\ counts}{mean\ control\ gene\ counts - mean\ disease\ gene\ counts}$. DM1 muscle biopsy RNASeq data was retrieved from http://DMSeq.org.

For the STRING analysis, the minimum required interaction score was set to medium confidence (0.400). Active interaction sources included textmining, experiments, databases, co-expression, neighborhood, gene fusion, and co-occurrence. Disconnected nodes were hidden from the network. Excluded lncRNAs include AL731556.1, AL606500.1, AL135999.1, AC124301.1, AC112907.3, AC009690.1, MYG1-AS1, SEMA3F-AS1.

## II.III. Protein extraction and analysis

### *II.III.I. Cells and mice extraction*

For total protein extraction, cells were sonicated and homogenized in Pierce RIPA buffer (Thermo Fisher Scientific) supplemented with protease and phosphatase inhibitor cocktails (Roche). Quantification of total protein was performed with a BCA protein assay kit (Pierce) using bovine serum albumin as the standard. For mouse tissue, the same buffer was used but instead of being sonicated, the tubes were then shaken vigorously by the TissueLyser machine for 5 min, then centrifuged for 15 min at 16,000 g at 4°C. The supernatant was then passed to a fresh tube and also analyzed by BCA.

### *II.III.II. QDB*

The QDB immunodetection assay was performed in collaboration with Estefanía Cerro-Herreros and Irene González-Martínez (Universitat de

Valencia). 1 μg/well of cell samples were denatured (100 °C for 5 min) and loaded in QDB plates (Quanticision Diagnostics Inc). Each cell sample was loaded at 2 μg/well in quadruplicate in two different plates; one was used to detect MBNL1 and the other for GAPDH, which was used here as an endogenous control. The QDB plate was placed in transfer buffer (0.039 M Glycine, 0.048 M Tris, 0.37% SDS, 20% methyl alcohol) and gently shaken for 1 min. The plate was then rinsed with TBST (137 mM NaCl, 2.7 mM KCl, 20 mM Tris, pH7.4, plus 0.1% Tween-20) three times, and soaked in blocking buffer (5% non-fat milk in TBST) and then incubated with primary mouse anti-MBNL1 (1:1000) or mouse anti-GAPDH (1:500) overnight at 4ºC. The plate was then washed three times with TBST and incubated again with the secondary antibody anti-mouse-POD (1:200, Sigma-Aldrich) for 2 hours before the plate was washed again for three times with TBST. The plate was inserted into a 96 well plate loaded with 100 μL/well ECL substrate (Pierce) solution for 1 minute before it was inserted into a white 96 well plate for chemiluminescence signal quantification using a Infinite M200 PRO plate reader (Zhang *et al.*, 2019).

### *II.III.III. Jess Simple Western*

For the immunodetection assay in DM1 cells the Jess Simple Western system was used to quantify MBNL1 by chemiluminescence using anti-MBNL1 (1:50, 4A8, anti-mouse). The capillaries are then subjected to a Replex step and again evaluated for total protein through chemiluminescence. For mouse tissues, Jess was used to quantify Mbnl1 protein chemiluminescence using anti-MBNL1 (1:10, ab45899, anti-rabbit) and normalized to total protein fluorescence without the Replex step.

### *II.III.IV. Western Blot*

20 μg of total protein was mixed with 6x loading buffer and $H_2O$ up to the final volume of 25 μL. Tubes were sealed with Parafilm, boiled for 5 min and

transferred to ice. The proteins were separated by electrophoresis in acrylamide/bisacrylamide SDS-PAGE gels with the Mini-protean Electrophoresis System in electrophoresis buffer (27 mM Tris, 200 mM glycine, 0.1% SDS) at 12 mA according to BioRad polyacrylamide electrophoresis protocol. Precision Plus Protein Dual Color Standard (Bio-Rad) was used as molecular marker. The resolving and stacking gel components can be found in Table MM15.

**Table MM15. Gel components for SDS-PAGE**

| Gel | Components |
|---|---|
| Stacking 4% | 0.13 M Tris-HCl pH 6.8 |
| | 4% acrylamide/bisacrylamide (5:1) |
| | 0.5% SDS |
| | 0.1% APS |
| | 0.1% TEMED |
| Resolving 12% | 0.39 M Tris-HCl pH 8.8 |
| | 12% acrylamide/bisacrylamide (5:1) |
| | 0.1% SDS |
| | 0.1% APS |
| | 0.04% TEMED |

After electrophoresis the membranes and filter paper were soaked in transfer buffer (48 mM Tris, 39 mM glycine, 0.025% SDS, 20% methanol) and transferred to a nitrocellulose membrane (GE Healthcare) using the Trans-Blot SD semi-dry transfer cell for 1 h at a constant voltage of 15 V according to BioRad protein blotting protocol. After, the membranes were dyed with Ponceau (0.5% Ponceau, 1% acetic acid) for approximately 1 min to confirm protein transfer and then washed with tap water until the stain was removed. Next, the membranes were blocked with blocking solution (5% of non-fat milk in PBST; 1x PBS, 0.1% Tween 20) for at least 1 h shaking at room temperature. Membranes were incubated with the primary antibodies (see Table MM11) dissolved in the blocking solution overnight at 4°C. After the incubation, the membranes were washed with 1x PBST, three times for 5 min

shaking, and incubated with secondary antibodies conjugated with horseradish peroxidase (see Table MMII) for 1 h at room temperature shaking. After incubation, the membranes were washed with 1x PBST and chemiluminescence was detected with SuperSignal West Femto Maximum Sensitivity Substrate. Subsequently, the membranes were stripped of the attached antibodies to be re-used for the detection of the endogenous control protein. The stripping process was performed by washing the membrane for 5 min in distilled $H_2O$ followed by 5 min in NaOH 0.2 N, and another 5 min in distilled $H_2O$. Once the antibodies were removed, the membranes were blocked, then immunodetection was performed again as described above Chemiluminescence was imaged with ImageQuant LAS 4000 (GE Healthcare).

### *II.III.V. Immunofluorescence*

After transfection and four days of differentiation, DM1 cells were fixed with 4% PFA for 15 minutes at room temperature (RT) and washed three times with 1x PBS. Myotubes were permeabilized with PBS-T (0.3% Triton-X in PBS) and blocked (PBS-T, 0.5% BSA, 1% donkey serum) for 30 minutes at RT. They were then incubated with MBNL1 primary antibody (1:200, 4A8) at 4°C overnight. After three PBS-T washes, the cells were incubated for 1 hour with a biotinylated anti-mouse-IgG (1:200) and subsequent Avidin-Biotin amplification (Elite ABC kit) for 30 minutes at RT. They were followed by three PBS-T washes and incubation with streptavidin-FITC fluorophore (1:200) for 2 hours at RT. After three washes with PBS, the cells were mounted with Vectashield mounting medium containing 2 μg/mL DAPI to detect the nuclei. Images of DM1 cells were taken on an Olympus FluoView FV100 confocal microscope (Beesley, 1993). The images were taken at a 40x magnification and quantified using Image J with the following formula at a threshold of 10: Mean Pixel Intensity=Gray value/Area according to ImageJ guide by Dr. Christine Labno (University of Chicago) (Schneider *et al.*, 2012).

## II.IV. Mice handling

Mouse handling and experimental procedures conformed to the European law regarding laboratory animal care and experimentation (2003/65/CE) and were approved by the Conselleria de Agricultura, Generalitat Valenciana ("Respuesta terapéutica a blockmiRs modificados en un modelo de ratón de DM1", reference number 2020/VSC/PEA/0203).

### *II.IV.I. Grip strength*

The forelimb grip strength was measured with a Grip Strength Meter according to BioSeb protocol. The peak pull force (measured in grams) was recorded on a digital force transducer when the mouse grasped the bar. The gauge of force transducer was reset to 0 g after each measurement. Tension was recorded by the gauge at the time the mouse released its forepaws from the bar. The measurement was performed three consecutive times at 30 s intervals. The bodyweight measurement was performed in parallel. Percentage of normal force was calculated by normalizing the average strength after treatment to the strength before treatment and dividing this value by the body weight of each mouse.

### *II.IV.II. Blood biochemistry*

Blood serum was collected for each mouse and analyzed for biochemical parameters by Laboratorios Montoro Botella (Valencia, Spain).

### *II.IV.III. Immunohistochemistry*

Frozen 10 μm sections of mouse gastrocnemius and quadriceps muscles were cut with a cryostat. The sections were then stained with haematoxylin and eosin and mounted with Vectashield mounting medium (Feldman and Wolfe, 2014). Images were taken at a 100x magnification with a Leica DM2500 microscope. The percentage of fibers containing central nuclei was quantified

in an average of 500 fibers in each mouse. All images were labelled randomly during quantification to facilitate a blind analysis.

## II.V. Statistics

All statistical analyses were performed using Prism 8.2.1 (GraphPad) with special assistance from Dr. Juan Carbonell (Biostatistician, INCLIVA, Valencia, Spain). A normal distribution was assumed in order to compare samples using Student's t-test. Welch's correction was used in the case of unequal variance. When a normal distribution could not be assumed, specifically in the biochemical blood analysis, the Kruskal Wallis non-parametric test was used with the Wilcoxon correction when necessary.

# References

## References


Ala, U. (2020). Competing Endogenous RNAs, Non-Coding RNAs and Diseases: An Intertwined Story. *Cells* 9.

Andre, L.M., van Cruchten, R.T.P., Willemse, M., and Wansink, D.G. (2019). (CTG)n repeat-mediated dysregulation of MBNL1 and MBNL2 expression during myogenesis in DM1 occurs already at the myoblast stage. *PLoS One* 14: e0217317.

Arandel, L., Polay Espinoza, M., Matloka, M., Bazinet, A., De Dea Diniz, D., Naouar, N., Rau, F., Jollet, A., Edom-Vovard, F., Mamchaoui, K., *et al.* (2017). Immortalized human myotonic dystrophy muscle cell lines to assess therapeutic compounds. *Dis Model Mech* 10: 487-497.

Bargiela, A., Cerro-Herreros, E., Fernandez-Costa, J.M., Vilchez, J.J., Llamusi, B., and Artero, R. (2015). Increased autophagy and apoptosis contribute to muscle atrophy in a myotonic dystrophy type 1 Drosophila model. *Dis Model Mech* 8: 679-690.

Bartel, D.P. (2009). MicroRNAs: target recognition and regulatory functions. *Cell* 136: 215-233.

Batra, R., Manchanda, M., and Swanson, M.S. (2015). Global insights into alternative polyadenylation regulation. *RNA Biol* 12: 597-602.

Batra, R., Nelles, D.A., Pirie, E., Blue, S.M., Marina, R.J., Wang, H., Chaim, I.A., Thomas, J.D., Zhang, N., Nguyen, V., *et al.* (2017). Elimination of Toxic Microsatellite Repeat Expansion RNA by RNA-Targeting Cas9. *Cell* 170: 899-912 e810.

Batra, R., Nelles, D.A., Roth, D.M., Krach, F., Nutter, C.A., Tadokoro, T., Thomas, J.D., Sznajder, L.J., Blue, S.M., Gutierrez, H.L., *et al.* (2021). The sustained expression of Cas9 targeting toxic RNAs reverses disease phenotypes in mouse models of myotonic dystrophy type 1. *Nat Biomed Eng* 5: 157-168.

Beesley, J.E. (1993). Immunocyto-chemistry : a practical approach, *IRL Press at Oxford University Press*, Oxford ; New York.

Bigot, A., Klein, A.F., Gasnier, E., Jacquemin, V., Ravassard, P., Butler-Browne, G., Mouly, V., and Furling, D. (2009). Large CTG repeats trigger p16-dependent premature senescence in myotonic dystrophy type 1 muscle precursor cells. *Am J Pathol* 174: 1435-1442.

Bisset, D.R., Stepniak-Konieczna, E.A., Zavaljevski, M., Wei, J., Carter, G.T., Weiss, M.D., and Chamberlain, J.R. (2015). Therapeutic impact of systemic AAV-mediated RNA interference in a mouse model of myotonic dystrophy. *Hum Mol Genet* 24: 4971-4983.

Blain, A.M., Greally, E., McClorey, G., Manzano, R., Betts, C.A., Godfrey, C., O'Donovan, L., Coursindel, T., Gait, M.J., Wood, M.J., *et al.* (2018). Peptide-conjugated phosphodiamidate oligomer-mediated exon skipping has benefits for cardiac function in mdx and Cmah-/-mdx mouse models of Duchenne muscular dystrophy. *Plos One* 13: e0198897.

Blau, H.M., Pavlath, G.K., Hardeman, E.C., Chiu, C.P., Silberstein, L., Webster, S.G., Miller, S.C., and Webster, C. (1985). Plasticity of the differentiated state. *Science* 230: 758-766.

Bogue, M.A., Philip, V.M., Walton, D.O., Grubb, S.C., Dunn, M.H., Kolishovski, G., Emerson, J., Mukherjee, G., Stearns, T., He, H., *et al.* (2020). Mouse Phenome Database: a data repository and analysis suite for curated primary mouse phenotype data. *Nucleic Acids Res* 48: D716-D723.

Botros, M., and Sikaris, K.A. (2013). The de ritis ratio: the test of time. *Clin Biochem Rev* 34: 117-130.

Bouchard, J.P., Cossette, L., Bassez, G., and Puymirat, J. (2015). Natural history of skeletal muscle involvement in myotonic dystrophy type 1: a retrospective study in 204 cases. *J Neurol* 262: 285-293.

Brook, J.D., McCurrach, M.E., Harley, H.G., Buckler, A.J., Church, D., Aburatani, H., Hunter, K., Stanton, V.P., Thirion, J.P., Hudson, T., *et al.* (1992). Molecular basis of myotonic dystrophy: expansion of a trinucleotide (CTG) repeat at the 3' end of a transcript encoding a protein kinase family member. *Cell* 69: 385.

Burdick, A.D., Sciabola, S., Mantena, S.R., Hollingshead, B.D., Stanton, R., Warneke, J.A., Zeng, M., Martsen, E., Medvedev, A., Makarov, S.S., *et al.* (2014). Sequence motifs associated with hepatotoxicity of locked nucleic acid--modified antisense oligonucleotides. *Nucleic Acids Res* 42: 4882-4891.

Burnett, J.C., and Rossi, J.J. (2012). RNA-based therapeutics: current progress and future prospects. *Chem Biol* 19: 60-71.

Cabaniss, C.D. (1990). Creatine Kinase. In: rd, Walker, H.K., Hall, W.D., and Hurst, J.W. (eds). Clinical Methods: The History, Physical, and Laboratory Examinations: Boston.

Cappella, M., Perfetti, A., Cardinali, B., Garcia-Manteiga, J.M., Carrara, M., Provenzano, C., Fuschi, P., Cardani, R., Renna, L.V., Meola, G., *et al.* (2018). High-throughput analysis of the RNA-induced silencing complex in myotonic dystrophy type 1 patients identifies the dysregulation of miR-29c and its target ASB2. *Cell Death Dis* 9: 729.

Carpentier, C., Ghanem, D., Fernandez-Gomez, F.J., Jumeau, F., Philippe, J.V., Freyermuth, F., Labudeck, A., Eddarkaoui, S., Dhaenens, C.M., Holt, I., *et al.* (2014). Tau exon 2 responsive elements deregulated in myotonic dystrophy type I are proximal to exon 2 and synergistically regulated by MBNL1 and MBNL2. *Biochim Biophys Acta* 1842: 654-664.

Cerro-Herreros, E., Fernandez-Costa, J.M., Sabater-Arcis, M., Llamusi, B., and Artero, R. (2016). Derepressing muscleblind expression by miRNA sponges ameliorates myotonic dystrophy-like phenotypes in Drosophila. *Sci Rep* 6: 36230.

Cerro-Herreros, E., Gonzalez-Martinez, I., Moreno, N., Espinosa-Espinosa, J., Fernandez-Costa, J.M., Colom-Rodrigo, A., Overby, S.J., Seoane-Miraz, D., Poyatos-Garcia, J., Vilchez, J.J., *et al.* (2021). Preclinical characterization of antagomiR-218 as a potential treatment for myotonic dystrophy. *Mol Ther Nucleic Acids* 26: 174-191.

Cerro-Herreros, E., Gonzalez-Martinez, I., Moreno-Cervera, N., Overby, S., Perez-Alonso, M., Llamusi, B., and Artero, R. (2020). Therapeutic Potential of AntagomiR-23b for Treating Myotonic Dystrophy. *Mol Ther Nucleic Acids* 21: 837-849.

Cerro-Herreros, E., González-Martínez, I., Moreno, N., Espinosa-Espinosa, J., Fernández-Costa, J.M., Colom-Rodríguez, A., Overby, S.J., Seoane-Miraz, D., Poyatos-Garcia, J., Vilchez, J.J., López de Munain, A., Varela, M.A., Wood, M.J., Pérez-Alonso, M., Llamusí, B., Artero, R. (2021). Preclinical characterization of antagomiR-218 as a potential treatment for Myotonic Dystrophy. *Mol Ther Nucleic Acids*.

Cerro-Herreros, E., Sabater-Arcis, M., Fernandez-Costa, J.M., Moreno, N., Perez-Alonso, M., Llamusi, B., and Artero, R. (2018). miR-23b and miR-218 silencing increase Muscleblind-like expression and alleviate myotonic dystrophy phenotypes in mammalian models. *Nat Commun* 9: 2482.

Chakraborty, M., Sellier, C., Ney, M., Pascal, V., Charlet-Berguerand, N., Artero, R., and Llamusi, B. (2018). Daunorubicin reduces MBNL1 sequestration caused by CUG-repeat expansion and rescues cardiac dysfunctions in a Drosophila model of myotonic dystrophy. *Dis Model Mech* 11.

Chakraborty, M., Selma-Soriano, E., Magny, E., Couso, J.P., Perez-Alonso, M., Charlet-Berguerand, N., Artero, R., and Llamusi, B. (2015). Pentamidine rescues contractility and rhythmicity in a Drosophila model of myotonic dystrophy heart dysfunction. *Dis Model Mech* 8: 1569-1578.

## References


Chamberlain, C.M., and Ranum, L.P. (2012). Mouse model of muscleblind-like 1 overexpression: skeletal muscle effects and therapeutic promise. *Hum Mol Genet* 21: 4645-4654.

Champy, M.F., Selloum, M., Zeitler, V., Caradec, C., Jung, B., Rousseau, S., Pouilly, L., Sorg, T., and Auwerx, J. (2008). Genetic background determines metabolic phenotypes in the mouse. *Mamm Genome* 19: 318-331.

Chan, J.H., Lim, S., and Wong, W.S. (2006). Antisense oligonucleotides: from design to therapeutic application. *Clin Exp Pharmacol Physiol* 33: 533-540.

Charizanis, K., Lee, K.Y., Batra, R., Goodwin, M., Zhang, C., Yuan, Y., Shiue, L., Cline, M., Scotti, M.M., Xia, G., *et al.* (2012). Muscleblind-like 2-mediated alternative splicing in the developing brain and dysregulation in myotonic dystrophy. *Neuron* 75: 437-450.

Charlet, B.N., Savkur, R.S., Singh, G., Philips, A.V., Grice, E.A., and Cooper, T.A. (2002). Loss of the muscle-specific chloride channel in type 1 myotonic dystrophy due to misregulated alternative splicing. *Mol Cell* 10: 45-53.

Chery, J. (2016). RNA therapeutics: RNAi and antisense mechanisms and clinical applications. *Postdoc J* 4: 35-50.

Choi, J., Dixon, D.M., Dansithong, W., Abdallah, W.F., Roos, K.P., Jordan, M.C., Trac, B., Lee, H.S., Comai, L., and Reddy, S. (2016). Muscleblind-like 3 deficit results in a spectrum of age-associated pathologies observed in myotonic dystrophy. *Sci Rep* 6: 30999.

Choi, J., Personius, K.E., DiFranco, M., Dansithong, W., Yu, C., Srivastava, S., Dixon, D.M., Bhatt, D.B., Comai, L., Vergara, J.L., *et al.* (2015). Muscleblind-Like 1 and Muscleblind-Like 3 Depletion Synergistically Enhances Myotonia by Altering Clc-1 RNA Translation. *EBioMedicine* 2: 1034-1047.

Christou, M., Wengel, J., Sokratous, K., Kyriacou, K., Nikolaou, G., Phylactou, L.A., and Mastroyiannopoulos, N.P. (2020). Systemic Evaluation of Chimeric LNA/2'-O-Methyl Steric Blockers for Myotonic Dystrophy Type 1 Therapy. *Nucleic Acid Ther* 30: 80-93.

Crooke, S.T., Wang, S., Vickers, T.A., Shen, W., and Liang, X.H. (2017). Cellular uptake and trafficking of antisense oligonucleotides. *Nat Biotechnol* 35: 230-237.

Dastidar, S., Majumdar, D., Tipanee, J., Singh, K., Klein, A.F., Furling, D., Chuah, M.K., and VandenDriessche, T. (2021). Comprehensive transcriptome-wide analysis of spliceopathy correction of myotonic dystrophy using CRISPR-Cas9 in iPSCs-derived cardiomyocytes. *Mol Ther* 10.1016/j.ymthe.2021.08.004.

de Die-Smulders, C.E., Howeler, C.J., Thijs, C., Mirandolle, J.F., Anten, H.B., Smeets, H.J., Chandler, K.E., and Geraedts, J.P. (1998). Age and causes of death in adult-onset myotonic dystrophy. *Brain* 121 ( Pt 8): 1557-1563.

de Haro, M., Al-Ramahi, I., De Gouyon, B., Ukani, L., Rosa, A., Faustino, N.A., Ashizawa, T., Cooper, T.A., and Botas, J. (2006). MBNL1 and CUGBP1 modify expanded CUG-induced toxicity in a Drosophila model of myotonic dystrophy type 1. *Hum Mol Genet* 15: 2138-2145.

Della Valle, F., Thimma, M.P., Caiazzo, M., Pulcrano, S., Celii, M., Adroub, S.A., Liu, P., Alanis-Lobato, G., Broccoli, V., and Orlando, V. (2020). Transdifferentiation of Mouse Embryonic Fibroblasts into Dopaminergic Neurons Reactivates LINE-1 Repetitive Elements. *Stem Cell Reports* 14: 60-74.

Denis, J.A., Gauthier, M., Rachdi, L., Aubert, S., Giraud-Triboult, K., Poydenot, P., Benchoua, A., Champon, B., Maury, Y., Baldeschi, C., *et al.* (2013). mTOR-dependent proliferation defect

in human ES-derived neural stem cells affected by myotonic dystrophy type 1. *J Cell Sci* 126: 1763-1772.

Dhont, S., Callens, R., Stevens, D., Bauters, F., De Bleecker, J.L., Derom, E., and Van Braeckel, E. (2020). Myotonic dystrophy type 1 as a major risk factor for severe COVID-19? *Acta Neurol Belg* 10.1007/s13760-020-01514-z.

Dixon, D.M., Choi, J., El-Ghazali, A., Park, S.Y., Roos, K.P., Jordan, M.C., Fishbein, M.C., Comai, L., and Reddy, S. (2015). Loss of muscleblind-like 1 results in cardiac pathology and persistence of embryonic splice isoforms. *Sci Rep* 5: 9042.

Dong, W., Chen, X., Wang, M., Zheng, Z., Zhang, X., Xiao, Q., and Peng, X. (2019). Mir-206 partially rescues myogenesis deficiency by inhibiting CUGBP1 accumulation in the cell models of myotonic dystrophy. *Neurol Res* 41: 9-18.

Dowdy, S.F. (2017). Overcoming cellular barriers for RNA therapeutics. *Nat Biotechnol* 35: 222-229.

Du, H., Cline, M.S., Osborne, R.J., Tuttle, D.L., Clark, T.A., Donohue, J.P., Hall, M.P., Shiue, L., Swanson, M.S., Thornton, C.A., *et al.* (2010). Aberrant alternative splicing and extracellular matrix gene expression in mouse models of myotonic dystrophy. *Nat Struct Mol Biol* 17: 187-193.

Evans, T.C., and Jehle, D. (1991). The red blood cell distribution width. *J Emerg Med* 9 Suppl 1: 71-74.

Feldman, A.T., and Wolfe, D. (2014). Tissue processing and hematoxylin and eosin staining. *Methods Mol Biol* 1180: 31-43.

Fernandez-Costa, J.M., Garcia-Lopez, A., Zuniga, S., Fernandez-Pedrosa, V., Felipo-Benavent, A., Mata, M., Jaka, O., Aiastui, A., Hernandez-Torres, F., Aguado, B., *et al.* (2013). Expanded CTG repeats trigger miRNA alterations in Drosophila that are conserved in myotonic dystrophy type 1 patients. *Hum Mol Genet* 22: 704-716.

Fernandez-Costa, J.M., Llamusi, M.B., Garcia-Lopez, A., and Artero, R. (2011). Alternative splicing regulation by Muscleblind proteins: from development to disease. *Biol Rev Camb Philos Soc* 86: 947-958.

Ferrari, N., Bergeron, D., Tedeschi, A.L., Mangos, M.M., Paquet, L., Renzi, P.M., and Damha, M.J. (2006). Characterization of antisense oligonucleotides comprising 2'-deoxy-2'-fluoro-beta-D-arabinonucleic acid (FANA): specificity, potency, and duration of activity. *Ann N Y Acad Sci* 1082: 91-102.

Fleming, J.L., Gable, D.L., Samadzadeh-Tarighat, S., Cheng, L., Yu, L., Gillespie, J.L., and Toland, A.E. (2013). Differential expression of miR-1, a putative tumor suppressing microRNA, in cancer resistant and cancer susceptible mice. *PeerJ* 1: e68.

Flower, M., Lomeikaite, V., Ciosi, M., Cumming, S., Morales, F., Lo, K., Hensman Moss, D., Jones, L., Holmans, P., Investigators, T.-H., *et al.* (2019). MSH3 modifies somatic instability and disease severity in Huntington's and myotonic dystrophy type 1. *Brain* 10.1093/brain/awz115.

Forand, A., Muchir, A., Mougenot, N., Sevoz-Couche, C., Peccate, C., Lemaitre, M., Izabelle, C., Wood, M., Lorain, S., and Pietri-Rouxel, F. (2020). Combined Treatment with Peptide-Conjugated Phosphorodiamidate Morpholino Oligomer-PPMO and AAV-U7 Rescues the Severe DMD Phenotype in Mice. *Mol Ther Methods Clin Dev* 17: 695-708.

Francois, V., Klein, A.F., Beley, C., Jollet, A., Lemercier, C., Garcia, L., and Furling, D. (2011). Selective silencing of mutated mRNAs in DM1 by using modified hU7-snRNAs. *Nat Struct Mol Biol* 18: 85-87.

## References


Freyermuth, F., Rau, F., Kokunai, Y., Linke, T., Sellier, C., Nakamori, M., Kino, Y., Arandel, L., Jollet, A., Thibault, C., *et al.* (2016). Splicing misregulation of SCN5A contributes to cardiac-conduction delay and heart arrhythmia in myotonic dystrophy. *Nat Commun* 7: 11067.

Friedmann, T., and Rossi, J.J. (2007). Gene transfer : delivery and expression of DNA and RNA : a laboratory manual, *Cold Spring Harbor Laboratory Press*, Cold Spring Harbor, N.Y.

Froger, A., and Hall, J.E. (2007). Transformation of plasmid DNA into E. coli using the heat shock method. *J Vis Exp* 10.3791/253: 253.

Fugier, C., Klein, A.F., Hammer, C., Vassilopoulos, S., Ivarsson, Y., Toussaint, A., Tosch, V., Vignaud, A., Ferry, A., Messaddeq, N., *et al.* (2011). Misregulated alternative splicing of BIN1 is associated with T tubule alterations and muscle weakness in myotonic dystrophy. *Nat Med* 17: 720-725.

Furling, D., Lemieux, D., Taneja, K., and Puymirat, J. (2001). Decreased levels of myotonic dystrophy protein kinase (DMPK) and delayed differentiation in human myotonic dystrophy myoblasts. *Neuromuscul Disord* 11: 728-735.

Gao, Y., Guo, X., Santostefano, K., Wang, Y., Reid, T., Zeng, D., Terada, N., Ashizawa, T., and Xia, G. (2016). Genome Therapy of Myotonic Dystrophy Type 1 iPS Cells for Development of Autologous Stem Cell Therapy. *Mol Ther* 24: 1378-1387.

Garber, K. (2017). Worth the RISC? *Nat Biotechnol* 35: 198-202.

Garcia-Lopez, A., Llamusi, B., Orzaez, M., Perez-Paya, E., and Artero, R.D. (2011). In vivo discovery of a peptide that prevents CUG-RNA hairpin formation and reverses RNA toxicity in myotonic dystrophy models. *Proc Natl Acad Sci U S A* 108: 11866-11871.

Garcia-Lopez, A., Monferrer, L., Garcia-Alcover, I., Vicente-Crespo, M., Alvarez-Abril, M.C., and Artero, R.D. (2008). Genetic and chemical modifiers of a CUG toxicity model in Drosophila. *PLoS One* 3: e1595.

Geary, R.S., Norris, D., Yu, R., and Bennett, C.F. (2015). Pharmacokinetics, biodistribution and cell uptake of antisense oligonucleotides. *Adv Drug Deliv Rev* 87: 46-51.

Gomes-Pereira, M., Cooper, T.A., and Gourdon, G. (2011). Myotonic dystrophy mouse models: towards rational therapy development. *Trends Mol Med* 17: 506-517.

Gomes-Pereira, M., Foiry, L., Nicole, A., Huguet, A., Junien, C., Munnich, A., and Gourdon, G. (2007). CTG trinucleotide repeat "big jumps": large expansions, small mice. *PLoS Genet* 3: e52.

Gonzalez-Barriga, A., Kranzen, J., Croes, H.J., Bijl, S., van den Broek, W.J., van Kessel, I.D., van Engelen, B.G., van Deutekom, J.C., Wieringa, B., Mulders, S.A., *et al.* (2015). Cell membrane integrity in myotonic dystrophy type 1: implications for therapy. *Plos One* 10: e0121556.

Gonzalez-Barriga, A., Mulders, S.A., van de Giessen, J., Hooijer, J.D., Bijl, S., van Kessel, I.D., van Beers, J., van Deutekom, J.C., Fransen, J.A., Wieringa, B., *et al.* (2013). Design and analysis of effects of triplet repeat oligonucleotides in cell models for myotonic dystrophy. *Mol Ther Nucleic Acids* 2: e81.

Gonzalez-Barriga, A., Nillessen, B., Kranzen, J., van Kessel, I.D.G., Croes, H.J.E., Aguilera, B., de Visser, P.C., Datson, N.A., Mulders, S.A.M., van Deutekom, J.C.T., *et al.* (2017). Intracellular Distribution and Nuclear Activity of Antisense Oligonucleotides After Unassisted Uptake in Myoblasts and Differentiated Myotubes In Vitro. *Nucleic Acid Ther* 27: 144-158.

Goodwin, M., Mohan, A., Batra, R., Lee, K.Y., Charizanis, K., Fernandez Gomez, F.J., Eddarkaoui, S., Sergeant, N., Buee, L., Kimura, T., *et al.* (2015). MBNL Sequestration by Toxic RNAs and RNA Misprocessing in the Myotonic Dystrophy Brain. *Cell Rep* 12: 1159-1168.

Gowda, S., Desai, P.B., Hull, V.V., Math, A.A., Vernekar, S.N., and Kulkarni, S.S. (2009). A review on laboratory liver function tests. *Pan Afr Med J* 3: 17.

Harper, P.S. (2009). Myotonic dystrophy, *Oxford University Press*, Oxford ; New York.

Harshe, R.P., Xie, A., Vuerich, M., Frank, L.A., Gromova, B., Zhang, H., Robles, R.J., Mukherjee, S., Csizmadia, E., Kokkotou, E., *et al.* (2020). Endogenous antisense RNA curbs CD39 expression in Crohn's disease. *Nat Commun* 11: 5894.

Heatwole, C., Johnson, N., Goldberg, B., Martens, W., and Moxley, R., 3rd (2011). Laboratory abnormalities in patients with myotonic dystrophy type 2. *Arch Neurol* 68: 1180-1184.

Ho, T.H., Charlet, B.N., Poulos, M.G., Singh, G., Swanson, M.S., and Cooper, T.A. (2004). Muscleblind proteins regulate alternative splicing. *EMBO J* 23: 3103-3112.

Hu, B., Zhong, L., Weng, Y., Peng, L., Huang, Y., Zhao, Y., and Liang, X.J. (2020). Therapeutic siRNA: state of the art. *Signal Transduct Target Ther* 5: 101.

Jang, Y.N., and Baik, E.J. (2013). JAK-STAT pathway and myogenic differentiation. *JAKSTAT* 2: e23282.

Jauvin, D., Chretien, J., Pandey, S.K., Martineau, L., Revillod, L., Bassez, G., Lachon, A., MacLeod, A.R., Gourdon, G., Wheeler, T.M., *et al.* (2017). Targeting DMPK with Antisense Oligonucleotide Improves Muscle Strength in Myotonic Dystrophy Type 1 Mice. *Mol Ther Nucleic Acids* 7: 465-474.

Jiang, H., Mankodi, A., Swanson, M.S., Moxley, R.T., and Thornton, C.A. (2004). Myotonic dystrophy type 1 is associated with nuclear foci of mutant RNA, sequestration of muscleblind proteins and deregulated alternative splicing in neurons. *Hum Mol Genet* 13: 3079-3088.

Johnson, N.E., Butterfield, R.J., Mayne, K., Newcomb, T., Imburgia, C., Dunn, D., Duval, B., Feldkamp, M.L., and Weiss, R.B. (2021). Population-Based Prevalence of Myotonic Dystrophy Type 1 Using Genetic Analysis of Statewide Blood Screening Program. *Neurology* 96: e1045-e1053.

Kalra, S., Montanaro, F., and Denning, C. (2016). Can Human Pluripotent Stem Cell-Derived Cardiomyocytes Advance Understanding of Muscular Dystrophies? *J Neuromuscul Dis* 3: 309-332.

Kalsotra, A., Singh, R.K., Gurha, P., Ward, A.J., Creighton, C.J., and Cooper, T.A. (2014). The Mef2 transcription network is disrupted in myotonic dystrophy heart tissue, dramatically altering miRNA and mRNA expression. *Cell Rep* 6: 336-345.

Kanadia, R.N., Johnstone, K.A., Mankodi, A., Lungu, C., Thornton, C.A., Esson, D., Timmers, A.M., Hauswirth, W.W., and Swanson, M.S. (2003a). A muscleblind knockout model for myotonic dystrophy. *Science* 302: 1978-1980.

Kanadia, R.N., Shin, J., Yuan, Y., Beattie, S.G., Wheeler, T.M., Thornton, C.A., and Swanson, M.S. (2006). Reversal of RNA missplicing and myotonia after muscleblind overexpression in a mouse poly(CUG) model for myotonic dystrophy. *Proc Natl Acad Sci U S A* 103: 11748-11753.

Kanadia, R.N., Urbinati, C.R., Crusselle, V.J., Luo, D., Lee, Y.J., Harrison, J.K., Oh, S.P., and Swanson, M.S. (2003b). Developmental expression of mouse muscleblind genes Mbnl1, Mbnl2 and Mbnl3. *Gene Expr Patterns* 3: 459-462.

## References


Kartha, R.V., and Subramanian, S. (2014). Competing endogenous RNAs (ceRNAs): new entrants to the intricacies of gene regulation. *Front Genet* 5: 8.

Khvorova, A., and Watts, J.K. (2017). The chemical evolution of oligonucleotide therapies of clinical utility. *Nat Biotechnol* 35: 238-248.

Kimura, T., Nakamori, M., Lueck, J.D., Pouliquin, P., Aoike, F., Fujimura, H., Dirksen, R.T., Takahashi, M.P., Dulhunty, A.F., and Sakoda, S. (2005). Altered mRNA splicing of the skeletal muscle ryanodine receptor and sarcoplasmic/endoplasmic reticulum Ca2+-ATPase in myotonic dystrophy type 1. *Hum Mol Genet* 14: 2189-2200.

Klein, A.F., Varela, M.A., Arandel, L., Holland, A., Naouar, N., Arzumanov, A., Seoane, D., Revillod, L., Bassez, G., Ferry, A., *et al.* (2019). Peptide-conjugated oligonucleotides evoke long-lasting myotonic dystrophy correction in patient-derived cells and mice. *J Clin Invest* 10.1172/JCI128205.

Koebis, M., Kiyatake, T., Yamaura, H., Nagano, K., Higashihara, M., Sonoo, M., Hayashi, Y., Negishi, Y., Endo-Takahashi, Y., Yanagihara, D., *et al.* (2013). Ultrasound-enhanced delivery of morpholino with Bubble liposomes ameliorates the myotonia of myotonic dystrophy model mice. *Sci Rep* 3: 2242.

Konieczny, P., Stepniak-Konieczna, E., and Sobczak, K. (2014). MBNL proteins and their target RNAs, interaction and splicing regulation. *Nucleic Acids Res* 42: 10873-10887.

Konieczny, P., Stepniak-Konieczna, E., and Sobczak, K. (2017). MBNL expression in autoregulatory feedback loops. *RNA Biol* 10.1080/15476286.2017.1384119: 1-8.

Koscianska, E., Witkos, T.M., Kozlowska, E., Wojciechowska, M., and Krzyzosiak, W.J. (2015). Cooperation meets competition in microRNA-mediated DMPK transcript regulation. *Nucleic Acids Res* 43: 9500-9518.

Koutalianos, D., Koutsoulidou, A., Mastroyiannopoulos, N.P., Furling, D., and Phylactou, L.A. (2015). MyoD transcription factor induces myogenesis by inhibiting Twist-1 through miR-206. *J Cell Sci* 128: 3631-3645.

Kubowicz, P., Zelaszczyk, D., and Pekala, E. (2013). RNAi in clinical studies. *Curr Med Chem* 20: 1801-1816.

Ladd, A.N., Charlet, N., and Cooper, T.A. (2001). The CELF family of RNA binding proteins is implicated in cell-specific and developmentally regulated alternative splicing. *Mol Cell Biol* 21: 1285-1296.

Landfeldt, E., Nikolenko, N., Jimenez-Moreno, C., Cumming, S., Monckton, D.G., Gorman, G., Turner, C., and Lochmuller, H. (2019). Disease burden of myotonic dystrophy type 1. *J Neurol* 266: 998-1006.

Langlois, M.A., Boniface, C., Wang, G., Alluin, J., Salvaterra, P.M., Puymirat, J., Rossi, J.J., and Lee, N.S. (2005). Cytoplasmic and nuclear retained DMPK mRNAs are targets for RNA interference in myotonic dystrophy cells. *J Biol Chem* 280: 16949-16954.

Lee, K.M., Choi, K.H., and Ouellette, M.M. (2004). Use of exogenous hTERT to immortalize primary human cells. *Cytotechnology* 45: 33-38.

Lee, K.S., Cao, Y., Witwicka, H.E., Tom, S., Tapscott, S.J., and Wang, E.H. (2010). RNA-binding protein Muscleblind-like 3 (MBNL3) disrupts myocyte enhancer factor 2 (Mef2) {beta}-exon splicing. *J Biol Chem* 285: 33779-33787.

Lee, K.S., Smith, K., Amieux, P.S., and Wang, E.H. (2008). MBNL3/CHCR prevents myogenic differentiation by inhibiting MyoD-dependent gene transcription. *Differentiation* 76: 299-309.

Lee, K.Y., Li, M., Manchanda, M., Batra, R., Charizanis, K., Mohan, A., Warren, S.A., Chamberlain, C.M., Finn, D., Hong, H., *et al.* (2013). Compound loss of muscleblind-like function in myotonic dystrophy. *EMBO Mol Med* 5: 1887-1900.

Leger, A.J., Mosquea, L.M., Clayton, N.P., Wu, I.H., Weeden, T., Nelson, C.A., Phillips, L., Roberts, E., Piepenhagen, P.A., Cheng, S.H., *et al.* (2013). Systemic delivery of a Peptide-linked morpholino oligonucleotide neutralizes mutant RNA toxicity in a mouse model of myotonic dystrophy. *Nucleic Acid Ther* 23: 109-117.

Li, Y., and Kowdley, K.V. (2012). MicroRNAs in common human diseases. *Genomics Proteomics Bioinformatics* 10: 246-253.

Lim, K.R., Maruyama, R., and Yokota, T. (2017). Eteplirsen in the treatment of Duchenne muscular dystrophy. *Drug Des Devel Ther* 11: 533-545.

Lin, X., Miller, J.W., Mankodi, A., Kanadia, R.N., Yuan, Y., Moxley, R.T., Swanson, M.S., and Thornton, C.A. (2006). Failure of MBNL1-dependent post-natal splicing transitions in myotonic dystrophy. *Hum Mol Genet* 15: 2087-2097.

Livak, K.J., and Schmittgen, T.D. (2001). Analysis of relative gene expression data using real-time quantitative PCR and the 2(-Delta Delta C(T)) Method. *Methods* 25: 402-408.

Llamusi, B., Munoz-Soriano, V., Paricio, N., and Artero, R. (2014). The use of whole-mount in situ hybridization to illustrate gene expression regulation. *Biochem Mol Biol Educ* 42: 339-347.

Lopez Castel, A., Overby, S.J., and Artero, R. (2019). MicroRNA-Based Therapeutic Perspectives in Myotonic Dystrophy. *Int J Mol Sci* 20.

Lopez-Martinez, A., Soblechero-Martin, P., de-la-Puente-Ovejero, L., Nogales-Gadea, G., and Arechavala-Gomeza, V. (2020). An Overview of Alternative Splicing Defects Implicated in Myotonic Dystrophy Type I. *Genes (Basel)* 11.

Lueck, J.D., Lungu, C., Mankodi, A., Osborne, R.J., Welle, S.L., Dirksen, R.T., and Thornton, C.A. (2007). Chloride channelopathy in myotonic dystrophy resulting from loss of posttranscriptional regulation for CLCN1. *Am J Physiol Cell Physiol* 292: C1291-1297.

Machuca-Tzili, L., Brook, D., and Hilton-Jones, D. (2005). Clinical and molecular aspects of the myotonic dystrophies: a review. *Muscle Nerve* 32: 1-18.

Maniatis, T., Fritsch, E.F., and Sambrook, J. (1982). Molecular cloning : a laboratory manual, *Cold Spring Harbor Laboratory*, Cold Spring Harbor, N.Y.

Mankodi, A., Logigian, E., Callahan, L., McClain, C., White, R., Henderson, D., Krym, M., and Thornton, C.A. (2000). Myotonic dystrophy in transgenic mice expressing an expanded CUG repeat. *Science* 289: 1769-1773.

Mankodi, A., Takahashi, M.P., Jiang, H., Beck, C.L., Bowers, W.J., Moxley, R.T., Cannon, S.C., and Thornton, C.A. (2002). Expanded CUG repeats trigger aberrant splicing of ClC-1 chloride channel pre-mRNA and hyperexcitability of skeletal muscle in myotonic dystrophy. *Mol Cell* 10: 35-44.

Mankodi, A., and Thornton, C.A. (2002). Myotonic syndromes. *Curr Opin Neurol* 15: 545-552.

Manning, K.S., Rao, A.N., Castro, M., and Cooper, T.A. (2017). BNA(NC) Gapmers Revert Splicing and Reduce RNA Foci with Low Toxicity in Myotonic Dystrophy Cells. *ACS Chem Biol* 12: 2503-2509.

## References


Marteyn, A., Maury, Y., Gauthier, M.M., Lecuyer, C., Vernet, R., Denis, J.A., Pietu, G., Peschanski, M., and Martinat, C. (2011). Mutant human embryonic stem cells reveal neurite and synapse formation defects in type 1 myotonic dystrophy. *Cell Stem Cell* 8: 434-444.

Martineau, L., Racine, V., Benichou, S.A., and Puymirat, J. (2018). Lymphoblastoids cell lines - Derived iPSC line from a 26-year-old myotonic dystrophy type 1 patient carrying (CTG)200 expansion in the DMPK gene: CHUQi001-A. *Stem Cell Res* 26: 103-106.

Matloka, M., Klein, A.F., Rau, F., and Furling, D. (2018). Cells of Matter-In Vitro Models for Myotonic Dystrophy. *Front Neurol* 9: 361.

Matynia, A., Ng, C.H., Dansithong, W., Chiang, A., Silva, A.J., and Reddy, S. (2010). Muscleblind1, but not Dmpk or Six5, contributes to a complex phenotype of muscular and motivational deficits in mouse models of myotonic dystrophy. *PLoS One* 5: e9857.

McDonald, C.M., Shieh, P.B., Abdel-Hamid, H.Z., Connolly, A.M., Ciafaloni, E., Wagner, K.R., Goemans, N., Mercuri, E., Khan, N., Koenig, E., *et al.* (2021). Open-Label Evaluation of Eteplirsen in Patients with Duchenne Muscular Dystrophy Amenable to Exon 51 Skipping: PROMOVI Trial. *J Neuromuscul Dis* 10.3233/JND-210643.

Mignon, L. (2017). IONIS-DMPKRx Clinical Program in Myotonic Dystrophy Myotonic Dystrophy Foundation.
https://www.myotonic.org/sites/default/files/MDF_Mignon_09Sep2017.pdf.

Miller, J.W., Urbinati, C.R., Teng-Umnuay, P., Stenberg, M.G., Byrne, B.J., Thornton, C.A., and Swanson, M.S. (2000). Recruitment of human muscleblind proteins to (CUG)(n) expansions associated with myotonic dystrophy. *EMBO J* 19: 4439-4448.

Misiak, P., Markiewicz, K.H., Szymczuk, D., and Wilczewska, A.Z. (2020). Polymeric Drug Delivery Systems Bearing Cholesterol Moieties: A Review. *Polymers (Basel)* 12.

Mladenovic, J., Pekmezovic, T., Todorovic, S., Rakocevic-Stojanovic, V., Savic, D., Romac, S., and Apostolski, S. (2006). Survival and mortality of myotonic dystrophy type 1 (Steinert's disease) in the population of Belgrade. *Eur J Neurol* 13: 451-454.

Mulders, S.A., van den Broek, W.J., Wheeler, T.M., Croes, H.J., van Kuik-Romeijn, P., de Kimpe, S.J., Furling, D., Platenburg, G.J., Gourdon, G., Thornton, C.A., *et al.* (2009). Triplet-repeat oligonucleotide-mediated reversal of RNA toxicity in myotonic dystrophy. *Proc Natl Acad Sci U S A* 106: 13915-13920.

Nakajima, K. (2016). Low serum amylase and obesity, diabetes and metabolic syndrome: A novel interpretation. *World J Diabetes* 7: 112-121.

Nakamori, M., Gourdon, G., and Thornton, C.A. (2011). Stabilization of expanded (CTG)*(CAG) repeats by antisense oligonucleotides. *Mol Ther* 19: 2222-2227.

Nakamori, M., Sobczak, K., Puwanant, A., Welle, S., Eichinger, K., Pandya, S., Dekdebrun, J., Heatwole, C.R., McDermott, M.P., Chen, T., *et al.* (2013). Splicing biomarkers of disease severity in myotonic dystrophy. *Ann Neurol* 74: 862-872.

Neil, E.E., and Bisaccia, E.K. (2019). Nusinersen: A Novel Antisense Oligonucleotide for the Treatment of Spinal Muscular Atrophy. *J Pediatr Pharmacol Ther* 24: 194-203.

Northrop-Clewes, C.A., and Thurnham, D.I. (2013). Biomarkers for the differentiation of anemia and their clinical usefulness. *J Blood Med* 4: 11-22.

O'Connell, K.E., Mikkola, A.M., Stepanek, A.M., Vernet, A., Hall, C.D., Sun, C.C., Yildirim, E., Staropoli, J.F., Lee, J.T., and Brown, D.E. (2015). Practical murine hematopathology: a comparative review and implications for research. *Comp Med* 65: 96-113.

Overby, S.J., Cerro-Herreros, E., Llamusi, B., and Artero, R. (2018). RNA-mediated therapies in myotonic dystrophy. *Drug Discov Today* 10.1016/j.drudis.2018.08.004.

Ozimski, L.L., Sabater-Arcis, M., Bargiela, A., and Artero, R. (2021). The hallmarks of myotonic dystrophy type 1 muscle dysfunction. *Biol Rev Camb Philos Soc* 96: 716-730.

Pandey, S.K., Wheeler, T.M., Justice, S.L., Kim, A., Younis, H.S., Gattis, D., Jauvin, D., Puymirat, J., Swayze, E.E., Freier, S.M., *et al.* (2015). Identification and characterization of modified antisense oligonucleotides targeting DMPK in mice and nonhuman primates for the treatment of myotonic dystrophy type 1. *J Pharmacol Exp Ther* 355: 329-340.

Pang, P.D., Alsina, K.M., Cao, S., Koushik, A.B., Wehrens, X.H.T., and Cooper, T.A. (2018). CRISPR -Mediated Expression of the Fetal Scn5a Isoform in Adult Mice Causes Conduction Defects and Arrhythmias. *J Am Heart Assoc* 7: e010393.

Pascual, M., Vicente, M., Monferrer, L., and Artero, R. (2006). The Muscleblind family of proteins: an emerging class of regulators of developmentally programmed alternative splicing. *Differentiation* 74: 65-80.

Pascual-Gilabert, M., Lopez-Castel, A., and Artero, R. (2021). Myotonic dystrophy type 1 drug development: A pipeline toward the market. *Drug Discov Today* 26: 1765-1772.

Philips, A.V., Timchenko, L.T., and Cooper, T.A. (1998). Disruption of splicing regulated by a CUG-binding protein in myotonic dystrophy. *Science* 280: 737-741.

Pinto, R.M., Dragileva, E., Kirby, A., Lloret, A., Lopez, E., St Claire, J., Panigrahi, G.B., Hou, C., Holloway, K., Gillis, T., *et al.* (2013). Mismatch repair genes Mlh1 and Mlh3 modify CAG instability in Huntington's disease mice: genome-wide and candidate approaches. *PLoS Genet* 9: e1003930.

Poulos, M.G., Batra, R., Li, M., Yuan, Y., Zhang, C., Darnell, R.B., and Swanson, M.S. (2013). Progressive impairment of muscle regeneration in muscleblind-like 3 isoform knockout mice. *Hum Mol Genet* 22: 3547-3558.

Rau, F., Freyermuth, F., Fugier, C., Villemin, J.P., Fischer, M.C., Jost, B., Dembele, D., Gourdon, G., Nicole, A., Duboc, D., *et al.* (2011). Misregulation of miR-1 processing is associated with heart defects in myotonic dystrophy. *Nat Struct Mol Biol* 18: 840-845.

Rau, F., Laine, J., Ramanoudjame, L., Ferry, A., Arandel, L., Delalande, O., Jollet, A., Dingli, F., Lee, K.Y., Peccate, C., *et al.* (2015). Abnormal splicing switch of DMD's penultimate exon compromises muscle fibre maintenance in myotonic dystrophy. *Nat Commun* 6: 7205.

Reynolds, M.A., Hogrefe, R.I., Jaeger, J.A., Schwartz, D.A., Riley, T.A., Marvin, W.B., Daily, W.J., Vaghefi, M.M., Beck, T.A., Knowles, S.K., *et al.* (1996). Synthesis and thermodynamics of oligonucleotides containing chirally pure R(P) methylphosphonate linkages. *Nucleic Acids Res* 24: 4584-4591.

Rigoutsos, I., and Furnari, F. (2010). Gene-expression forum: Decoy for microRNAs. *Nature* 465: 1016-1017.

Rinaldi, C., and Wood, M.J.A. (2018). Antisense oligonucleotides: the next frontier for treatment of neurological disorders. *Nat Rev Neurol* 14: 9-21.

Roberts, T.C., Langer, R., and Wood, M.J.A. (2020). Advances in oligonucleotide drug delivery. *Nat Rev Drug Discov* 19: 673-694.

Rupaimoole, R., and Slack, F.J. (2017). MicroRNA therapeutics: towards a new era for the management of cancer and other diseases. *Nat Rev Drug Discov* 16: 203-222.

Sarma, P.R. (1990). Red Cell Indices. In: rd, Walker, H.K., Hall, W.D., and Hurst, J.W. (eds). Clinical Methods: The History, Physical, and Laboratory Examinations: Boston.

Savkur, R.S., Philips, A.V., and Cooper, T.A. (2001). Aberrant regulation of insulin receptor alternative splicing is associated with insulin resistance in myotonic dystrophy. *Nat Genet* 29: 40-47.

Schneck, K., Washington, M., Holder, D., Lodge, K., and Motzel, S. (2000). Hematologic and serum biochemical reference values in nontransgenic FVB mice. *Comp Med* 50: 32-35.

Schneider, C.A., Rasband, W.S., and Eliceiri, K.W. (2012). NIH Image to ImageJ: 25 years of image analysis. *Nat Methods* 9: 671-675.

Senior, J.R. (2012). Alanine aminotransferase: a clinical and regulatory tool for detecting liver injury-past, present, and future. *Clin Pharmacol Ther* 92: 332-339.

Seth, P.P., Tanowitz, M., and Bennett, C.F. (2019). Selective tissue targeting of synthetic nucleic acid drugs. *J Clin Invest* 129: 915-925.

Seznec, H., Agbulut, O., Sergeant, N., Savouret, C., Ghestem, A., Tabti, N., Willer, J.C., Ourth, L., Duros, C., Brisson, E., *et al.* (2001). Mice transgenic for the human myotonic dystrophy region with expanded CTG repeats display muscular and brain abnormalities. *Hum Mol Genet* 10: 2717-2726.

Sharma, S., Pujani, M., Pahuja, S., Chandra, J., Rath, B., and Labhchand (2010). Critical evaluation of peripheral smear in cases of anemia with high mean corpuscular hemoglobin concentration in children: a series of four cases. *Indian J Pathol Microbiol* 53: 820-823.

Sharma, V.K., Rungta, P., and Prasad, A.K. (2014). Nucleic acid therapeutics: basic concepts and recent developments. *RSC Advances* 4: 16618–16631.

Shen, W., De Hoyos, C.L., Sun, H., Vickers, T.A., Liang, X.H., and Crooke, S.T. (2018). Acute hepatotoxicity of 2' fluoro-modified 5-10-5 gapmer phosphorothioate oligonucleotides in mice correlates with intracellular protein binding and the loss of DBHS proteins. *Nucleic Acids Res* 46: 2204-2217.

Shen, X., Soibam, B., Benham, A., Xu, X., Chopra, M., Peng, X., Yu, W., Bao, W., Liang, R., Azares, A., *et al.* (2016). miR-322/-503 cluster is expressed in the earliest cardiac progenitor cells and drives cardiomyocyte specification. *Proc Natl Acad Sci U S A* 113: 9551-9556.

Shi, R., Sun, Y.H., Zhang, X.H., and Chiang, V.L. (2012). Poly(T) adaptor RT-PCR. *Methods Mol Biol* 822: 53-66.

Sobczak, K., Wheeler, T.M., Wang, W., and Thornton, C.A. (2013). RNA interference targeting CUG repeats in a mouse model of myotonic dystrophy. *Mol Ther* 21: 380-387.

Song, K.Y., Guo, X.M., Wang, H.Q., Zhang, L., Huang, S.Y., Huo, Y.C., Zhang, G., Feng, J.Z., Zhang, R.R., Ma, Y., *et al.* (2020). MBNL1 reverses the proliferation defect of skeletal muscle satellite cells in myotonic dystrophy type 1 by inhibiting autophagy via the mTOR pathway. *Cell Death Dis* 11: 545.

Souleimanian, N., Deleavey, G.F., Soifer, H., Wang, S., Tiemann, K., Damha, M.J., and Stein, C.A. (2012). Antisense 2'-Deoxy, 2'-Fluroarabino Nucleic Acids (2'F-ANAs) Oligonucleotides: In Vitro Gymnotic Silencers of Gene Expression Whose Potency Is Enhanced by Fatty Acids. *Mol Ther Nucleic Acids* 1: e43.

Suenaga, K., Lee, K.Y., Nakamori, M., Tatsumi, Y., Takahashi, M.P., Fujimura, H., Jinnai, K., Yoshikawa, H., Du, H., Ares, M., Jr., *et al.* (2012). Muscleblind-like 1 knockout mice reveal novel splicing defects in the myotonic dystrophy brain. *PLoS One* 7: e33218.

Sugo, T., Terada, M., Oikawa, T., Miyata, K., Nishimura, S., Kenjo, E., Ogasawara-Shimizu, M., Makita, Y., Imaichi, S., Murata, S., *et al.* (2016). Development of antibody-siRNA conjugate targeted to cardiac and skeletal muscles. *J Control Release* 237: 1-13.

Suominen, T., Bachinski, L.L., Auvinen, S., Hackman, P., Baggerly, K.A., Angelini, C., Peltonen, L., Krahe, R., and Udd, B. (2011). Population frequency of myotonic dystrophy: higher than expected frequency of myotonic dystrophy type 2 (DM2) mutation in Finland. *Eur J Hum Genet* 19: 776-782.

Swayze, E.E., Siwkowski, A.M., Wancewicz, E.V., Migawa, M.T., Wyrzykiewicz, T.K., Hung, G., Monia, B.P., and Bennett, C.F. (2007). Antisense oligonucleotides containing locked nucleic acid improve potency but cause significant hepatotoxicity in animals. *Nucleic Acids Res* 35: 687-700.

Tabas, I. (2002). Cholesterol in health and disease. *J Clin Invest* 110: 583-590.

Taketo, M., Schroeder, A.C., Mobraaten, L.E., Gunning, K.B., Hanten, G., Fox, R.R., Roderick, T.H., Stewart, C.L., Lilly, F., Hansen, C.T., *et al.* (1991). FVB/N: an inbred mouse strain preferable for transgenic analyses. *Proc Natl Acad Sci U S A* 88: 2065-2069.

Tang, Z.Z., Yarotskyy, V., Wei, L., Sobczak, K., Nakamori, M., Eichinger, K., Moxley, R.T., Dirksen, R.T., and Thornton, C.A. (2012). Muscle weakness in myotonic dystrophy associated with misregulated splicing and altered gating of Ca(V)1.1 calcium channel. *Hum Mol Genet* 21: 1312-1324.

Tanner, M.K., Tang, Z., and Thornton, C.A. (2021). Targeted splice sequencing reveals RNA toxicity and therapeutic response in myotonic dystrophy. *Nucleic Acids Res* 49: 2240-2254.

Teplyuk, N.M., Uhlmann, E.J., Gabriely, G., Volfovsky, N., Wang, Y., Teng, J., Karmali, P., Marcusson, E., Peter, M., Mohan, A., *et al.* (2016). Therapeutic potential of targeting microRNA-10b in established intracranial glioblastoma: first steps toward the clinic. *EMBO Mol Med* 8: 268-287.

Terenzi, F., and Ladd, A.N. (2010). Conserved developmental alternative splicing of muscleblind-like (MBNL) transcripts regulates MBNL localization and activity. *RNA Biol* 7: 43-55.

Ting, K.K., Zhao, Y., Shen, W., Coleman, P., Yam, M., Chan-Ling, T., Li, J., Moller, T., Gillies, M., Vadas, M.A., *et al.* (2019). Therapeutic regulation of VE-cadherin with a novel oligonucleotide drug for diabetic eye complications using retinopathy mouse models. *Diabetologia* 62: 322-334.

Tome, S., and Gourdon, G. (2020). DM1 Phenotype Variability and Triplet Repeat Instability: Challenges in the Development of New Therapies. *Int J Mol Sci* 21.

Tran, H., Gourrier, N., Lemercier-Neuillet, C., Dhaenens, C.-M., Vautrin, A., Fernandez-Gomez, F.J., Arandel, L., Carpentier, C., Obriot, H., Eddarkaoui, S., *et al.* (2011). Analysis of Exonic Regions Involved in Nuclear Localization, Splicing Activity, and Dimerization of Muscleblind-like-1 Isoforms. *Journal of Biological Chemistry* 286: 16435-16446.

Tsilfidis, C., MacKenzie, A.E., Mettler, G., Barcelo, J., and Korneluk, R.G. (1992). Correlation between CTG trinucleotide repeat length and frequency of severe congenital myotonic dystrophy. *Nat Genet* 1: 192-195.

## References


Ueki, J., Nakamori, M., Nakamura, M., Nishikawa, M., Yoshida, Y., Tanaka, A., Morizane, A., Kamon, M., Araki, T., Takahashi, M.P., *et al.* (2017). Myotonic dystrophy type 1 patient-derived iPSCs for the investigation of CTG repeat instability. *Sci Rep* 7: 42522.

van Agtmaal, E.L., Andre, L.M., Willemse, M., Cumming, S.A., van Kessel, I.D.G., van den Broek, W., Gourdon, G., Furling, D., Mouly, V., Monckton, D.G., *et al.* (2017). CRISPR/Cas9-Induced (CTGCAG)n Repeat Instability in the Myotonic Dystrophy Type 1 Locus: Implications for Therapeutic Genome Editing. *Mol Ther* 25: 24-43.

Veenstra, J., Smit, W.M., Krediet, R.T., and Arisz, L. (1994). Relationship between elevated creatine phosphokinase and the clinical spectrum of rhabdomyolysis. *Nephrol Dial Transplant* 9: 637-641.

Vihola, A., Bachinski, L.L., Sirito, M., Olufemi, S.E., Hajibashi, S., Baggerly, K.A., Raheem, O., Haapasalo, H., Suominen, T., Holmlund-Hampf, J., *et al.* (2010). Differences in aberrant expression and splicing of sarcomeric proteins in the myotonic dystrophies DM1 and DM2. *Acta Neuropathol* 119: 465-479.

Vihola, A., Sirito, M., Bachinski, L.L., Raheem, O., Screen, M., Suominen, T., Krahe, R., and Udd, B. (2013). Altered expression and splicing of Ca(2+) metabolism genes in myotonic dystrophies DM1 and DM2. *Neuropathol Appl Neurobiol* 39: 390-405.

Wagner, S.D., Struck, A.J., Gupta, R., Farnsworth, D.R., Mahady, A.E., Eichinger, K., Thornton, C.A., Wang, E.T., and Berglund, J.A. (2016). Dose-Dependent Regulation of Alternative Splicing by MBNL Proteins Reveals Biomarkers for Myotonic Dystrophy. *PLoS Genet* 12: e1006316.

Wahbi, K., and Furling, D. (2020). Cardiovascular manifestations of myotonic dystrophy. *Trends Cardiovasc Med* 30: 232-238.

Wallace, L.M., Garwick-Coppens, S.E., Tupler, R., and Harper, S.Q. (2011). RNA interference improves myopathic phenotypes in mice over-expressing FSHD region gene 1 (FRG1). *Mol Ther* 19: 2048-2054.

Wang, E.T., Cody, N.A., Jog, S., Biancolella, M., Wang, T.T., Treacy, D.J., Luo, S., Schroth, G.P., Housman, D.E., Reddy, S., *et al.* (2012). Transcriptome-wide regulation of pre-mRNA splicing and mRNA localization by muscleblind proteins. *Cell* 150: 710-724.

Wang, E.T., Treacy, D., Eichinger, K., Struck, A., Estabrook, J., Olafson, H., Wang, T.T., Bhatt, K., Westbrook, T., Sedehizadeh, S., *et al.* (2019). Transcriptome alterations in myotonic dystrophy skeletal muscle and heart. *Human Molecular Genetics* 28: 1312-1321.

Wang, E.T., Ward, A.J., Cherone, J.M., Giudice, J., Wang, T.T., Treacy, D.J., Lambert, N.J., Freese, P., Saxena, T., Cooper, T.A., *et al.* (2015). Antagonistic regulation of mRNA expression and splicing by CELF and MBNL proteins. *Genome Res* 25: 858-871.

Wang, G.S., Kuyumcu-Martinez, M.N., Sarma, S., Mathur, N., Wehrens, X.H., and Cooper, T.A. (2009). PKC inhibition ameliorates the cardiac phenotype in a mouse model of myotonic dystrophy type 1. *J Clin Invest* 119: 3797-3806.

Wang, P.Y., Chang, K.T., Lin, Y.M., Kuo, T.Y., and Wang, G.S. (2018). Ubiquitination of MBNL1 Is Required for Its Cytoplasmic Localization and Function in Promoting Neurite Outgrowth. *Cell Rep* 22: 2294-2306.

Wheeler, T.M., Leger, A.J., Pandey, S.K., MacLeod, A.R., Nakamori, M., Cheng, S.H., Wentworth, B.M., Bennett, C.F., and Thornton, C.A. (2012). Targeting nuclear RNA for in vivo correction of myotonic dystrophy. *Nature* 488: 111-115.

Wheeler, T.M., Lueck, J.D., Swanson, M.S., Dirksen, R.T., and Thornton, C.A. (2007). Correction of ClC-1 splicing eliminates chloride channelopathy and myotonia in mouse models of myotonic dystrophy. *J Clin Invest* 117: 3952-3957.

Wheeler, T.M., Sobczak, K., Lueck, J.D., Osborne, R.J., Lin, X., Dirksen, R.T., and Thornton, C.A. (2009). Reversal of RNA dominance by displacement of protein sequestered on triplet repeat RNA. *Science* 325: 336-339.

Wienholds, E., and Plasterk, R.H. (2005). MicroRNA function in animal development. *FEBS Lett* 579: 5911-5922.

Wojtkowiak-Szlachcic, A., Taylor, K., Stepniak-Konieczna, E., Sznajder, L.J., Mykowska, A., Sroka, J., Thornton, C.A., and Sobczak, K. (2015). Short antisense-locked nucleic acids (all-LNAs) correct alternative splicing abnormalities in myotonic dystrophy. *Nucleic Acids Res* 43: 3318-3331.

Xia, G., Santostefano, K.E., Goodwin, M., Liu, J., Subramony, S.H., Swanson, M.S., Terada, N., and Ashizawa, T. (2013). Generation of neural cells from DM1 induced pluripotent stem cells as cellular model for the study of central nervous system neuropathogenesis. *Cell Reprogram* 15: 166-177.

Yamashita, Y., Matsuura, T., Shinmi, J., Amakusa, Y., Masuda, A., Ito, M., Kinoshita, M., Furuya, H., Abe, K., Ibi, T., *et al.* (2012). Four parameters increase the sensitivity and specificity of the exon array analysis and disclose 25 novel aberrantly spliced exons in myotonic dystrophy. *J Hum Genet* 57: 368-374.

Yanovsky-Dagan, S., Avitzour, M., Altarescu, G., Renbaum, P., Eldar-Geva, T., Schonberger, O., Mitrani-Rosenbaum, S., Levy-Lahad, E., Birnbaum, R.Y., Gepstein, L., *et al.* (2015). Uncovering the Role of Hypermethylation by CTG Expansion in Myotonic Dystrophy Type 1 Using Mutant Human Embryonic Stem Cells. *Stem Cell Reports* 5: 221-231.

Young, J.A., Ting, K.K., Li, J., Moller, T., Dunn, L., Lu, Y., Moses, J., Prado-Lourenco, L., Khachigian, L.M., Ng, M., *et al.* (2013). Regulation of vascular leak and recovery from ischemic injury by general and VE-cadherin-restricted miRNA antagonists of miR-27. *Blood* 122: 2911-2919.

Yuan, Y., Compton, S.A., Sobczak, K., Stenberg, M.G., Thornton, C.A., Griffith, J.D., and Swanson, M.S. (2007). Muscleblind-like 1 interacts with RNA hairpins in splicing target and pathogenic RNAs. *Nucleic Acids Res* 35: 5474-5486.

Zhang, B.W., Cai, H.F., Wei, X.F., Sun, J.J., Lan, X.Y., Lei, C.Z., Lin, F.P., Qi, X.L., Plath, M., and Chen, H. (2016). miR-30-5p Regulates Muscle Differentiation and Alternative Splicing of Muscle-Related Genes by Targeting MBNL. *Int J Mol Sci* 17.

Zhang, W., Yu, G., Zhang, Y., Tang, F., Lv, J., Tian, G., Zhang, Y., Liu, J., Mi, J., and Zhang, J. (2019). Quantitative Dot Blot (QDB) as a universal platform for absolute quantification of tissue biomarkers. *Anal Biochem* 576: 42-47.

Zhou, J., and Rossi, J. (2017). Aptamers as targeted therapeutics: current potential and challenges. *Nat Rev Drug Discov* 16: 440.

# Annex

# Proof of concept of peptide-linked blockmiR induced MBNL functional rescue in Myotonic Dystrophy Type 1 mouse model

**Sarah J. Overby[1,2], Estefanía Cerro-Herreros[1,2], Irene González-Martínez[1,2], Miguel A. Varela[3,4], David Seoane-Miraz[3,4], Yahya Jad[3,4], Richard Raz[3,4], Thorleif Møller[5], Manuel Pérez-Alonso[1,2], Matthew J. Wood[3,4], Beatriz Llamusí[1,2,6], Rubén Artero[1,2]**

[1]University Institute of Biotechnology and Biomedicine (BIOTECMED), Universidad de Valencia, 46100 Burjassot, Spain; [2]Translational Genomics Group, Incliva Biomedical Research Institute, 46010 Valencia, Spain; [3]Department of Paediatrics, University of Oxford, John Radcliffe Hospital, OX3 9DU, Oxford, UK; [4]MDUK Oxford Neuromuscular Centre, University of Oxford, Oxford, UK.[5]Ranger Biotechnologies; [6]ARTHEx Biotech S.L, Calle Catedrático Agustín Escardino 9 (current address)

**Myotonic Dystrophy Type 1 is a debilitating neuromuscular disease causing muscle weakness, myotonia, and cardiac dysfunction. The phenotypes are caused by Muscleblind-like (MBNL) protein sequestration by toxic RNA in the DM1 Protein Kinase (*DMPK*) gene. DM1 patients exhibit a pathogenic number of repetitions in *DMPK* which leads to down-stream symptoms. Another disease characteristic is altered miRNA expression. It was previously shown that miR-23b regulates the translation of *MBNL1* into protein (Cerro-Herreros et al. 2018). Antisense oligonucleotide (AON) treatment targeting this miRNA can improve disease symptoms (Cerro-Herreros et al. 2020). Here we present a refinement of this strategy targeting a miR-23b binding site on the *MBNL1* 3'-UTR in DM1 model cells and mice by using AONs called BlockmiRs. BlockmiRs linked to novel cell-penetrating peptide chemistry showed an increase in MBNL1 protein in DM1 model cells and HSA$^{LR}$ mice. They also showed an increase in muscle strength and significant rescue of downstream splicing and histological phenotypes in mice.**

## INTRODUCTION

Myotonic Dystrophy Type 1 (DM1) is a dominantly-inherited neuromuscular disorder characterized by muscle weakness and involuntary muscle contraction. These symptoms have a significant impact in the quality of life of patients especially when muscle strength is needed.[1] Other symptoms include cardiac arrhythmias, cataracts, insulin resistance, and respiratory difficulties (OMIM; MIM: 160900). The disease originates in a toxic CUG repeat expansion in the DM1 Protein Kinase (*DMPK*) gene transcripts inducing the sequestration of Muscleblind-like (MBNL) proteins.[2] MBNL proteins play a critical role in regulating mRNA metabolism specifically post-transcription alternative splicing and alternative polyadenylation.[3-5] MBNL1 and 2 have similar expression patterns post-natally encouraging adult alternative splicing patterns. They also show functional overlap and can compensate for one another when necessary.[6] MBNL3 principally functions during the embryonic prenatal phase or in adult regenerating tissues. Consequently, aberrant fetal splicing patterns in certain transcripts are hallmarks of the DM1 disease profile and lead to the DM1 phenotype.[6] Indeed, human-induced pluripotent stem cells (hiPSCs) that were CRISPR/Cas9 edited to reduce MBNL proteins recapitulated DM1 phenotypes such as mis-splicing and impairment of late myogenic fusion.[7]

Additionally, as MBNL proteins are sequestered, CUGBP Elav-Like Family Member 1 (CELF1) proteins are up-regulated.[8] CELF1 proteins also function as splicing regulators and their increase also contributes to splicing abnormalities in DM1. Indeed, CELF and MBNL proteins show an antagonistic relationship that effects splicing patterns.[9]

Antisense oligonucleotides (AONs) are a promising nucleic acid therapy across a variety of neuromuscular disorders.[10] Indeed, various AONs have also shown promise for treatment of DM1.[11] For example, short locked-nucleic acid (LNA), charge-neutral morpholino (PMO), and cell-penetrating peptide-linked morpholino (P-PMO) based AONs targeting the toxic *DMPK* repetitions were able to block the binding of MBNL proteins.[12-14] Specifically, one P-PMO produced therapeutic results in DM1 HSA$^{LR}$ mice, including splicing rescue, myotonia and reduction of nuclear foci.[14]

PMOs have a neutral charge that create a highly stable compound and facilitate efficient delivery to the cell. A PMO called Eteplirsen has already obtained FDA approval for the treatment of Duchenne muscular dystrophy (DMD).[15] PMOs can also be covalently linked with cell penetrating peptides to further promote cell uptake like the Pip6a-PMO compound that previously showed cardiac improvements in DMD mouse models.[16, 17]

AONs have also been used as therapy in DM1 by targeting miRNAs regulating MBNL protein synthesis instead of the CUG repetitions. In this way, increased MBNL production can compensate for non-functional MBNL sequestered by toxic repeats. It has been previously shown that antagomiRs targeting miR-218 and miR-23b increase MBNL1 production by blocking *MBNL* transcript regulation.[18] Rescue of MBNL1 protein was observed after treatment in DM1 cells[18] as well as in HSA$^{LR}$ mice.[19] Other rescue observed in these studies include alternative splicing, histological phenotypes, myotonia, and grip strength. Concurrently, miRNA activity is increasingly being investigated in the context of DM1 namely the roles of miR-7[20] and miR-1.[21]

AntimiRs or "antagomiRs" have been well characterized for their capability in blocking miRNA activity[22, 23]. However, because miRNAs can have hundreds of target transcripts,[24] it is difficult to set apart their specific effects on MBNLs versus their additional effects on several other mRNAs. In this paper we describe an alternative to antimiR technology called "blockmiRs". BlockmiRs are similar to antimiRs in that they both use antisense technology to reduce miRNA regulation. However, instead of binding to miRNAs, they bind specifically to the 3' untranslated region (UTR) binding site on the target transcript. This blocks interaction with miRNAs thereby allowing translation to occur. In this way, blockmiRs are binding site sequence specific and not miRNA sequence specific.

Here, we show the effects of a novel blockmiR strategy with linkage to a new peptide called Pip9b2. The peptide is designed to facilitate efficient entry into the cell without the use of transfection reagents. Pip9b2 peptide-linked PMO blockmiRs were designed against a binding site of miR-23b on *MBNL1* and tested in immortalized patient-derived DM1 fibroblasts transdifferentiated into myotubes (DM1 cells).[25] After treatment in cells, the blockmiR increased the amount of *MBNL1* transcripts and protein with low toxicity. The compound was then tested in HSA$^{LR}$ mice. Therapeutic effects include increased grip strength, splicing rescue, increase in Mbnl1 protein, and histological improvements.

**Correspondence:** Ruben Artero; University Institute for Biotechnology and Biomedicine (BIOTECMED), Universidad de Valencia, 46100 Burjassot, Spain
**Email:** ruben.artero@uv.es

RESULTS

**Pip9b2-linked PMO blockmiR increases MBNL1 in cells**

Pip9b2 is a cell penetrating peptide that contains two flanking regions enriched with arginines (cationic amino acids) and a central hydrophobic core. The sequence can be found in Materials and Methods. The peptide-linkage to the PMO blockmiR is designed to facilitate cell entry without the need for transfection reagent. To test for cell toxicity, the P-PMO blockmiR and a peptide-linked with a scrambled PMO (P-SC), a chemistry control, were administered in DM1 cells at increasing concentrations (Figure 1A). The peptide-linked oligos showed little to no cell growth inhibition across all concentrations in contrast to those treated with transfection reagent which began to show 50% cell growth inhibition after 50 nM. Therefore, for the rest of the experiments, P-PMO and P-SC were administered at 1 μM per manufacturer's recommendation.

DM1 cells showed an increase in *MBNL1* and 2 transcript expression levels after P-PMO blockmiR treatment (Figures 1B-C). Aberrant fetal splicing patterns in *MBNL1* and *NFIX* transcripts show a strong phenotype in DM1 cells. After treatment with the blockmiR, a slight but significant return to the adult splicing pattern was observed. The cells also showed a striking increase in MBNL1 protein immunofluorescence through analysis of confocal microscopy images (Figures 1F-I).

From a qualitative standpoint, the cells treated with cell-penetrating peptide blockmiRs were visibly more prolific and showed a large increase in MBNL1 fluorescence in the cytoplasm. Quantification of the mean pixel intensity for each cell confirmed this increase (Figure 1J).

**miR-23b binding site is conserved in mice**

The success of the blockmiRs *in vitro* led to *in vivo* testing in mice. But before this experiment could take place, the binding site of miR-23b needed to be confirmed in mouse. Site 1 on the *MBNL1* 3'-UTR has previously been confirmed in HeLa cells through dual luciferase assay.[18] This site shares sequence homology with Site 2 of the two predicted miR-23b binding sites in mice save for one nucleotide (Figure 2A). To confirm these predicted sites, another luciferase assay was performed in mouse C2C12 cells using *Mbnl1* 3'-UTR constructs. Three reporter plasmids were generated, one containing the wildtype *Mbnl1* (WT), one with deletion of the respective miR-23b seed region in the binding site (Del), and one with a complementary perfect match to the full miR-23b sequence (PM). The plasmids were transfected in C2C12 cells and the GLuc and SEAP luminescence was read after 48 h. If miRNA binding occurs, GLuc translation is inhibited and therefore luminescence decreases.

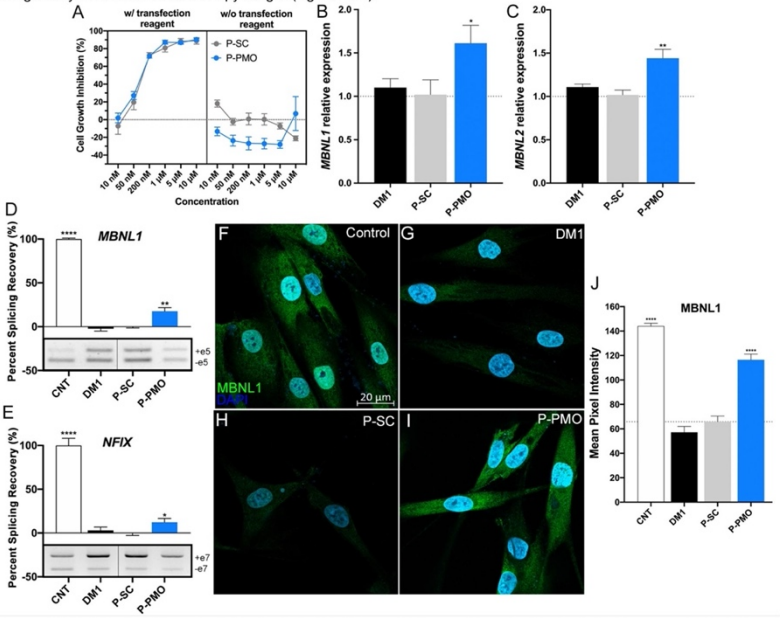


**Figure 1. P-PMO blockmiR effects on DM1 cells.** (A) The P-PMO blockmiR along with the scramble control (P-SC) was tested for cell viability at increasing concentrations with and without the use of transfection reagent. The peptide conjugation is designed to penetrate the cell without the need for transfection reagent. Expression of (B) *MBNL1* and (C) *MBNL2* transcripts was relatively quantified in triplicate from cells after treatment with the P-PMO blockmiR at 1 μM. Percent Splicing Recovery (PSR) was calculated after RT-PCR and exon band quantification for (D) *MBNL1* exon 5 and (E) *NFIX* exon 7 and normalized to CNT samples. Representative gels can be seen below each graph. *GAPDH* was run as an endogenous control (not shown). Immunofluoresence of MBNL1 protein (green) and DAPI (blue) was observed in DM1 and control cells (F-I) and the mean pixel intensity of each was quantified (J). Cell count: CNT n=118, DM1 n=83, P-SC n=96, P-PMO n=108. All statistical comparisons were performed against P-SC via Student's t-test. P-value GP style: 0.1234 (ns), 0.0332 (*), 0.0021 (**), 0.0002 (***), <0.0001 (****). Error bars = SEM.

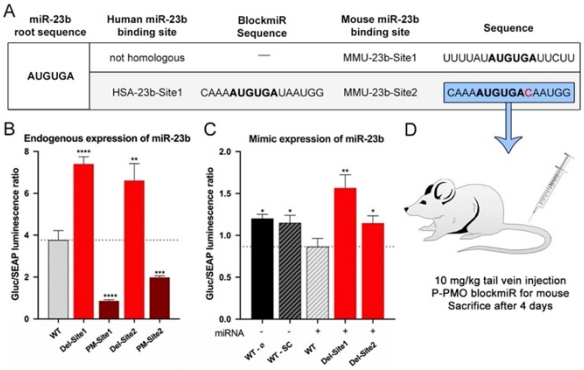


**Figure 2. Dual luciferase assay confirms conservation of miR-23b binding site.** (A) Sequence analysis (shown 5' to 3') shows that the predicted mouse Site 2 is identical to human Site 1 for miR-23b except for one nucleotide difference marked in red. miRNA seed region is marked in bold. (B) Gluc and SEAP luminescence was quantified in C2C12 mouse cells after transfection with reporter plasmids containing the 3'-UTR of Mbnl1 either wildtype (WT), the miR-23b seed region deleted (Del) or perfect match to miR-23b (PM). (C) To further confirm the luminescence observed was due to miR-23b, the experiment was repeated with co-transfection of a miRNA mimic of miR-23b. Two mimic controls were used, one with no mimic (WT-∅) and one with a scrambled mimic (WT-SC). All dual luciferase assays were normalized to SEAP and compared to WT for statistical comparison using Student's t-Test. P-value GP style: 0.1234 (ns), 0.0332 (*), 0.0021 (**), 0.0002 (***), <0.0001 (****). Error bars = SEM. (D) After site confirmation, a new P-PMO blockmiR was generated matching the mouse sequence along with a scramble control. They were administered by tail vein injection at 12.5 mg/kg and left for four days before sacrifice and muscle isolation.

SEAP is constitutively translated as a normalization control. Endogenous expression of miR-23b binding in the C2C12 cells was apparent through the increase of luminescence in the miR-23b binding site deletion plasmids in comparison to the wildtype (Figure 2B). In contrast, GLuc signal was decreased upon transfection with perfect match plasmids. This confirms that miR-23b is directly binding to these sites.

In order to further validate these binding sites, the experiment was repeated using a miR-23b mimic. Upon seed region deletion, GLuc luminescence increased once again. Also supporting this information was the wildtype no-mimic control and the wildtype scrambled-mimic control which both showed less miRNA repression compared to wildtype and mimic co-transfection. Through these assays, Sites 1 and 2 were both confirmed as miR-23b binding sites in the mouse *Mbnl1* 3'-UTR. Therefore, P-PMO blockmiR was tested *in vivo*. A new compound was generated accounting for the single nucleotide difference and was administered at 10 mg/kg through tail vein injection in HSA$^{LR}$ DM1 model mice (n = 6). A scramble control was also injected at the same concentration (n = 6). A group of FVB healthy mice (n = 5) and a group of HSA$^{LR}$ mice (n = 5) were administered PBS as two separate controls. After four days, mice were sacrificed and analyzed for disease phenotypes.

**P-PMO is non-toxic to mice and increases grip strength**

Mice grip strength was measured before and after treatment and the percent normal force was calculated for each group (Figure 3A). The P-PMO treated mice showed a large increase in percentage of normal force. The change was statistically significant compared to the same mice treated with PBS through Student's t-Test.

After treatment, blood serum was extracted from the mice for biochemical analysis (Figure 3B). The FVB levels were set as the healthy control level to which all other treatments were compared. One of the few significant changes was a decrease in creatine phosphokinase (CPK) levels. CPK is released into the blood during muscle tissue damage.[26] The lower amounts seen here indicate a lack of tissue damage and are within the range for normal levels in healthy mice. Also significantly different from FVB are the amylase levels after treatment with the P-PMO and, curiously, the PBS control. However, after closer look, these levels were also within the normal range for healthy mice. Importantly, the rest of the parameters indicating hepatotoxicity or tissue damage, including ALT, AST, bilirubin, bile acids, and LDH, remained unchanged after blockmiR treatment. Other health indicators such as creatinine, cholesterol, glucose, and triglycerides, as well as mouse weight were also stable.

**BlockmiR induces rescue of HSA$^{LR}$ mice phenotypes**

After seeing promising results at the physiological level, the mice were analyzed at the molecular level for changes in the DM1 phenotype specifically in the quadriceps leg muscle.

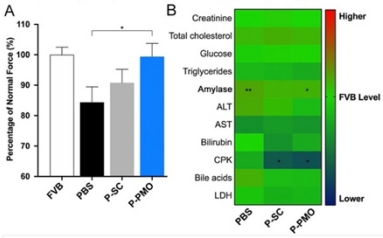


**Figure 3. Pip9b2-linked blockmiR affects grip strength without toxicity.** (A) Mouse grip strength was measured before and after treatment with P-PMO or P-SC by grip meter to calculate the percent of normal force normalized to mouse weight. Student's t-Test was used for statistical comparison. (B) Blood serum biochemistry was analyzed after treatments. All samples were statistically compared to FVB mice through Kruskal-Wallis ANOVA and Wilcoxon test if applicable. All parameters were within the normal range for healthy mice. P-value GP style: 0.1234 (ns), 0.0332 (*), 0.0021 (**), 0.0002 (***), <0.0001 (****). Error bars = SEM.

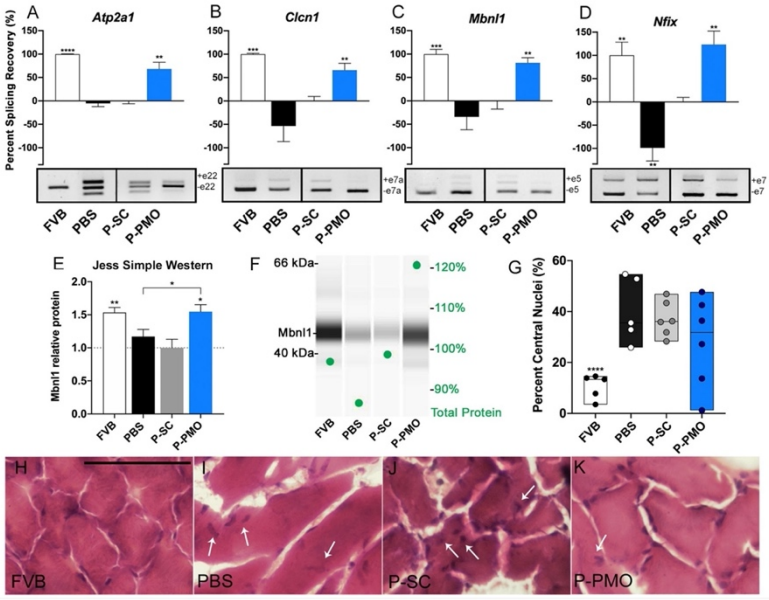


**Figure 4. P-PMO blockmiR rescues molecular and histological phenotypes of HSA$^{LR}$ mice.** RT-PCR was performed to analyze alternative splicing patterns in exons of interest for (A) *Atp2a1* (B) *Clcn1* (C) *Mbnl1* and (D) *Nfix* transcripts. *Gapdh* was run as an endogenous control (not shown). PSR was calculated normalized to FVB samples. Representative gels can be seen below each graph. (E) Relative protein was quantified using Jess Simple Western technology. (F) A representative lane view shows the bands observed compared to total protein normalization (green dots and scale). Finally, 10 µm sections of quadriceps muscle were cut and stained with hematoxylin and eosin in order to visualize the localization of central nuclei within the muscle fibers. (G) An average of 500 fibers were analyzed per mouse. Representative images of each treatment can be seen in (H-K). Black scale bar = 50 µm. The white arrows signal nuclei that have central localization. All samples were statistically compared to P-SC through Student's t-Test. P-value GP style: 0.1234 (ns), 0.0332 (*), 0.0021 (**), 0.0002 (***), <0.0001 (****). Error bars = SEM.

Transcripts *Atp2a1*, *Clcn1*, *Mbnl1*, and *Nfix* all show abnormal fetal splicing patterns in the DM1 mice model.[27-30] After blockmiR administration, correction was seen in all four transcripts (Figures 4A-D). The percent splicing recovery compared to the P-SC control showed significant rescue.

As seen in DM1 cell microscopy, the P-PMO also increased the amount of Mbnl1 protein (Figures 4E-F). Jess Simple Western technology was used to quantify the level of Mbnl1 normalized to the total protein level. The P-PMO showed significant increase compared to the P-SC and the HSA$^{LR}$ PBS control.

Finally, a histological analysis was made of 10 µm sections of the quadriceps muscle (Figure 4G-K). After staining with hematoxylin and eosin, the percent of muscle fibers with central nuclei were quantified. The migration of muscle fiber nuclei towards the center of the muscle fibers is a well-known phenotype of HSA$^{LR}$ mice muscle.[31] Although not statistically significant when averaging all six mice, a decrease in the percent of fibers with central nuclei was observed in comparison to the P-SC samples. There were two specific mice that showed particularly strong rescue. The image in Fig. 4K is representative of one of these mice and shows a striking resemblance to the FVB cuts.

DISCUSSION

A significant increase in MBNL1 protein was observed after treatment with P-PMO blockmiR through Simple Western analysis. Importantly, the treatment also did not over rescue the abundance of MBNL1 as the levels reached were comparable to the healthy controls. The MBNL1 protein increase was also functional as evidence by the significant splicing rescue in cells and mice. MBNL proteins play a critical role in the alternative splicing patterns of the transcripts. Specifically, a recent study comparing mis-spliced transcripts in HSA$^{LR}$ mice to MBNL¾ knockout mice showed 81% overlap which included *Atp2a1*, *Clcn1*, *Mbnl1*, and *Nfix*.[30] Indeed, *ATP2A1*, *MBNL1*, and *NFIX* splicing correction showed a dose response to MBNL1 knockout in human cells.[32] Likewise, *Clcn1* also shows response to *MBNL* knockout.[33] The results of P-PMO blockmiR treatment not only indicates an increase in MBNL1 protein but the rescue of these four transcripts also indicates an upstream rescue of MBNL1 functionality.

These transcripts also play important roles in cell function. For example, *ATP2A1* codes for a key enzyme for $Ca^{2+}$ metabolism in muscle cells.[34] *Mbnl1* ex5 splicing patterns are related to MBNL1 subcellular localization and functionality.[35] Furthermore, *Clcn1* mis-splicing is directly related to myotonia and muscle weakness.[36, 37] Therefore, splicing rescue could be responsible for the increase in mice grip strength in this

experiment. Other DM1 phenotypes such as myotonia should be analyzed for therapeutic effects in future P-PMO blockmiR treatment.

Although not significant for n=6, the abundance of central nuclei decreased greatly for two mice in particular. Indeed, even when just omitting a pair of mice with the highest percentage values, the statistical comparison to P-SC quickly becomes significant with a p-value of 0.0384. The error for nuclei quantifications was low for each individual mouse (Table S2). Nuclei quantification was done blindly after randomizing images to avoid bias.

One of the principal delimiting factors in antisense therapy is transporting the ASOs across the cell membrane barrier.[38] In an experiment testing the cell membrane of $HSA^{LR}$ mice, it was concluded that their cell membranes have a fully functional barrier.[39] Therefore, all ASO treatments in DM1 must consider the integrity of the cell. The therapeutic effects of P-PMO blockmiR seen here in cells and mice suggest that the cell-penetrating peptides are indeed capable of crossing the cell membrane. Additionally, the peptide technology did not cause any toxic effects *in vitro* or *in vivo*. This is a critical advantage for the P-PMO design and chemistry and merits further *in vivo* study that could potentially be applied to other antisense treatment strategies.

Finally, the results seen in this study confirm the concept of blockmiR therapy in DM1. Indeed, the site-specific strategy showed similar therapeutic results to miRNA-specific antagomiR strategies.[18, 40] Both strategies are capable of increasing MBNL1 protein and grip strength in $HSA^{LR}$ mice as well as inducing therapeutic splicing alterations. The blockmiR technology presented here merits further exploration particularly in regard to quantifying how much compound successfully reached the muscles.

MATERIALS AND METHODS

**P-PMO BlockmiR design**

Phosphorodiamidate morpholino oligonucleotides (PMOs) are non-ionic oligonucleotides since the phosphodiester bonds are replaced by phosphoroamidate linkages and the riboses by morpholino moieties. The PMO blockmiR contains the following sequence: CCAUUAUCACAUUUUGCUCUU. It is covalently linked to the cationic peptide Pip9b2: RXRRBRR FQILY RBRXRB. Peptides were synthesized and conjugated to PMOs as described previously.[41] A negative scrambled control Pip9b2-PMO was also generated with the following PMO sequence: TCTTACCTCAGTTACAATTTA. Conjugates were centrifuged through 3k Amicon filters followed by filtration through 0.22 um. Quality control was performed after each of the conjugations (HPLC: >99%, MALDI-TOF: acceptance error of molecular weight is 0.1%). Following each freeze thaw cycle peptide-PMOs are vortexed briefly and incubated for 30 mins in a 37C water bath. Subsequently, peptide-PMOs are sonicated for 30 seconds with a probe sonicator or 5 mins with a water bath sonicator.

**Cell culture**

Healthy immortalized control-derived fibroblasts (CNT) and immortalized patient-derived fibroblasts carrying 1300 CTG repeats (DM1) were provided by Dr. Furling[25] (Institute of Myology, Paris) and were transdifferentiated into myotubes by inducing MyoD expression. The fibroblasts were grown in DMEM with 4.5 g/L glucose, 1% penicillin and streptomycin (P/S), and 10% FBS (Sigma). Transdifferentiation was prompted by muscle differentiation medium (MDM) containing DMEM with 4.5 g/L glucose, 1% P/S, 2% horse serum, 1% apo-transferrin (10 mg/mL), 0.1% insulin (10 mg/mL), and 0.02% doxycycline (10 mg/mL). C2C12 cells were also grown in in DMEM with 4.5 g/L glucose, 1% penicillin and streptomycin (P/S), and 10% FBS (Sigma). All cells were grown at 37°C in a humidified atmosphere containing 5% $CO_2$.

**Toxicity assay**

Immortalized DM1 fibroblasts were plated in a 96-well plate (Falcon) at a concentration of $1.0x10^5$ cells per mL. After 24 hours, P-PMO blockmiRs and P-SC were transfected at 10 nM, 50 nM, 200 nM, 1 µM, 5 µM, and 10 µM in triplicate in MDM with X-tremeGENE HP DNA Transfection Reagent (Roche) according to manufacturer instructions and transdifferentiated into myotubes for 4 days. The same experiment was duplicated without the use of transfection reagent. To measure cell viability, 20 µl of MTS/PMS tetrazolium salt from the CellTiter 96 Aqueous Non-Radioactive Cell Proliferation Assay (Promega) was added to each well and cells were incubated for four hours at 37°C in a humidified chamber with 5% $CO_2$. The conversion of MTS into soluble formazan was measured by absorbance at 490 nm using an Infinite 200 PRO plate reader (Tecan). Data were normalized to non-transfected DM1 controls.

**Cell transfection**

DM1 cells and CNT cells were plated at $1.0x10^5$ cells per mL in 10 mL petri dishes (Falcon). DM1 cells were transfected with 1 µM of P-PMO or P-SC and transdifferentiated with MDM. CNT cells and DM1 cells treated with PBS were used as controls. The cells were left four days to transdifferentiate into myotubes.

**Immunofluorescence**

Immortalized DM1 fibroblasts were seeded at $4.0x10^4$ cells per well in a 24-well plate (Falcon). After transfection and four days of differentiation, the transdifferentiated myotubes were fixed with 4% PFA for 15 minutes at room temperature (RT) and washed three times with 1x PBS. Myotubes were permeabilized with PBS-T (0.3% Triton-X in PBS) and blocked (PBS-T, 0.5% BSA, 1% donkey serum) for 30 minutes at RT. They were then incubated with MBNL1 primary antibody (1:200, MB1a (4A8), Developmental Studies Hybridoma Bank[42]) at 4°C overnight. After three PBS-T washes, the cells were incubated for 1 hour with a biotinylated anti-mouse-IgG (1:200, Sigma-Aldrich) and subsequent Avidin-Biotin amplification (Elite ABC kit, VECTASTAIN) for 30 minutes at RT. They were followed by three PBS-T washes and incubation with streptavidin-FITC fluorophore (1:200, Vector) for 2 hours at RT. After three washes with PBS, the cells were mounted with VECTASHIELD mounting medium containing 2 µg/mL DAPI (Vector) to detect the nuclei.

Images of DM1 cells were taken on an Olympus FluoView FV100 confocal microscope. The images were taken at a 40× magnification and quantified using Image J with the following formula at a threshold of 10: Mean Pixel Intensity=Gray value/Area.

**Dual Luciferase Assay**

Luminesence of Gaussian luciferase (GLuc) and alkaline phosphatase (SEAP) were measured using the secreted-pair dual luminescence kit (GeneCopoeia) according to the manufacturer's protocols. Gaussian luciferase activity was normalized to alkaline phosphatase activity (GLuc/SEAP). Luminescence was measured using a Tecan Infinite M200 PRO plate reader (Life Sciences). Mbnl1 3'-UTR reporter pEZX-MT05 plasmids were designed containing wildtype Mbnl1 (WT), deletion of miR-23b seed region (Del), and perfect match of the full miR-23b sequence (PM). The plasmids were transfected in C2C12 cells and their luminescence was measured. The same assay was repeated with C2C12 cells co-transfected with miR-23b mimic, scrambled mimic, and no mimic controls. Full plasmid sequences can be found in SI Appendix.

**RNA extraction, RT-qPCR and RT-PCR**

Total RNA was isolated from transdifferentiated myotubes or gastrocnemius muscle using QIAzol Lysis Reagent and RNeasy

Mini Kit (Qiagen) following manufacturer's recommendations. One microgram of RNA was digested with DNase (Zymo) and reverse-transcribed with SuperScript II Reverse Transcriptase (Invitrogen) using random hexanucleotides (Roche).

Semiquantitative PCR was performed using approximately 4 ng of template cDNA with TaqMan probes (Qiagen) for *MBNL1* and *MBNL2* with FAM-labeled probes and *GAPDH* as an endogenous control with MAX-labeled probes. Three technical replicates were performed for each sample. Expression levels were measured using an Applied Biosystems StepOnePlus Real Time PCR System. Samples were normalized to *GAPDH* calibrated with the P-SC control group using the $2^{-\Delta\Delta Ct}$ method. Samples were compared to P-SC using Student's t-test applying Welch's correction when necessary.

Alternative splicing was analyzed using approximately 200 ng of cDNA in a standard PCR reaction with GoTaq polymerase (Promega, Inc). *MBNL1* and *NFIX* specific primers were used to analyze splicing patterns for cells cDNA and *Atp2a1*, *Clcn1*, *Mbnl1*, and *Nfix* specific primers were for mouse cDNA (*SI Appendix*, Table S1). *GAPDH* and a No Reverse Transcriptase (NRT) were run as cDNA controls (Figure S1). PCR products were run on a 2% agarose gel and the exons quantified with Image J software (NIH). Percentage splice recovery (PSR) index was defined as value$\%_{SI}$ minus $\bar{X}\%_{DSI}$, divided by $\bar{X}\%_{DSI}$ minus $\bar{X}\%_{HSI}$ (where SI is splicing inclusion of each sample, DSI is disease splicing inclusion, and HSI is healthy splicing inclusion). Samples were compared to P-SC using Student's t-test applying Welch's correction when necessary.

**Transgenic mice and blockmiR administration**
Mouse handling and experimental procedures conformed to the European law regarding laboratory animal care and experimentation (2003/65/CE) and were approved by the Conselleria de Agricultura, Generalitat Valenciana ("Respuesta terapéutica a blockmiRs modificados en un modelo de ratón de DM1", reference number 2020/VSC/PEA/0203). Homozygous transgenic $HSA^{LR}$ (line 20 b) mice[31] were provided by Prof. C. Thornton (University of Rochester Medical Center, Rochester, NY, USA) and mice with the corresponding genetic background (FVB) were used as controls. Age-matched $HSA^{LR}$ (~3.5 months old) mice received one intravenous tail vein injection of 150 $\mu$l of either 1× PBS (n = 5), P-PMO 10 mg/kg (n = 6), or P-SC 10 mg/kg (n = 6) and FVB mice of the same age also received one intravenous tail vein injection of 150 $\mu$l of 1× PBS (n = 5). Four days after injection, the mice were sacrificed blood, muscles, and organs of interest were extracted. Muscles were divided into two tubes: one part was frozen in liquid nitrogen for the molecular analyses, and the other was fixed with -80°C chilled isopentane before histological processing.

**Forelimb grip strength test**
The forelimb grip strength was measured with a Grip Strength Meter (BIO-GS3; Bioseb, USA). The peak pull force (measured in grams) was recorded on a digital force transducer when the mouse grasped the bar. The gauge of force transducer was reset to 0 g after each measurement. Tension was recorded by the gauge at the time the mouse released its forepaws from the bar. The measurement was performed three consecutive times at 30 s intervals. The bodyweight measurement was performed in parallel. Percentage of normal force was calculated by normalizing the average strength after treatment to the strength before treatment and dividing this value by the body weight of each mouse.

**Blood biochemistry**
Blood serum was collected for each mouse and analyzed for biochemical parameters by Laboratorios Montoro Botella (Valencia, Spain). All samples were statistically compared to FVB mice through Kruskal-Wallis ANOVA and Wilcoxon test if applicable.

**Protein extraction and Jess Simple Western**
For total protein extraction, human DM1 cells or mouse tissues were sonicated and homogenized in Pierce RIPA buffer (Thermo Scientific) supplemented with protease and phosphatase inhibitor cocktails (Roche Applied Science). Quantification of total protein was performed with a BCA protein assay kit (Pierce) using bovine serum albumin as standard. For the immunodetection assay in mouse tissues, the Jess Simple Western system was used to quantify Mbnl1 protein chemiluminescence (1:50, MB1a (4A8), Developmental Studies Hybridoma Bank[42]) and normalized to total protein fluorescence.

**Muscle histology**
Frozen 10 µm sections of mouse quadriceps muscles were stained with haematoxylin and eosin and mounted with VECTASHIELD mounting medium (Vector) according to standard procedures. Images were taken at a 100× magnification with a Leica DM2500 microscope. The percentage of fibers containing central nuclei was quantified in an average of 500 fibers in each mouse. All images were labelled randomly during quantification to facilitate a blind analysis.

**Statistical analysis**
All statistical analyses were performed using Prism 8.2.1 (GraphPad) with special assistance from Dr. Juan Carbonell (Biostatistician, INCLIVA, Valencia, Spain).

ACKNOWLEDGMENTS
This projected was funded by the Myotonic Dystrophy Foundation (MDF) and the Tatami project funded by "La Caixa" Banking Foundation under the project code HR17-00268.
S.J.O. was funded by Santiago Grisolía code GRISOLIAP/2017/015.
Special thanks to Developmental Studies Hybridoma Bank for the MB1a antibodies and to Arantxa García Redón for research assistance.

AUTHOR CONTRIBUTIONS
S.J.O., E.C.-H., I.G.-M., B.L., and D.S.M. performed research; S.J.O., R.A., and B.L. designed research; M.A.V., Y.J. and R.R. provided the compounds. R.A., M.J.W., and M.P.A. contributed to conceptualization and funding acquisition; S.J.O. analyzed data and wrote the paper.

# Annex


REFERENCES

1. Landfeldt, E, Nikolenko, N, Jimenez-Moreno, C, Cumming, S, Monckton, DG, Faber, CG, Merkies, ISJ, Gorman, G, Turner, C, and Lochmuller, H (2020). Activities of daily living in myotonic dystrophy type 1. *Acta Neurol Scand* **141**: 380-387.
2. Miller, JW, Urbinati, CR, Teng-Umnuay, P, Stenberg, MG, Byrne, BJ, Thornton, CA, and Swanson, MS (2000). Recruitment of human muscleblind proteins to (CUG)(n) expansions associated with myotonic dystrophy. *EMBO J* **19**: 4439-4448.
3. Konieczny, P, Stepniak-Konieczna, E, and Sobczak, K (2014). MBNL proteins and their target RNAs, interaction and splicing regulation. *Nucleic Acids Res* **42**: 10873-10887.
4. Konieczny, P, Stepniak-Konieczna, E, and Sobczak, K (2017). MBNL expression in autoregulatory feedback loops. *RNA Biol*: 1-8.
5. Batra, R, Charizanis, K, Manchanda, M, Mohan, A, Li, M, Finn, DJ, Goodwin, M, Zhang, C, Sobczak, K, Thornton, CA, *et al.* (2014). Loss of MBNL leads to disruption of developmentally regulated alternative polyadenylation in RNA-mediated disease. *Mol Cell* **56**: 311-322.
6. Sznajder, LJ, and Swanson, MS (2019). Short Tandem Repeat Expansions and RNA-Mediated Pathogenesis in Myotonic Dystrophy. *Int J Mol Sci* **20**.
7. Merien, A, Tahraoui-Bories, J, Cailleret, M, Dupont, JB, Leteur, C, Polentes, J, Carteron, A, Polveche, H, Concordet, JP, Pinset, C, *et al.* (2021). CRISPR gene editing in pluripotent stem cells reveals the function of MBNL proteins during human in vitro myogenesis. *Hum Mol Genet*.
8. Wheeler, TM, and Thornton, CA (2007). Myotonic dystrophy: RNA-mediated muscle disease. *Curr Opin Neurol* **20**: 572-576.
9. Wang, ET, Ward, AJ, Cherone, JM, Giudice, J, Wang, TT, Treacy, DJ, Lambert, NJ, Freese, P, Saxena, T, Cooper, TA, *et al.* (2015). Antagonistic regulation of mRNA expression and splicing by CELF and MBNL proteins. *Genome Res* **25**: 858-871.
10. Rinaldi, C, and Wood, MJA (2018). Antisense oligonucleotides: the next frontier for treatment of neurological disorders. *Nat Rev Neurol* **14**: 9-21.
11. Xiong, H, Veedu, RN, and Diermeier, SD (2021). Recent Advances in Oligonucleotide Therapeutics in Oncology. *Int J Mol Sci* **22**.
12. Wojtkowiak-Szlachcic, A, Taylor, K, Stepniak-Konieczna, E, Sznajder, LJ, Mykowska, A, Sroka, J, Thornton, CA, and Sobczak, K (2015). Short antisense-locked nucleic acids (all-LNAs) correct alternative splicing abnormalities in myotonic dystrophy. *Nucleic Acids Res* **43**: 3318-3331.
13. Wheeler, TM, Sobczak, K, Lueck, JD, Osborne, RJ, Lin, X, Dirksen, RT, and Thornton, CA (2009). Reversal of RNA dominance by displacement of protein sequestered on triplet repeat RNA. *Science* **325**: 336-339.
14. Leger, AJ, Mosquea, LM, Clayton, NP, Wu, IH, Weeden, T, Nelson, CA, Phillips, L, Roberts, E, Piepenhagen, PA, Cheng, SH, *et al.* (2013). Systemic delivery of a Peptide-linked morpholino oligonucleotide neutralizes mutant RNA toxicity in a mouse model of myotonic dystrophy. *Nucleic Acid Ther* **23**: 109-117.
15. Lim, KR, Maruyama, R, and Yokota, T (2017). Eteplirsen in the treatment of Duchenne muscular dystrophy. *Drug Des Devel Ther* **11**: 533-545.
16. Blain, AM, Greally, E, McClorey, G, Manzano, R, Betts, CA, Godfrey, C, O'Donovan, L, Coursindel, T, Gait, MJ, Wood, MJ, *et al.* (2018). Peptide-conjugated phosphodiamidate oligomer-mediated exon skipping has benefits for cardiac function in mdx and Cmah-/-mdx mouse models of Duchenne muscular dystrophy. *Plos One* **13**: e0198897.
17. Forand, A, Muchir, A, Mougenot, N, Sevoz-Couche, C, Peccate, C, Lemaitre, M, Izabelle, C, Wood, M, Lorain, S, and Pietri-Rouxel, F (2020). Combined Treatment with Peptide-Conjugated Phosphorodiamidate Morpholino Oligomer-PPMO and AAV-U7 Rescues the Severe DMD Phenotype in Mice. *Mol Ther Methods Clin Dev* **17**: 695-708.
18. Cerro-Herreros, E, Sabater-Arcis, M, Fernandez-Costa, JM, Moreno, N, Perez-Alonso, M, Llamusi, B, and Artero, R (2018). miR-23b and miR-218 silencing increase Muscleblind-like expression and alleviate myotonic dystrophy phenotypes in mammalian models. *Nat Commun* **9**: 2482.
19. Cerro-Herreros, E, Gonzalez-Martinez, I, Moreno-Cervera, N, Overby, S, Perez-Alonso, M, Llamusi, B, and Artero, R (2020). Therapeutic Potential of AntagomiR-23b for Treating Myotonic Dystrophy. *Mol Ther Nucleic Acids* **21**: 837-849.
20. Sabater-Arcis, M, Bargiela, A, Furling, D, and Artero, R (2020). miR-7 Restores Phenotypes in Myotonic Dystrophy Muscle Cells by Repressing Hyperactivated Autophagy. *Mol Ther Nucleic Acids* **19**: 278-292.
21. Rau, F, Freyermuth, F, Fugier, C, Villemin, JP, Fischer, MC, Jost, B, Dembele, D, Gourdon, G, Nicole, A, Duboc, D, *et al.* (2011). Misregulation of miR-1 processing is associated with heart defects in myotonic dystrophy. *Nat Struct Mol Biol* **18**: 840-845.
22. Lopez Castel, A, Overby, SJ, and Artero, R (2019). MicroRNA-Based Therapeutic Perspectives in Myotonic Dystrophy. *Int J Mol Sci* **20**.
23. Rupaimoole, R, and Slack, FJ (2017). MicroRNA therapeutics: towards a new era for the management of cancer and other diseases. *Nat Rev Drug Discov* **16**: 203-222.
24. Bartel, DP (2009). MicroRNAs: target recognition and regulatory functions. *Cell* **136**: 215-233.
25. Arandel, L, Polay Espinoza, M, Matloka, M, Bazinet, A, De Dea Diniz, D, Naouar, N, Rau, F, Jollet, A, Edom-Vovard, F, Mamchaoui, K, *et al.* (2017). Immortalized human myotonic dystrophy muscle cell lines to assess therapeutic compounds. *Dis Model Mech* **10**: 487-497.
26. Veenstra, J, Smit, WM, Krediet, RT, and Arisz, L (1994). Relationship between elevated creatine phosphokinase and the clinical spectrum of rhabdomyolysis. *Nephrol Dial Transplant* **9**: 637-641.

27. Du, H, Cline, MS, Osborne, RJ, Tuttle, DL, Clark, TA, Donohue, JP, Hall, MP, Shiue, L, Swanson, MS, Thornton, CA, *et al.* (2010). Aberrant alternative splicing and extracellular matrix gene expression in mouse models of myotonic dystrophy. *Nat Struct Mol Biol* **17**: 187-193.
28. Dixon, DM, Choi, J, El-Ghazali, A, Park, SY, Roos, KP, Jordan, MC, Fishbein, MC, Comai, L, and Reddy, S (2015). Loss of muscleblind-like 1 results in cardiac pathology and persistence of embryonic splice isoforms. *Sci Rep* **5**: 9042.
29. Lin, X, Miller, JW, Mankodi, A, Kanadia, RN, Yuan, Y, Moxley, RT, Swanson, MS, and Thornton, CA (2006). Failure of MBNL1-dependent post-natal splicing transitions in myotonic dystrophy. *Hum Mol Genet* **15**: 2087-2097.
30. Tanner, MK, Tang, Z, and Thornton, CA (2021). Targeted splice sequencing reveals RNA toxicity and therapeutic response in myotonic dystrophy. *Nucleic Acids Res* **49**: 2240-2254.
31. Mankodi, A, Logigian, E, Callahan, L, McClain, C, White, R, Henderson, D, Krym, M, and Thornton, CA (2000). Myotonic dystrophy in transgenic mice expressing an expanded CUG repeat. *Science* **289**: 1769-1773.
32. Wagner, SD, Struck, AJ, Gupta, R, Farnsworth, DR, Mahady, AE, Eichinger, K, Thornton, CA, Wang, ET, and Berglund, JA (2016). Dose-Dependent Regulation of Alternative Splicing by MBNL Proteins Reveals Biomarkers for Myotonic Dystrophy. *PLoS Genet* **12**: e1006316.
33. Choi, J, Personius, KE, DiFranco, M, Dansithong, W, Yu, C, Srivastava, S, Dixon, DM, Bhatt, DB, Comai, L, Vergara, JL, *et al.* (2015). Muscleblind-Like 1 and Muscleblind-Like 3 Depletion Synergistically Enhances Myotonia by Altering Clc-1 RNA Translation. *EBioMedicine* **2**: 1034-1047.
34. Vihola, A, Sirito, M, Bachinski, LL, Raheem, O, Screen, M, Suominen, T, Krahe, R, and Udd, B (2013). Altered expression and splicing of Ca(2+) metabolism genes in myotonic dystrophies DM1 and DM2. *Neuropathol Appl Neurobiol* **39**: 390-405.
35. Terenzi, F, and Ladd, AN (2010). Conserved developmental alternative splicing of muscleblind-like (MBNL) transcripts regulates MBNL localization and activity. *RNA Biol* **7**: 43-55.
36. Tang, ZZ, Yarotskyy, V, Wei, L, Sobczak, K, Nakamori, M, Eichinger, K, Moxley, RT, Dirksen, RT, and Thornton, CA (2012). Muscle weakness in myotonic dystrophy associated with misregulated splicing and altered gating of Ca(V)1.1 calcium channel. *Hum Mol Genet* **21**: 1312-1324.
37. Wheeler, TM, Lueck, JD, Swanson, MS, Dirksen, RT, and Thornton, CA (2007). Correction of ClC-1 splicing eliminates chloride channelopathy and myotonia in mouse models of myotonic dystrophy. *J Clin Invest* **117**: 3952-3957.
38. Crooke, ST, Wang, S, Vickers, TA, Shen, W, and Liang, XH (2017). Cellular uptake and trafficking of antisense oligonucleotides. *Nat Biotechnol* **35**: 230-237.
39. Gonzalez-Barriga, A, Kranzen, J, Croes, HJ, Bijl, S, van den Broek, WJ, van Kessel, ID, van Engelen, BG, van Deutekom, JC, Wieringa, B, Mulders, SA, *et al.* (2015). Cell membrane integrity in myotonic dystrophy type 1: implications for therapy. *PLoS One* **10**: e0121556.
40. Cerro-Herreros, E, González-Martínez, I., Moreno, N., Espinosa-Espinosa, J., Fernández-Costa, J.M., Colom-Rodríguez, A., Overby, S.J., Seoane-Miraz, D., Poyatos-Garcia, J., Vílchez, J.J., López de Munain, A., Varela, M.A., Wood, M.J., Pérez-Alonso, M., Llamusí, B., Artero, R. (2021). Preclinical characterization of antagomiR-218 as a potential treatment for Myotonic Dystrophy. *Mol Ther Nucleic Acids*.
41. Betts, C, Saleh, AF, Arzumanov, AA, Hammond, SM, Godfrey, C, Coursindel, T, Gait, MJ, and Wood, MJ (2012). Pip6-PMO, A New Generation of Peptide-oligonucleotide Conjugates With Improved Cardiac Exon Skipping Activity for DMD Treatment. *Mol Ther Nucleic Acids* **1**: e38.
42. Holt, I, Mittal, S, Furling, D, Butler-Browne, GS, Brook, JD, and Morris, GE (2007). Defective mRNA in myotonic dystrophy accumulates at the periphery of nuclear splicing speckles. *Genes Cells* **12**: 1035-1048.

SUPPLEMENTAL INFORMATION

**Table S1. Primer and probe sequences used in RT-qPCR and RT-PCR.**

| Primers | Sequence | Analysis |
|---|---|---|
| *MBNL1* F | CTGCATCTGTCTATGCCAAACT | RT-qPCR |
| *MBNL1* R | GGGAATCTCCTCACAGCTGAAT | RT-qPCR |
| *MBNL1* Probe | ACCGATTGCACCACCAAACTCCATTGCA | RT-qPCR |
| *MBNL2* F | CCACCACGCCTGTTATTGTT | RT-qPCR |
| *MBNL2* R | CAGTCCTGAGAAGTTTCTGAGTTG | RT-qPCR |
| *MBNL2* Probe | ACCGGTCACTGTCCCGGGCTCAACT | RT-qPCR |
| *MBNL1* exon 5 F | AGGGAGATGCTCTCGGGAAAAGTG | RT-PCR |
| *MBNL1* exon 5 R | GTTGGCTAGAGCCTGTTGGTATTGGAAAATAC | RT-PCR |
| *NFIX* exon 7 F | GAGCCCTGTTGATGACGTGTTCTA | RT-PCR |
| *NFIX* exon 7 R | CTGCACAAACTCCTTCAGTGAGTC | RT-PCR |
| *GAPDH* F | CAACGGATTTGGTCGTATTGG | RT-qPCR & RT-PCR |
| *GAPDH* R | TGATGGCAACAATATCCACTTTACC | RT-qPCR & RT-PCR |
| *GADPH* Probe | CGCCTGGTCACCAGGGCTGCT | RT-qPCR |
| *Atp2a1* exon 22 F | GGGTCAGTGCCTCAGCTTTG | RT-PCR |
| *Atp2a1* exon 22 R | GCTCATGGTCCTCAAGATCTCAC | RT-PCR |
| *Clcn1* exon 7a F | GTCCTCAGCAAGTTTATGTCC | RT-PCR |
| *Clcn1* exon 7a R | GAATCCTCGCCAGTAATTCC | RT-PCR |
| *Mbnl1* exon 5 F | AGGGGAGATGCTCTCGGGAAAAGTG | RT-PCR |
| *Mbnl1* exon 5 R | GTTGGCTAGAGCCTGTTGGTATTGGAAAATAC | RT-PCR |
| *Nfix* exon 7 F | TCGACGACAGTGAGATGGAG | RT-PCR |
| *Nfix exon 7 R* | CAAACTCCTTCAGCGAGTCC | RT-PCR |
| *Gapdh F* | GAACGGATTTGGCCGTATTGG | RT-PCR |
| *Gapdh R* | GATGGCAACAATCTCCACTTTGCC | RT-PCR |

**Table S2. Statistical data for histological image quantification**

| Mouse | Mean | SEM | # of fibers |
|---|---|---|---|
| FVB1 | 38.91 | ±0.32 | 1791 |
| FVB2 | 39.61 | ±0.57 | 455 |
| FVB3 | 32.79 | ±0.38 | 877 |
| FVB4 | 28.50 | ±0.71 | 452 |
| FVB5 | 38.36 | ±0.34 | 816 |
| PBS1 | 77.86 | ±1.38 | 276 |
| PBS2 | 50.92 | ±1.00 | 297 |
| PBS3 | 60.57 | ±1.24 | 424 |
| PBS4 | 79.69 | ±0.98 | 342 |
| PBS5 | 57.89 | ±0.75 | 799 |
| P-SC1 | 68.36 | ±1.42 | 214 |
| P-SC2 | 71.89 | ±0.98 | 575 |
| P-SC3 | 56.83 | ±1.09 | 332 |
| P-SC4 | 60.90 | ±1.21 | 178 |
| P-SC5 | 53.32 | ±0.67 | 738 |
| P-SC6 | 61.24 | ±1.02 | 482 |
| P-PMO1 | 61.41 | ±1.48 | 238 |
| P-PMO2 | 39.29 | ±0.59 | 1325 |
| P-PMO3 | 72.69 | ±1.28 | 180 |
| P-PMO4 | 26.22 | ±0.93 | 325 |
| P-PMO5 | 52.22 | ±0.86 | 953 |
| P-PMO6 | 67.55 | ±7.20 | 88 |

**From:** **Molecular Therapy - Nucleic Acids** em@editorialmanager.com
**Subject:** Molecular Therapy - Nucleic Acids Editorial Decision MTNA-D-21-01327
**Date:** October 15, 2021 at 4:37 AM
**To:** Sarah Overby sarah.overby@ext.uv.es

Oct 14, 2021

MTNA-D-21-01327
Proof of concept of peptide-linked blockmiR induced MBNL functional rescue in Myotonic Dystrophy Type 1 mouse model

Dear Dr. Overby,

Thank you for allowing us to review your manuscript, MTNA-D-21-01327, "Proof of concept of peptide-linked blockmiR induced MBNL functional rescue in Myotonic Dystrophy Type 1 mouse model" which has now been seen by the reviewers whose comments are attached. While they find the work of potential interest, important concerns have been raised that preclude publication, as least at this time. We would like to request that you prepare a revision in response to the comments below, which will need to be seen again by one or more of the reviewers.

Please be aware that this offer to consider a revision does not in itself guarantee an eventual positive outcome and that a final decision will be taken based on a review of your revisions and assessment of the strength of your response to the reviewers' concerns.

Your revision is due on Jan 12, 2022. To submit a revision, go to https://www.editorialmanager.com/mtna/ and log in as an Author. You will see a menu item call Submission Needing Revision. You will find your submission record there.

Please remember to include your response to the reviewers' comments in the "Rebuttal Letter". You also have the option to withdraw your paper and submit it elsewhere, in which case we should be notified. However if you choose to revise it and resubmit it here, we will be pleased to consider the manuscript further.

Authors are granted three months from the date of decision to submit their revised manuscripts, although an extension can be granted by writing the editors closer to the due date.

Did you know that ASGCT members benefit from significantly discounted publication charges and open-access fees? The benefits associated with ASGCT membership are described here. If you are not currently an ASGCT member, but are interested in becoming one, please visit www.asgct.org for more details. For questions or assistance, email the Society Office.

Best regards,

Xavier Bofill-De Ros, PhD
Associate Editor, Molecular Therapy - Nucleic Acids

==========

**COMMENTS FROM THE EDITORIAL OFFICE:**

-- an eTOC Synopsis and Graphical Abstract are required with your revision (see instructions below).

-- include 5-10 keywords in a "Keywords" section before the References

-- Include a "Conflict of Interest" statement before the “Reference” section in the "Manuscript" file.

-- Only include Figures (1-4) and their captions in the “PDF FILE OF ALL FIGURES” file. Remove all other text.

-- Remove the title and author list from the “Supplemental Material” file. We will add a cover sheet in-house with this information.

==========

**COMMENTS FROM THE REVIEWERS:**

Reviewer #1: In the paper "Proof of concept of peptide-linked blockmiR induced MBNL functional rescue in Myotonic Dystrophy Type 1 mouse model" by Overby S et al., the authors used a blockmiR targeting the miR-23b binding site on the MBNL1 3'-UTR of Myotonic Dystrophy Type 1 in cell and mouse models to rescue DM1. Following injection, HSA(LR mice showed increased muscle strength and a rescue of downstream splicing. The rescue of the histological phenotype is less evident. This manuscript offers an interesting proof of concept to use blockmiRs as a potential therapeutic agent to rescue DM1. However, there are several weaknesses in the data and text that should be addressed to validate and support the authors' conclusions.

Specific Comments:
1. It has been previously shown that antagomiRs targeting miR-218 and miR-23b increase MBNL1 production by blocking MBNL transcript regulation. The authors should discuss and justify why they targeted only miR-23b in this study. Would a combination of targeting both miR-218 and miR-23b offer better rescue?

2. Muscles were analyzed only 4 days post-injection in mice. The authors should show different time points and justify why only 4

2. Muscles were analyzed only 4 days post injection in mice. The authors should show different time points and justify why only 4 days was studied. What happens after multiple adminstrations of the blockmiR? Does multiple injections at various timepoints provide better rescue?

3. The histological analysis of the quadriceps muscle in Figure 4 shows high variability and weakens the conclusion. Stating that two mice showed strong rescue is not rigorous data to support the conclusion. Especially when the results are not statistically significant. Revise text or add more supportive data.

4. It is critical to know how much compound reaches the myofibers. The authors should quantitate the compound in myofibers and in other cell types.

5. Nuclear foci should be assessed after administration of compound since it's a hallmark feature of DM1.

6. qRT-PCR is performed for quantitate analysis. However in this manuscript the authors used RT-PCR for quantitate analysis. RT-PCR can be used for qualitative assessment but not quantitative analysis. Authors must perform qRT-PCR for data in Figures 1D, 1E, 4A, 4B, 4C, and 4D or remove the graphs.

7. Style comment: The authors should consider not labeling each panel. For example, Figure A-D should just be Figure A. Having each panel labeled does not add to the clarity of the text.

8. Check grammar.

9. Authors should include references about blockmiRs (line 76). In addition, authors should enhance the description of the mechanism of action of blockmiRs in the Introduction section (eg. describe the difference between siRNAs and blockmiRs with respect to the target RNA).

Minor comments

1. Authors should indicate figures 1D and 1E in the paragraph (line 101).

2. When NFIX is first cited, authors should include a reference (line 102).

3. Authors should include figure 2C in the paragraph (line 124).

4. Figure 2 describes in vitro data obtained in C2C12. Authors should move Figure 2D to Figure 3 with the other in vivo data.

5. Line 499, the dose indicated in the figure legend is different from the dose in Figure 2D. Please correct.

6. In Figure 3B, it is difficult to discern the different levels among the replicates. The authors should include a supplementary figure showing the level of the compounds for each mouse.

7. Line 155 is unclear. The authors should modify the sentence: "As seen in DM1 cell microscopy, the P-PMO also increased the amount of Mbnl1 protein in vivo (Figures 4E-F)". Please explain and clarify.

8. For Figure 4H-K, include whole sections of the muscles in the supplementary figures.

Reviewer #2: The manuscript present a refinement of a previous strategy for targeting a miR-23b binding site on the MBNL1 3'-UTR in DM1 model cells and mice using a AONs called BlockmiRs.
Although the strategy of using ASO technology to block miRNA regulatory action on transcript may be more clear when associated to a novel terminology (blockmiR), the mechanism of action through steric hindrance is the same as previously described ASOs. It is therefore confusing the association of a commonly known RNA based therapeutic with the 'proof of concept' definition in the title. The reader expects a new class of nucleic acid therapeutic.
The structure of the sequence is the one of a regular ASO and the mechanism of blockage the same. Recently, several new therapeutic means based on ASO steric blockage have been described, such as translation enhancers, but all have been classified as antisense oligonucleotides. I would suggest rephrasing to specify that the novelty is not on the ASO itself but on the hybridization to a 'unexplored element' in the 3′ UTRs.
On a general note, since the authors propose here a new proof of concept, I find the manuscript lacking a more in depth initial study on the most efficient length of the ASO and type of modifications to be introduced in the sequence. We now known that those factors influence vastly the action of ASO due to protein binding and off target effects. This was overcome by the choice of testing the ASOs in mice model, but resulted in a design that is most probably not optimal.

CPP Pip9b2 was previously designed and described to facilitate efficient entry into the cell without the use of transfection reagents. In Figure 1A it is clear that the peptide-linked oligos showed little to no cell growth inhibition across all concentrations in contrast to those treated with transfection reagents and as a conclusion the authors have used transfecting agents and 1 μM concentration. In no experiment in the manuscript it has been shown the positive effect of appending Pip9b2 to the ASO. Although it was shown in a previous article, I would have liked to see a control where the PMO sequence is injected in mice or tested in cells as unconjugated, without peptide moiety, to have an idea of the influence of the peptide on the naked oligo. If possible having a control of the peptide alone as well.

In Figure 1D, GAPDH was run as an endogenous control but is not shown. It would be preferable to have an extra line with the image of GAPDH already in this figure. I suggest to add the full gels uncut in the supporting information as well if possible.

In order to confirm that the previously shown result in Figure 2B was due to miR-23b, the authors repeated the luminescence experiment with co-transfection controls, one with no mimic (WT-Ø) and one with a scrambled mimic (WT-SC). In the text the authors claim that the wildtype no-mimic control and the wildtype scrambled-mimic control both showed less miRNA repression compared to wildtype and mimic cotransfection. The statement is puzzling since the controls seems to have a higher value. Why the signal is higher than WT? Should not be expected to have no change or at least not the same effect as the mimic on Del site

2?

One of the few significant changes described at biochemistry level is a decrease in creatine phosphokinase (CPK) which connection to the disease seems to be very important. CPK is in fact released into the blood during muscle tissue damage. Scramble and PMO sequence seems to have an overall similar effect on the biochemistry and especially on CPK level. How can this be justified if the changes compared to PBS treatment should be dependent only on blockmir action?

Figure 4G-K: As the authors highlight, the decrease in the percent of fibers with central nuclei observed in comparison to the P-SC samples is not statistically significant when averaging all six mice. Is there a theory behind this large difference?
ATP2a1 WB coming from PBS treatment shows several bands, compared to other treatment. Is it a splicing effect?

Reviewer #3: The manuscript by Overby et al. is a well designed and clearly described preclinical study in mice using blockmiRs targeting the binding sites of miR23b in the 3'UTR of the MBNL1 transcript, as potential therapeutical approach for DM1. The results show the increase in MBNL1 protein levels, and, what is more relevant, the increase in mice grip strength and the partial recovery in splicing pattern of genes involved in the pathophysiology. As such, the study represents the proof of concept of blockmiR therapy in this disease, although several points need to be addressed, mainly with the aim of improving the manuscript:
- The discussion of the pros and cons of this strategy in relation to the use of antimiRs/ antagomiRs, previously used by the authors, should be extended. There is just a brief sentence in the discussion (line 201) mentioning similar effects for both treatments.
- toxic effects: page7, lines 195-196, the authors mention there is no toxic effect in vio or in vitro. I am not sure if this refers to the use of a peptide-linked PMO or to the use of the blockmiR. In vivo, the P-PMO was administered and 4 days later the mice were sacrificed, I assume no evident toxic effects were observed in such a short period. However, I think it would be useful to know if the blockmiR per se has any secondary off-target effects through binding to other transcripts and blocking phsyiological mir23b function. mir23b is expressed in different tissues and is involved in different pathways in relation to cancer and other diseases, so it would be useful to know if the blockmiR is binding elsewhere and its effects.

Minor issues:
- Page 4, line 103: "…a signficant return to the adult splicing pattern was observed." And indication that this seen in Fig 1 D,E is missing. In addition, please explain the choice of these two genes : MBNL1 and NF1X
-page 6, line 187: the sentence "Indeed, even when just omitting a pair of mice with the highest percentage values, the statistical comparison to P-SC quickly becomes significant …" should be deleted, as statistically, this is not allowed.

==========

**IMPORTANT DETAILS ON LENGTH RESTRICTIONS AND STYLE SPECIFICATIONS:**

1. The abstract should be succinct and refrain from editorializing. Please limit its length to between 150 and 200 words.

2. All text must be in (Word [.doc] format, font size 12, Times or Times Roman font preferred). Pdf format is NEVER acceptable for any text item.

3. Reference Guidelines:

- **PLEASE SPELL OUT THE NAMES AND INITIALS OF THE FIRST TEN AUTHORS, FOLLOWED BY ET AL FOR THOSE REFERENCES WITH GREATER THAN TEN AUTHORS.**
- Items must be numbered in the order they appear in the text **as a superscript, and not in parenthesis**. Additional items may be referenced as part of the supplemental information online, provided they relate to the supplemental information.

4. **All art should be saved as EPS or TIFF files. POWERPOINT AND MICROSOFT IMAGING FILES ARE NEVER, EVER ACCEPTABLE.**

- All art files should be high resolution. At least 300 dots per inch for photos and 1000 dots per inch for line drawings.
- All color files should be saved as RGB (not CMYK).
- All files should be sized as large as possible - either size the art for a ¼ page or ½ page size.
- do not imbed art in AI or .doc files.

5. Figure legends should simply describe what is shown in the figures, and should not discuss results or methodology, unless absolutely necessary for the reader to understand the data shown. Each figure legend must have a short title.

6. While the editors fully understand the extra challenges posed to authors whose native language is not English, we must ask that all manuscripts be reviewed and edited by a native speaker of English prior to submission.

7. eTOC Synopsis is required - The eTOC synopsis is a short summary of the main take-home message of the paper. This synopsis should be 50 words or fewer and should describe the context and significance of the findings for the broader readership. The goal is to highlight the major conceptual advance in the paper in order to attract the attention of the non-specialist without including extensive experimental detail. Submit this file in Word format under the "eTOC" category.

8. Graphical Abstract is required - A graphical abstract allows readers to quickly gain an understanding of the main take-home message of the paper. It should be entirely diagrammatic and not contain any original data images. The size specifications are 5.5 inches square at 300dpi. Accepted file types are TIFF, PDF, and JPG. Upload this file under the "Graphical Abstract" category.